



Deliverable D12.1

Civil Engineering requirements, architecture, inspection and monitoring report

Project acronym:	FP3 - IAM4RAIL
Starting date:	01/12/2022
Duration (in months):	48
Call (part) identifier:	HORIZON-ER-JU-2022-01
Grant agreement no:	101101966
Due date of deliverable:	Month 24
Actual submission date:	30-11-2024
Responsible/Author:	Jose Solís Hernández / CEMOSA Paula Lopez Arevalo / CEMOSA
Dissemination level:	PU
Status:	Issued

Reviewed: (yes/no)

Document history		
Revision	Date	Description
0.1	15/01/2024	First issue circulated
0.2	29/02/2024	Use Cases section revision
0.3	30/04/2024	Architecture section revision
0.4	30/06/2024	Installation and Initial Data Analysis section revision
0.5	31/08/2024	Internal revision
0.6	28/10/2024	Internal review
1.0	25/11/2024	Final version submitted to ERJU

Report contributors		
Name	Beneficiary Short Name	Details of contribution
Pedro Martín Pérez Martínez	ADIF	Contribution on sections 5.2, 6.3, 6, 7.2 and 7.3.
Paula López Arévalo, Israel Alejandro Hernández González	CEM	Deliverable leader, contribution on sections 3, 4, 5.2, 6, 7.2 and 8. Internal revision.
Miquel Morata Royes	COM	Contribution on sections 5.2, 6 and 7.2.
Chiara Cesali	FS	Contribution on sections 5.1, 6 and 7.1.
Vincenzo Scarnera, Teodora Palmas, Simone Lelli, Fabbri Castagni Davide, Ignazio Rana	MER	Contribution on sections 5.1, 6 and 7.1.
Margherita Lupi, Nazzareno Lopez, Giulia Polimanti; Marco Fussotto	FS	Contribution on sections 5.1. and 7.1.2. Final Revision
Rune Schlanbusch, Christos Sakaris	NRD	Contribution on section 5.4, 6 and 7.4.
Amine Dhemaied, Dorine Chenier	SNCF	Contribution on sections 5.3, 6, 7.3.
Vincenzo Scarnera	MER	Work Package Leader, final internal revision
David Villalmanzo	ADIF	Quality check and official submission to the JU
Mariya Kayalova	RINA	Revision

Disclaimer

The information in this document is provided “as is”, and no guarantee or warranty is given that the information is fit for any particular purpose. The content of this document reflects only the author’s view – the Joint Undertaking is not



responsible for any use that may be made of the information it contains. The users use the information at their sole risk and liability.

The content of this Deliverable does not reflect the official opinion of the Europe's Rail Joint Undertaking (EU-Rail JU). Responsibility for the information and views expressed in the therein lies entirely with the author(s).

Table of Contents

1.	Executive Summary	12
2.	Abbreviations and acronyms	13
3.	Background	16
4.	Objective/aim.....	17
5.	Use Cases: Functional and Technical Requirements	18
5.1.	Multiscale Monitoring of Civil Assets (Italy)	18
5.2.	Bridges and Earthworks Asset Management aided by Geotechnics (Spain).....	28
5.3.	Monitoring of Tunnel, Sub-ballast layers, Subsoil (France).....	36
5.4.	Data Analysis for Condition Monitoring (The Netherlands, Norway).	46
6.	Architecture and Data Interoperability.....	63
6.1.	Architecture	63
6.2.	User Interface	66
6.3.	Standards	69
7.	Civil engineering inspection and monitoring technologies: Installation and initial data collection.....	72
7.1.	Multiscale Monitoring of Civil Assets (Italy)	72
7.2.	Bridges and Earthworks Asset Management aided by Geotechnics (Spain).....	128
7.3.	Monitoring of Tunnel, Sub-ballast layers, Subsoil (France).....	169
7.4.	Data Analysis for Condition Monitoring (The Netherlands, Norway)	197
8.	Conclusion.....	213
9.	References.....	216
10.	Annexes.....	220

List of Figures

Figure 1. Number of French tunnels railways built per decade.	37
Figure 2. Traditional tunnel inspection.	37
Figure 3. Use of conventional geotechnical and geophysical methods for better diagnosis to reduce maintenance operations and improve solution design.	39
Figure 4. Example of a new tunnel inspection system.	40
Figure 5. Application in tunnel convergence monitoring.	41
Figure 6. Topographical precision control works.	41
Figure 7. Study areas of transition zones at the double-track railway bridge (Unsiwilai, et al. 2023).	54
Figure 8. Tasks planned for the current UC.	55
Figure 9. Layout monitoring plan for transition zones and bridge.	57
Figure 10. ABA responses of Track I at an example bridge (Unsiwilai, et al. 2023).	59
Figure 11. GWPS of the ABA signals measured at different rails for Track I at an example bridge (Unsiwilai, et al. 2023).	59
Figure 12. SAWP of the ABA signals and track geometries at an example bridge (Unsiwilai, et al. 2023).	60
Figure 13. WP 12 Database structure (Oracle MySql WorkBench).	63
Figure 14. WP 12/13 Data Explorer web interface (Apache Tomcat). Home page.	66
Figure 15. WP 12/13 Data Explorer we interface (Apache Tomcat). Campaigns Table.	66
Figure 16. WP 12/13 Data Explorer we interface (Apache Tomcat). Measurements Table.	67
Figure 17. WP 12/13 Data Explorer we interface (Apache Tomcat). Processing Table.	67
Figure 18. WP 12/13 Data Explorer we interface (Apache Tomcat). Processing Table.	68
Figure 19. ALL WP12-13 data view (there are already 115 rows and 40 columns).	68
Figure 20. Upload Table Pop Up.	68
Figure 21. 30 cm resolution orthoimage for neural network training.	72
Figure 22. Ground truth data: classified point cloud from aerial survey (left) and CHM (right).	73
Figure 23. Additional ground truth data: classification map.	73
Figure 24. Intersection of the areas.	74
Figure 25. Pipeline structure for training with available classification map.	74
Figure 26. Pipeline structure for inference.	75
Figure 27. Left: comparison between histograms of predicted and ground truth values for the "Terrain" class. Right: Difference histogram.	78
Figure 28. Raster of the difference between the predicted CHM and the ground truth for the "Terrain" class.	78
Figure 29. Left: comparison between histograms of predicted and ground truth values for the "Vegetation" class. Right: Difference histogram.	79
Figure 30. Raster of the difference between the predicted CHM and the ground truth for the "Vegetation" class.	79
Figure 31. Example of pixels erroneously assigned to the Vegetation class.	80
Figure 32. Left: comparison between histograms of predicted and ground truth values for the "Buildings" class. Right: Difference histogram.	80
Figure 33. Raster of the difference between the predicted CHM and the ground truth for the "Buildings" class.	81
Figure 34. Classif. map from point cloud.	81

Figure 35. Predicted classification map.	81
Figure 36. Classif. map from point cloud.	81
Figure 37. Predicted classification map.	81
Figure 38. Left: comparison between histograms of predicted and ground truth values for the "Vegetation" class. Right: Difference histogram. Results obtained after training both model A & B.	82
Figure 39. Raster of the difference between the predicted CHM and the ground truth for the "Vegetation" class. Results obtained after training both model A and B.	82
Figure 40. The three structures in the first batch of data. From left to right: concrete viaduct, bricks viaduct and steel girder.	83
Figure 41. Distribution of markers by category. M: "defects in masonry elements", C: "defects in reinforced concrete (R.C.) and pre-stressed concrete (P.C.) elements", A: "defects in steel elements", MCG: "defects in joint connection mechanisms", MCA: "defects in support connection mechanisms", V: "defects in superstructures".	84
Figure 42. Distribution of markers by category (colour) and type.	85
Figure 43. Different types of defects reported on indistinguishable areas.	86
Figure 44. High density of markers emphasising a problematic area.	86
Figure 45. Ambiguous markers placement on surface with vegetation.	87
Figure 46. High density of markers signifying an area that requires monitoring.	87
Figure 47. Examples of defects covered by branches and leaves.	88
Figure 48. The crack in this piece of steel is not visible due to the dark colour and the image resolution.	88
Figure 49. Defects on backlit structures are even more difficult to identify.	89
Figure 50. Example of data and respective ground truth for a classification dataset. In this case there are two overlapping types of defects: efflorescence and corrosion stain. Hence, the orange bounding box is multi-labelled.	90
Figure 51. Example of data and relative ground truth for a semantic segmentation dataset. The green shapes cover the pixels associated to the class "weathering", while the blue ones are for the class "efflorescence".	91
Figure 52. Milano-Novara and Tortona-Voghera AOI.	93
Figure 53. Data download and elaboration scheme.	94
Figure 54. GPM IMERG Final precipitation L3 Half Hourly 0.1° x 0.1° (GPM_3IMERGHH).	97
Figure 55 - GPM_3IMERGHH over the AOI.	98
Figure 56. GPM IMERG Late precipitation L3 Half Hourly 0.1° x 0.1° (GPM_3IMERGHH).	98
Figure 57. GLDAS-2.1 Noah 3-hourly 0.25 degree 0-10 cm soil moisture [kg m ⁻²] for 03Z Jan 01, 2000.	100
Figure 58. GLDAS soil moisture over the AOI (acquisition ID: NASA/GLDAS/V021/NOAH/G025/T3H/A20230101_0000).	101
Figure 59. Summary of the C6 MODIS LST products (source: (NASA, MODIS 2024)).	102
Figure 60. MOD11A1 over the AOI (acquisition ID: MODIS/061/MOD11A1/2011_01_01).	103
7.1.3.3.2. Figure 61. MOD11A1 over the AOI (acquisition ID: MODIS/061/MOD11A1/2011_01_01) resampled to 10 km. Data Processing and Correlation	103
Figure 62. Example of CSV output. (a) cumulated 1 h, (b) daily, (c) monthly, (d) climatological average for precipitation parameter.	106
Figure 63. GLDAS anomalies series for year 2000 and variable vsm_0_10 (AOI Milano-Novara). ...	108
Figure 64. GPM anomalies time series for year 2002 and variable precipitationCal (AOI Milano-	

Novara).....	109
Figure 65. MODIS Terra anomalies time series for year 2023 and variable LST (AOI Milano-Novara).	109
Figure 66. GLDAS box plot for year 2010 and parameter vsm_0_10 (AOI Tortona-Voghera).	110
Figure 67. GPM box plot for year 2011 and parameter precipitationCal (AOI Tortona-Voghera). .	111
Figure 68. MODIS Terra box plot for year 2002 and parameter LST (AOI Tortona-Voghera).	111
Figure 69. GPM cross plot precipitationCal-vsm_0_10 for year 2014 (AOI Tortona-Voghera).	113
Figure 70. GPM cross plot precipitationCal-vsm_0_10 for year 2014 (AOI Tortona-Voghera). Zoomed version.	113
Figure 71. Cross plot precipitationCal-vsm_0_10 for year 2015 (AOI Tortona-Voghera).	114
Figure 72. Cross plot precipitationCal-vsm_0_10 for year 2015 (AOI Tortona-Voghera). Zoom version.	115
Figure 73. Cross plot precipitation Cal-LST for year 2004 (AOI Milano-Novara).	116
Figure 74. Cross plot precipitation Cal-LST for year 2004 (AOI Milano-Novara). Zoom version.	116
Figure 75. Workflow.....	117
Figure 76. Fully connected NN architecture.	118
Figure 77. Loss function and accuracy for AOI Milano-Novara for training (in blue) and validation set (in orange).	119
Figure 78. Loss function and accuracy for AOI Tortona-Voghera for training (in blue) and validation set (in orange).	119
Figure 79. IWS TOPS SAR Mode Acquisition Scheme.	121
Figure 80 SW installed.....	122
Figure 81. EGM Service and example of Reports per point (Vertical and East-West Displacement).	122
Figure 82 EGM Service Vertical Displacement on Cerignola Area.	123
Figure 83 EGM Service Vertical Displacement on Talud Briones Area.	123
Figure 84 Copernicus Browse and Data Download.	124
Figure 85 SAR Acquisition Concept.	124
Figure 86. Left: repeating Ground Track. Right: Interferometric Concept.	125
Figure 87 Operation sequence for DEM and displacement retrieval.	126
Figure 88. Subsidence on Cerignola AOI.	127
Figure 89. Subsidence on Talud Briones AOI.	128
Figure 90. Triaxial accelerometer image.....	131
Figure 91. Concrete wall box 40x40 inside without bottom.	132
Figure 92. Example of Gateway + solar panel installed on catenary pole.	134
Figure 93. Detail of the Gateway and the solar panel to be installed on the catenary pole that is located in front of the unstable slope.	134
Figure 94. Type clinometers to be installed on the slope on rebar. Specifically, 14 clinometers of the same type as the one shown on the right of the image will be installed.	135
Figure 95. Mode of installation of rebar.	135
Figure 96. Example of a weather station installed on a shed.	136
Figure 97. Type video camera installed on catenary pole.	136
Figure 98. Detail of the Inclinator installed.	136
Figure 99. Inclinator installed on the Corrugated Bar	136
Figure 100. Schematic of the proposed architecture.	137
Figure 101. Installation of tiltmeter on a mast embedded in the ground.....	139

Figure 102. Tiltmeter orientation.	139
Figure 103. Clinometer power batteries.	139
Figure 104. Tiltmeter installed on a rock.	140
Figure 105. Tiltmeter installed on sleeper.	140
Figure 106. Installation scheme.	142
Figure 107. Plans of the installation of the monitoring system for dynamic analysis of the structure.	144
Figure 108. Viaduct cross-section.	145
Figure 109. Trench between communications channel and wall.	145
Figure 110. Elevation section and plan of the viaduct.	146
Figure 111. Affected section of Adif's RC Line 700.	147
Figure 112. Detail of the slope slip.	147
Figure 113. General architecture for the study slope.	148
Figure 114. Location of the unstable slope under study.	149
Figure 115. Location plan of installed clinometers.	150
Figure 116. Flowchart of the implemented S-DT-based continuous St-Id of bridges.	153
Figure 117. Flowchart for the analysis and detection of anomalies in tiltmeter time series.	158
Figure 118. Tiltmeters installation with local coordinates systems.	159
Figure 119. LSTM network architecture.	161
Figure 120. (a) Definition of limits based on the training period. (b) Alarm activation mechanism.	162
Figure 121. Recording Differences to Identify Peak Values.	163
Figure 122. Alarm mechanism based on value predictions.	163
Figure 123. (a) Deviation in railway sleepers and (b) damage mechanism based on deviation limit values.	164
Figure 124. Tests set-up. Example 1.	165
Figure 125. Tests set-up. Example 2.	165
Figure 126. Tests set-up. Example 3.	165
Figure 127. Tests set-up. Example 4.	165
Figure 128. Platform interface.	167
Figure 129. Example of log of alarms.	167
Figure 130. Platform interface. Example 1.	168
Figure 131. Platform interface. Example 2.	168
Figure 132 : Photograph of the hammer-type active seismic source on a metal plate between two geophones (black and blue).	169
Figure 133 : (A) Photograph of a seismic setup placed on the cess and of the hammer-type source used during seismic active acquisitions (2022). (B) Seismic setup recording seismic waves generated by the train passage (2022).	170
Figure 134. Workflow of the active seismic method.	171
Figure 135. Workflow of the passive seismic method.	172
Figure 136. Example of shear-waves velocity pseudo-section and complementarity with GPR data along a railway trackbed disorder zone.	172
Figure 137. (top) Example of groundwater table map generated using passive MASW and Artificial Intelligence. (bottom) Example of geologic profiles and groundwater table profiles inferred using passive MASW and Artificial Intelligence.	173
Figure 138. Active seismic device : a. Conventional on the cess, b. Landstreamer on the cess, c.	

Landstreamer on the track.....	174
Figure 139. Example of a defect survey conducted using the RADIS module (AutoCAD software).	175
Figure 140. Example of rating for an underground structure (source database 2023).....	176
Figure 141. Analysis of the relationships between the identified factors of change.	177
Figure 142. Synthetic example of how a decision tree model works.	179
Figure 143. Synthetic example of how a neural network model works.	179
Figure 144. Performance results for the neural network model. 75% of the predictions fall within the [rating-5; rating+5] interval.	181
Figure 145. Performance results for the Gradient Boosting model. 76,6% of the predictions fall within the [rating-5; rating+5] interval.	181
Figure 146. Screenshot of the Decision Support Tool Developed by SNCF.	183
Figure 147. TS4 system from German company SPACETEC with line-scan cameras.	184
Figure 148. Scantubes system from the French company SITES with matrix cameras.	184
Figure 149. ELISE system from the Swiss company AMBERG for SNCF Réseau.	185
Figure 150. ELISE system from the Swiss company AMBERG for SNCF Réseau.	186
Figure 151. Example of a photorealistic 3D model.	187
Figure 152. Superposition of a damage survey with a pseudo-orthophotograph obtained from a scanner.	187
Figure 153. Automatic detection of a brick exfoliation zone by comparison between the profiles measured by a scanner and a theoretical profile and photograph of the zone taken in-situ during an inspection.	188
Figure 154. Superposition of an orthophotograph with the temperature reading.	188
Figure 155. Superposition of an orthophotograph with the temperature reading.	189
Figure 156. Creation of damages.	189
Figure 157. Measurement.	189
Figure 158. Examples of orthophotographs corresponding to different degradation moments. ..	190
Figure 159. Pixel-to-pixel subtraction and identification of visible differences between two moments (ScanTubes® – SITES) – SNCF Network Tunnel.	191
Figure 160. Geometric processing and detection of damage depths between two moments (ScanTubes® – SITES) – SNCF Network Tunnel.	191
Figure 161. View of the microwire under the microscope. Source: IMA	192
Figure 162. Project Timeline. Source: Own Elaboration	194
Figure 163. Microwire patches of different lengths. Source: Own Elaboration.....	195
Figure 164. Optimal microthread patch. Source: Own elaboration	195
Figure 165. PCV prototype with microwire patch. Source: Own elaboration	196
Figure 166. Parts of the experimental setup. Source: Own elaboration	196
Figure 167. BBMS system interface (ProRail, Factsheet ProRail - Dataset Spoorgeometrie 2022). ..	198
Figure 168. ABA measurement system sensor layout.	202
Figure 169. UFM120 sensors layout (ProRail, Factsheet ProRail - Meetsystemen UFM120 2022). ..	202
Figure 170. Situational map of Sørsterbekk area on Ofotbanen railway line.	203
Figure 171. Installation plan for Sørsterbekk bridge 1.	204
Figure 172. Installation plan for Sørsterbekk bridge 2.	204
Figure 173. Transition zones between Dordrecht station and Lage Zwaluwe station (Unsiwilai, et al. 2023).	205
Figure 174. The average speed of the ABA measurement system at each transition zone.	206

Figure 175. Responses of the ABA signals from 4 wheelsets measured at the inner rail of Track I at Bridge 6, ABA signals with 100 Hz cutoff frequency (source of aerial photographs: BBMS, ProRail) (Unsiwilai, et al. 2023).....	207
Figure 176. GWPS of the ABA signals of the transition zones at the inner rail of Track I at Bridge 6. A-I to C-I are areas on the entrance side, and D-I to F-I are areas on the exit side (Unsiwilai, et al. 2023).	207
Figure 177. SAWP of the ABA signals from 4 wheelsets at the inner rail of Track I at Bridge 6 (Unsiwilai, et al. 2023).....	208
Figure 178. ABA responses (with 100 Hz cutoff frequency) at Bridge 3 in wheelset 1 on the inner rail of Track I: (a) and (b) ABA and its WPS, measured at 15.7 m/s; and (c) and (d) ABA and its WPS, measured at 24.2 m/s (source of aerial photographs: BBMS, ProRail) (Unsiwilai, et al. 2023).	208
Figure 179. GWPS of ABA signals from two different measurement speeds at Bridge 3 in wheelset 1 on the inner rail of Track I (Unsiwilai, et al. 2023).	209
Figure 180. SAWP of the ABA signals from two different measurement speeds at Bridge 3 for the inner rail of Track I (Unsiwilai, et al. 2023).	209
Figure 181. SAWP of the ABA signals and track geometries at Bridge 6, Track I (Unsiwilai, et al. 2023).	210
Figure 182. The overview of Delft – Schiedam Line (source of the map and aerial photographs: BBMS, ProRail).	211
Figure 183. The ABA measurement train passed the Delft Campus station (between Delft and Schiedam).....	211

List of Tables

Table 1. Abbreviations and Acronyms	15
Table 2. Example of Versatile JSON entry for measurements and processing	65
Table 3. Training paraments.	76
Table 4. Training paraments for the two models	77
Table 5. GPM Level 3 data.....	96
Table 6. List of data fields, their variable names (in the data structure), and the data units for 3IMERGHH data files.....	97
Table 7. Main characteristics of precipitation data.	99
Table 8. Main characteristics of “GLDAS-2.1: Global Land Data Assimilation System”	101
Table 9. Main characteristics of LST data.	103
Table 10. Summary of the produced output.	106
Table 11. Training configuration and test results.	118
Table 12. Sentinel-1A and Sentinel-1B orbital parameters.	120
Table 13. IWS TOPS incidence and Offnadir per subswath.	121
Table 14. Sentinel-1 IWS TOPS Swath and resolution geometric parameters.	121
Table 15. Triaxial accelerometer specifications.....	131
Table 16. Information on the location of installed clinometers.	151
Table 17. Influence of factors on speed (examples).....	176
Table 18. Description of the measured signals from the ABA measurement system.....	198
Table 19. Description of the considered track geometry parameters.	199
Table 20. Specification of the considered track geometry parameters (ProRail, Factsheet ProRail - Dataset Spoorgeometrie 2022).....	199
Table 21. List of major specifications for bridge measurement system.....	200
Table 22. Summary of the planned measurement system.....	201

1. Executive Summary

WP12 deals with intelligent inspection technologies and management of civil works. On top of the assets themselves (e.g. bridges, viaduct, rail, tunnels), the surrounding environment / environmental conditions are part of this work (e.g. slopes, vegetations, floods). This deliverable establishes requirements, architecture and presents initial measurements pertaining monitoring techniques on civils, paving henceforth the way for WP13.

The present document is divided in the following sections:

- The first section **Use Cases: Functional and Technical Requirements** (Section 5) presents one subsection per Use Case, describing for each one (1) Problem to be solved, (2) Industry current position/baseline, (3) Subproblem addressed by the use case and measurable objectives, (4) Influence of the proposed innovation on the IM/RU problem and (5) Refinement of Key Performance Indicators (KPIs). These sections (5.1, 5.2, 5.3 and 5.4) provide the general information for the project technologies, providing also an overview on the technologies state of the art review and other socio-economic factors.
- The following section (Section 6) is **Architecture and Data interoperability**, which presents (1) The architecture of the WP, (2) the user interface developed to visualise the data of the interoperability database to browse WP12 and 13 contents and (3) the different standards that each UC applies to the WP as well as the standards applied for interoperability and retrievability.
- Next, on Section 7, **Civil engineering inspection and monitoring technologies: Installation and initial data collection**, a detailed report on the current development status of each project Use Case technology is provided per UC including Selected equipment, technical specifications and justification, Data selection and collection, Algorithms and implementation, Preliminary results, Workflow and Demonstration Plan.
- There is a final section of **Conclusions** (Section 8), a section for **References** (Section 9) and another referring the different **Appendices** of the document (Section 10).

2. Abbreviations and acronyms

Abbreviation / Acronym	Description
ABA	Axle Box Acceleration
ADIF	Administrador de Infraestructuras Ferroviarias
AOI	Area Of Interest
AR	Auto Regressive
BIM	Building Information Modeling
BMS	Bridge Management Systems
CAPEX	Capital Expenditure
CEDEX	Centro de Estudios y Experimentación de Obras Públicas
CEMOSA	Centro de Estudios de Materiales y Control de Obra, S.A.
CHM	Canopy Height Model
CoSD	Combined Standard Deviation
CSV	Comma Separated Value
CWT	Continuous Wavelet Transform
DAQ	Data Acquisition System
DT	Digital Twin
DTM	Digital Terrain Model
EGMS	European Ground Motion Service
EOC	Environmental Conditions
EOCs	Environmental and Operating Conditions
ESA	European Space Agency
FA	Flagship Areas
FEA	Finite Element Analysis
FEM	Finite Element Model
GDLAS	Global Land Data Assimilation System
GEE	Google Earth Engine
GIS	Geographic Information System
GPM	Global Precipitation Measurement
GPS	Global Positioning System
IM	Infrastructure Manager

Abbreviation / Acronym	Description
IMERG	Integrated Multi-satellite Retrievals
INECO	Ingeniería y Economía del Transporte
InSAR	Interferometric Synthetic Aperture Radar
IOT	Internet Of Things
JAXA	Japan Aerospace Exploration Agency
KNN	K-Nearest Neighbour
KPI	Key Performance Indicators
LL	Longitudinal Level
LST	Land Surface Temperature
LVDT	Linear Variable Differential Transformer
MAE	Mean Absolute Error
MASW	Multichannel Analysis of Surface Waves
MGT	Million Gross Tonnes
ML	Machine Learning
MODIS	Moderate-Resolution Imaging Spectroradiometer
MOMIT	Multi-Scale Observation & Monitoring of Railway Infrastructure Threats
NASA	National Aeronautics and Space Administration
NDE	Non-destructive Evaluation
NDI	Non-Destructive Inspections
NIR	Near Infrared
NN	Neural Network
OMA	Operational Modal Analysis
OPEX	Operational Expenditure
PCA	Principal Component Analysis
PSD	Power Spectral Density
PVC	Polyvinyl chloride
RADIS	Detailed Computerized Record of Underground Defects
RFI	Rete Ferrovie Italiane
RFN	French National Railway Network
RU	Railway Undertaking

Abbreviation / Acronym	Description
SAR	Synthetic Aperture Radar
SAWP	Scale Average Wavelet Power
SHM	Structural Health Monitoring
SLC	Single-Look Complex
SNAP	Sentinel's Application Platform
SNAPHU	Statistical-Cost, Network-Flow Algorithm for Phase Unwrapping
SNCF	Société nationale des chemins de fer français
SOAR	Regional civil engineering specialists
SQL	Sequel Query Language
SVM	Support Vector Machine
TG	Track Geometry
TRMM	Tropical Rainfall Measuring Mission
UC	Use Case
UI	User Interface
VNA	Vector network analyzer
WPS	Wavelet Power Spectrum
WSN	Wireless Sensor Network

Table 1. Abbreviations and Acronyms



3. Background

The present document constitutes the Deliverable D12.1 “Civil Engineering requirements, architecture, inspection and monitoring report” in the framework of the Flagship Project FP3-IAM4RAIL as described in the EU-RAIL MAWP. The work focuses on improving the life-cycle management of civil assets, encompassing a range of components and systems, including railway civil structures like tunnels and bridges, as well as civil works such as earthworks and their surrounding environments. Additionally, it addresses external factors that impact railway infrastructure, including vegetation, landslides, floods, and other influences from various sources. The comprehensive background information for the different technologies is presented in section 5. In relation to each individually threatened Use Case, the background information covers the overall problems to be solved by the Infrastructure Managers (IM) or the Railway Undertakings, the IM’s/RU’s baselines/positions, the (sub)problems addressed by the Use Cases, plus the targeted measurable objectives and the influence on the IM/RU problem of the innovation proposed by the Use Case.

4. Objective/aim

This deliverable D12.1's main goal is to present the requirements and the architecture of the technologies across WP12 and WP13. The document also presents the installation and initial data collection from monitoring and inspection systems, setting the baseline for the work around civil assets to be performed in WP13. In this report, different assets are normally discussed in different regions. When the same kind of asset is threatened in two or more regions, different technologies apply for its inspection and management. Technologies adopted are vary, spanning across space, air, ground and underground (e.g. satellites, airplanes, drones, ground vehicles, tilt-meters, accelerometers, displacement transducers, geophones). Four main use case are defined across five countries. Every section of the deliverable addresses the 4 different UCs which are part of WP12 and that are internally composed by different technologies and demonstration scenarios:

- **Multiscale Monitoring of Civil Assets** (Italian UC). This UC works with three different assets:
 - Vegetation.
 - Bridge inspection.
 - Hydrogeological risk satellite-based monitoring.
- **Bridges and Earthworks Asset Management aided by Geotechnics** (Spanish UC). Two different types of assets are analyzed:
 - Bridges.
 - Earthworks. Two different locations are used for the earthwork's demonstration:
 - Briones.
 - Vilar de Silva.
- **Monitoring of Tunnel, Sub-ballast layers, Subsoil** (French UC). Three different technologies are addressed by this UC:
 - Evaluation of mechanical properties of sub-ballast layers and subsoil.
 - High efficiency tunnel inspection systems and predictive maintenance for tunnels.
 - Passive contactless magnetic microwire sensors arrays for high definition tunnel convergence monitoring systems in tunnels.
- **Data Analysis for Condition Monitoring** (The Netherlands and Norway UC). Two different developments are englobed within this UC:
 - Railway track monitoring in The Netherlands using a combination of dynamic responses from axle box acceleration system and track geometry measurements.
 - Condition assessment of existing concrete bridge and transition zones in Norway.

The document structure, organized by UCs and their corresponding technologies, enables a comprehensive description that thoroughly addresses all deliverable objectives with a high level of detail.

5. Use Cases: Functional and Technical Requirements

This section details the analysis of the four Use Cases of the project (1) Multiscale Monitoring of Civil Assets, (2) Bridges and Earthworks Asset Management aided by Geotechnics, (3) Monitoring of Tunnel, Sub-ballast layers, Subsoil and (4) 2.4. Data Analysis for Condition Monitoring. To fully define the different Use Cases the following sections are presented:

- Problem to be solved.
- Industry current position/baseline.
- Subproblem addressed by the use case and measurable objectives.
- Influence of the proposed innovation on the IM/RU problem.
- Refinement of Key Performance Indicators (KPIs).

5.1. Multiscale Monitoring of Civil Assets (Italy)

5.1.1. Problem to be solved

During the last years, FS Group has set the goal of designing, developing and implementing a system of control and management of the entire life cycle of civil infrastructure assets (e.g. bridges), railway infrastructure and the surrounding territory (vegetation, landslides, floods and other external factors affecting railway infrastructure). In this system, information from various data sources (from different technologies) is jointly exploited, providing support to the operators involved in maintenance. Exploiting merged data sources, will make such data more usable to those involved in the maintenance activities (currently data is managed separately and not integrated). Another objective that must be pursued is to minimize response times during emergency phases.

5.1.2. Industry current position/baseline

The industry current position/baseline will be analysed regarding (1) civil infrastructure monitoring, (2) Hydrogeological risk and (3) Vegetation encroachment and third parties' interference.

5.1.2.1. Civil infrastructure monitoring (railway bridges)

The Italian railway network, due to the complex orographic structure of the national territory, is among those with the highest number of bridges in Europe. Most of existing infrastructures was developed since the second half of the nineteenth century. Currently RFI S.p.A. (a company of the FS group) manages about 17000 km of network and about 23.100 civil infrastructures (bridges, viaducts, underpasses and overpasses).

The total basin of civil infrastructures present on the Italian territory is composed by 37% of underpasses, 34% of bridges, 22% of overpasses and 7% of viaducts.

RFI monitors the entire railway network assessing the state of conservation and maintenance of civil infrastructures (i.e., bridges, viaducts, underpasses, etc.). In accordance with the national and international provisions/legislation, RFI conducts cycles of inspection visits for bridges, viaducts and underpasses, with the following frequencies:

- Annual, defined as "routine",
- Triennial, or also called "principal",
- Six-year, every six years, defined as "general".

The corporate regulatory framework guarantees the integrity, safety, regularity and functionality of railway operation. The framework compels the corporate's bodies to adhere to specific procedures and operating methods. These procedure and methods regulate the inspection of bridges and other civil infrastructures. Two documents are available and used as reference:

1. Procedure "Inspections of bridges, tunnels and other structures of the railway infrastructure"
2. Operational Methodology Manual "Compilation of minutes for civil infrastructure inspection"

The procedure regulates inspections of bridges, tunnels and other railway civil infrastructure. The procedure defines the bodies in charge of the inspections, the rules to keep track of asset's status and the frequencies of the inspections. The operation manual, on the other hand, identifies the procedures to conduct the inspection and store its results, describes the Bridge Management System (DOMUS) the preliminary activities to be performed and list the tools required for the execution of the inspections.

The pondered inspections must include places surrounding the infrastructure such as watercourse and slopes; in fact, these could affect the stability of the infrastructure.

The general visit (performed every six years) is characterized by a greater in-depth inspection as all the structural components of the bridge (i.e. decks, piles, abutments, etc.) must be inspected at "contact distance". In this case, the activity can require the use of elevating work platforms, special by-bridge vehicles, boats, ladders, scaffoldings, etc. and other suitable means to overcome natural and anthropic obstacles.

The purpose of the inspection visit is to identify, characterize and quantify the defects of the infrastructure in accordance with the DOMUS system (Diagnostics Artwork Unified Maintenance Standard), BMS System (DOMUS) is a set of procedures, models and algorithms allowing the railway infrastructure manager to monitor the state of conservation of civil works, plan optimally the maintenance and keep control of civil infrastructure, considering all the structural and operational factors.

In some cases, due to the orography of the territory, some works are difficult to inspect even through the use of special tools/means (elevating work platforms, special by-bridge vehicles, boats, ladders, scaffoldings, etc.) and consequently, the use of remotely piloted aircraft vehicles (UAVs - drones) has been introduced which provide valid support to the inspectors who carry out the visit activities.

5.1.2.2. Hydrogeological risk

Referring to the mitigation of hydrogeological instability, current common best practices provide differentiated solutions according to the type of problems to be addressed. For instance, geomorphological and hydraulic phenomena are treated differently, although it is acknowledged that rainfalls can trigger both phenomena.

FSI continuously maps real and/or potential hazards that may involve the infrastructure, striving to apply the appropriate policies for ordinary and extraordinary maintenance. These mappings

(specifically for hazards as flooding and landslides) are prevalently based on the Hydrogeological Structure Plans and the Flood Risk Management Plans issued by the District Authorities. GIS tools are employed to associate these specific hazards to the infrastructural assets by assigning a priority to the mitigating actions. Mitigating actions are guaranteed by acting with over time strategies and by constant real-time monitoring, making risk management more effective.

The onset of potentially hazardous conditions is studied in situ following critical events (also involving on site-specific numerical calculation models). However Hydrogeological Structure Plans and Flood Risk Management Plans are seldomly updated by the District Authorities. This limits the confidence achievable by the risk mapping, resulting in a limited awareness of the risk.

5.1.2.3. Vegetation encroachment and third parties' interference

Hazards due to Vegetation and other possible interference along the railway (e.g. proximity of buildings), are controlled by carrying out periodic field visits and by the means of dedicated video surveillance, often leading to a labour-intensive, time-consuming, costly, and inefficient vegetation management process.

Routinely field inspections provide a wide range of checks on:

- General infrastructure's health, including track, structure, roads, fences, level crossing, signalling equipment, overhead catenary line, paying special attention to the effects of water floods.
- Violation of the Railway Police Regulation such as illegally constructed buildings, excavation, vegetation and any other material within safety distance, including violation of trespassing and free cattle roaming in the vicinity.

Filed inspections related activities, are then reported on the maintenance management system. Visits are performed during operation interruption during and outside service time (i.e. with possible interruption of revenue service). Frequency and means of the inspections depend on the line type and its typical maintenance requirement (lines are grouped according to commercial profiles, traffic types and generally exposure to wearing factors).

Current best practices require:

- Daily check of the way's clearance from obstacles performed by the first train running at reduced speed.
- From weekly to monthly surveys with diagnostic trains.
- Bi-monthly visual inspection by a single walking maintainer.

The maintenance actions are then focused based on the results of the surveys as evaluated by the maintainers.

5.1.3. Subproblem addressed by the use case and measurable objectives

The subproblem addressed are described following (1) Civil infrastructure monitoring and (2) Hydrogeological risk, vegetation encroachment and third parties' interference.

5.1.3.1. Civil infrastructure monitoring (railway bridges)

Inspections, carried out on civil works via remotely piloted aircraft systems, guarantee the total coverage the civil work with its structural elements (e.g. piles, abutments, vaults, scaffolding, etc.). These activities are characterized by the field surveys and the post-processing phases described below.

5.1.3.1.1. Field surveys

Field activities consist of direct inspection, consisting of photogrammetric campaigns acquired during multiple UAV flights. The UAV capture the images of the civil works and enable recognising the characteristic defects of the structures under investigation. The detected imperfections are then stored and characterised, according to the nomenclature established of the Bridge Management System software (BMS). Calibration procedures are often conducted along with the survey. During calibration, drone data are re-calibrated based on classic field measurements. The flight path and the spatial frequency of the pictures are finely tuned to have full coverage of the civil work.

5.1.3.1.2. Preliminary inspection of the civil works

Before the flights, preliminary inspections allow to rule out critical issues that can hinder the aerial surveys or result in delays during the acquisition phase. The surrounding of the civil work is carefully analysed to pre-address a list of possible problems, such as:

- Vegetation hindering the view of the drone (concealing the civil work)
- Accessibility problems preventing to reach the area of interest by the drone or by the operator piloting the drone (e.g. steep slopes, private properties, wire nets etc.)
- Any possible problematic scenarios not covered by the national authority regulation.
- Need of special equipment for inspections (e.g. LEDs to illuminate areas with poor lighting, special optical payloads for the creation of photographic material)
- Environmental conditions that limit flight activity (e.g. areas of the structure exposed to strong winds).

Following this activity, an inspection plan is drawn up to mitigate all the issues spotted in the above-described phase.

5.1.3.1.3. Flight mode

It is necessary to carry out enough flights to investigate all the structural elements of the civil work under inspection (piles, abutments, vaults, decks, etc.). To characterise all the defects within DOMUS BMS system, the following minimum number of flights must be carried out:

- Minimum 2 flights below each vault/deck of bridge with the optical unit mounted below or above the drone, depending on the areas of the work to be inspected
- Minimum 1 flight for each front of every bridge span
- Minimum 1 flight above the bridge. Flights above the bridges are carried out under conditions of interruption of railway traffic.

For steel bridges, the number of flights below the deck and at deck's sides must be optimised based on the complexity and number of structural details (nodes, joints and supports). If the supports present difficulties in inspecting, further flights and field surveys can be rearranged/repeated.

5.1.3.1.4. Post-processing activities

The photographic material acquired during the flights is then post-processed, yielding the following material:

- General report of the work.
- Complete photographic report of the inspection.
- Sparse Point cloud. This document is provided in .psz/.psz files. From the point cloud, the inspector can extrapolate the position and orientation of each individual photograph inserted within the photographic report. Consulting the photographic report, the inspector can label the defects according to the DOMUS defect catalogue.
- Dense Point cloud. This document is provided in .psz/.psz files and it is basically an interpolation of the sparse cloud (mesh model). The sparse elements of the measurement are glued together by mean of georeferencing and appropriate model mashing. The Dense Point cloud provides the inspector with a general overview of the civil work's structural elements.
- 3D Graphic rendering.

The results shown by two experimental campaigns carried out starting from 2016, highlighted the feasibility and efficacy of aerial technology in structural inspections. The immediate advantage related to physical accessibility and time saving (e.g. by drone usage), is complemented by abundance of digital details, unashing the potential of artificial intelligence.

Both application of Artificial Intelligence algorithms and analysis of the photographic material by an expert, result in the identification of most of types of defects for the different types of structural and material (masonry and concrete arch bridges, steel, reinforced and pre-stressed concrete deck bridges), in accordance with the provisions of the RFI BMS system.

5.1.3.2. Hydrogeological risk, vegetation encroachment and third parties' interference

Coexistence of different assets and associated issues require various, dedicated ways of inspection. Managing different inspections techniques, conducting these with the right frequency and making timely decision is an arduous task, especially considering the trade-off between performances and costs. The possibility to conduct these inspections by means of satellite would allow to make the

data collection process far more efficient, given the satellite capability to keep the whole infrastructure under control, inspecting the assets' condition with the right frequency.

5.1.4. Influence of the proposed innovation on the IM/RU problem

These sections are subdivided into (1) Civil infrastructure monitoring and (2) Hydrogeological risk, vegetation encroachment and third parties' interference.

5.1.4.1. Civil infrastructure monitoring (railway bridges)

The aim of FS within the ERJU project is to:

- Automate the identification of structural problems and defects of the civil infrastructure by means of Machine Learning models for data analysis (Neural Networks). Machine learning algorithms shall therefore classify defects (according to classification indicated in the RFI Defect Catalogue).
- Application of techniques is also envisaged for residual life's estimation and Predictive Maintenance of the civil assets under inspection.
- Design and develop of an Asset Management Platform, integrating image acquisition, processing and classification service for the automatic detection of defects and for the estimation of the residual lifetime of the civil infrastructures. The platform will become a new tool to support decisions pertaining maintenance.
- The developed methodology & tool will respectively reduce the cost of the in-situ inspections and the cost of asset management. As by product, this methodology of inspection will indirectly reduce the cost related to asset unavailability (e.g. quicker in-situ inspection).
- The integration of the bridge platform as part of a holistic Asset Management platform for monitoring the infrastructure works of the railway line.

Compared with the existing methodology (based on inspection by means of cranes, platform and scaffolding and followed by manual data inspection and manual defect classification), the introduction of automated aerial data gathering (by drones) and application of novel processing techniques (machine learning) would reduce the cumulative time to conduct the assessment.

5.1.4.2. Hydrogeological risk, vegetation encroachment and third parties' interference

Currently, the following methodologies have been tested:

- SANF: is project to process data from a net of rainfall detectors distributed on a large scale to predict the occurrence of critical rainfall events and provide a risk estimation for the sites.
- Ramses: the project employs radar-based monitoring of cloud formations, monitoring of lightning strikes, and develops climate models to short-term forecast the onset of intense stormy micro-cells over small water basins. The aim is to forecast imminent consequences

of heavy rainfalls (bridges occlusion, track flooding in cuts, landslides at tunnel entrance, etc.).

- PSF: fixed radar stations for radar monitoring of landslides in critical spots. The system automatically interrupts the train operations when dangerously sized obstacles are detected.
- Unmanned drone monitoring: BVLOS (Beyond Visual Line of Sight) flights returning 3D models and imagery of the infrastructure and surroundings to identify dangerous growth of vegetation and some track defects. The system uses AI for the identification of hazardous conditions.
- Satellite monitoring of the infrastructure: a collection of initiatives to study the advantage of satellite imagery processing to assess hydrological instability, structure within safety distance and vegetation growth.

Those initiatives, including the projects Multi-Scale Observation and Monitoring of Railway Infrastructure Threats (M.O.M.I.T., developed within the H2020-S2R-2017 EU initiative) and Earth Observation 4 Infrastructure Mapping and Planning (EO4I), have shown the feasibility and the effectiveness of the satellite-based monitoring techniques.

All those initiatives address specific hazard individually or are currently in a proof-of-concept stage. Individual initiatives do not provide mature and integrated means to improve large scale monitoring of the assets. These previous results will be the background for the further developments to achieve high / expected TRL.

5.1.5. Refinement of Key Performance Indicators (KPIs)

KPIs are indicated for control and management system of the entire life cycle of civil infrastructure assets such as bridges, railway infrastructure and the surrounding territory, vegetation, landslides, floods and other external factors affecting railway infrastructure presented in the Italian use case. KPIs are intended to measure the optimization of costs and times (referring to reduction of maintenance cost and reduction of in-service failures) resulting from the application of new technologies and integrated approaches (vs current and traditional monitoring and data processing methodologies). Three different KPIs are defined that will be described on the following subsections.

5.1.5.1. KPI1. Reduction of maintenance time and cost

- **Short description.** The main objective of this KPI is to measure the time reduction obtained on the time needed to perform bridge inspection and post-processing data and the assessment of the state of conservation and maintenance of civil infrastructure comparing systems and models that do not involve the use of artificial intelligence with the system developed during the project.

For this aim, for the same activity, bridge inspector can use drones as support for bridge inspections (without interruption of railway traffic and unavailability of the line) and AI analytics for post-processing.

This factor is directly related to a correct preventive maintenance by getting a faster assessment of the state of health of the infrastructure, this allows infrastructure managers to detect any infrastructural damage or defect early and take corrective action if necessary.

- **How to compute KPI1.** For computing KP1, it is possible to estimate the time (hour/ man referred to activity on singular bridge span) to perform the inspection and post-processing data and compare it with traditional methods to establish the time saving ratio that could be achieved with the application of this technological approach. To evaluate this KPI we can use the following formula:

$$KP1 (\% \text{ time savings}) = \frac{Time_{traditional \ method} - Estimated \ time_{new \ method}}{Time_{traditional \ method}} \times 100 \quad (1)$$

Time Traditional Method is the time required to perform an inspection by the traditional method. *Estimated time new method* is the time required to perform an inspection by the new method.

A positive KP1 indicates that the estimated time for the new method is less than the time required for the traditional method (time saving or a reduction in the time required to complete the task). A negative KP1 indicates that the estimated time for the new method is greater than the time required for the traditional method. A negative value indicates that the new method would require more time compared to the traditional method.

Therefore, the cost of personnel (h/m. referred to activity on singular bridge span) is indicated below:

$$KP1 (\% \text{ cost savings}) = \frac{Cost_{traditional \ method} - Estimated \ Cost_{new \ method}}{Cost_{traditional \ method}} \times 100 \quad (2)$$

Cost Traditional Method is the cost required to perform an inspection by the traditional method. *Estimated Cost new method* is the cost required to perform an inspection by the new method.

A positive KP1, indicates that the estimated cost for the new method is less than the time required for the traditional method (time saving or a reduction in the cost required to complete the task). A negative KP1 indicates that the estimated cost for the new method is greater than the cost required for the traditional method. A negative value indicates that the new method would require more cost compared to the traditional method.

5.1.5.2. KPI2. Reduction of traffic disruption caused by traditional bridge inspection in the railway infrastructure

- **Short description.** Bridge inspection with current procedures needs of traffic interruptions for infrastructures to be monitored which repercussions on the availability of the railway line and impact on circulation. In the Italian use case, the use of drones for the inspection activity will make it possible to considerably reduce the interruption of railway traffic while improving safety.

The use of AI analytics speeds up the post processing (defect classification) and paves the way for predictive maintenance (e.g. estimating asset remaining lifetime due to a propagating defect). This can help to improving the reliability and availability of rail infrastructure, reducing the need of speed restrictions and improving overall passenger experience.

- **How to compute KPI2.** To compute this KPI the number of traffic disruption caused by traditional inspection on bridges can be compared to the number of traffic disruptions caused by the new method approach. The evaluation period will be determined on the basis of the available data. KPI2 has follows the equation below:

$$KPI\ 2(\% \text{ disruption}) = \frac{LTV_n}{LTV_t} \times 100 \% \quad (3)$$

Where LTV_t is the number of total traffic disruption caused by traditional inspection on bridges and LTV_n is the number of traffic disruption caused by new method approach.

5.1.5.3. KPI3. Reduction of track-data collection time

- **Short Description.** This KPI assess the reduction of time (and cost of personnel) associated with track-data collection and respective information retrieval. Here, information retrieval includes the state of conservation and maintenance of the railway track, plus that of surroundings.

IM operators can jointly use data remotely acquired from satellites, drones, in-situ measurements and ancillary data as support for track and surrounding monitoring (without the need to interrupt the railway traffic). This KPI is related to a correct preventive maintenance: knowing the state of health of the infrastructure in a faster time allows infrastructure managers to detect any critical area along the track and to take appropriate actions if necessary, including high resolution data gathering, activation of emergency procedure and mitigation actions among others.

- **How to compute KPI3.** For computing KP3, it's possible to estimate the time (man/hour) required for data collection along the track and its surrounding before and after the application on the developed monitoring approach based on the use of remotely acquired data. To evaluate this KPI3 the following formula will be applied:

$$KP3 (\% \text{ time savings}) = \frac{Time_{traditional\ method} - Estimated\ time_{new\ method}}{Time_{traditional\ method}} \times 100 \quad (4)$$

Traditional Method Time is the time required to perform the conventional data collection and Estimated time new method is the time required to gather the still needed data after the application of the new monitoring approach.

A positive KPI3 indicates that the estimated time for the new method is less than the time required for the traditional method (time saving or a reduction in the time required to complete the task). If KP3 is negative, the estimated time for the new method is greater than the time required for the traditional method. A negative value indicates that the new method would require more time compared to the traditional method.

Another formula with the cost of personnel is indicated below:

$$KP3 (\% \text{ cost savings}) = \frac{Cost_{traditional\ method} - Estimated\ Cost_{new\ method}}{Cost_{traditional\ method}} \times 100 \quad (5)$$

Traditional Method Cost is the cost required to perform the conventional data collection and Estimated new method Cost is the cost required to gather the still needed data after the application of the new monitoring approach.

A positive KP3 indicates that the estimated cost for the new method is less than the time required for the traditional method (time saving or a reduction in the cost required to complete the task). If KP3 is negative, the estimated cost for the new method is greater than the cost required for the traditional method. A negative value indicates that the new method would require more cost compared to the traditional method.

5.2. Bridges and Earthworks Asset Management aided by Geotechnics (Spain)

5.2.1. Problem to be solved

The problems to be solved are subdivided into the two types of assets analyzed: (1) bridges and (2) earthworks.

5.2.1.1. Bridge Assets Management

ADIF is particularly interested in the analysis of a specific structural pathology: damage to the POT supports of long bridges (about 1000 metres) without an intermediate fixed support, especially if they are designed in curves from a floor with trains passing at speeds above 300 km/h. These bridges are subjected to high torsional stresses which cause damage to support elements such as POT bearings. These elements have a much shorter life cycle than the structure itself (estimated at 100 years). The objective is to develop a predictive maintenance tool to anticipate this damage or failure in order to know the optimal time to replace these assets before failure occurs. To address this use case, it is necessary to design an inspection system that provides relevant information on the condition of the POT supports and the dynamic behaviour of the structure that can feed into maintenance decisions.

In ADIF, bridges with a total length of more than 1,000 metres have an intermediate fixed support to minimise axial movement of the deck. For this reason, a 999 m long bridge has been selected for this demonstrator, called Viaducto sobre el Arroyo de las Huertas de Mateo, located on line 040 (Bif. Torrejón de Velasco - Valencia Joaquim Sorolla pk 284+989), which is supposed to be one of the bridges with more axial displacements of the entire railway network. In addition, its plan layout is curved, which is why we consider it to be the most representative bridge for the study of damage to POT supports. Its typology is representative of a large number of viaducts on the Spanish High Speed rail network; a bridge with continuous girders with several spans made of prestressed concrete and spans of 43-45 m.

5.2.1.2. Earthworks Assets Management

The scope of this demonstrator is the detailed study of the intrinsic movement of a slope. To this end, two specific slopes of great interest to ADIF are going to be analysed.

The first of these two slopes has a long history of problems associated with instabilities even before the construction of the railway line in 1880. This area presents high frequency of rainfall, presence of a reservoir with continuous rise and fall of the water level favouring the instability of the slope that consequently can cause problems in the infrastructure such as loss of track geometry and imbalance in train operations. The selected area for demonstration is the slope of tunnel 40, located between PP.KK. 277+100 to 277+457 of the Palencia-La Coruña line, that besides all the characteristics described above has currently active landslides.

The scope is the set-up of a predictive maintenance tool based in a low-cost sensors network that will allow to monitor the slope movement and to identify the progressive damage caused on the railway line and compare results with conventional sensors. On the other hand, a strategic analysis will be carried out based on satellite images comparing the variability and the difference that may

exist between the different images taken in each time interval.

The new sensor network formed by tiltmeters installed on the slope as well as the satellite images and the historical geotechnical data will provide relevant information related to the behaviour of the slope and its evolution, in particular, the detection of the movements will be used for the generation and calibration of a Digital Platform to perform different analysis in relation to anomaly detection and future behaviour analysis of the slope movements.

The second of these is an unstable slope located on line 700 of the Castejón - Bilbao Conventional Network, in the section PK 124.050- PK 124.100, Briones (La Rioja), identified in the Trench Plan dated 30/04/2016, with HIGH risk. This is a mobilised area of very significant magnitude, where it is difficult to apply stabilisation measures. The slope has masonry walls with mortar as a corrective measure for the clearing, indicating that stability problems were already detected at the time on this slope. To date, it has been recommended to place containment/protection measures close to the track (static/dynamic barriers), but the real-time monitoring of the movements by means of clinometers is considered a very positive complementary safety measure to establish alerts in the event of activation of the movements.

These sensors will allow in situ data collection in real time and with a configurable frequency of the movements and inclinations occurring on the slope. These new sensors will provide relevant information related to the behaviour of the slope and its evolution, which will be equipped with embedded intelligence to manage the exceeding of thresholds, such as sending an alert in real time, sending the data that breaks the threshold or increasing the frequency of data collection, fully configurable remotely via an App.

5.2.2. Industry current position/baseline

This section is subdivided into the two types of assets analysed: (1) bridges and (2) earthworks.

5.2.2.1. Bridge Assets Management

The current Maintenance System is based on the performance of Principal and Regular Inspections. Visual Inspections by personnel specialized in structural pathology (Principal Inspection) or basic training (Regular Inspection) with a certain frequency each of them, from these visual inspections the failure can only be identified when it has already occurred, which leads to the affection of the exploitation.

5.2.2.2. Earthworks Assets Management

Regarding earthworks and more specifically this slope, the current Maintenance System is based on the realization of the reading of measuring instruments such as inclinometers, piezometers, obtaining the data every four months, currently four inclinometers are in operation although it is ruled out that two have stopped working due to the movement of the slope in addition to the realization of a topography of the affected area so it is only possible to identify the failure when it has already occurred, which leads to the affection of the exploitation.

5.2.3. Subproblem addressed by the use case and measurable objectives

This section is subdivided into the two types of assets analyzed: (1) bridges and (2) earthworks.

5.2.3.1. Bridge Assets Management

The main objective of the project is to acquire the necessary knowledge and develop an initial tool to transform the maintenance strategy for these assets. The goal is to shift from corrective maintenance (replacement after damage) or preventive maintenance (replacement at the end of its useful life, regardless of damage) to predictive maintenance. Predictive maintenance provides warnings about the deterioration of assets before failure occurs, allowing for replacement when the asset's functionality is nearly exhausted.

5.2.3.2. Earthworks Assets Management

One of the main objectives of the project is to gather the necessary knowledge and the development of a tool to change the maintenance strategy of these assets, moving from corrective maintenance (stabilization when the failure has occurred) to predictive maintenance with real time data, which warns that an instability is occurring in the slope and can cause affection to the traffic. In addition, other objective is to verify that no movements occur once the projected stabilizing measures have been implemented.

5.2.4. Influence of the proposed innovation on the IM/RU problem

Advantages over corrective action:

- The impact on railway operation is minimized, due to the lack of establishment of restrictions, usually speed restrictions, which could serve as a parameter that quantifies the impact: accumulated lost time due to the presence of speed limits or cuts in the line due to the loss of geometry in the track.
- The planning of the work and the tendering by an open procedure of free competition is more economically advantageous for the IM than the use of emergency procedures or negotiated by urgency.

Advantages over preventive:

- The impact on the railway operation is minimized.
- The costs of the work are reduced.

5.2.4.1. Bridge assets management

According to the POT bearings specifications provided by manufacturers, these assets have a much shorter life cycle than the structure itself (100 years the structure vs 25-50 years POT bearings, depending on the manufacturer). We would like to configure a predictive maintenance tool that allows us to know the progressive damage of the supports to identify the optimal moment of

replacement of the bearings before the failure or the blockage of them occurs. This is a very specific use case and it could be part of a predictive maintenance tool that covers more structural pathologies. To address this, it seems necessary to design an architecture based on local monitoring in bearings as LVDT sensors, but also, we aim to be able to correlate variations on the dynamic behaviour of the bridge with possible damages in bearings. For this reason, we have also designed an instrumentation based on accelerometers spread across the interior of the girder. A continuous monitoring of the dynamic behaviour based on operational modal analysis (OMA) techniques to provide modal parameters (natural frequencies, damping ratios, mode shapes). In addition of these accelerometers and in order to understand the overall behaviour of the infrastructure, some tiltmeters and accelerometers are to be installed in the transition area of the bridge and on the platform above the bridge. They will allow to realise a correlation between the bridge structure and the railway platform. Complementary data may be obtained thanks to the FO laid all along the tracks.

To avoid the lack of monitoring data during the period between the start of the project and the installation of the surveillance system, remote surveillance from space is proposed, based on interferometry applied to synthetic aperture radar images (InSAR). In addition to covering the aforementioned period of absence of data (with a much lower sampling frequency), this technique makes it possible to establish a baseline of "normal" behaviour of the bridge, providing, for example, seasonal movements due to thermal effects, and even identify past anomalies by means of a historical study of the available images.

The new sensors projected to be installed in the viaduct will provide us with relevant information related with the structural behaviour of the bridge and its evolution, in particular, the functioning and the measurement of the displacements of a continuous girder over the POT bearings, as well as its dynamic behaviour that will be seen for the generation and calibration of a Digital Twin with which to predict future behaviour.

The information obtained from these sensors can be compared to the manufacturer's specifications regarding the useful life of the POT bearings. Typically, this useful life is expressed in terms of accumulated distance or years of use. By comparing the data provided by the sensors to these specifications, we can gain insight into the current condition of the bearings and make informed decisions regarding maintenance or replacement.

The first viaducts built on the high-speed rail network in Spain date back to 1990 (HSL Madrid - Seville), so according with the specifications provided by manufacturers some of these assets are very close to reach the end of their useful life. This project will help us to evaluate the behaviour of these elements in a real environment, the movements they undergo according to the design of the viaduct and the ambient temperature. Ultimately, we will draw conclusions to be extrapolated to viaducts of this same typology to analyse the most optimal time for its replacement.

Three types of monitoring will be installed for the bridge management:

1. **Monitoring system for POT bearings.** The objective of this installation is to analyse the POT support equipment in detail to analyse pathologies and service life and to optimise their maintenance.
2. **Monitoring system for dynamic analysis of the structure.** The objective is to identify any alteration in the dynamic behaviour of the structure resulting from a malfunction of the

support devices (change in the boundary conditions) in the area of greatest stroke across the entire viaduct.

3. **Monitoring system for correlation.** The objective is to collate data in order to enable correlation with data measured by CEDEX and INECO and processed by CEMOSA through information received from the project database. This will facilitate the detection of any existing damage and observation of variations in the behaviour of the structure over time, with the aid of an AI layer that allows:
 - **Monitor the track platform** in order to provide information to implement performance indicators of the POT type supports to optimize the decision-making process for their maintenance.
 - **Variations** in the platform **inclination**.
 - **The acceleration** generated by the train's passage.
 - Determine the **optimal maintenance schedules** based on the above values using a decision support system. In particular, the extensive experience gained in the RESILTRACK project, completed in 2022, which was entirely dedicated to the experimental and theoretical development of this same issue, is available.

5.2.4.2. Earthworks Assets Management

For the first slope, it is intended to deploy a network of low-cost sensors with the objective of gathering real time on site data correlated with those provided by the inclinometers, both the existing ones and those that would be installed by the Conventional Network Project Management when the stabilization project is executed in order to meet another objective, to analyse how effective are the measures adopted for slope stabilization, once it is executed after approximately one and a half years.

On the other hand, a strategic analysis will be carried out based on satellite images comparing the variability and the difference that may exist between the different images taken in each time interval.

The monitoring systems will provide us with relevant information related to the behaviour of the slope and its evolution. In particular, the detection of the movements will be used for the generation and calibration of a Digital Platform to perform a statistical analysis to predict the future behaviour related to the movements on the slope and to verify that the stabilizing measures implemented are working properly.

Instead, for the second one, the proposed instrumentation is of the WSN (wireless sensor network) type, i.e., formed by a network of contact sensors that measure terrain or environmental variables but communicate without wiring. In other words, a data acquisition network based on IoT technology, capable of autonomously and reliably capturing data at remote measurement points by means of dataloggers with telematic capacity without the need for external connectivity and low power consumption.

The system consists in the first instance of 14 wireless tiltmeters, endowed with embedded intelligence. These are connected individually or in very close groups to reading nodes, which act as local dataloggers, measuring, recording and sending data in a network or directly to a gateway that acts as a central datalogger or hub, using LoRa (Long Range) protocol, Flat Mesh or any other low-power wireless mesh network. The tiltmeters will be distributed over the entire surface of the slope

and will be installed on masts or embedded in the ground. To this end, the successful tenderer shall provide the necessary auxiliary means of clamp-type fastening for their installation.

The system is completed by a weather station capable of simultaneously reading rainfall, ambient temperature and relative humidity.

5.2.5. Refinement of Key Performance Indicators (KPIs)

The KPIs indicated in the two use cases that build the Spanish demonstrator are aimed at measuring the cost and time that is optimized with the development of a predictive maintenance tool, both for the replacement of POT bearings in bridges and the monitoring of slopes with active movements in earthworks with low-cost sensor networks:

- Predictive maintenance tool for the POT bearings replacement in bridges (KPI 1, KPI 2 and KPI 4).
- Predictive maintenance tool for the monitoring of slope with active movements (KPI 1, KPI 2, KPI 3 and KPI 5).

5.2.5.1. KPI1. Infrastructure changes.

- **Short description.** This KPI hereby described focuses on determining the frequency and characteristic traces of failures that evolve in time (i.e., which undergo a degradation process), since this type of failures are the ones that can, in principle, be predicted by models.
- **How to compute.** Consider records from bridges and earthworks to develop methods for:
 - Automatic identification of systematic trends and
 - Modelling degradation rate and making future projections.

The objective will be to have one model for earthworks and another one for bridges supporting the characterisation of two trends in each case, such as:

- Bridges: Changes due to temperature and degradation of elements.
- Earthworks: Changes induced by rainfall.

5.2.5.2. KPI2. Time saving.

- **Short description.** Predictive maintenance can significantly influence the reduction of speed restrictions on rail infrastructure by enabling early detection of potential problems before they become critical failures that may have an impact on circulation. These speed restrictions represent a reduction in the theoretical time lost for each circulation.

By analysing the information collected by the sensors network, the predictive models to be developed will be able to detect patterns and anomalies that indicate potential problems before they become critical failures. This allows them to schedule maintenance before it is needed, helping to reduce unplanned downtime and improve the reliability and availability of rail infrastructure.

- **How to compute KPI2.** Speed restrictions caused by failures in POT bearings on bridges and by problems of slope movements will be quantified with the current corrective / preventive maintenance approach compared to the future predictive maintenance approach in which maintenance activities can be scheduled without affecting circulation. Time period will be determined based on the available data following the equation below:

$$KPI\ 2 = \frac{TTLa}{TTLt} \times 100 \% \quad (6)$$

TTLt: Theoretical time lost for each circulation in the RFIG (Red Ferroviaria de Interés General) caused by problems in bridges and earthworks. TTLa: Theoretical time lost for each circulation caused by failures in POT bearings on bridges and by problems of slope movements with current maintenance strategy.

5.2.5.3. KPI3. Monitoring cost saving.

- **Short description.** The main objective of this KPI is to check whether the reduction in costs involved in the implementation of the instrumentation necessary to monitor the hillside occurs. The installation of planned sensors will be low cost and will be compatible with the instruments already installed.
- **How to compute KPI3.** To calculate the reduction of the costs in the instrumentation equipment of the slope, it is essential to know the cost of the previous monitoring instruments and from this data, see the evolution with respect to the years, that is, establish a comparison between 2 successive years. Steps to follow:
 - Obtaining the historical costs for each year of the instrumentation devices of the hillside.
 - Obtaining the costs associated with the network of low-cost sensors for each year.

$$KPI3 = \left(\frac{COSTS_n - COSTS_{n-1}}{COSTS_{n-1}} \right) \times 100 \% \quad (7)$$

n is the current year in which the comparison is to be made and n-1 is the year before to the current year. Finally, as an interpretation of results, if the value of the KP3 indicator is negative, it means that costs have been reduced compared to the previous year.

5.2.5.4. KPI4. Emergency cost.

- **Short description.** The application of this KPI is proposed to analyse the reduction of the cost of emergency works respect to a model based on predictive maintenance in which the works are planned through public tender. Indeed, emergency works are often more expensive than works with public tenders.
- **How to compute KPI4.** A comparison of the costs of a typical emergency work will be carried out with respect to the cost through an open public tendering procedure following the equation below:

$$KPI\ 4 = \left(\frac{COSTEW - COSTPT}{COSTPT} \right) \times 100 \% \quad (8)$$

COSTEW: Cost Emergency Work to replace POT bearings. COSTPT: Cost Public tender to replace POT bearings + monitoring costs.

KPI5.

- **Short description.** When severe instabilities occur in an earthwork, measures are designed in order to solve this stability issue. Sometimes, these stabilizing measures are not fully effective, and problems continue to occur.
Therefore, the main objective of this KPI is to measure the degree of effectiveness of these stabilizing measures that are executed on the hillside. This indicator can only be measured if the installation of the sensor network is carried out before the execution of the works.
- **How to compute KPI5.** The objective here is to verify whether there are movements, deformations once the stabilization measures have been executed, for this, the trend of the data from the low-cost sensors installed before and after the stabilizing measures will be studied.

$$KPI\ 5 = \left(\frac{Tb - Ta}{Tb} \right) \times 100 \% \quad (9)$$

Tb: Trend sensor data before measurements. Ta: Trend sensor data after measurements. Interpreting the results, if the KPI is equal to 100% it will mean that the stabilization measures implemented have been correct and it will not be necessary to do any other type of action on the hillside.

5.3. Monitoring of Tunnel, Sub-ballast layers, Subsoil (France)

This task will contribute to the development of:

- Evaluation of mechanical properties of sub-ballast layers and subsoil in order to understand and apprehend the emergence of disorders in the subsoil by using the MASW method.
- High efficiency tunnel inspection systems to automatically detect visual damages evolution and Predictive maintenance for tunnels.
- An analysis of the use of passive contactless magnetic microwire sensor arrays for high-definition tunnel convergence monitoring systems.

5.3.1. Problem to be solved

This section is divided into the three previously presented developments: (1) Evaluation of mechanical properties of sub-ballast layers and subsoil, (2) High efficiency tunnel inspection systems and predictive maintenance for tunnels and (3) Passive contactless magnetic microwire sensor arrays for high-definition tunnel convergence monitoring systems in tunnels.

5.3.1.1. Evaluation of mechanical properties of sub-ballast layers and subsoil

The design, regeneration and maintenance of railway lines require a regular assessment and control (both qualitative and quantitative) of the mechanical condition of the bedding structures and the supporting soil.

Thus, the multi-scale diagnosis of the railway platform, concerns:

- The platforms to evaluate and control the mechanical state of the subgrade structures.
- The supporting soil to understand the phenomena of the appearance of disorders in the track, generated by a deterioration of the underlying cavity.

This risk is increasing because there is not enough evidence of a disorder before the incident occurs. This risk is a major concern for SNCF Réseau, not only in terms of safety but also in terms of economic and social impacts. Emergency maintenance operations must be carried out by SNCF Réseau to ensure the continuity and safety of the traffic, which implies a temporary limitation of the speed, the stopping of the traffic, periodical surveys of the track geometry, permanent monitoring, filling and injection works, etc.

Our aim is approach to reach a predictive maintenance by developing and testing new geophysical approach on railway context.

5.3.1.2. High efficiency tunnel inspection systems and predictive maintenance for tunnels

French railway tunnels are numerous (1430 tunnels) and old (average age: 135), as depicted in Figure 1.

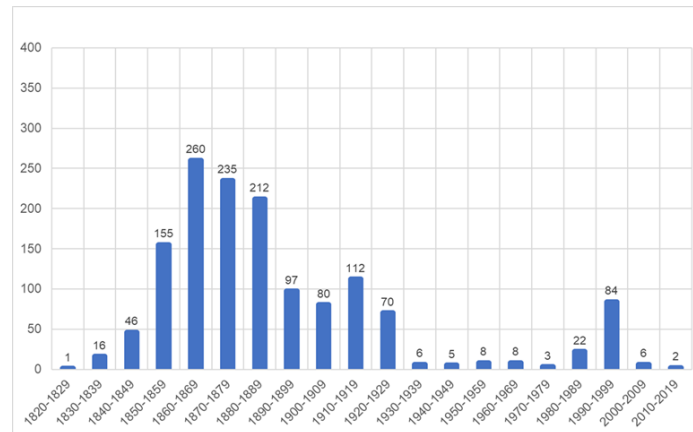


Figure 1. Number of French tunnels railways built per decade.

Due to the difficult access conditions to these structures and the important interface with rail traffic, regular assessment and control (inspection) require the use of special trains during periods of traffic interruption.



Figure 2. Traditional tunnel inspection.

Although tunnel inspections may be successful, they come at a significant cost. The recent development of new mobile inspection technologies is an opportunity to reduce these costs. These new technologies can also reduce the part of subjectivity of inspections (performed manually). In addition, tunnel regeneration operations are very costly due to the specificity, complexity and important interface with rail traffic. Temporary speed restrictions are necessary. Sometimes, long term traffic interruptions are also necessary. Defining the needs and planning these operations is a critical issue for Infrastructure Managers.

Since 2006, SNCF Réseau has collected data on damages detected during inspections. The quotation

reflects the state of the tunnel. All this data collected is an opportunity to develop algorithms to predict tunnel degradation to optimise the asset management (planning of maintenance operations).

5.3.1.3. Passive contactless magnetic microwire sensor arrays for high-definition tunnel convergence monitoring systems in tunnels.

Railway tunnels are one of the essential assets of the rail transport infrastructure. ADIF has almost 1,300 tunnels totalling almost 500 km in length, which gives us an idea of the importance of this railway asset. Tunnels facilitate the transportation of people and goods, connecting cities, regions, and even entire countries. However, they present unique challenges for engineers and designers, who must ensure that trains can pass through safely and efficiently.

Convergence is a term that refers to the distance between the tunnel walls. If the convergence is too narrow, there may be a risk of collision or derailment, which can endanger the lives of passengers and train staff. In addition, convergence also affects the efficiency of the railway system in terms of time and costs. Therefore, periodic measurement of convergence in railway tunnels is an essential part of ensuring that safety and efficiency standards are maintained in the railway system. Monitoring and checking the convergence of a railway tunnel is essential to ensure that there are no structural safety problems and to ensure the efficiency of the railway asset. Inadequate convergence in railway tunnels can be dangerous and costly.

Convergence sections enable the recording of deformations in the element being monitored (such as a tunnel or the space between screens) by measuring length variations in various representative chords. These distance measurements can be carried out using a variety of systems, including strain gauges, high-precision total stations, or continuous measurement laser systems. In addition to the aforementioned safety risks, inadequate convergence can affect the efficiency of the railway system.

The design of the convergence must consider factors such as tunnel width, ceiling height, degree of curvature, and the maximum permitted speed within the tunnel. It is essential to account for the characteristics of the trains using the tunnel, ensuring that the convergence accommodates their size and speed.

Currently, techniques used to measure convergence in tunnels do not support automated inspections and are wireless to facilitate the process.

In conclusion, it is crucial that convergence is carefully designed and complies with safety standards to prevent collisions or derailments. The convergence must also allow trains to operate without significant speed reductions or interruptions. Furthermore, it is important to develop monitoring methods that are automatic and easy to implement.

5.3.2. Industry current position/baseline

This section is divided into the three previously presented developments: (1) Evaluation of mechanical properties of sub-ballast layers and subsoil, (2) High efficiency tunnel inspection systems and predictive maintenance for tunnels and (3) Passive contactless magnetic microwire sensor arrays for high-definition tunnel convergence monitoring systems in tunnels.

5.3.2.1. Evaluation of mechanical properties of sub-ballast layers and subsoil

For mechanical characterization of sub-ballast layer and sub-soil and to diagnosis the soil support for the risk of subsidence, we use classical geotechnical and geophysical method which are punctual, not accurate in some case and not compatible with the constraints of the railway. This work will help us to gain a better knowledge of our infrastructure, to adapt and to reduce maintenance operation and better design the solution (Figure 3). Obviously, safety and economic benefits.

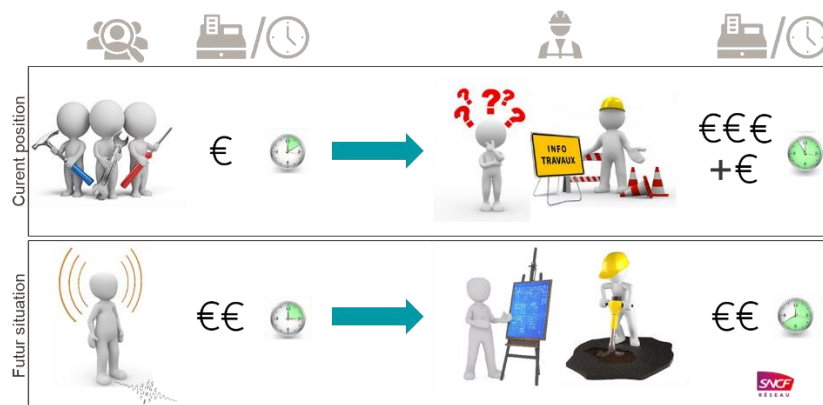


Figure 3. Use of conventional geotechnical and geophysical methods for better diagnosis to reduce maintenance operations and improve solution design.

5.3.2.2. High efficiency tunnel inspection systems and predictive maintenance for tunnels

Currently, regular tunnel inspections are led by human specialist by using special trains but without digital technologies. Damages are detected visually and by using a hammer.

New tunnel inspection systems have developed the last few years. These systems are mainly based on photography, lidar and infrared thermography technologies (see Figure 4. Example of a new tunnel inspection system. They offer opportunity to ensure a realistic and very high-definition representation of the tunnels, in 2D and in 3D. The latest technological developments also allow high-performance acquisition on mobile vectors.



Figure 4. Example of a new tunnel inspection system.

The use of these new technologies for surveillance is an opportunity for SNCF Réseau to further improve its management processes and its assets knowledge. Several tests in operational situations have therefore been carried out with different systems to assess the potential of these new tools and to define their field application for SNCF Réseau structures. The initial feedback shows that these new tools can be a valuable aid in identifying and characterizing damage without replacing traditional inspections, which remain essential.

The gain provided by these new technologies is mainly to be found in the accuracy of the damage records, which facilitates the assessment of the heritage structures deterioration. They also help prepare for inspections and end-of-mission self-checks. They can save time during inspections and thus do more inspections during periods of traffic disruption. Obviously, safety and economic benefits.

On the other hand, since 2006, SNCF Réseau has built digital data on damages detected during inspections (digital report and damages maps). The quotation reflects the state of the tunnel. All this data will be used to create algorithms for predicting tunnel degradation.

5.3.2.3. Passive contactless magnetic microwire sensor arrays for high-definition tunnel convergence monitoring systems in tunnels

Due to the great importance of knowledge of convergence in tunnels, auscultation has now become a fundamental tool in the service of engineering, responding to the need to know and adequately control the behaviour of our increasingly complex and ambitious works.

Auscultation is particularly important in tunnels, where design is generally based on empirical methods or theoretical calculations, according to complex and somewhat uncertain models. In addition, there are also major uncertainties in the properties and behaviour of the ground to be excavated, as well as in its homogeneity along the route, beyond the points where the surveys have been carried out. Both methods, convergence tapes and topography, are used to provide a complete picture of the tunnel convergence. The frequency of monitoring depends on the complexity of the project and the geological conditions in the tunnel area.

Convergence tapes are devices that are fixed to the ceiling and wall of the tunnel and measure the distance between them at different points along the tunnel. These measurements are used to calculate the convergence of the tunnel and detect any deformation or deviation from the desired alignment. High-precision convergence tapes have a very high measurement resolution and can

detect even small deviations from the desired alignment. Figure 5 shows an example of the application of convergence tapes for convergence measurement.

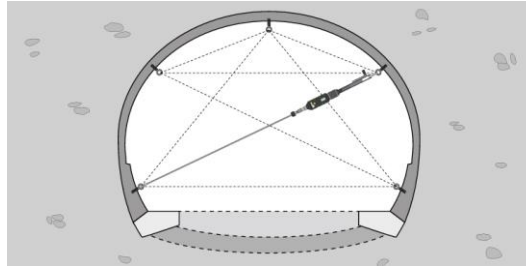


Figure 5. Application in tunnel convergence monitoring.

Topography is another tool used for monitoring tunnel convergence. It is used to measure the position and elevation of points along the tunnel and is used to detect any deformation or deviation from the desired alignment. To measure the convergence of a tunnel with topography, control points are established on the ceiling and wall of the tunnel on both sides. These points are measured using high-precision surveying instruments, such as theodolites and total stations, to determine their position in XYZ coordinates. Periodic measurements of these control points are made to measure the convergence of the tunnel. The convergence is calculated by comparing the XYZ coordinates of the control points at different points in time. Deformations and deviations in the tunnel alignment can be detected by comparing the measured values with the expected values. An example of the application of topographical methods for convergence measurement is shown in Figure 6.



Figure 6. Topographical precision control works.

5.3.3. Subproblem addressed by the use case and measurable objectives

This section is divided into the three previously presented developments: (1) Evaluation of mechanical properties of sub-ballast layers and subsoil, (2) High efficiency tunnel inspection systems and predictive maintenance for tunnels and (3) Passive contactless magnetic microwire sensor arrays for high-definition tunnel convergence monitoring systems in tunnels.

5.3.3.1. Evaluation of mechanical properties of sub-ballast layers and subsoil

In order to characterize the mechanical behaviour of sub-ballast /sub-soil and monitor areas with sinkhole hazard we aim to:

- Develop an active seismic surface waves method and creation of a toolbox (methodology, equipment, software, ...) allowing guide choices in terms of design, monitoring and maintenance. This will be tested on specific sites on high-speed line.
- Develop a passive seismic surface waves method to characterize the mechanical properties of the shallow subsurface, analyse the variation of the shear velocity due to cavity in the subsurface and study the influence of hydrogeological context on the shear wave velocity analysis. This will be tested on conventional line with gypsum dissolution hazard context.

To reach this objective, we need to:

- Carry out in-situ geophysical tests, define measurement protocols, test processing routines, model physical phenomena of wave propagation in a railway context.
- Correlate the results with field data including geotechnics.
- Clarify the expectation on the railway/industrial side for the exploitation of technical results and the adaptation expected on maintenance and works.

5.3.3.2. High efficiency tunnel inspection systems and predictive maintenance for tunnel

The aim is to deploy new inspection technologies and to predict the evolution of tunnel degradation. The tasks necessary for the achievement of the objective of this demonstrator include:

- Concerning the utilization of new inspection technologies:
 - Define specifications of the technologies to ensure a correct level of damage detection.
 - Define specifications of the measuring system.
 - Define the process and means of data processing and management.
 - Carry out tests in tunnels to verify performance and define limits.
- Concerning the prediction of the evolution of tunnel degradation:
 - Develop algorithms for predicting the degradation of tunnels.
 - Evaluate the performance of these algorithms (comparison between predictions and reality).
 - Define the process and means of data processing and management.
 - Create an asset management tool based on prediction models.

5.3.3.3. Passive contactless magnetic microwire sensor arrays for high-definition tunnel convergence monitoring systems in tunnels

The tasks necessary for the achievement of the objectives of this demonstrator include:

- To carry out all the laboratory tests to study the best direction of the microwires in order to obtain the most accurate and real information possible.

- To carry out all the laboratory tests to study the best way to carry out the set up.
- Carry out measurements and calculate the convergence on laboratory samples.
- Estimates of the time required to perform measurements in a relevant environment will be conducted, along with economic estimates associated with the process.

5.3.4. Influence of the proposed innovation on the IM/RU problem

This work by infrastructure managers (SNCF and ADIF) will improve the approach to the following points:

- To better quantify the disorders on sub-ballast and sub-soil, and anticipate the development of certain disorders.
- To limit the number of emergency maintenance operation.
- To propose an adapted design to the situation.
- To check that the work has been carried out properly.
- To optimize the maintenance operations in terms of methodology an economic point of view.
- To ensure the safety and operability of the tunnels.

5.3.5. Refinement of Key Performance Indicators (KPIs)

5.3.5.1. KPI 1. Reduction of maintenance time

- **Short description.** The main objective of this KPI is to check whether the time needed to perform a measurement:
 - To adapt the type/nature of maintenance and work for sub-ballast and sub-soil;
 - To make tunnel inspections and the planning of repairs operations;
 - To control the convergence of the tunnels can be reduced. For this purpose, sensors ("micro-wires") capable of providing accurate information on the convergence of the tunnels will be used. This factor is directly related to a correct preventive maintenance, by knowing in real time what data is being generated, this allows infrastructure managers to detect any changes in convergence early and take corrective action if necessary.
- **How to compute KPI1:** For the two first demonstrator which aim to reach the TRL 7, the estimation of the KPI1 for the two SNCFR demonstrator will adopt the following formula:

$$KPI1 (\% \text{ time savings}) = \frac{Time_{traditional_method} - Estimated\ time_{new_method}}{Time_{traditional_method}} \times 100 \quad (10)$$

Traditional Method Time is the time required to maintenance and works including investigation by the traditional method and Estimated time new method is the time required to maintenance and works including investigation by the new method.

For the third demonstrator, as it has a low technological maturity level (TRL4), it will not be tested in a relevant environment, but will be tested in laboratories, **we can obtain estimates of the time it may take to perform the inspection** and compare it with traditional methods to establish the time saving ratio that could be achieved with the application of this technology. To evaluate this KPI we can use the following formula:

$$KP1 (\% \text{ time savings}) = \frac{Time_{traditional_method} - Estimated\ time_{new_method}}{Time_{traditional_method}} \times 100 \quad (11)$$

Traditional Method Time is the time required to perform an inspection by the traditional method and the Estimated time new method is the time required to perform an inspection by the new method.

If KP1 is positive: Indicates that the estimated time for the new method is less than the time required for the traditional method. In this case, a positive value indicates a time saving or a reduction in the time required to complete the task, however, if KP1 is negative: Indicates that the estimated time for the new method is greater than the time required for the traditional method. In this case, a negative value indicates that the new method would require more time compared to the traditional method.

5.3.5.2. KPI2. Reduction of maintenance cost

- **Short description.** The main objective of this KPI is to check whether or not the reduction of maintenance cost is achieved by:
 - Reducing number and type of corrective maintenance operations and adapt the solution of rehabilitation to the context.
 - Reducing the tunnel inspections times and number of repair operations per year.
 - Implementing the necessary instrumentation to control the convergence of the tunnels. For this purpose, sensors ("microwire") will be used, which are able to provide accurate information on the convergence of the tunnels. This factor is directly related to a correct preventive maintenance, by knowing in real time what data is being generated, this allows infrastructure managers to detect any changes in convergence early and take corrective action if necessary.
- **How to compute KPI2.** For the two first demonstrator which aim to reach the TRL 7, the estimation of the KPI2 for the two SNCFR demonstrator which will be tested in a relevant environment, will be done by the following formula:

$$KP2 \% (\text{cost savings}) = \frac{Equ.\ cost_{t.m.} - Equ.\ Esti_{n.m.}}{Equ.\ cost_{t.m.}} \times 100 \quad (12)$$

Traditional Method cost is the cost required to maintenance and works including investigation by the traditional method ($Eq.cost_{t.m.}$) and Estimated new method cost is the cost required to maintenance and works including investigation by the new method ($Eq.Esti_{n.m.}$).

As it has a low technological maturity level (TRL4), it will not be tested in a relevant environment, but will be tested in laboratories, **we can obtain estimates of the cost it may take to perform the inspection** and compare it with traditional methods to establish the cost ratio that could be reduced with the application of this technology. To evaluate this KPI we can use the following formula.

$$KP2 \% (cost\ savings) = \frac{(Eq.cost_{t.m.} + Wf.cost_{t.m.}) - (Eq.Esti_{n.m.} + Wf.Esti_{n.m.})}{Eq.cost_{t.m.} + Eq.cost_{t.m.}} \times 100 \quad (13)$$

Equipment costs traditional method of an inspection ($Eq.cost_{t.m.}$): Refers to the costs associated with the purchase, maintenance and calibration of the equipment necessary to carry out the inspection. Workforce cost traditional method of an inspection ($Wf.cost_{t.m.}$): This is the expenditure related to the time and human effort required to perform the inspection. Estimated Equipment cost of new method of an inspection ($Eq.Esti_{n.m.}$): Refers to the estimated costs associated with the acquisition, maintenance and calibration of the equipment necessary to carry out the inspection. Estimated Workforce cost of new method of an inspection of an inspection ($Wf.Esti_{n.m.}$): This is the expenditure related to the time and human effort required to perform the inspection.

If KP2 is positive it indicates that the estimated costs of the new method (n.m.) are lower than the total costs of the old method (t.m.). In this case, a positive value indicates an economic saving or a reduction in costs, but if the KP2 is negative, it indicates that the estimated costs of the new method are lower than the total costs of the old method (t.m.). KP2 is negative: Indicates that the estimated costs of the new method (n.m.) are higher than the total costs of the old method (t.m.). In this case, a negative value indicates an increase in costs or a lack of economic savings in the new method.

5.4. Data Analysis for Condition Monitoring (The Netherlands, Norway).

5.4.1. Problem to be solved

This section is subdivided into two different developments and locations: (1) Track condition monitoring using a combination of ABA measurements and track geometry measurements in The Netherlands and (2) Condition assessment of existing concrete bridge and transition zones in Norway.

5.4.1.1. The Netherlands-Track condition monitoring

Track condition monitoring is an essential activity in supporting track maintenance decision-making. Track geometry faults cause poor condition track which can deteriorate resulting in speed restrictions, having a negative impact on train performance and in extreme cases result in derailments. Hence, a current practice for track condition monitoring relies on track geometry measurements.

Nevertheless, track geometry measurements cannot strongly reflect track conditions in other aspects, such as train-track interaction, embankment and subsoil conditions. In addition, track geometry measurements rely on a track recording car. Its availability is a constraint for frequent inspection activities. Therefore, additional techniques are required for comprehensive track condition monitoring.

This task aims to develop a new framework for monitoring track conditions based on both axle box acceleration (ABA) measurements and track geometry measurements. The research will assess the effectiveness with a major focus on embankment properties. Embankment is the focus of this task due to the generally poor bearing capacity of the Dutch soil. In FP3-IAM4RAIL project, a natural first step is the analysis of railway transition zones because the changes in its embankment composition. That is from the conventional ballast track that is supported by a typical embankment to the track on the bridge that is supported by a civil structure.

5.4.1.2. Norway–Condition assessment of existing concrete bridge and transition zones

In Norway and Europe there is a need to increase the railway transportation capacity to accommodate more frequent and heavier trains, which increases the requirements on railway infrastructure. A sustainable approach to accommodate the needs is to upgrade and reinforce the existing infrastructure and prolong their service life. However, there is limited information about the health conditions of existing bridges, especially pre-stressed concrete bridges. This makes the upgrading of railway infrastructure a more complex task. Most of condition monitoring systems of bridges are focusing on detecting signs of damage or deterioration. They do not provide evidence on the link between the signals measured by the sensors and the failure mechanism in the bridge to allows quantitative assessment of the health conditions. Moreover, some measurements like actual prestress loss of existing concrete bridges can be difficult (even impossible) or very costly. Therefore, the design loads for existing bridges such as strength capacity and remaining lifetime are mainly determined based on original design models (NS-EN & Eurocodes) which are very conservative and do not account for real contributions from materials and structural boundary

conditions during the service time. To this end, the present use case aims at the development of predictive tools for multi-level assessment procedure of existing railway bridges combining advanced structural models with data from continuous monitoring systems. The development of such predictive tool requires specific measurements with high accuracy for calibration and validation of the predictive models. An improved monitoring system integrating multiple sensing technologies installed on the bridge, in the transition zones and on the train will be considered. The predictive tool will be demonstrated on an existing prestressed bridge located at Sørsterbekk on the Ofoten line. The bridge which was built in 1989 as a part of the Ofoten Line (single track) serving iron ore trains between the mine in Kiruna and the Port of Narvik. Daily there are 11 to 13 iron ore trains in each direction. The ore trains operate at 50 kilometres per hour, while the empty return trains operate at 60 kilometres per hour.

5.4.2. Industry current position/baseline

This section is subdivided into two different developments and locations: (1) Track condition monitoring using a combination of ABA measurements and track geometry measurements in The Netherlands and (2) Condition assessment of existing concrete bridge and transition zones in Norway, as well as a last section on damage diagnosis in steel bridges.

5.4.2.1. The Netherlands-Track condition monitoring

The current baseline in track condition monitoring is track geometry, in which two major indicators can be considered:

- **The indicator for isolated defects.** There are 5 track geometry parameters defined in EN 13848-1: track gauge, longitudinal level, cross level, alignment, and twist (CEN, NEN-EN 13848-1:2019 (E) - Railway applications - track - track geometry quality - part 1: characterization of track geometry 2019). According to EN 13848-5, three levels are determined on each geometry parameters for maintenance decision-making: Immediate Action Limit, Intervention Limit, and Alert Limit (CEN, NEN-EN 13848-5:2017 (E) - Railway applications - track - track geometry quality - part 5: geometric quality levels - plain line, switches and crossing 2017). Besides the limits according to EN standard, ProRail, the Dutch railway infrastructure manager, has followed the principle of EN standard and established limit values for the Dutch railway network, which is stated in ProRail document number IHS00001-1 (ProRail, Instandhoudingsspecificatie - Spoor - Deel 1: Onderhoudswaarden, Interventiewaarden, Onmiddellijke actiewaarden 2021).
- **The indicator for assessment of the overall track geometry quality, TQI, over a defined length of tracks (typically 200 m).** According to EN 13848-6, TQI is referred to combined standard deviation (CoSD), which can be done by a combination of weighted standard deviations of individual geometric parameters (CEN, NEN-EN 13848-6:2014 (E) - Railway applications - track - track geometry quality - part 6: characterization of track geometry quality 2014).

However, the current baseline has the following limitations:

- The limit values determined in EN 13848-5 are not optimal in terms of delays due to speed restrictions (Andrade and Teixeira 2018).
- Track geometry cannot always indicate locations corresponding to poor train-track interaction since deviation of geometry parameters is only one of the causes of changes in train-track interaction (Li, et al. 2006, Xu 2017).
- Track geometry has positioning errors, which affect the accuracy in the localization of damage and the further use of the data (Wang, et al. 2018).
- Track geometry cannot effectively characterize short wave irregularities, which can accelerate degradation and fault in substructure (Loidolt and Marschnig 2024).

5.4.2.2. Norway–Condition assessment of existing concrete bridge and transition zones

The Ofoten line is 43-kilometre railway with a single track in Narvik (North of Norway). The line stretches from the Port of Narvik to Riksgränsen on the Norway – Sweden border, where it is connected to the Iron ore line (Malmbanan) via Kiruna and Gällivare to Luleå. Today, more than 30 million gross tonnes (MGT) of goods are transported annually on the Ofoten line. Iron ore accounts for 22 million tons. There is a need to further increase the transportation volume and frequency on the line. This requires upgrading the Ofoten line infrastructure. A challenging task for upgrading the infrastructure is the structural assessment of existing prestressed concrete bridges which is a complex process that involves the evaluation of their condition, integrity, and performance. It is required for changing the bridge's specifications or evaluating the impact of deterioration or damage. Traditional and standardised methods, which are used when designing the new structure are mainly considered for the assessment of existing bridges. However, to account for real contributions from materials and structural boundary conditions during the service time, enhanced assessment which integrate inspection and monitoring data is critical. This can be realized by combining improved non-linear analysis and simulations with improved inspection, Destructive & Non-destructive (material) tests (DT & NDT) and monitoring technologies. The condition monitoring systems of interest are those which can support the assessment of existing concrete bridges by providing reference base for evaluating their condition and structural performance and remaining service life:

- Automated visual monitoring and inspection: They are used for monitoring the dynamic response of the bridge and detecting visual damage during the service time. The deflection measurements by vision-based inspection provide large data sets characterizing the bridge and the transition zones. These are key data not only for condition monitoring, but also for calibration and validation of structural model.
- Impact hammer tests measurements are used for measuring the resonant frequency of the track, ballast, wheel, etc. to deduce the stiffness. The change in the measurements during the service time indicates potential defects in the associated structure. At the same time, the measured stiffness is key inputs to the structural model of the railway bridge.

- Measurements from bridge and transition zones Instrumentation: The aim is to use multiple sensing technologies of which the emplacement on the bridges is optimized to provide local detailed measurement and account for the contribution from the bridge structures. The deflection measurements will be used for the calibration and validation of the FE analysis.
- Axle Box Measurements and on board measurements to improve the quality and the accuracy of the data from the sensing systems installed on the train (on board and train axle). These will be obtained by the measuring train Roger 1000. The data from the bridge sensing system will be used as a reference for the analysis of axle box data, enabling mobile monitoring system with improved accuracy.
- Proof loading tests measurements are performed to assess the bridge's structural performance under controlled load. The measurements from the test are interesting for model validation.
- Traffic load and environmental records: The existing measuring station at Haugfjell, near Sørsterbekk, will be used to extract measurement data (traffic loads) from all trains passing the bridge. In addition to traffic loads, the station provides detailed information about train speed and climatic data such as temperature and relative humidity (RH).

5.4.2.3. Damage diagnosis in steel bridges

The bridges in which steel is the main material, are used mainly as railway bridges (Vagnoli, Prescott and Andrews 2018, Ghiasi, Ng and Sheikh 2022, Svendsen, Oiseth, et al. 2023, Sonbul 2023) and in a smaller degree as highway bridges (Catbas, Gokce and Gul 2012, Sunca, et al. 2021). These bridges constitute essential components of the transport infrastructure and their uninterrupted operation is imperative for the normal operation of the society (Vagnoli, Prescott and Andrews 2018). However, they are affected by increasingly demanding operational conditions such as intense traffic loads and harsh environmental conditions which lead to the development of deterioration mechanisms (Ghiasi, Ng and Sheikh 2022, Svendsen, Oiseth, et al. 2023). The mechanisms include fatigue, fracture, buckling, corrosion and scour and their early diagnosis including detection, localization, quantification (Svendsen, Oiseth, et al. 2023), is crucial as they can lead to catastrophic failure, the collapse of the bridge, high maintenance costs and the loss of human lives among other dire environmental, social, and economic consequences (Imam and Chrysanthopoulos 2012, Azim and Gul 2021). Structural Health Monitoring (SHM) in steel bridges is pivotal for the early diagnosis of such deterioration mechanisms. Additionally, the variability of the operational and environmental conditions (EOCs) hinders the SHM's effectiveness as the EOCs partially or fully "mask" the effects of damages on the structural dynamics (Svendsen, Oiseth, et al. 2023).

5.4.2.3.1. Methods

Currently, SHM in steel bridges is conducted via Non-destructive Evaluation (NDE) methods based on ultrasound, radiography, eddy current and mostly on visual inspections. However, these methods require a priori knowledge of and access to the vicinity of the suspected damage location, they are typically time consuming and costly, and they can be applied only when the bridges are not operational (Vagnoli, Prescott and Andrews 2018, Azim and Gul 2021). SHM in steel bridges has also

been investigated via methods based on vibration signals.

The main premise of the vibration-based methods is that a damage alters the stiffness or mass of the examined structure, which, in turn, alter the structure's measured global dynamic response properties and damage diagnosis is achieved via the examination of changes in the structure's vibration characteristics (Vagnoli, Prescott and Andrews 2018, Sonbul 2023). These methods operate with vibration signals acquired via installed sensors on the bridges, resulting in a reduced SHM cost and a continuous availability of SHM data, as opposed to sporadic and expensive NDE based inspections. The vibration signals are typically naturally available and are easily measurable through various types of sensors and data acquisition systems (Rageh, Linzell and Azam 2018, Svendsen, Oiseth, et al. 2023). Additionally, the methods offer advantages such as capability of automation, no requirement of access to the location of damage and application during a bridge's normal operation.

The vibration-based methods employ mathematical models for modelling a bridge's dynamics and treating the effects of the varying EOCs on the dynamics. The modelling for the treatment of the varying EOCs can be either explicit or implicit. Implicit-based methods attempt to remove the effects of varying EOCs on the dynamics via the use of techniques such as the Principal Component Analysis (PCA) for the selection of features of the dynamics that are insensitive to changes due to the varying EOCs, assuming that they are sensitive to damage (Guo, et al. 2012, Laory, Ali, et al. 2012, Laory, Trinh, et al. 2013, Vagnoli, Prescott and Andrews 2018, Azim and Gul 2021, Maes, et al. 2022). On the other hand, explicit-based methods attempt to model the effects of the varying EOCs on the dynamics (Laory, Ali, et al. 2012, Rageh, Linzell and Azam 2018, Neves, Gonzalez and Karoumi 2022, Sarmadi, et al. 2022, Svendsen, Froseth, et al. 2022, Zhou, et al. 2022, Svendsen, Oiseth, et al. 2023, Yano, et al. 2023).

In the implicit-based methods and in most of the explicit-based methods, data-based models developed exclusively through the acquired vibration signals from the structure are used. These models are able of representing partially the structural dynamics and they can be either multivariate models such as Neural Networks (NNs) (Rageh, Linzell and Azam 2018, Neves, Gonzalez and Karoumi 2022), linear regression models (Laory, Ali, et al. 2012, Laory, Trinh, et al. 2013, Maes, et al. 2022), state space models (Maes, et al. 2022, Svendsen, Oiseth, et al. 2023) or univariate models such as AutoRegressive (AR) models (Laory, Trinh, et al. 2013, Svendsen, Froseth, et al. 2022). Some of the explicit-based methods employ detailed and accurate physical models, as for instance Finite Element Models (FEMs) which describe the complete structural dynamics and need to be updated with vibration response signals from multiple sensors (Zhou, et al. 2022). Of course, there are studies where vibration-based methods equipped with state space models (Sunca, et al. 2021, Torres, et al. 2023), NNs (Ngoc, et al. 2019, Parisi, et al. 2022, Dang, Tatipamula and Nguyen 2022, Sonbul 2023) and models based on Power Spectral Density (PSD) (Beskhyroun, Oshima and Mikami 2010, Oshima, et al. 2013, Sunca, et al. 2021, Ghiasi, Ng and Sheikh 2022, Torres, et al. 2023), cross-correlation function (Catbas, Gokce and Gul 2012) & wavelets (Beskhyroun, Oshima and Mikami 2010), are applied in steel bridges but varying EOCs are not considered (Beskhyroun, Oshima and Mikami 2010, Catbas, Gokce and Gul 2012, Oshima, et al. 2013, Ngoc, et al. 2019, Sunca, et al. 2021, Ghiasi, Ng and Sheikh 2022, Parisi, et al. 2022, Dang, Tatipamula and Nguyen 2022, Torres, et al. 2023).

Many of the methods equipped with data-based models are confined only to the first level of damage diagnosis, which is damage detection (Beskhyroun, Oshima and Mikami 2010, Catbas,

Gokce and Gul 2012, Guo, et al. 2012, Laory, Ali, et al. 2012, Oshima, et al. 2013, Laory, Trinh, et al. 2013, Vagnoli, Prescott and Andrews 2018, Rageh, Linzell and Azam 2018, Ngoc, et al. 2019, Azim and Gul 2021) (Sunca, et al. 2021, Parisi, et al. 2022, Dang, Tatipamula and Nguyen 2022, Ghiasi, Ng and Sheikh 2022, Maes, et al. 2022, Neves, Gonzalez and Karoumi 2022, Sarmadi, et al. 2022, Svendsen, Froseth, et al. 2022, Zhou, et al. 2022, Yano, et al. 2023) (Sonbul 2023, Svendsen, Oiseth, et al. 2023, Torres, et al. 2023). The models are developed with vibration signals from the healthy structure and potentially measurements of the EOCs, with features sensitive to damage, such as its structural parameters, residual signals, modal parameters, principal components, being acquired from the models. Damage detection is achieved based on the detection of dissimilarities between the features from the healthy structure to their counterparts from a present unknown structural state. Damage localization and quantification (Beskhyroun, Oshima and Mikami 2010, Catbas, Gokce and Gul 2012, Oshima, et al. 2013, Azim and Gul 2021, Svendsen, Froseth, et al. 2022, Parisi, et al. 2022, Dang, Tatipamula and Nguyen 2022, Ghiasi, Ng and Sheikh 2022, Sonbul 2023, Svendsen, Oiseth, et al. 2023) is achieved with the detected damage state being roughly classified either to a prespecified damaged state of specific location and magnitude or to the nearest sensor with the corresponding highest damage index acting as an indication of damage quantity (severity). Machine learning techniques such as Support Vector Machine (SVM) (Vagnoli, Prescott and Andrews 2018, Svendsen, Froseth, et al. 2022, Ghiasi, Ng and Sheikh 2022, Svendsen, Oiseth, et al. 2023), K-Nearest Neighbour (KNN) (Guo, et al. 2012, Ghiasi, Ng and Sheikh 2022, Svendsen, Froseth, et al. 2022, Sonbul 2023), Random Forest (RF) (Svendsen, Froseth, et al. 2022, Sonbul 2023) and NNs (Vagnoli, Prescott and Andrews 2018, Rageh, Linzell and Azam 2018, Ngoc, et al. 2019, Parisi, et al. 2022, Dang, Tatipamula and Nguyen 2022, Sonbul 2023) are used for the treatment of damage detection, localization and quantification as classification problems. Additionally, the NNs can treat damage localization and quantification as precise estimation problems by providing a precise value of the damage location and quantity (severity) (Rageh, Linzell and Azam 2018, Ngoc, et al. 2019).

In the context of the FEM based methods, the treatment for the problem of damage diagnosis requires the structure to be divided into a number of elements (substructures) and the identification of changes in the structural parameters (stiffness coefficients or Young's moduli) leads subsequently to the identification of the damaged element(s) which correspond(s) to the damage location(s) and magnitude(s) (Laory, Ali, et al. 2012). However, the modelling of structures of complex geometry (structures with bolted nodes connecting multiple components) may lead to large in size FEMs whose updating is difficult because the inverse problem posed may prove to be ill-conditioned when the number of the updating parameters is large. Moreover, signals from several sensors are needed for updating FEMs of structures of higher complexity (Brownjohn, et al. 2001, Friswell, Mottershead and Ahmadian 2001).

5.4.2.3.2. Types of steel bridges

The steel bridges on which the considered vibration-based methods for SHM have been applied, are mostly railway bridges (Beskhyroun, Oshima og Mikami 2010, Guo, et al. 2012, Laory, Ali, et al. 2012, Laory, Trinh, et al. 2013, Oshima, et al. 2013, Rageh, Linzell og Azam 2018, Vagnoli, Prescott og Andrews 2018, Ngoc, et al. 2019, Azim og Gul 2021, Parisi, et al. 2022) (Dang, Tatipamula and Nguyen 2022, Zhou, et al. 2022, Maes, et al. 2022, Neves, Gonzalez and Karoumi 2022, Sarmadi, et al. 2022, Svendsen, Froseth, et al. 2022, Ghiasi, Ng and Sheikh 2022, Svendsen, Oiseth, et al. 2023, Yano, et al. 2023, Sonbul 2023) (Torres, et al. 2023) and in a smaller degree highway bridges (Catbas, Gokce and Gul 2012, Sunca, et al. 2021). The examined railway bridges include the Quisi bridge in

Spain (Torres, et al. 2023), the KW51 bridge in Belgium (Maes, et al. 2022, Neves, Gonzalez and Karoumi 2022, Sarmadi, et al. 2022, Yano, et al. 2023), the Hell Bridge Test Arena bridge in Norway (Svendsen, Froseth, et al. 2022, Svendsen, Oiseth, et al. 2023), the Zangenberg bridge in Germany (Laory, Ali, et al. 2012, Laory, Trinh, et al. 2013), the Adour Bridge in France (Guo, et al. 2012), the Port Adelaide bridge in Australia (Ghiasi, Ng and Sheikh 2022), the Nam O bridge in Vietnam (Ngoc, et al. 2019, Dang, Tatipamula and Nguyen 2022) and others whereas some of the examined highway bridges include the Eynel bridge in Turkey (Sunca, et al. 2021) and the Sunrise Boulevard bridge in USA (Catbas , Gokce and Gul 2012). Some of these bridges have distinctive forms such as bowstring truss (Ngoc, et al. 2019, Maes, et al. 2022, Neves, Gonzalez and Karoumi 2022, Sarmadi, et al. 2022, Dang, Tatipamula and Nguyen 2022, Yano, et al. 2023), bailey truss (Guo, et al. 2012, Oshima, et al. 2013, Torres, et al. 2023), parker truss (Svendsen, Froseth, et al. 2022, Zhou, et al. 2022, Svendsen, Oiseth, et al. 2023), pratt truss (Rageh, Linzell and Azam 2018, Azim and Gul 2021) and Pennsylvania petit truss (Laory, Ali, et al. 2012, Laory, Trinh, et al. 2013) with their length ranging between 6.9 m and 300 m. In a few studies, only one or two of spans instead of the whole bridge have been examined (Laory, Trinh, et al. 2013, Azim and Gul 2021, Parisi, et al. 2022, Torres, et al. 2023). Additionally, several of the examined railway bridges have been decommissioned and some of them have been replaced by new ones (Beskhyroun, Oshima and Mikami 2010, Laory, Ali, et al. 2012, Guo, et al. 2012, Oshima, et al. 2013, Laory, Trinh, et al. 2013, Svendsen, Froseth, et al. 2022, Zhou, et al. 2022, Svendsen, Oiseth, et al. 2023).

5.4.2.3.3. Details about sensors, damages, environmental conditions and the methods effectiveness

Although, a combination of experimental and simulation signals is used for damage diagnosis in the majority of the considered steel bridges (Beskhyroun, Oshima and Mikami 2010, Catbas , Gokce and Gul 2012, Guo, et al. 2012, Oshima, et al. 2013, Rageh, Linzell and Azam 2018, Sunca, et al. 2021, Dang, Tatipamula and Nguyen 2022, Zhou, et al. 2022, Maes, et al. 2022, Neves, Gonzalez and Karoumi 2022) (Sarmadi, et al. 2022, Svendsen, Froseth, et al. 2022, Yano, et al. 2023, Svendsen, Oiseth, et al. 2023, Torres, et al. 2023), there are cases where only simulated signals are used (Laory, Ali, et al. 2012, Laory, Trinh, et al. 2013, Vagnoli, Prescott and Andrews 2018, Ngoc, et al. 2019, Azim and Gul 2021, Ghiasi, Ng and Sheikh 2022, Parisi, et al. 2022). These signals correspond to acceleration (Beskhyroun, Oshima and Mikami 2010, Guo, et al. 2012, Oshima, et al. 2013, Ngoc, et al. 2019, Sunca, et al. 2021, Dang, Tatipamula and Nguyen 2022, Zhou, et al. 2022, Ghiasi, Ng and Sheikh 2022, Maes, et al. 2022, Neves, Gonzalez and Karoumi 2022) (Sarmadi, et al. 2022, Svendsen, Froseth, et al. 2022, Yano, et al. 2023, Svendsen, Oiseth, et al. 2023, Torres, et al. 2023), strain (Catbas , Gokce and Gul 2012, Laory, Ali, et al. 2012, Laory, Trinh, et al. 2013, Rageh, Linzell and Azam 2018, Azim and Gul 2021, Neves, Gonzalez and Karoumi 2022, Parisi, et al. 2022), displacement (Ngoc, et al. 2019) and deflection signals (Torres, et al. 2023) within frequency bandwidths up to 800 Hz, with the last two types used only in a very few cases. Additionally, they are based on sensors or measuring points whose number range between 4 and 76 and their usual considered locations are the truss bridges' sides and the central and side girders (stringers) below the deck. The top of the truss and the deck constitute alternative locations for the sensors and the measuring points. Hiltec (Catbas , Gokce and Gul 2012), Dytran (Svendsen, Oiseth, et al. 2023), Bridge Diagnostics (Rageh, Linzell and Azam 2018) and B&K (Sunca, et al. 2021, Torres, et al. 2023) sensors are used for the acquirement of experimental signals.

The actual damages which have been examined in the steel bridges include loosened or removed bolts, removed shims, cracks (Beskhyroun, Oshima and Mikami 2010, Catbas , Gokce and Gul 2012, Oshima, et al. 2013, Svendsen, Froseth, et al. 2022, Svendsen, Oiseth, et al. 2023). Also, retrofitting is considered as a form of damage which results to the change of the bridge dynamics (Maes, et al. 2022, Neves, Gonzalez and Karoumi 2022, Sarmadi, et al. 2022, Yano, et al. 2023). Only the bridges where the retrofitting and the shim removal have been considered, are still operational (Catbas , Gokce and Gul 2012, Maes, et al. 2022, Neves, Gonzalez and Karoumi 2022, Sarmadi, et al. 2022, Yano, et al. 2023). Moreover, the examined simulated damages correspond to reduction of stiffness, elasticity modulus and cross sectional area and to removal of elements (Guo, et al. 2012, Laory, Ali, et al. 2012, Laory, Trinh, et al. 2013, Rageh, Linzell and Azam 2018, Ngoc, et al. 2019, Azim and Gul 2021, Ghiasi, Ng and Sheikh 2022, Zhou, et al. 2022, Parisi, et al. 2022, Dang, Tatipamula and Nguyen 2022). Multiple damages corresponding to simultaneous damages of the same or different type and of different magnitudes and at different locations have been examined (Beskhyroun, Oshima and Mikami 2010, Catbas , Gokce and Gul 2012, Ngoc, et al. 2019, Azim and Gul 2021, Svendsen, Froseth, et al. 2022, Svendsen, Oiseth, et al. 2023, Torres, et al. 2023).

In most of the studies about damage diagnosis in steel bridges, varying EOCs are considered. The environmental conditions include bridge temperature (Maes, et al. 2022, Yano, et al. 2023), air temperature (Laory, Ali, et al. 2012, Laory, Trinh, et al. 2013, Neves, Gonzalez and Karoumi 2022, Sarmadi, et al. 2022, Svendsen, Oiseth, et al. 2023), wind speed (Svendsen, Froseth, et al. 2022, Svendsen, Oiseth, et al. 2023) whereas the operational conditions include train and traffic load (Rageh, Linzell and Azam 2018, Laory, Trinh, et al. 2013, Maes, et al. 2022, Torres, et al. 2023), train speed (Guo, et al. 2012, Azim and Gul 2021, Neves, Gonzalez and Karoumi 2022), number of cars of a train (Azim and Gul 2021) and coefficient of different types of springs (Zhou, et al. 2022).

Although most of the used vibration-based methods provide satisfactory results about damage detection, localization and quantification in steel bridges, there are few of them which are not able to detect (Rageh, Linzell and Azam 2018, Azim and Gul 2021, Neves, Gonzalez and Karoumi 2022, Torres, et al. 2023), localize (Rageh, Linzell and Azam 2018, Zhou, et al. 2022) and quantify (Rageh, Linzell and Azam 2018, Parisi, et al. 2022) adequately damages and especially small ones. Additionally, the effectiveness of the most methods is examined based only on damage scenarios which may be quite few during the evaluation phase and thus with no results on the methods' false alarm rate (Beskhyroun, Oshima and Mikami 2010, Laory, Ali, et al. 2012, Oshima, et al. 2013, Laory, Trinh, et al. 2013, Ngoc, et al. 2019, Azim and Gul 2021, Parisi, et al. 2022, Dang, Tatipamula and Nguyen 2022). Also, the effectiveness of the methods is tested only with the same damage magnitudes, locations and EOCs values considered in the training phase and no other values are considered (Guo, et al. 2012, Laory, Ali, et al. 2012, Laory, Trinh, et al. 2013, Rageh, Linzell and Azam 2018, Ngoc, et al. 2019, Azim and Gul 2021, Parisi, et al. 2022, Dang, Tatipamula and Nguyen 2022, Zhou, et al. 2022, Ghiasi, Ng and Sheikh 2022) (Svendsen, Froseth, et al. 2022, Svendsen, Oiseth, et al. 2023, Yano, et al. 2023). Finally, there are damages such as retrofitting for which only a specific magnitude is considered (Maes, et al. 2022, Neves, Gonzalez and Karoumi 2022, Sarmadi, et al. 2022).

5.4.3. Subproblem addressed by the use case and measurable objectives

This section is subdivided into two different developments and locations: (1) Track condition monitoring using a combination of ABA measurements and track geometry measurements in The Netherlands and (2) Condition assessment of existing concrete bridge and transition zones in

Norway.

5.4.3.1. Track condition monitoring in The Netherlands

The final goal of the task is to monitor embankment stability with a use case on the track section between Delft and Schiedam in The Netherlands. At the current stage, we take transition zones as case studies since they exhibit significant changes in track support conditions when connecting plain tracks supported by embankments and rigid structures, such as bridges, culverts, and tunnels. The differences in the track substructures at transition zones lead to drastic train-track interaction and fast track degradation due to the unevenness in the track support conditions. In The Netherlands, maintenance activities in transition zones are reported to be at least twice as frequent as those conducted on plain tracks. The health condition of the transition zones is estimated by analyzing the measurements at different locations. These locations include the entrance and exit sides on each of the two tracks, abutments, and the inner and outer rails, as shown in the next figure.

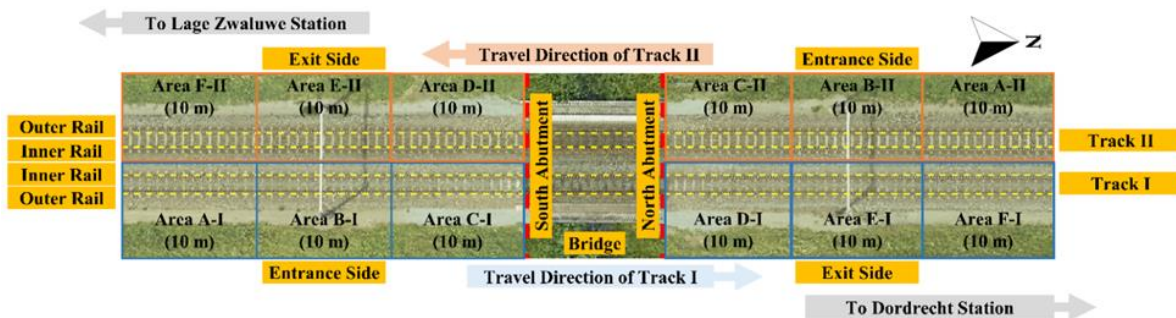


Figure 7. Study areas of transition zones at the double-track railway bridge (Unsiwilai, et al. 2023).

The key subproblem addressed by the case studies is how to use ABA signals to characterize the dynamic response due to changes in embankment properties and assess their health conditions. We develop a multiple-axle box acceleration (multi-ABA) monitoring technique to characterize the ABA responses at railway bridge transition zones. Multi-ABA measurements include acceleration signals in the vertical direction on multiple wheelsets. The energy of the ABA responses is used to represent the degradation level of tracks. Larger ABA energies should be observed for tracks with more degradation. Furthermore, we develop KPIs based on multi-ABA measurements to evaluate the differences in energy levels between different abutments, tracks, sides, and rails at each bridge. The objective is to develop a comprehensive method for track conditions assessment regarding geometry deviation and train-track interaction. Rather than solely considering track geometry, ABA could provide more insights in terms of dynamic responses of track components, especially embankment.

5.4.3.2. Condition assessment of existing concrete bridge and transition zones in Norway

The use case aims at the following subobjectives:

- To develop and validate FEA enabling the consideration of the contributions from material and structural boundary conditions of the bridge and its transition zones,
- To develop an improved monitoring and condition assessment systems,
- To connect the results and provide insights on the relation between the monitoring and modelling data and the failure modes, providing support for decision-making processes in the bridge and transition zone maintenance,
- To establish the predictive tools required for condition assessments and upgrading the concrete bridge.

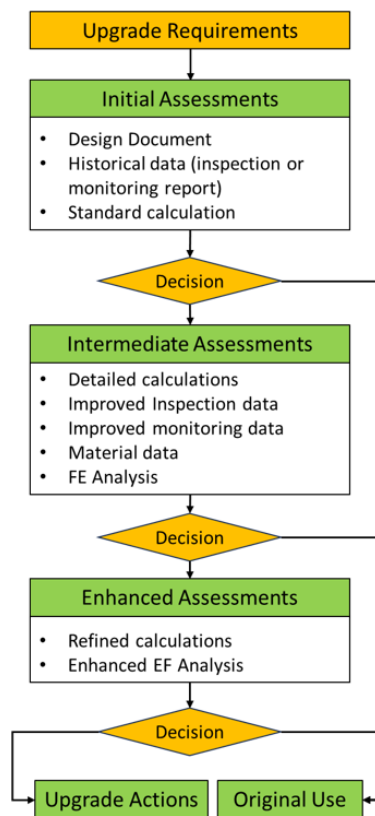


Figure 8. Tasks planned for the current UC.

Figure 8 shows the main tasks planned for the current use case, including:

- **Initial assessment of the bridge and the transition zone** aims to offer a comprehensive understanding of the structure's condition and performance. In general, this assessment serves as a crucial guide for decision-making concerning maintenance, repair, rehabilitation, or replacement strategies, all aimed at ensuring the safety and longevity of the infrastructure.

In the case of the Sørsterbekk bridge use case, the initial assessment involves a review of historical records, such as construction/ design documents, inspection and maintenance logs, and review and analysis of monitoring data collected during the 32.5-ton axle load test. These records can yield valuable insights into the bridge's design, construction methods, past inspections, repairs, and maintenance history. Furthermore, the initial assessment of the bridge entails conducting simplified structural calculation to determine the distribution of internal forces and moments under specific loading conditions.

- **Intermediate assessments**, which typically involves a more detailed evaluation of the bridge structural integrity, performance, and any changes since the initial assessment. It involves:
 - Improved inspection data could be established with a thorough visual inspection (supported by NDT tests) which is conducted to identify any new signs of deterioration, cracks, spalling, or other structural issues that may have developed since the last special/ main inspection of the bridge including transition zones.
 - More detailed calculation will be employed to evaluate the bridge's response to various and actual loading conditions from increased axle load and new rolling stock, including static and dynamic loads. As input for detailed calculations available historical data supported with new monitoring data will form a more detailed understanding of the current condition and structural behaviour of the bridge.
 - Historical dataset includes:
 - Train-borne measurements of the Ofoten line track structure including bridges and transition zones from Track-Logger (2019) and diagnostic vehicle Roger 1000 measurements (performed 2 time/ year).
 - Monitoring data from Sørsterbekk bridges performed by Rambøll in connection with the 32,5-ton test train campaign 2016-20.

Dataset includes bridge deflection, strain in reinforcement bars and vibration measurements from multiple train passes from iron ore trains with 30- and 32,5-ton axle load.

In addition, track measuring data from Haugfjell measuring station will be used to investigate the actual traffic loads from all train passing the Sørsterbekk bridge. Both historical and present data are available.

For the Norwegian use case partner intend to instrument the pre-stressed concrete at Sørsterbekk monitoring to measure the structural response of the bridge and transition zones from iron ore train. A proposed monitoring setup is outlined for the IM. New measuring data from Roger 1000 and Track Logger is planned which will form additional input for further calculations and analysis. Based on research studies, empirical material data will be applied in the detailed structural analysis. This includes an investigation of concrete elements condition, pre-tension losses in tendon cables, track structure and ballast degradation on bridge and transitions zones.

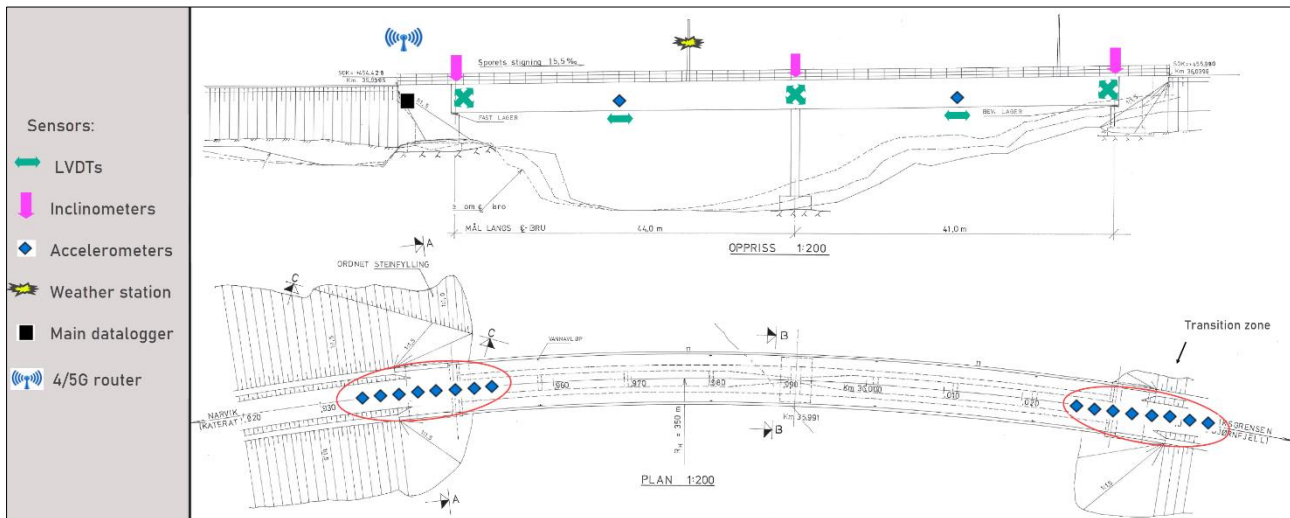


Figure 9. Layout monitoring plan for transition zones and bridge.

The FE Analysis aims at recreating the behaviour of the concrete bridge and its transition zone within some domain of interest. Considering that the bridge and transition zone were constructed decades ago and have been subjected to wear and maintenance, building a model capable of representing the bridge and transition zone in their current state will be challenging. Some key difficulties are expected to be found in:

- The settlement of the transition zones before and after the bridge. It is generally known that the response of transition zones changes over time due to crushing of ballast stone and settlement of the ballast and weak subsoil. It is also influenced by the maintenance (tamping) aiming to reset the settlement effects. Settlement may have a notable influence on the dynamic forces from the train-wheels as the train enters or exits the bridge.
- The steel cables used for post-tensioning the concrete elements of the bridge will experience a loss of tension over time. Given that this is an older bridge, this kind of stress relaxation will have already happened. It is not clear how much of an influence this value will have on the structural response of the bridge, but it plays an important role on its strength capacity.
- The long-term use may have influences on the material response of the track structural components or the bridge itself. Modelling an idealised version of the bridge might not be sufficient for direct comparison with data, requiring the model to go one step further and account for any significant changes which may have occurred in the bridge throughout its life thus far.
- **Enhanced Assessments:** A numerical model requires data from a monitoring system for calibration and validation. However, once established the model would be able to describe the properties and behaviour of the bridge and transition zone in much greater detail than what can be provided by the monitoring system itself. This can be used to support the measurements, provide insight, and extend our understanding of the bridge, and to conduct parametric studies to investigate the influence of design parameters. Defects and damage may also be introduced

to study the most common failure modes for prestressed concrete bridges. It is important to note that predictions made by a simulation must be understood within the context of model validity – the map is not the territory.

For the Norway-condition assessment of existing concrete bridge and transition zones, the Sjøsterbekk bridge was originally designed to accommodate 25-ton axle load. However, due to the growing demand for increased rail traffic capacity along the Ofoten line, there has been a need to elevate the axle load to 30-ton, a change implemented in 2008. This adjustment was made feasible with the introduction of new iron ore trains. After a 32.5-ton axle load test campaign the maximum allowable load was further increased to 31-ton.

Currently, Bane NOR is in the process of preparing for another upgrade, aiming to raise the axle load capacity to 32.5 tons (32.5-ton axle load is considered to be the upper limit for existing ore trains). This necessitates a thorough structural assessment of the Sjøsterbekk bridge to ascertain its ability to accommodate the anticipated 32.5-ton axle load. Such an assessment is critical to ensure the bridge's continued safety and functionality amidst evolving operational requirements and increased loads on the rail network. The technical and functional requirements for the measurement system is found in Annex 6.

5.4.4. Influence of the proposed innovation on the IM/RU problem

This section is subdivided into two different developments and locations: (1) Track condition monitoring using a combination of ABA measurements and track geometry measurements in The Netherlands and (2) Condition assessment of existing concrete bridge and transition zones in Norway, as well as a last section on Damage diagnosis in steel bridges.

5.4.4.1. Track condition monitoring in The Netherlands

The objective of this use case is to develop a comprehensive method for track conditions assessment regarding geometry deviation and train-track interaction. Rather than solely considering track geometry, ABA could provide more insights regarding the dynamic responses of track components, especially embankments. The analysis and preliminary results presented in this deliverable have been published open access in (Unsiwilai, et al. 2023), which acknowledges the FP3-IAM4RAIL project.

Measurements (ABA and TG) at an example bridge in the Dutch railway network are presented to showcase the value of the developed technology. The next figure presents the responses of the inner and the outer rails. The ABA signals from the inner and outer rails yield similar peak positions. However, the inner rail signal shows a significantly larger amplitude than the outer rail signal at a peak close to the South Abutment. This suggests that at Track I, the South Abutment experiences a stronger uneven degradation than the North Abutment. Then, ABA signals are transformed from the time domain to the time-frequency domain using the continuous wavelet transform (CWT). Consequently, the wavelet power spectrum (WPS), the energy of ABA signal regarding CWT, of the inner rail close to the South Abutment are significantly larger than those from the outer rail.

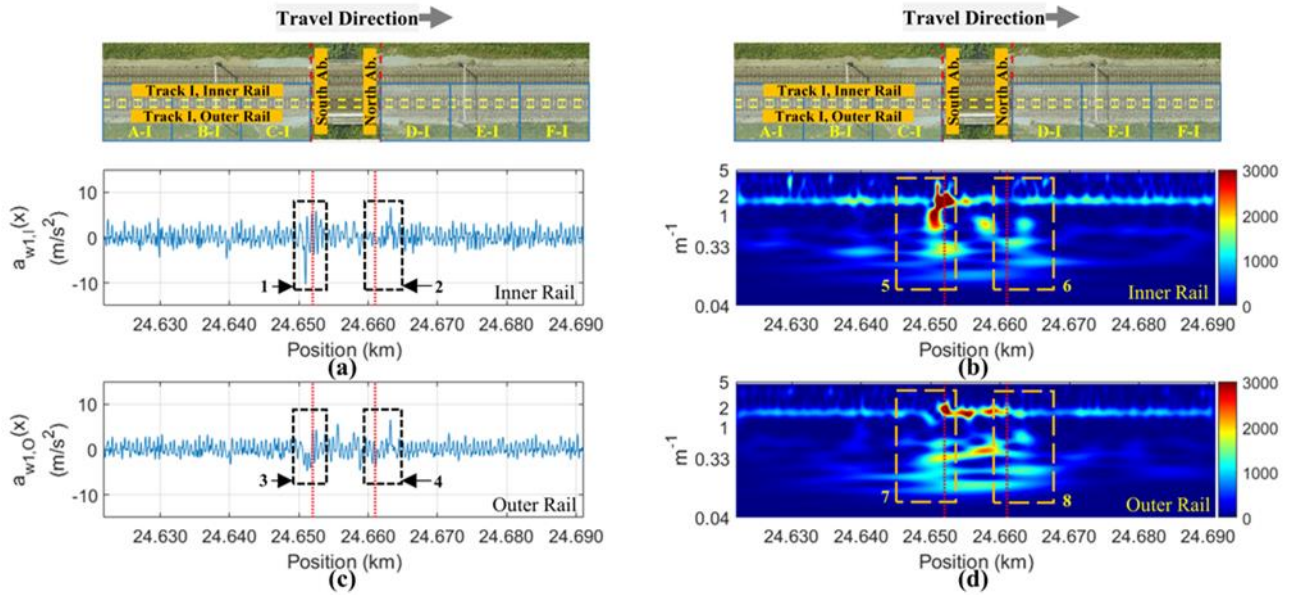


Figure 10. ABA responses of Track I at an example bridge (Unsiwilai, et al. 2023)

Then, multi-ABA signals from both rails in terms of the global wavelet power spectrum (GWPS) and the distribution of WPS with respect to the frequencies in each study area are compared in the next figure. Signals from the inner and outer rails show differences in the frequencies and amplitudes of the dominant peaks in the study areas. Areas C-I and D-I show noticeable response differences between the two rails in the spatial frequency range below 0.33 m^{-1} . In addition, remarkable differences between the two rails are also found at spatial frequencies above 0.33 m^{-1} .

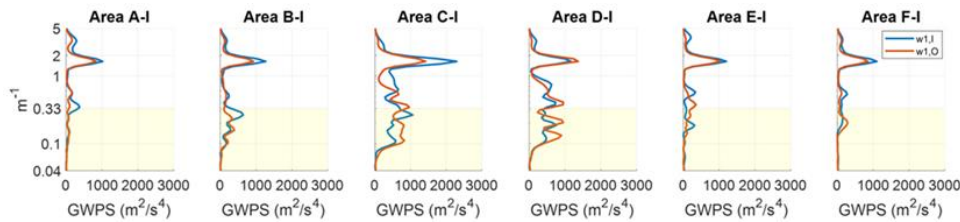


Figure 11. GWPS of the ABA signals measured at different rails for Track I at an example bridge (Unsiwilai, et al. 2023).

Next, the scale average wavelet power (SAWP), the distribution of WPS with respect to the positions of the signals at both rails in Tracks I and II, and the corresponding track geometry parameters at the transition zones are shown in the next figure. The figure shows noticeable differences in Areas B-I, C-I, and D-I regarding the location and amplitude of the SAWP peak responses between the inner and outer rails. The inner rail shows larger energies than the outer rail in Area B-I, while the outer rail shows larger energies in Areas C-I and D-I. While longitudinal levels measured at both inner and outer rails are not significantly different. These findings suggest a sensitivity of the multi-ABA to estimate responses from signals measured at different rails. It can be observed that ABA measurement provides results with higher sensitivity than track geometry measurement, the current practice technology.

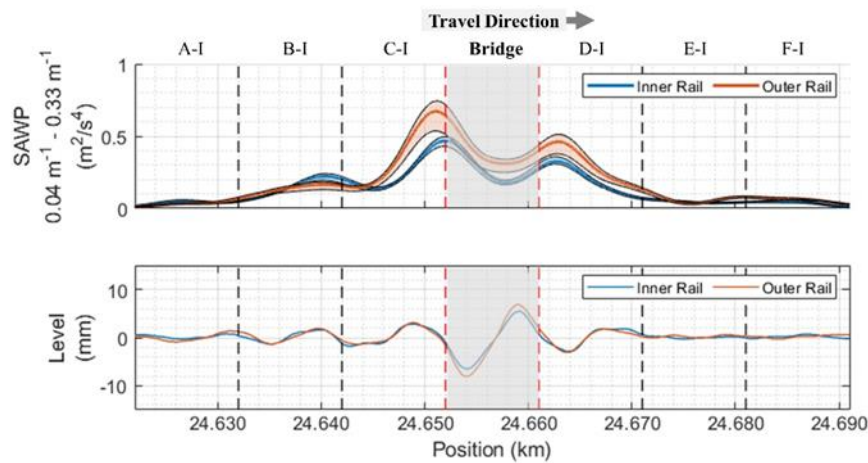


Figure 12. SAWP of the ABA signals and track geometries at an example bridge (Unsiwilai, et al. 2023).

5.4.4.2. Condition assessment of existing concrete bridge and transition zones in Norway

The combination of advanced modelling and instrumentation which is developed and demonstrated in the current use case will significantly contribute to the development of new condition assessment and maintenance systems for IM. The predictive tool for condition assessment of existing bridges and the database from the continuous condition monitoring instrumentation will support understanding the effects of the service condition on the bridge to develop sustainable management strategy for the railway infrastructure. In addition, modelling combined with multiple sensing technologies will improve understanding the impact of specific failure mode on the dynamic signals as received by the condition monitoring sensing system. This will significantly contribute to increasing the accuracy of monitoring system. Finally, the predictive tool combined with continuous monitoring of the transition zone will support IR for improving their maintenance and reduce its impact on the structural health of the bridge.

5.4.5. Refinement of Key Performance Indicators (KPIs)

No further refinements to the KPIs are identified at the present stage. The KPIs will be refined upon analysis of the data acquired at the asset using the measurement system.

This section is subdivided into two different developments and locations: (1) Track condition monitoring using a combination of ABA measurements and track geometry measurements in The Netherlands and (2) Condition assessment of existing concrete bridge and transition zones in Norway.

5.4.5.1. KPI1. Track condition monitoring in The Netherlands

- **Short description.** The current baseline for track condition assessment solely relies on track geometry parameters. However, some limitations in utilizing track geometry are indicated before. This use case considers ABA measurements, which can capture train-track

interaction, as an additional source of information for track condition assessment. The preliminary results suggest that ABA measurements provide higher sensitivity than track geometry measurements, indicating a higher capability of ABA measurements in detecting track positions with poor embankment conditions, which can be called defects. In addition, due to higher sensitivity and more frequent monitoring operation of ABA measurements than track geometry measurements, an early warning detection framework for track embankment failures is allowed to be developed in the future.

- **How to compute KPI1.** Therefore, in this state, the KPI is developed to quantify the capability of ABA measurements in track condition assessment regarding the number of detected defects, as follows.

$$\text{KPI1} = \frac{(\text{defect}_{\text{ABA}} - \text{defect}_{\text{TG}})}{\text{defect}_{\text{TG}}} \times 100 \quad (14)$$

where: $\text{defect}_{\text{TG}}$ is the number of defects regarding track geometry measurements, from location $x = 1$ to $x = n$. In this case, a longitudinal level at location x , $LL(x)$, is a considered track geometry parameter. Defects must provide a higher longitudinal level than the established limit value, \widehat{LL} .

$\text{defect}_{\text{ABA}}$ is the number of defects regarding ABA measurements, from location $x = 1$ to $x = n$. To identify defects, the SAWP (ABA energy) at location x , $\text{SAWP}(x)$, is considered. Defects must provide higher SAWP than the minimum SAWP at locations with a longitudinal level equal to the limit value.

A positive KPI value suggests that ABA measurements more effectively detect defects than track geometry parameter measurements, indicating a higher capability for assessing track conditions, particularly in the embankment component.

5.4.5.2. KPI2. Detectability of incipient known failures

- **Short description.** At baseline, incipient faults are either detected through regular inspections (noticed, reported, and assessed by ad-hoc inspection) or, worst case, through failure if the fault is fully developed. Regular inspections may not capture all relevant faults at a sufficiently early stage, e.g., due to accessibility or due to long periods between inspections. Early detection will increase safety and give time to plan and execute maintenance actions at a lower overall cost without compromising safety. If successful, the numerical model coupled with data from continuous monitoring instrumentation will enable describing the properties and behaviour of the bridge and transition zones in much greater

detail than what can be provided by instrumentation. This will provide insight on the link between the measurements and degradation mechanisms. Defects and damage may also be introduced to study their impact on the bridge response. This allows earlier prediction of failure. However, it is important to note that predictions made by a simulation must be understood within the context of model validity and assumptions.

- **How to compute de KPI.** The KPI will be computed based on a statistical comparison of performance on the detectability of known incipient faults compared with regular baseline inspection (manual inspection). The KPI will be computed by:

$$\text{KPI2} = \frac{n_{mon}}{n_{mon} + m_{ins}} \times 100 (\%),$$

where n_{mon} is the number of faults detected by the monitoring system deployed in this project, while m_{ins} is the number of faults detected by inspection or other means without first being detected by the monitoring system. The main failure cases targeted will be:

1. Loss of prestress in tendons,
2. Loss of stiffness in transition zones.

The KPI will be calculated individually for the two failure cases.

6. Architecture and Data Interoperability

6.1. Architecture

The general architecture of this work package can be associated to the structure of a database. The dependencies between the tables of this database represent how Infra-managers (owning the sites) and technology providers (performing the measurements & processing) interacts during the works of this WP. Data upload follows the typical rigid rules of database data injection, implying interoperability and data homogeneity. The database provides a convenient interface between the UCs of this work package. Furthermore, once this database is filled, it will enable data retrievability, aligning to the FAIR principles in terms of Findability and Accessibility (providing data owner concede access). This database can then be exposed to other 'FA' (Transversal topics) within ERJU to implement the two remaining 'IR' attributes (Interoperability and Reusability).

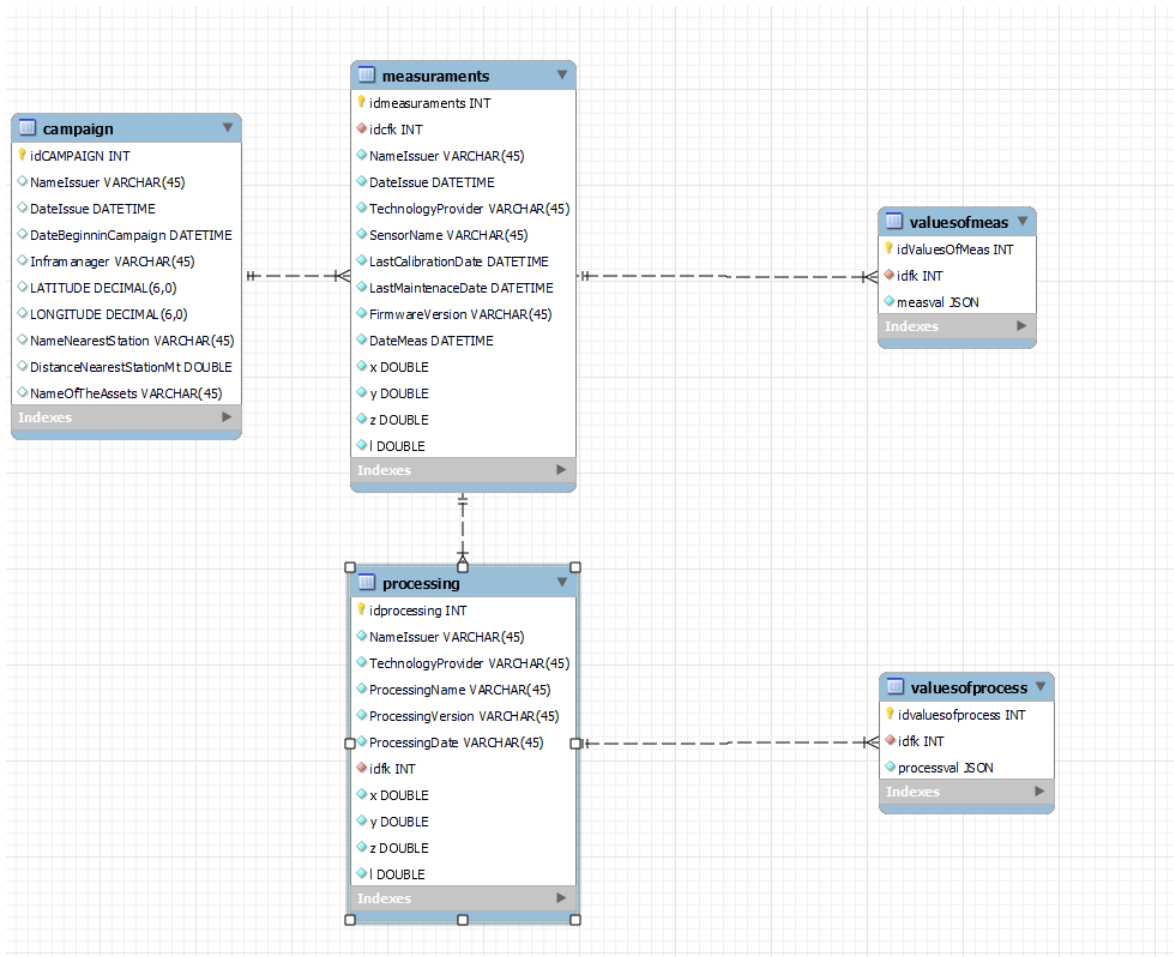


Figure 13.WP 12 Database structure (Oracle MySql WorkBench).

6.1.1. Campaign Table

Each test site is most likely owned by an Infra-manager. In this view, the fields' description is as follows:

- Inframanager: Name of the Infra-manager managing or owning the site (eg. FSI, ADIF, SNCF).
- NameOfTheAsset: Name of the asset or of the location (eg. Viadotto Pugliese).
- Latitude: Latitude of the centre of mass of the site (eg. 41.11148).
- Longitude: Longitude of the centre of mass of the site (eg. 16.8554).
- NameNearestStation: Name of the nearest station (eg. Bari Central Station).
- DistanceNearestStation: Linear Distance along the track from the nearest station (30 km).
- NameIssuer: Name of the person who created this record (es. Vincenzo Scarnera).
- DateIssuer: Creation date of this record (01/01/2024).
- DateBeginningCampaign: Date of the start measurement of the campaign on this site (01/02/2024).

The Campaign Table is connected to the children tables ("measurements") in a one-to-many fashion.

6.1.2. Measurement Table

In each campaign/site, different technology providers could be operating at the same time. The technology provider performing a measurement on a specific site shall declare a record for this table. In this view, the fields' description is described as follows:

- NameIssuer: Name of the person who created this record.
- DateIssue: Creation date of this record (includes minutes and seconds).
- TechnologyProvider: Name of the technology provider (eg. Mermec).
- SensorName: Name of the sensor (eg. Track Geometry, geophone, georadar).
- LastCalibrationDate: Date of the last calibration for the sensor.
- LastMaintenanceDate: Date of the last maintenance for this sensor.
- Firmwareversion: Version of the firmware currently installed.
- X,Y,Z,L: coordinate of the sensor relative to the centre of mass declared in the parent Campaign.
- L: Linear coordinate (along the track) of the sensor relative to the centre of mass declared in the parent Campaign.

NOTE: X,Y,Z,L indicate the point where the sensor is located at the beginning of the measurement and not necessary where the measurement comes from. For instance, a geophone is fixed, but the measurement comes from underground. Same thing for a moving measuring vehicle: the initial location is to be indicated.

The Measurement Table is connected to the children tables ("valueofmeas") in a one-to-many fashion.

VALUE OF MEAS TABLE: Whilst the Measurement table refers to the instance of the measurement

(when, how, by who), the table “valueofmeas”, refers to the value of the measurements itself (time, voltages, temperatures etc). The valueofmeas table leverage on the agility of JSON format.

Let us say, for example, that 100 values of temperature at consecutive times were gathered at the same site, same day, same spot, same date, same person, same sensor. In this example the architecture calls for: 1 record in the table measurements connected to 100 records in the valueofmeas table.

Carrying on, let us say, that another 321 values of temperatures need to be taken during the same day, at same site, same spot, by same person & same sensor of the example above. In this case another record for the ‘measurement’ table needs to be instantiated with another DateIssue (different minutes). To this record, 321 records will be associated in the children table “valueofmeas”.

6.1.3. Processing Table

The Measurement Table is connected to the children tables (“processing”) in a one-to-many fashion. Each measurement can be, in principle, associated with several kind of processing (one-to-many relationship). In this view, the fields’ description is as follows:

- NameIssuer: Name of the person who created this record.
- DateIssue: Creation date of this record (includes minutes and seconds).
- TechnologyProvider: Name of the technology provider (eg. Mermec).
- Processing Name.
- Processing Version.
- Processing Date.
- X,Y,Z,L: coordinate of the processed zone, relative to the centre of mass declared in the parent folder Measurement . These should be by default the same of the parent table (‘measurement’), however a sensor located in a place could generate data processing that refers to another place (ranging sensors).

6.1.4. Tables ‘valueofmeas’ and ‘valueofproc’

The tables ‘valueofmeas’ and ‘valueofproc’ contain respectively the value of the measurement and of the processing. These tables leverage on the flexibility of the JSON format, so each entry can have multiple values. Unlike in all the other table presented, the format of these entries is not predefined in the database, but it is rather managed at last by the operator performing the SQL injection.

DateTime	Voltage	Current	Temperature	Acceleration	Humidity	Temperature
----------	---------	---------	-------------	--------------	----------	-------------

Table 2. Example of Versatile JSON entry for measurements and processing

The table above exemplify one hypothetical record that could be injected in these tables. At a determined time stamp (DateTime), the values read for voltages, currents, temperature, acceleration, humidity & Temperature are all uploaded, giving rise to a record.

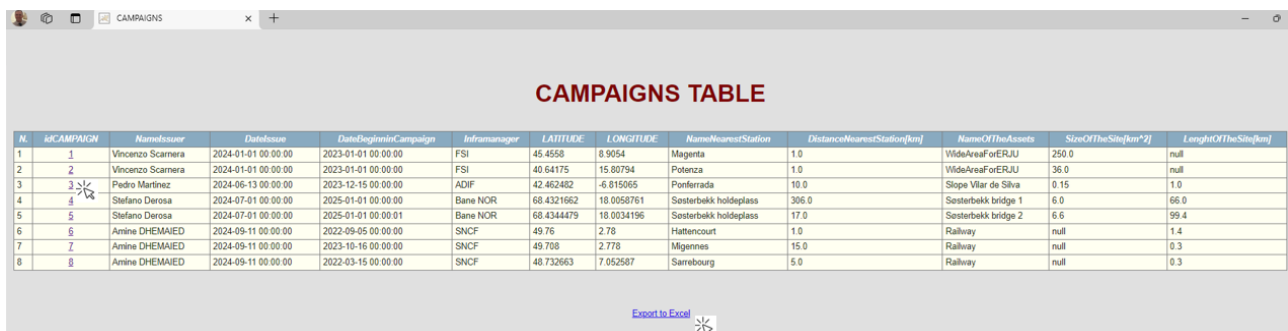
6.2. User Interface

A web interface has been built to visualise the data of the interoperability database. In this way, users that have no SQL knowledge, can freely browse and inject WP12-13 contents, as described by the databases tables.



Figure 14. WP 12/13 Data Explorer web interface (Apache Tomcat). Home page.

The interface runs on whichever computer endowed with internet browser. Clicking on 'View campaign' is the entry point to search through the children tables (e.g. Measurement, Campaigns).



N.	IDCAMPAGN	NameIssuer	DateIssue	DateBegininCampaign	Inframanager	LATITUDE	LONGITUDE	NameNearestStation	DistanceNearestStation[km]	NameOfTheAssets	SizeOfTheSite[km*2]	LengthOfTheSite[km]
1	1	Vincenzo Scamera	2024-01-01 00:00:00	2023-01-01 00:00:00	FSI	45.4558	8.9054	Magenta	1.0	VideAreaForERJU	250.0	null
2	2	Vincenzo Scamera	2024-01-01 00:00:00	2023-01-01 00:00:00	FSI	40.64175	15.20794	Polenza	1.0	VideAreaForERJU	36.0	null
3	3	Pedro Martinez	2024-06-13 00:00:00	2023-12-15 00:00:00	ADIF	42.462482	-6.815065	Ponferrada	10.0	Slope Vilar de Silva	0.15	1.0
4	4	Stefano Derosa	2024-07-01 00:00:00	2025-01-01 00:00:00	Bane NOR	68.4321662	18.0058761	Søsterbakk hoidglass	306.0	Søsterbakk bridge 1	6.0	66.0
5	5	Stefano Derosa	2024-07-01 00:00:00	2025-01-01 00:00:01	Bane NOR	68.4344479	18.0034196	Søsterbakk hoidglass	17.0	Søsterbakk bridge 2	6.6	99.4
6	6	Amine DHEMAIED	2024-09-11 00:00:00	2022-09-05 00:00:00	SNCF	49.76	2.78	Hattenecourt	1.0	Railway	null	1.4
7	7	Amine DHEMAIED	2024-09-11 00:00:00	2023-10-16 00:00:00	SNCF	49.708	2.778	Migennes	15.0	Railway	null	0.3
8	8	Amine DHEMAIED	2024-09-11 00:00:00	2022-03-15 00:00:00	SNCF	48.732663	7.052587	Sarrebourg	5.0	Railway	null	0.3

Figure 15. WP 12/13 Data Explorer we interface (Apache Tomcat). Campaigns Table.

As shown in Figure 15, so far, there are 8 Campaigns (sites) listed. The information pertaining the overall geography of the sites, along with the owner of the site are all listed in this view. The entries viewed can be exported by mean of the 'Export to Excel' link.

To find out more about the multiple measurements taken in any of these Campaigns (Sites), the user can click to the correspondent 'idCampaign' column (as indicated by the mouse cursor). In this way, for instance, the measurements conducted in the site of Ponferrada will appear in the Measurement view.

MEASUREMENTS TABLE																
N.	Idmeasurement	idcfr	NameIssuer	DateIssue	TechnologyProvider	SensorName	LastCalibrationDate	LastMaintenanceDate	FirmwareVersion	DateMeas	x	y	z	l	latitude	longitude
1	17	3	ADIF	2024-06-13 00:00:00	WORLDSENSING	Tiltometer- 91776	2023-12-15 00:00:00	2023-12-15 00:00:00	1	2023-12-15 00:00:00	0.0	0.0	0.0	0.0	-42.46326111	-6.816294444
2	18	3	ADIF	2024-06-13 00:00:01	WORLDSENSING	Tiltometer- 91785	2023-12-15 00:00:00	2023-12-15 00:00:00	1	2023-12-15 00:00:00	0.0	0.0	0.0	0.0	-42.46381944	-6.815913889
3	19	3	ADIF	2024-06-13 00:00:02	WORLDSENSING	Tiltometer- 91848	2023-12-15 00:00:00	2023-12-15 00:00:00	1	2023-12-15 00:00:00	0.0	0.0	0.0	0.0	-42.46345278	-6.815447222
4	20	3	ADIF	2024-06-13 00:00:03	WORLDSENSING	Tiltometer- 91858	2023-12-15 00:00:00	2023-12-15 00:00:00	1	2023-12-15 00:00:00	0.0	0.0	0.0	0.0	-42.46285833	-6.815613889
5	21	3	ADIF	2024-06-13 00:00:04	WORLDSENSING	Tiltometer- 91909	2023-12-15 00:00:00	2023-12-15 00:00:00	1	2023-12-15 00:00:00	0.0	0.0	0.0	0.0	-42.46245	-6.815336111
6	22	3	ADIF	2024-06-13 00:00:05	WORLDSENSING	Tiltometer- 91973	2023-12-15 00:00:00	2023-12-15 00:00:00	1	2023-12-15 00:00:00	0.0	0.0	0.0	0.0	-42.46294444	-6.815388889
7	23	3	ADIF	2024-06-13 00:00:06	WORLDSENSING	Tiltometer- 91979	2023-12-15 00:00:00	2023-12-15 00:00:00	1	2023-12-15 00:00:00	0.0	0.0	0.0	0.0	-42.46348889	-6.817347222
8	24	3	ADIF	2024-06-13 00:00:07	WORLDSENSING	Tiltometer - 91987	2023-12-15 00:00:00	2023-12-15 00:00:00	1	2023-12-15 00:00:00	0.0	0.0	0.0	0.0	-42.46267778	-6.815744444
9	25	3	ADIF	2024-06-13 00:00:08	WORLDSENSING	Tiltometer - 91988	2023-12-15 00:00:00	2023-12-15 00:00:00	1	2023-12-15 00:00:00	0.0	0.0	0.0	0.0	-42.46256667	-6.816022222
10	26	3	ADIF	2024-06-13 00:00:09	WORLDSENSING	Tiltometer - 91993	2023-12-15 00:00:00	2023-12-15 00:00:00	1	2023-12-15 00:00:00	0.0	0.0	0.0	0.0	-42.46218889	-6.815230556
11	27	3	ADIF	2024-06-13 00:00:10	WORLDSENSING	Tiltometer - 92002	2023-12-15 00:00:00	2023-12-15 00:00:00	1	2023-12-15 00:00:00	0.0	0.0	0.0	0.0	-42.46235	-6.815152778
12	28	3	ADIF	2024-06-13 00:00:11	WORLDSENSING	Tiltometer - 92029	2023-12-15 00:00:00	2023-12-15 00:00:00	1	2023-12-15 00:00:00	0.0	0.0	0.0	0.0	-42.46237778	-6.81515
13	29	3	ADIF	2024-06-13 00:00:12	WORLDSENSING	Tiltometer - 102876	2023-12-15 00:00:00	2023-12-15 00:00:00	1	2023-12-15 00:00:00	0.0	0.0	0.0	0.0	-42.46254722	-6.815063889
14	30	3	ADIF	2024-06-13 00:00:13	WORLDSENSING	Tiltometer - 103220	2023-12-15 00:00:00	2023-12-15 00:00:00	1	2023-12-15 00:00:00	0.0	0.0	0.0	0.0	-42.46275556	-6.815041667
15	31	3	ADIF	2024-06-13 00:00:14	WORLDSENSING	Tiltometer - 103799	2023-12-15 00:00:00	2023-12-15 00:00:00	1	2023-12-15 00:00:00	0.0	0.0	0.0	0.0	-42.462975	-6.815033333
16	32	3	ADIF	2024-06-13 00:00:15	WORLDSENSING	Tiltometer - 103364	2023-12-15 00:00:00	2023-12-15 00:00:00	1	2023-12-15 00:00:00	0.0	0.0	0.0	0.0	-42.46236111	-6.815111111
17	33	3	ADIF	2024-06-13 00:00:16	WORLDSENSING	Tiltometer - 115792	2023-12-15 00:00:00	2023-12-15 00:00:00	1	2023-12-15 00:00:00	0.0	0.0	0.0	0.0	-42.463767	-6.817296

Figure 16. WP 12/13 Data Explorer we interface (Apache Tomcat). Measurements Table.

Figure 16 lists the measurement lot performed by WORLDSENSING by mean of 17 Tiltometers in the site pointed by the parent table (Ponferrada). This view nails the sensors' location for the measurements, along with their condition (Start of the acquisition, calibration date, firmware etcetera). As explained, the coordinate of the device, in this view, can either be relative to the centre of gravity of the parent 'Campaign' record, or absolute (in this case we have the absolute longitude latitude of the 17 tiltometers). The entries viewed can be exported by mean of the 'Export to Excel' link.

Generally speaking, more sensors can be jointly exploited to create one or more processing. In the case above, we have the 11 sensors that are used together to trigger a 'Soil Alarm'. The 'Soil Alarm' is a processing. Clicking on 'IdMeasurement=33' (as indicated by the mouse cursor in Figure 17), will open the Processing view, pertaining the correspondently clicked Tiltometer-115792, plus all those that jointly contribute to the 'Soil Alarm'.

VIEW MEASUREMENTS

X

MERGED PROCESSING NAMES

N.	Idprocessing	idfk	NameIssuer	TechnologyProvider	ProcessingName	ProcessingVersion	ProcessingDate	x	y	z	l
1	19	17	Jose Solis	Cemosa	Soil Alarm	1	2024-03-15 00:00:00	0.0	0.0	0.0	0.0
2	20	18	Jose Solis	Cemosa	Soil Alarm	1	2024-03-15 00:00:00	0.0	0.0	0.0	0.0
3	21	19	Jose Solis	Cemosa	Soil Alarm	1	2024-03-15 00:00:00	0.0	0.0	0.0	0.0
4	22	20	Jose Solis	Cemosa	Soil Alarm	1	2024-03-15 00:00:00	0.0	0.0	0.0	0.0
5	23	21	Jose Solis	Cemosa	Soil Alarm	1	2024-03-15 00:00:00	0.0	0.0	0.0	0.0
6	24	22	Jose Solis	Cemosa	Soil Alarm	1	2024-03-15 00:00:00	0.0	0.0	0.0	0.0
7	25	23	Jose Solis	Cemosa	Soil Alarm	1	2024-03-15 00:00:00	0.0	0.0	0.0	0.0
8	26	29	Jose Solis	Cemosa	Soil Alarm	1	2024-03-15 00:00:00	0.0	0.0	0.0	0.0
9	27	30	Jose Solis	Cemosa	Soil Alarm	1	2024-03-15 00:00:00	0.0	0.0	0.0	0.0
10	28	31	Jose Solis	Cemosa	Soil Alarm	1	2024-03-15 00:00:00	0.0	0.0	0.0	0.0
11	29	32	Jose Solis	Cemosa	Soil Alarm	1	2024-03-15 00:00:00	0.0	0.0	0.0	0.0

[Export to Excel](#)

Figure 17. WP 12/13 Data Explorer we interface (Apache Tomcat). Processing Table.

In another processing insisting on this site, five sensors are jointly used to generate a 'Rock Tunnel Alarm'. Clicking on 'IdMeasurement=24' will open the Processing view, pertaining Tiltometer-91987 and all those Tiltometers that contribute to the 'Rock Tunnel Alarm'. The entries viewed can be exported by mean of the 'Export to Excel' link.

MERGED PROCESSING NAMES

N.	idprocessing	idfk	Name/issuer	Technology/Provider	ProcessingName	ProcessingVersion	ProcessingDate	x	y	z	i
1	30	24	Jose Solis	Cemosa	Rock Tunnel Alarm	1	2024-03-15 00:00:00	0.0	0.0	0.0	0.0
2	31	25	Jose Solis	Cemosa	Rock Tunnel Alarm	1	2024-03-15 00:00:00	0.0	0.0	0.0	0.0
3	32	26	Jose Solis	Cemosa	Rock Tunnel Alarm	1	2024-03-15 00:00:00	0.0	0.0	0.0	0.0
4	33	27	Jose Solis	Cemosa	Rock Tunnel Alarm	1	2024-03-15 00:00:00	0.0	0.0	0.0	0.0
5	34	28	Jose Solis	Cemosa	Rock Tunnel Alarm	1	2024-03-15 00:00:00	0.0	0.0	0.0	0.0

[Export to Excel](#)

Figure 18. WP 12/13 Data Explorer we interface (Apache Tomcat). Processing Table.

Clicking on the 'VIEW ALL' of the home page (Figure 18) will let the user have access to the whole lot of Campigns/Measurement/Processing in one go (Figure 19), by mean of a cross inner join permed across all table. Disposing of all data will enable further processing & management related operations.



Figure 19. ALL WP12-13 data view (there are already 115 rows and 40 columns).

The button 'UPLOAD DATA' (Figure 20) allows the user to update the database, by injecting entries in the tables. Once clicked, the user is asked to upload .xls files, containing the entries.

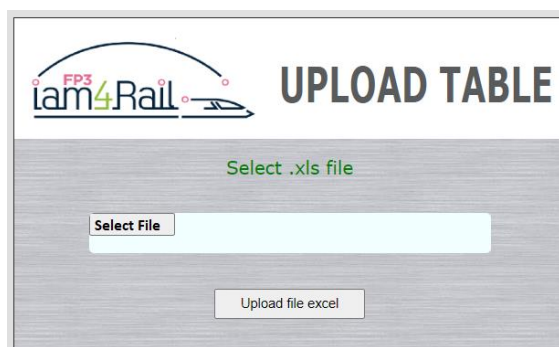


Figure 20. Upload Table Pop Up.

The xls. Files for the injection must mirror the format of the file obtained when clicking on 'Export to Excel'. This simplifies enormously the procedure, once again allowing a user not having any SQL skill, to perform otherwise complicated database injection.

6.3. Standards

To limit the problems related to technical interoperability, the standard used in the UC have been homogenised as much as possible and clearly stated. In this section the standards applied are initially presented for the standards, interoperability and retrievability part and then specified for each use case.

6.3.1. Standards used for interoperability & retrievability.

Data interoperability database (My SQL Workbench by Oracle Corporation)

- ANSI SQL (SQL-92, SQL:1999, SQL:200)
- JDBC (Java Database Connectivity)
- ODBC (Open Database Connectivity)

Data interoperability web interface (Apache Tomcat)

- Jakarta EE standards (Servlet, Pages, Expression Language, WebSocket, Annotations)

6.3.2. Standards used in in Multiscale Monitoring of Civil Assets (Italy).

Main standards are used for the project in the frame of spaceborn application:

- Hdf5 (Hierarchical Data Format) for SAR Data (e.g. used in mission like Sentinel-1C, CSK/CSG)
- TIF (Tagged Image File Format) for Multispectral Data (e.g. used in mission like Pleiades NEO)
- KML (Google Earth open format) for polygons delimiting area of interest.
- LAS (Lidar Laser) for point clouds used in training data.
- PT (PyTorch Model format) to store the weights and parameters of trained AI PyTorch models.

Main standards are used for the project for UAV application:

- TIF (Tagged Image File Format) for RGB images, multispectral images, DTM (Digital Terrain Model) and DSM (Digital Surface Model);
- LAS (Lidar Laser) for point clouds.
- PT (PyTorch Model format) to store the weights and parameters of trained AI PyTorch models.

6.3.3. Standards used in Bridges and Earthworks Asset Management aided by Geotechnics (Spain).

- MQTT (Message Queuing Telemetry Transport) with SSL/TLS protocol for communications and data confidentiality.
- JSON (JavaScript Object Notation) as a lightweight format for storing and transporting data.

6.3.4. Standards used in Monitoring of tunnel, sub-ballast layers, subsoil (France).

The standards are presented following the developments they are relative of:

- Evaluation of mechanical properties of sub-ballast layers and subsoil. Main standards are used for the project from geophysical instruments and processing:
 - DAT for binary measurements.
 - NPY python format.
 - Tiff (tag image file format).
- High efficiency tunnel inspection systems and predictive maintenance for tunnels.
 - LAS (Lidar Laser) for point clouds.
 - TIF (Tagged Image File Format) for Multispectra Data.
 - OBJ (wavefront 3D object file) for 3D models of tunnels.
 - Tiff (tag image file format) for ortophotography and damages maps.
 - DWG (DraWinG) for damages maps.
- Passive contactless magnetic microwire sensor.
 - The data to be employed in this UC will be derived from laboratory tests.

6.3.5. Standards in Data analysis for condition monitoring (The Netherlands, Norway).

The following standards will be used during the project:

- ISO 5725-2:2019 (E) "Accuracy (trueness and precision) of measurement methods and results – Part 2: Basic method for determination of repeatability and reproducibility of a standard measurement method".
- EN13306:2017(E) "Maintenance – Maintenance Terminology".
- ISO 16587:2004 "Mechanical vibration and shock – Performance parameters for condition monitoring of structures".
- ISO 14963:2003 "Mechanical vibration and shock – Guidelines for dynamic tests and investigations on bridges and viaducts".
- UIC 778-4R:2009 "Defects in railway bridges and procedures for maintenance".

- EN 13848-1: “Railway applications - Track - Track geometry quality - Part 1: Characterization of track geometry”.
- EN 13848-2: “Railway applications - Track - Track geometry quality - Part 2: Measuring systems - Track recording vehicles”.
- EN 13848-5: “Railway applications - Track - Track geometry quality - Part 5: Geometric quality levels - Plain line, switches and crossings”.
- EN 13848-6: “Railway applications - Track - Track geometry quality - Part 6: Characterisation of track geometry quality”.

7. Civil engineering inspection and monitoring technologies: Installation and initial data collection

This section provides detailed information on the current development status of each project Use Case technology. The following sections, whenever applicable to the use case /technology, cover the following trends:

- Selected equipment, technical specifications, and justification.
- Data selection and collection.
- Algorithms and implementation.
- Preliminary results.
- Workflow.
- Demonstration Plan.

7.1. Multiscale Monitoring of Civil Assets (Italy)

7.1.1. Vegetation encroachment and asset recognition

7.1.1.1. Data selection, collection and processes

The supervised training process of a neural network requires a pair of complementary data types: the raw data and the ground truth data. The ground truth data teaches the network what it should learn from the raw data.

The preliminary geographical area covered by available data is in the Basilicata region, in the vicinity of Potenza. We dispose of multispectral satellite orthoimage with 6 bands (R, G, B, NIR, Red Edge, and Deep Blue) and a resolution of 0.30 m.



Figure 21. 30 cm resolution orthoimage for neural network training.

The ground truth data, obtained through an aerial survey, consists of a classified point cloud. This means that each point carries not only the information of the object's elevation, but also other types of information, such as the object's class, which can be one of the following: terrain, vegetation or buildings.

The Canopy Height Model (CHM) is obtained from the difference between the Digital Surface Model (DSM) and the Digital Terrain Model (DTM). The DSM and the DTM, along with the point cloud, have a resolution of 1 m. In the CHM the pixel values represent the height calculated from the normalized ground, in meters.

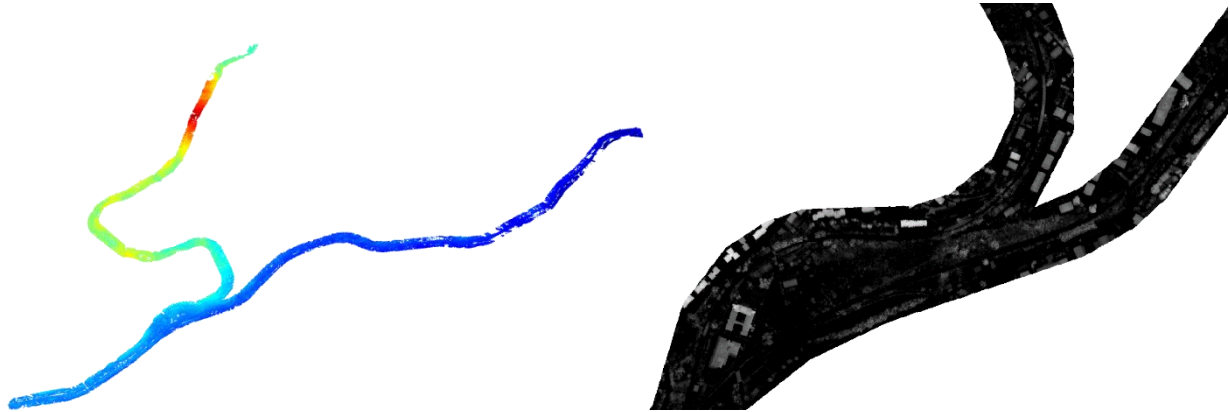


Figure 22. Ground truth data: classified point cloud from aerial survey (left) and CHM (right).

From the point cloud, additional ground truth data are extracted and used to maximize the information provided to the neural network. This additional piece of data consists of a segmentation mask, created by generating a grid where each cell has a side length of 0.30 m, analogous to the resolution of the satellite orthoimage. For each cell, the density of points in each class is assessed. Each cell thus represents a pixel and is assigned to the class with the highest point density. If no points are present in a pixel, the "vegetation" class is assigned to it by default. In this way, the network will be fed with the information of each asset classification in the image. Below, a portion of the segmentation mask is shown. The three classes are identified by a different grey scale value.



Figure 23. Additional ground truth data: classification map.

Since the areas of the raw data and the ground truth data do not perfectly coincide, only the intersection area, represented in the figure below by the green polygon, is retained for the training.



Figure 24. Intersection of the areas.

In the end, a total area of 1.26 km² is covered, of which 0.68 km² (54.4%) is classified as terrain, 0.46 km² (36.3%) as vegetation and 0.12 km² (9.31%) as buildings.

From this area, 4530 tiles of 128x128 pixels are extracted, which are then quadrupled through data augmentation, obtaining a total of 18120 tiles to be redistributed in the neural network dataset.

7.1.1.2. Algorithms and implementation

For the purposes of the project, a neural model pipeline has been developed, which varies depending on whether the classified point cloud relative to the orthoimage is available. If so, the classification map can be extracted from the point cloud. Otherwise, it will have to be obtained as a result of training another dedicated neural network.

1. Pipeline for training

The pipeline structure is displayed in the following image.

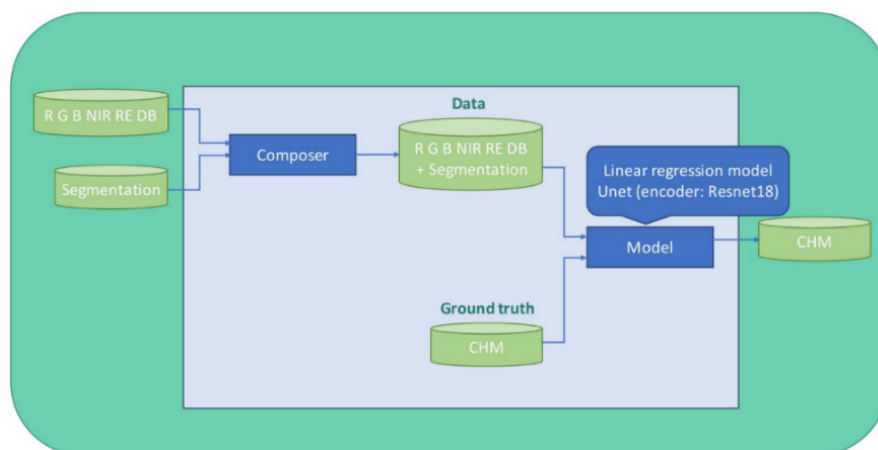


Figure 25. Pipeline structure for training with available classification map.

The neural network model of choice is a simple U-Net with a ResNet18 encoder and a linear activation function in the final layer, designed to complete a linear regression task.

The model is provided with a composite data input with 10 channels, where the first 6 are

the multispectral bands and the last 4 channels are the Boolean masks obtained by filtering the various classes from the assets' classification map. The fourth-to-last channel is reserved to the "background", which included all the pixels not associated with the 3 classes of interest.

2. Pipeline for inference

In the eventuality of having to predict a CHM using only a multispectral satellite image, the data should be adequately prepared to be submitted to the linear regression model for inference. This would mean being able to produce a classification map, to fill the last four channels of the data. To achieve this goal, a chain of two models where the first would be responsible for producing the segmentation mask and the second the CHM has been designed. An intermediate phase would combine the output of the first model with the 6 bands of the multispectral image, preparing the data for the second model.

Below is a schematic representation of the designed model chain.

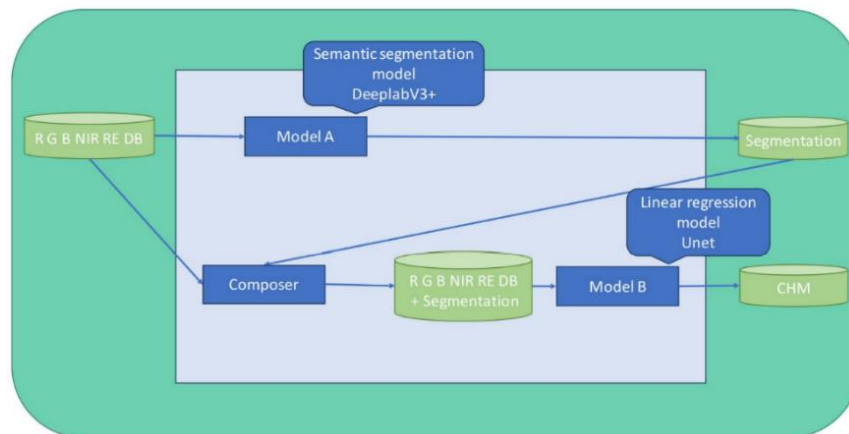


Figure 26. Pipeline structure for inference.

The first neural network could be a DeepLabV3+, a state-of-the-art model for solving semantic segmentation tasks.

7.1.1.3. Workflow

The workflow entails three main phases: preprocessing, neural network training and analysis of the extracted predictions.

- **Preprocessing of the data**

The data in input are resampled to the same resolution of 0.30 m and cut to the intersection between the data and the ground truth. The available area is then subdivided into 128,128 pixel tiles, with an overlap of 64 pixels on each side. This will reduce discontinuity effects on the predicted tiles borders and provide a better understanding of the context on the neural network part. The number of tiles is increased through reflections along the x-axis and y-axis.

Finally, the tiles are distributed into the training, validation and test sets. The first two portions will be actively used by the network for learning, while the test portion will remain unseen by the network and will be used to evaluate the quality of the training results, as ground truth data are still available for comparison.

- **Training**

Two training processes are conducted for the first type of pipeline and for the second type of pipeline.

- Training with available classification map

In this case the classification map is extracted from the point cloud, so there is only one neural network to train, that is, the U-Net. The table below shows the parameters used for the training.

	Input Data	Input Label	Dataset sets %	Training Batch Size	Validation Batch Size	Learning Rate Adam Optim.	Loss Function	Metric
Model	Multispectral satellite orthoimages + Classif. map Shape: (128,128,10)	CHM Shape: (128,128,1)	Training: 85% (15402) Validation: 10% (1812) Test: 5% (906)	32	16	0.01	MAE	MAE

Table 3. Training paraments.

The metric evaluated during training, which coincided with the loss function used, was the Mean Absolute Error (MAE).

- Training with no available classification map

If the only available data are the multispectral orthoimage, it is necessary to have a pre-trained semantic segmentation model that can output a classification map from the input multispectral orthoimage. This model, which we will call Model A, must therefore undergo its own training process before becoming part of the pipeline. The characteristics of the training for the model that extracts the predicted CHM, which we will call Model B, are the same as previously described.

Here is the table of parameters for the two training processes.

	Input Data	Input Label	Training Batch Size	Validation Batch Size	Learning Rate Adam Optim.	Loss Function	Metric
Model A	Multispectral satellite orthoimages Shape: (128,128,6)	Classif. map from clasified point cloud Shape: (128,128,1)	32	16	0.0001	Dice Loss	IoU
Model B	Multispectral satellite orthoimages + Classif. map Shape: (128,128,10)	CHM Shape: (128,128,1)	32	16	0.01	MAE	MAE

Table 4. Training paraments for the two models

For model A, the metric evaluated during training is the mean Intersection over Union (mIoU), while the loss function is the Dice Loss.

- Results analysis**

The final phase of the workflow is the extraction of CHM predictions by the best trained model from those parts of the orthoimage that were placed in the test set and had not been seen by the network during training. These results are then evaluated against the ground truth data to assess the effectiveness of the model.

7.1.1.4. Preliminary Results

In this section, the evaluation of the results obtained for each of the three classes of interest is presented: terrain, vegetation, buildings.

A distinction is made between the results of the first type of pipeline and the ones of the second type of pipeline.

1. Training with available classification map from point cloud

- Terrain

As evident from the comparison between the histograms of the predicted values and the ground truth values, and from the histogram of their difference, the model predicts the CHM with high precision for this class, differing on average by 0.51 m.

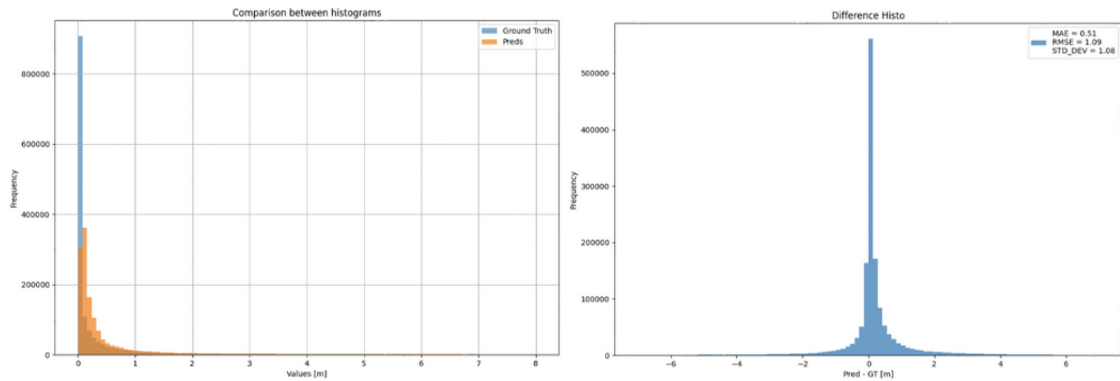


Figure 27. Left: comparison between histograms of predicted and ground truth values for the “Terrain” class. Right: Difference histogram.

Even from the raster of the differences, it is possible to observe how for the "Terrain" class the discrepancy between the predicted CHM and the ground truth is close to 0. It should be noted that this class was the most represented, covering 54.4% of the total area.

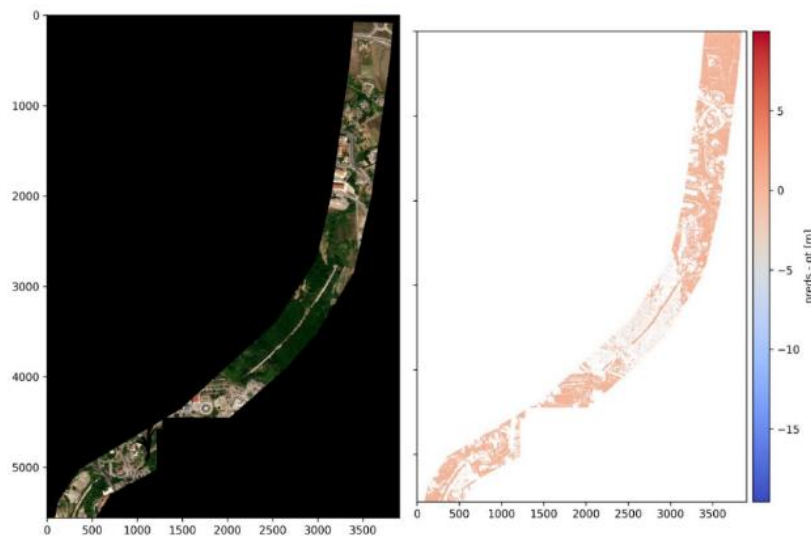


Figure 28. Raster of the difference between the predicted CHM and the ground truth for the “Terrain” class.

- Vegetation

For the "Vegetation" class, which is of the greatest interest, we see that while the height distribution of the ground truth data presents a single peak corresponding to a CHM of a few meters and then has a roughly monotonically decreasing decline, the predicted values distribution has two peaks, one around 0 m and one around 10 m.

On average, the predicted values differ from the ground truth by approximately 3.11 m.

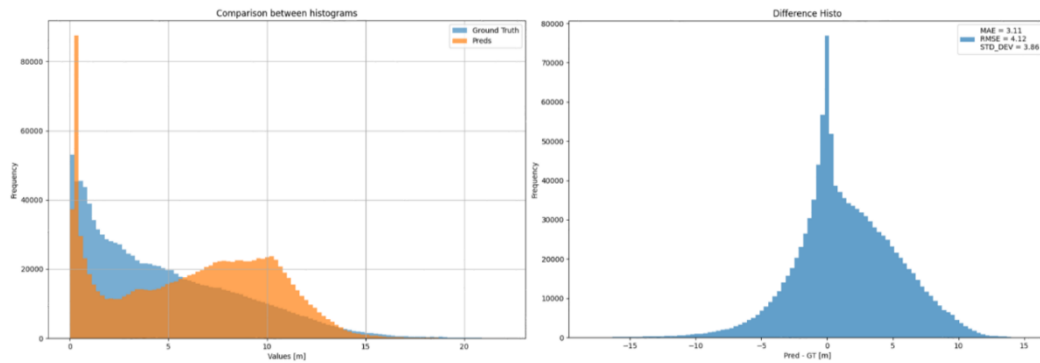


Figure 29. Left: comparison between histograms of predicted and ground truth values for the “Vegetation” class. Right: Difference histogram.

From the histogram of the differences, it is evident that the predominant tendency is towards overestimation, which is preferable to an underestimation tendency, as the latter could lead to erroneously overlooking hazardous situations.

The raster of the differences highlights overestimated regions corresponding to tall and isolated trees, which are likely underrepresented in the available data.

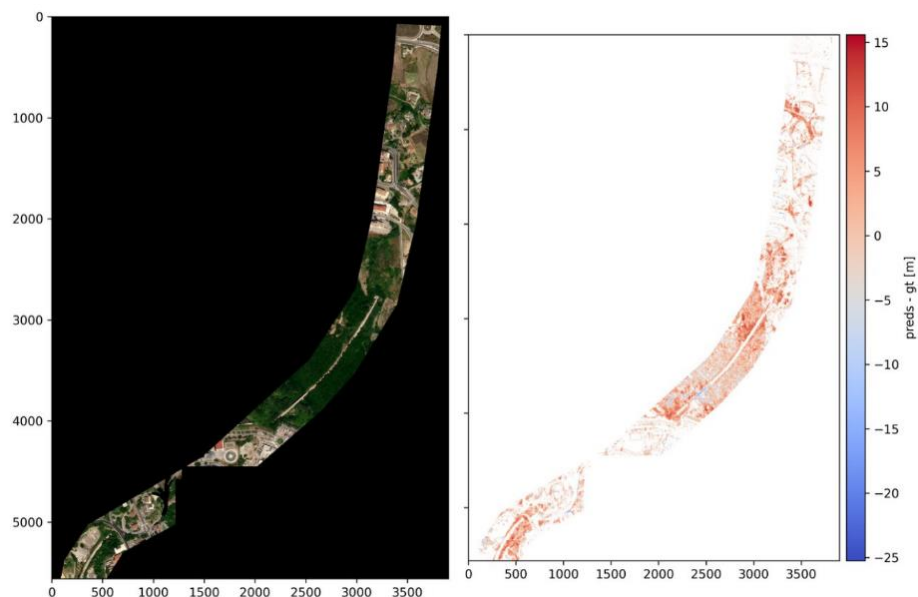


Figure 30. Raster of the difference between the predicted CHM and the ground truth for the “Vegetation” class.

Some pixels are erroneously assigned to the vegetation class due to the method used to construct the segmentation mask for filtering the classes. It should be noted that pixels without points in the point cloud were assigned by default to the vegetation class. Among these pixels, some are located along the railway and are underestimated. This section is actually a viaduct, but the network predicted its height as similar to that of the ground, thus close to 0 m. This example is shown in the image below.

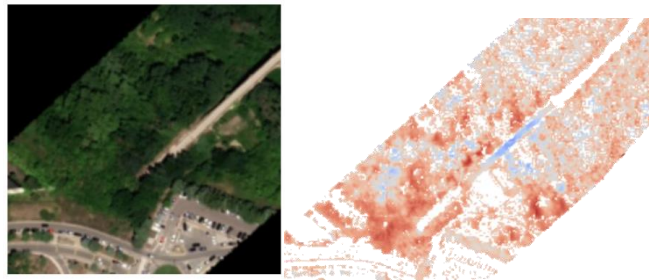


Figure 31. Example of pixels erroneously assigned to the Vegetation class.

- Buildings

Finally, the results obtained for the "Buildings" class are presented, for which we did not have high expectations. The network, in fact, could not learn to recognize them because the examples were too few.

Buildings above 15 m are not recognized and, on average, the error is 6.21 m.

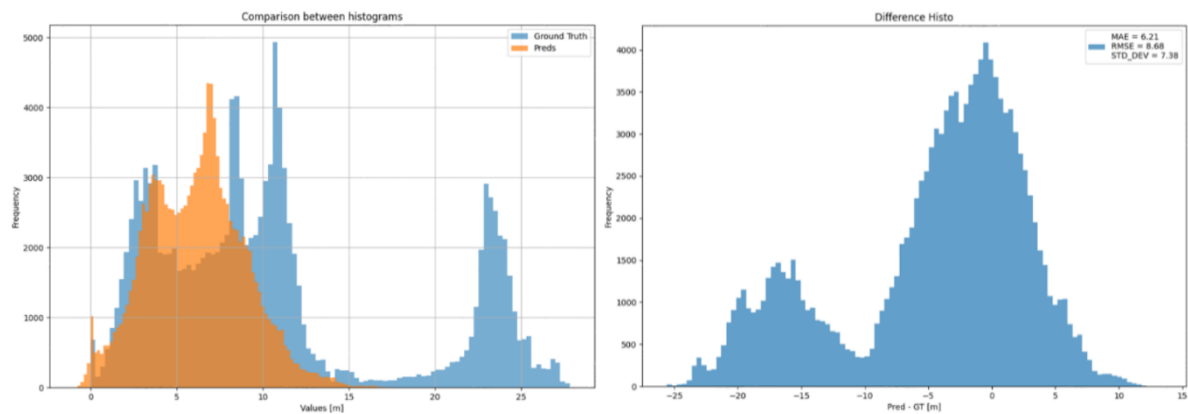


Figure 32. Left: comparison between histograms of predicted and ground truth values for the "Buildings" class. Right: Difference histogram.

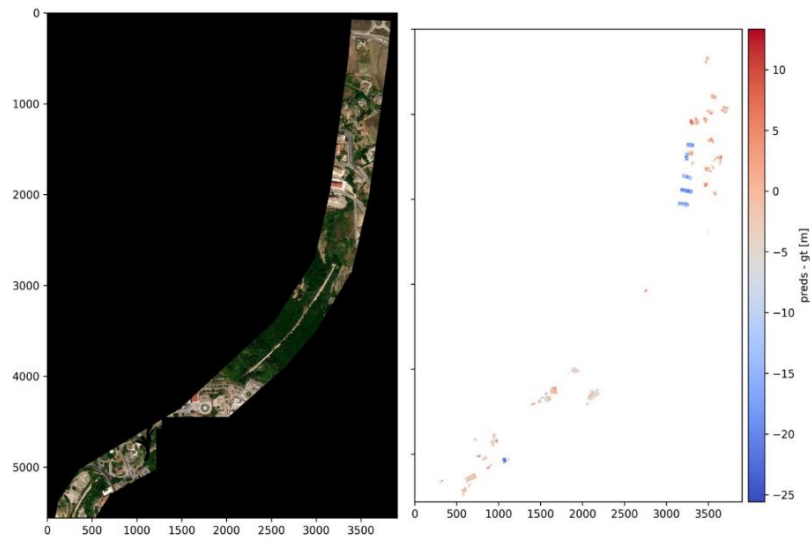


Figure 33. Raster of the difference between the predicted CHM and the ground truth for the “Buildings” class.

2. Training without an available classification map from point cloud

In this case, the classification map was previously predicted by a dedicated semantic segmentation model, specifically a DeepLabV3+.

Here are a few examples of the comparison between the predicted and the point cloud-derived segmentation map:

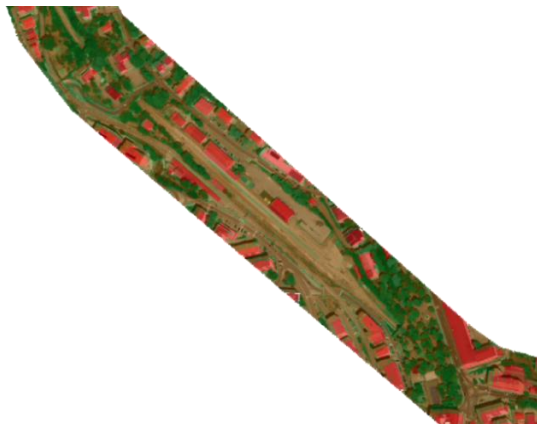


Figure 34. Classif. map from point cloud.

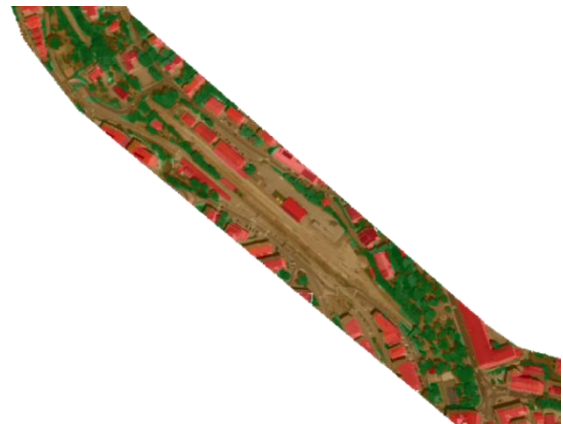


Figure 35. Predicted classification map.



Figure 36. Classif. map from point cloud.



Figure 37. Predicted classification map.

In conclusion, the two segmentation masks are substantially comparable. Moreover, the showcased utilisation of the semantic segmentation model proves how it is possible to recognise assets, paving the way for the recognition of illegal anthropic activities via change detection.

Model B was then trained with the predicted segmentation map as an input.

Below, the results obtained for the Vegetation class are shown.

- Vegetation

The average error is 2.96 m, but in this case, the tendency is towards underestimation. This is unsatisfactory because some hazardous situations could be erroneously overlooked.

Disposing of more data for the training (e.g. WP13), should reduce this error.

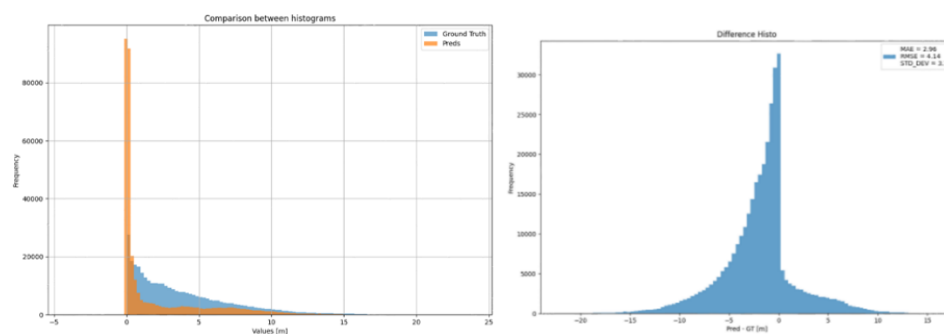


Figure 38. Left: comparison between histograms of predicted and ground truth values for the “Vegetation” class. Right: Difference histogram. Results obtained after training both model A & B.

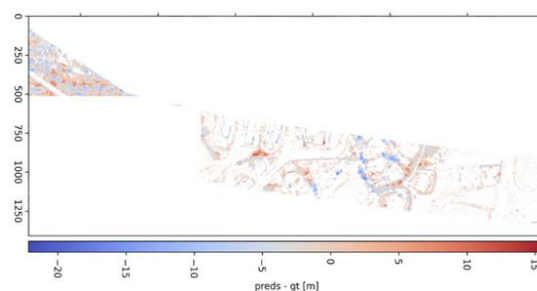


Figure 39. Raster of the difference between the predicted CHM and the ground truth for the “Vegetation” class. Results obtained after training both model A and B.

To conclude, we consider the results promising and with a significant margin for improvement: achieving better results is having a larger amount of data. This would not only allow for a more comprehensive training of Model A and Model B but would also be fundamentally important for achieving the necessary generalization capability for a project dealing with a variable subject like vegetation through photographic images, even if they are multispectral. Vegetation is naturally

subject to seasonal changes, but not only that: in the images, the neural network can rely on variable features such as the shadow cast by the plant. This will depend not only on the height, but also on the time of day or atmospheric conditions.

7.1.1.5. Demonstration Plan

The demonstration plan will involve the training of the artificial intelligence algorithms on wider areas. The tackled area for the demonstration plan includes multiple aerial surveys and multiple, corresponding satellite orthophoto (Milano – Novara area). This will greatly expand both the training set and the labelling set (Area of vegetation, building and railway assets). As per the detection of anthropic activities, a demonstration of automatic detection/ change detection is showcased in annex 7 (for brevity not showed in this paragraph). The automatic detection/ change detection leverages on semantic segmentation neural network too and it has been implemented by adding the class ‘buildings’ class to the already trained classes (Terrain, Vegetation and Building). Once the network achieves better estimation performances, the work will focus on specific areas with updated satellite acquisition (multiple times every year, focusing on the areas with spotted issues). In this way, the possible problems arising from vegetation encroachment and anthropic activities can be flagged in a prompt way, resulting so in quantifiable KPIs.

7.1.2. Bridge inspection

The objective of this work is to use AI for the identification and the classification of defects according to standard RFI’s nomenclature. The bridges or elements of bridges are made of concrete, bricks or steel, which are part of the Italian railway network. Currently, this operation is performed by field experts who indicate the position of defects on images acquired via drone. The whole set of images gives rise to a 3D model of the civil infrastructures under inspection.

7.1.2.1. Initial data collection and results

The data has been provided by RFI in two batches and includes 6 viaducts. These batches function as dataset for the initial training of the neural network. The evaluation of this data concerns the first batch and has been later extended to the second one. The first batch includes three bridges, one made of concrete, one made of masonry, and one made of steel.



Figure 40. The three structures in the first batch of data. From left to right: concrete viaduct, bricks viaduct and steel girder.

Among the numerous files, multiple XML files are provided containing various information, including the coordinates of point markers in 2D and 3D, which thus identify them on both the images and the 3D models. Markers are point identifiers that aim to indicate the presence of certain defects in space. Defects are categorized according to a notation convention established by RFI, using one or more letters followed by a number. The literal part of the notation establishes the macro-category of defects, while the number specifies the micro-category. For example, the letter M indicates the category of “Defects in masonry elements” and, on a deeper level, M1 describes infiltrations through the masonry, M2 efflorescence, M3 the presence of vegetation and so on.

From the analysis of the distribution of defects by category, the following histogram is obtained:

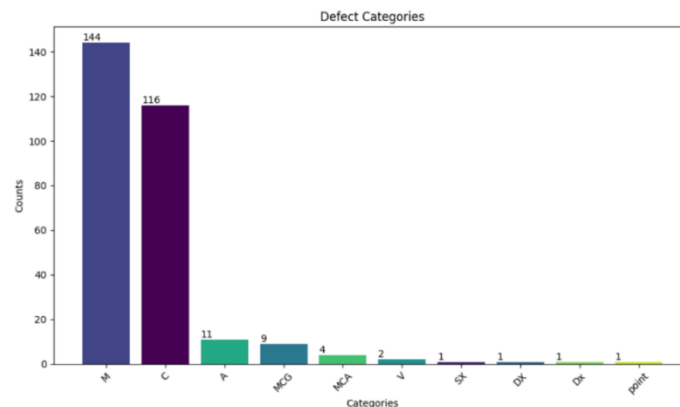


Figure 41. Distribution of markers by category. M: “defects in masonry elements”, C: “defects in reinforced concrete (R.C.) and pre-stressed concrete (P.C.) elements”, A: “defects in steel elements”, MCG: “defects in joint connection mechanisms”, MCA: “defects in support connection mechanisms”, V: “defects in superstructures”.

The most populated category is found to be “defects in masonry elements” (M) with 144 distinct occurrences, followed by “defects in reinforced concrete and pre-stressed concrete elements” (C) with 116 distinct occurrences. The other categories are sparsely populated.

Expanding the distribution of labels by micro-category, it is possible to spot how some categories are very underrepresented (**Figure 42**). This underrepresentation is further emphasised considering that each defect is present in multiple images, acquired from slightly or significantly different perspectives.

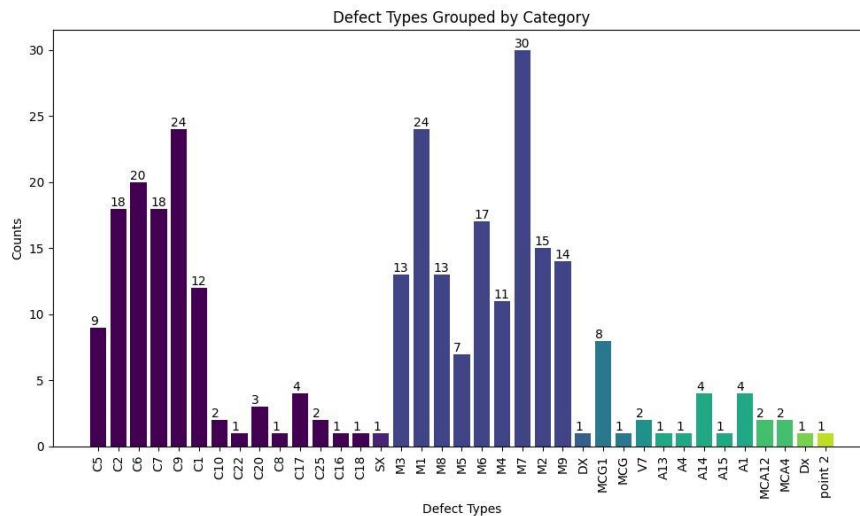


Figure 42. Distribution of markers by category (colour) and type.

Overall, there are 7503 images with markers for these three structures. Of these, 7067 images are 5280x2970 pixels in dimension, and 436 images are 5280x3956 pixels in dimension.

7.1.2.2. Labelling workflow

When drawing bounding boxes with a fixed side of 50 pixels centred on the markers on the images, to have visual feedback of the actual appearance of the defects, it becomes apparent that there are some significant issues. The issue arises since, from an inspector point of view, very often, the aim of a marker is merely to indicate the presence of a type of defect in a certain area, so the marker does not necessarily identify the defect extent. Often the marker is not exactly centred on the defect, or many markers are placed to indicate with a certain emphasis a problematic area. In other words, sometimes, flagging with extreme precision the location of the defects, is not a big concern. This is because repairs and associated scaffolding would generally involve areas way bigger than the defects themselves. However, when it comes to AI's training, a more precise defect location is of paramount importance. So, the purpose of the labelling for the inspector, that is sufficient for human intelligence, does not carry the necessary information needed to train a very naïve neural network (yet to be trained).

Here are some notable examples for the three structures.

- **Concrete viaduct**

Different types of defects are reported in areas appear indistinguishable.



Figure 43. Different types of defects reported on indistinguishable areas.

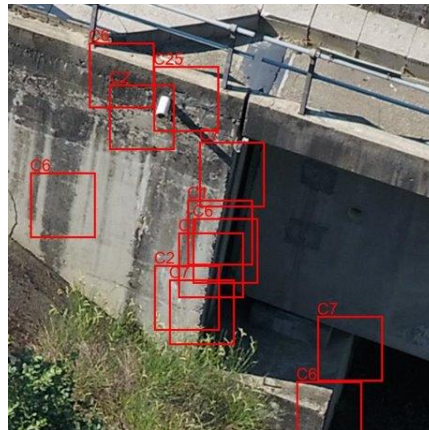


Figure 44. High density of markers emphasising a problematic area.

For example, in the image below, both M3 and C6 are present, and they both indicate the presence of vegetation, but the is first on masonry elements and the second on concrete elements. However, it cannot be determined from the image on which material the plants have grown. This would certainly be confusing during AI training. Labelling needs to be improved to be ready for AI training.

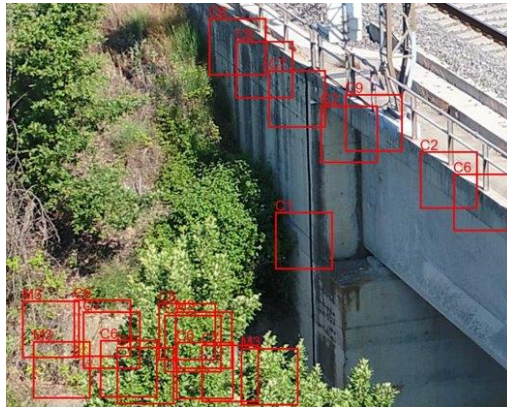


Figure 45. Ambiguous markers placement on surface with vegetation.

- **Masonry viaduct**

The same conclusions apply to the masonry viaduct: a high density of markers indicates an area requiring special attention, and often, areas with very similar appearances are marked by different types of markers. Again, this would certainly be confusing during AI training.

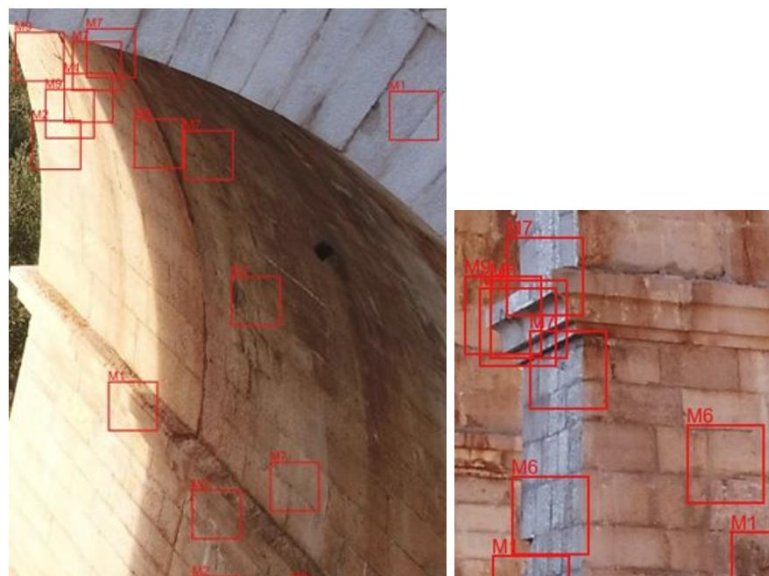


Figure 46. High density of markers signifying an area that requires monitoring.

It also frequently happens that markers are placed on top of tree branches because the defects are hidden behind them.



Figure 47. Examples of defects covered by branches and leaves.

- **Steel girder**

In the case of the metal girder, the situation is even more complex because it is inherently a very complicated structure. Colour, for instance, hides some of the most peculiar defects, such as rust. The difficulty is further increased by the resolution of the images, which may not be high enough to distinguish very small defects like cracks.



Figure 48. The crack in this piece of steel is not visible due to the dark colour and the image resolution.

In addition, when the images are acquired backlit, it becomes truly difficult to distinguish defects on such a dark structure.

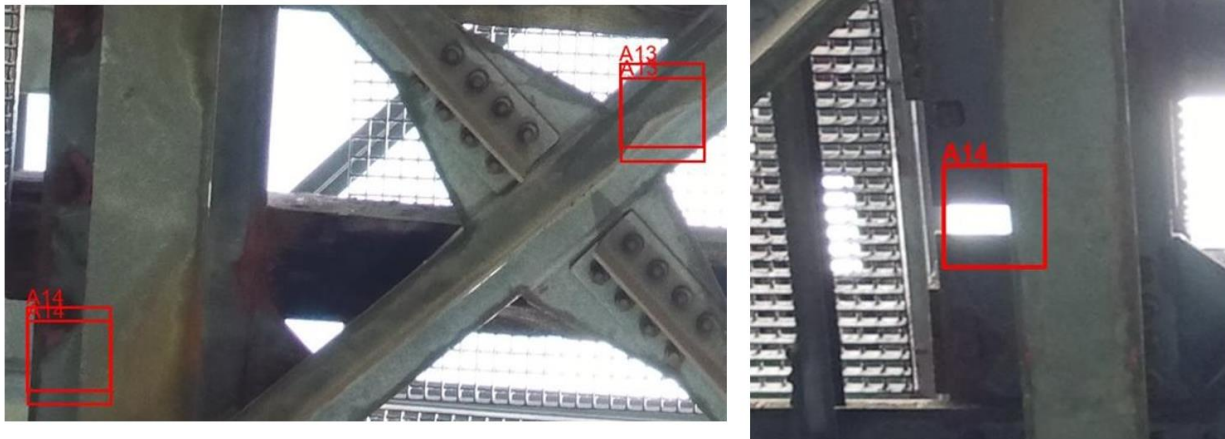


Figure 49. Defects on backlit structures are even more difficult to identify.

From this brief analysis of the provided data, several conclusions can be drawn to establish an effective strategy to better leverage on the available data.

It might be advisable to focus on two primary categories of defects, namely the most numerous ones: “defects in masonry elements” and “defects in reinforced concrete and pre-stressed concrete elements”. However, this narrowing down would still be insufficient because, even within these two categories, many defect types are underrepresented.

In addition to the number of occurrences, these data are challenging to seamlessly adapt for AI training purposes. The sub-optimal marker positioning and labelling, implies reviewing all defect labels and bounding boxes to accurately reflect the actual sizes of the defects.

This process would be extremely complex and time-consuming, particularly for operators without field expertise. Many markers would need to be discarded, further reducing the already limited number of examples available for training a neural network model.

Based on the analysis conducted and the issues identified, these data alone are deemed insufficient to form a complete dataset for training a neural network model. However, they will contribute to the learning and evaluation process.

7.1.2.3. AI processing strategies

To start with a limited, yet still challenging case, we decided to focus on the recognition of defects in concrete structures. To tackle this problem using AI techniques, two possible strategies have been developed, which will be illustrated below, namely: defect classification and defect semantic segmentation.

- **Defect classification**

As in all applications that leverage AI, one of the key points, if not the core of the work, is the dataset. There are some standard open-source datasets available for defects in concrete structures with corresponding ground truth data. These datasets consist of high-resolution images acquired by drones at different scales, angles, and weather conditions, depicting various levels of deterioration. In the ground truth data, defects are classified into particularly significant and recurring categories, such as cracks, spallation, exposed bars, efflorescence or corrosion stains, and are circumscribed

within bounding boxes that can also overlap if multiple types of defects are concurrent. Here is an example of how a data item with the corresponding ground truth can be presented.



Figure 50. Example of data and respective ground truth for a classification dataset. In this case there are two overlapping types of defects: efflorescence and corrosion stain. Hence, the orange bounding box is multi-labelled.

To integrate/reinforce RFI data, the first step can be to select defect classes that can be merged with the general ones represented in the open-source datasets. Given that the analysis of the available data highlights that the usable categories are few and with limited examples, this selection is advantageous. It potentially allows for the recognition of a wider variety of defects, as many types are present in the open-source datasets but not in the provided data.

After selecting the defect classes, a provisional bounding box is created around the marker and the image is cropped around this bounding box, possibly with some additional margin. These cropped images are then reviewed to adjust the bounding box size and to ensure that only those images where the defect is clearly visible and well-represented are included in the dataset.

The neural network model to be used will be a convolutional network, with its architecture tailored to the specific case.

Once the network is trained, the RFI images are cropped into smaller parts, the same size as the images submitted to the network for training, and its ability to recognize the defects is verified. From the bounding box of the defect predicted by the network, the marker and thus its 2D coordinates can be extracted in the system of reference of the image.

- **Semantic segmentation**

This second strategy focuses on pixel-by-pixel classification, which means that each pixel is assigned to a defect class. Specific open-source datasets can be found for high-resolution images of masonry or concrete structures captured by drones at various scales and angles, with ground truth data provided in the form of segmentation masks.

A segmentation mask is an image with the same dimensions as the RGB image, but with pixels coloured differently based on the defect class. Each defect class is assigned a specific grayscale value, while all pixels not associated to defects are classified as “background” and keep their own grayscale value/colour. This type of ground truth offers more detailed information than simple classification, as it also informs the network of the exact extent of the defect in the image. An example of image and respective segmentation mask can be found in the pictures below.



Figure 51. Example of data and relative ground truth for a semantic segmentation dataset. The green shapes cover the pixels associated to the class “weathering”, while the blue ones are for the class “efflorescence”.

Incorporating RFI data into this type of dataset (semantic segmentation datasets) requires more effort than defect classification (previous strategy) as the process of creating segmentation masks is laborious and time-consuming. Additionally, specific field expertise is needed to accurately identify the extent of the defects.

Open-source semantic segmentation datasets can be used to enhance Defect classification datasets (first strategy) by extracting bounding boxes that cover the minimum area containing the pixel group associated with the defect.

The neural network model planned for this task is a semantic segmentation model, such as DeepLabV3+, which has been successfully used in other works.

Once the model is trained, image crops with the same dimensions as those used during training are submitted. The network then returns a probability map, indicating, for each pixel, the probability of each defect class plus the background. The class with the highest probability is selected and a lower threshold for this probability is set to guarantee a high level of likelihood.

If the objective is to determine a marker for the defect, the 2D coordinates of the centroid of the pixel group related to a specific defect can be extracted as well.

7.1.2.4. Conclusion and future developments

The available data and labelling duo provided by FSI is perfectly suitable for the maintenance and analytics of the IM. However, the possibility of directly training a CNN from this duo is hindered by two main aspects.

- For the training of the AI (deep learning / CNN), the labelling needs to be adapted to be univocally intelligible by the machine.
- The number of defects divided by categories and sub-categories is very limited and the ground truth data is inadequate.

The analysis of the provided data has resulted in the development of two potential strategies for future efforts. Both strategies involve integrating the available data, after adjusting the ground truth data, with existing online datasets. The two approaches are defect classification and semantic segmentation. Both methods can achieve the same result: either a marker centered on the defect automatically recognized by the network, or more detailed information such as a bounding box around the defect or a pixel-by-pixel digital representation of the defect.

7.1.2.5. Demonstration Plan

The demonstration plan will entail the test of both the strategies previously described on various sets and types of data, which will integrate the images given by RFI, after undergoing appropriate pre-processing and transformations. This might include external open-source dataset. The expected results are represented by a classification of defects on concrete and masonry bridges, along with their georeferenced position. In this way, the identification of problematic areas in these types of structures will be automated.

7.1.3. Hydrogeological Risk

7.1.3.1. Selected equipment, technical specifications, and justification.

Hydrogeological instability represents the set of soil degradation processes, which mainly occur under certain weather conditions. In Italy, this phenomenon has a significant impact on the population and on the territory as highlighted in the Report on Hydrogeological Instability published by ISPRA in 2018. Obviously, the railway infrastructure being an important territorial element with more than 16,000 km of railway lines, in some cases it is strongly affected by this problematic.

To this purpose, it is intended to propose and develop a monitoring and forecasting tool based on the collection and analysis of satellite available data of sensitive “*climate*” variables (with respect to the phenomena that are intended to be monitored).

Data will be collected and processed using Google Earth Engine (GEE) platform (using JavaScript programming language) and Microsoft Visual Studio editing Python.

The integration of collected and pre-elaborated data will carry out through neural networks algorithms, on the basis of which the monitoring and forecasting tool will be developed.

7.1.3.2. Installation layout

Precipitation, soil moisture and Land Surface Temperature (LST) are the parameters considered for the flooding risk monitoring.

The analysis was executed for the Area Of Interest (AOI) “Milano-Novara. However, an additional AOI, “Tortona-Voghera”, was considered as a further case study for the validation of the processing and algorithms. AOIs are shown in the next figure.

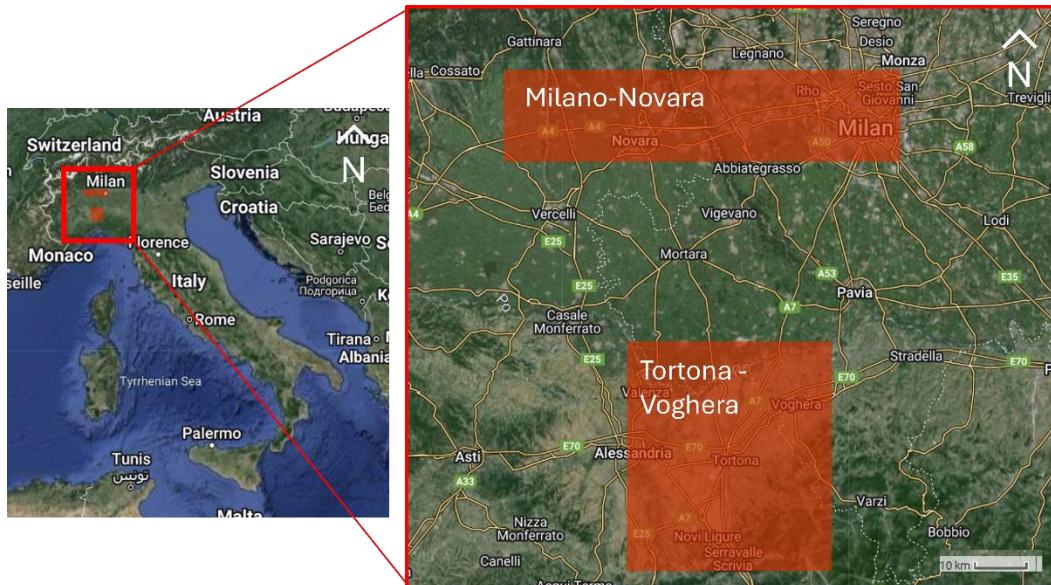


Figure 52. Milano-Novara and Tortona-Voghera AOI.

The considered analysis time ranges from 2000 to 2023. This choice aims to maximize the study years, considering data availability.

7.1.3.3. Initial data collection and results

7.1.3.3.1. Satellite Images/Data Selection and Collection

Figure 53 shows the general data processing. This procedure is applied for each parameter, i.e., precipitation, soil moisture, and LST. In particular, data are collected and processed using Google Earth Engine (GEE) platform and Microsoft Visual Studio editing Python, respectively highlighted in the blue and green areas of the Figure. GEE (Google 2024) is a cloud-based platform that facilitates geoprocessing. It includes geospatial data collections and a code editor which is an integrated development environment for the elaboration of algorithms using JavaScript programming language. Microsoft Visual Studio is also an integrated development environment for developing codes in different programming languages, including Python.

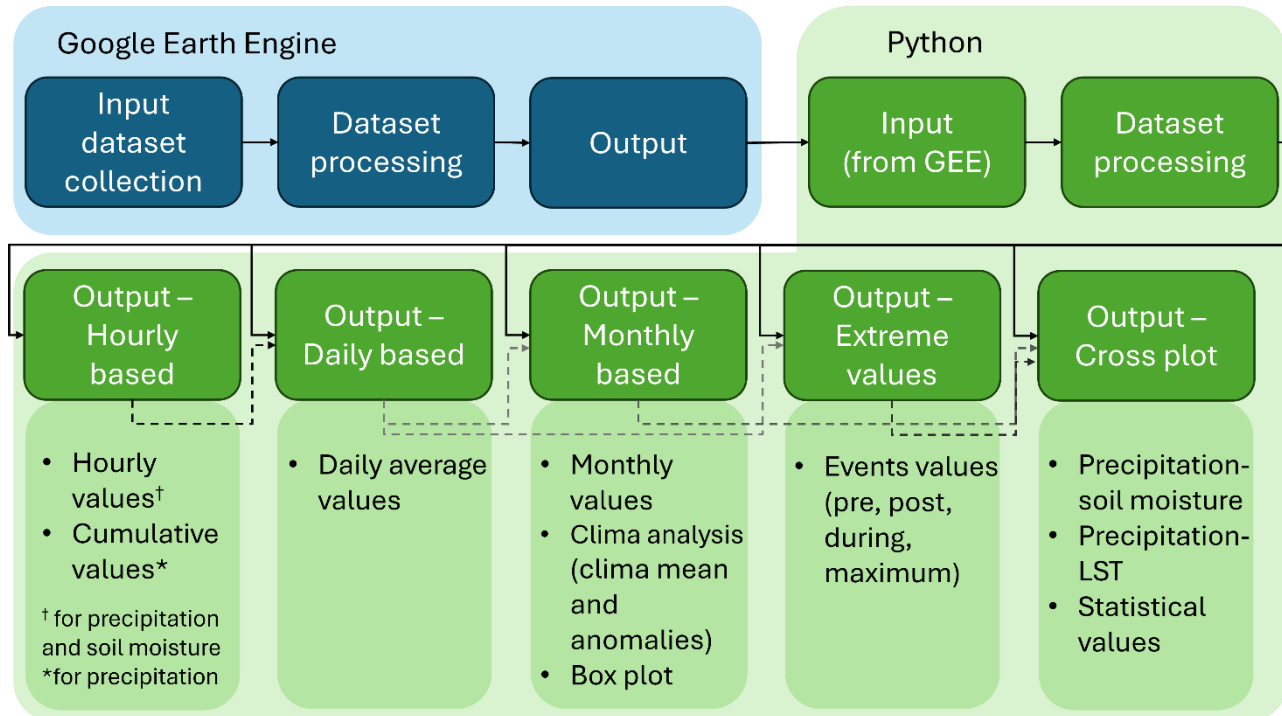


Figure 53. Data download and elaboration scheme.

The processing steps executed in GEE are shown in blue in Figure 53, while those executed in Python are in green. In GEE, after the collection via the Google Earth Engine Data Catalog of the input data, data of interest are processed and exported as CSV files for subsequent in-depth elaborations executed in Python.

In the Python environment, input data are the outputs from GEE which are additionally processed to obtain one or more products which can consist of CSV files or graphs. Produced outputs can be differentiated based on the time interval considered for the analysis (hourly, daily, or monthly). Additionally, analysis based on extreme values, i.e., values during or near the event and maximum values, were executed. This information was summarized in a final output consisting of cross plots that compare the different parameters for the different scenarios of event or non-event.

More detailed information is provided in Section 7.1.3.3.2.

The data used, which will be further described in the following section, are:

- **GPM IMERG** (<https://gpm.nasa.gov/missions/GPM>): Global Precipitation Measurement (GPM) data provide observations of rain and snow and were used to estimate precipitation. The following products were considered:
 - **GPM IMERG Final Precipitation L3 Half Hourly 0.1 degree x 0.1 degree V06**: this product reports precipitation data adjusted in accordance with gauge data and climatological.
 - **GPM IMERG Late Precipitation L3 Half Hourly 0.1 degree x 0.1 degree V06**: this product was considered only in case of unavailability of the first one, as it does not have the same corrections as the former.

- **GLDAS Soil Moisture Data** (<https://ldas.gsfc.nasa.gov/gldas>): Global Land Data Assimilation System (GLDAS) data provide hydrogeological products, and was used to estimate soil moisture. Two dataset versions exist, the following was considered:
 - **GLDAS-2.1**: this is the more recent version and climatologically more consistent compared to the previous one.
- **MODIS Terra Data** (<https://modis.gsfc.nasa.gov/>): Moderate Resolution Imaging Spectroradiometer (MODIS) measures were used to obtain LST. Among the data products available, the following from the current Collection-6 was considered:
 - **MODIS Land Surface Temperature and Emissivity (MOD11)**.

GPM IMERG Data

This data was used for the precipitation parameter. The following paragraphs describe the data and their characteristics.

Data description:

The Global Precipitation Measurement (GPM) mission is an international network of satellites that provide the next-generation global observations of rain and snow. The mission was initiated by National Aeronautics and Space Administration (NASA) and the Japan Aerospace Exploration Agency (JAXA) and comprises a consortium of international space agencies. The core satellite carries an advanced radar/radiometer system to measure precipitation from space and serve as a reference standard to unify precipitation measurements from a constellation of research and operational satellites. The satellite network surpasses its predecessor, the Tropical Rainfall Measuring Mission (TRMM) mission, by covering a larger area and using advanced sensors to measure precipitation more accurately, especially light and solid precipitation.

The Integrated Multi-satellitE Retrievals for GPM (IMERG) is the unified U.S. algorithm that provides the multi-satellite precipitation product. IMERG combines data from various sources, including infrared, microwave, and gauge observations, to create precipitation estimates at relatively high resolution both in terms of spatial, $0.1^\circ \times 0.1^\circ$, and temporal, 30 minutes, resolution over the entire globe. The system is run several times for each observation time, first giving a quick estimate and successively providing better estimates as more data arrive. Based on this, IMERG offers different datasets, which includes (Pradhan, et al. 2022):

- Near-real-time data, available within 4 to 14 hours, which are the IMERG-Early run (IMERG-E) and IMERG-Late run (IMERG-L);
- Final dataset, delayed by about 4 months, which is IMERG-Final run (IMERG-F) and is used for more in-depth research (Pradhan, et al. 2022).

IMERG-E, IMERG-L, and IMERG-F are Level 3 data, i.e., geophysical variable spatially and temporally resampled. GPM Level 3 data are summarized in the following table (NASA, Precipitation Data Directory 2024):

Data	Description	Version	Data availability	Spatial Resolution
IMERG Early run	Near real-time low-latency gridded global multi-satellite precipitation estimates.	06	2000-present	10km (0.1°)
IMERG Late run	Near real-time gridded global multi-satellite precipitation estimates with quasi-Lagrangian time interpolation.	06	2000-present	10km (0.1°)
IMERG Final run	Research-quality gridded global multi-satellite precipitation estimates with quasi-Lagrangian time interpolation, gauge data, and climatological adjustment.	06	2000-2021	10km (0.1°)
3B Combined	Gridded rainfall estimates from combined radar/radiometer data (GPM GMI & DPR, TRMM TMI & PR).	06	1997-2015 and 2014-present	0.25°-5°
3A Radar	Gridded rainfall estimates from radar data (GPM DPR, TRMM PR).	06	1997-2015 and 2014-present	0.25°-5°
3A Radiometer	Gridded rainfall estimates from GPM GMI, TRMM TMI, and constellation microwave radiometers.	06	2000-present	0.25°

Table 5. GPM Level 3 data.

IMERG was released in 2015 and has become a valuable tool used for various purposes, including simulating streamflow, predicting floods, and analyzing extreme weather events. Recently, IMERG expanded its data coverage back to the TRMM era, providing a 20-year record from 2000 to the present day (Pradhan, et al. 2022).

GPM IMERG Final Precipitation L3 Half Hourly 0.1 degree x 0.1 degree V06 (GPM_3IMERGHH)

Given the characteristics of the GPM Level 3 data reported in Table 5, GPM IMERG Final run data were considered for dataset creation, more specifically the “GPM IMERG Final Precipitation L3 Half Hourly 0.1 degree x 0.1 degree V06 (GPM_3IMERGHH)” product (hereafter GPM_3IMERGHH) (Huffman, et al. 2019). This choice was due to the following reasons:

- They are adjusted in accordance with gauge data and climatological;
- They are characterized by the finest spatial resolution, i.e., 0.1° x 0.1.

GPM_3IMERGHH includes different data field for users and data developers, summarized in the following table (Huffman, et al. 2019).

Data field	Variable name	Units
Multi-satellite precipitation estimate with gauge calibration (Final)	precipitationCal	mm/hr
Multi-satellite precipitation estimate (Early and Late)		
Multi-satellite precipitation estimate	precipitationUncal	mm/hr
Random error for precipitationCal	randomError	mm/hr
Merged microwave-only precipitation estimate	HQprecipitation	mm/hr
Microwave satellite source identifier	HQprecipSource	index values
Microwave satellite observation time	HQobservationTime	min. into half hour
IR-only precipitation estimate	IRprecipitation	mm/hr
Weighting of IR-only precipitation relative to the morphed merged microwave-only precipitation	IRkalmanFilterWeight	percent
Probability of liquid precipitation phase	probabilityLiquidPrecipitation	percent
Quality Index for precipitationCal field	precipitationQualityIndex	index

Table 6. List of data fields, their variable names (in the data structure), and the data units for 3IMERGHH data files.

Among the available variable, precipitationCal was considered, since it is recommended for general use and describes the multi-satellite precipitation estimate with gauge calibration, in mm/hr. Figure 54 shows the surface precipitation from GPM_3IMERGHH.

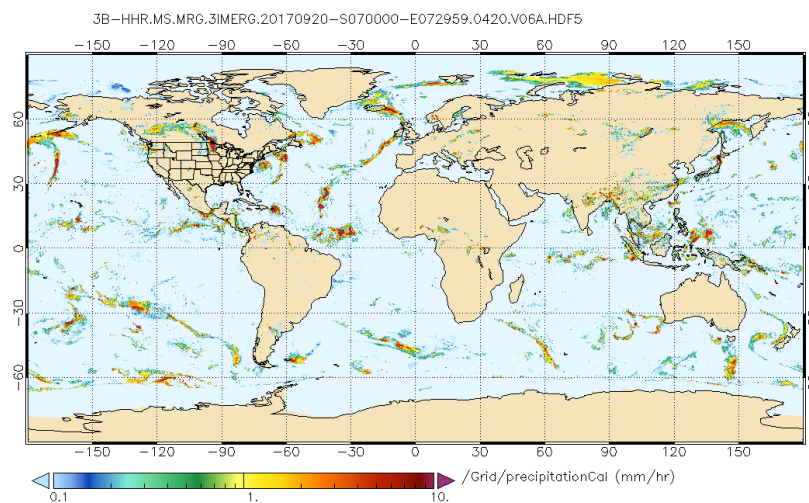


Figure 54. GPM IMERG Final precipitation L3 Half Hourly 0.1° x 0.1° (GPM_3IMERGHH).

Figure 54 shows as an example GPM_3IMERGHH data for the 21 October 2019 at 00:00:00 acquired

over the AOI. Also, rain gauge stations within the AOI are reported.

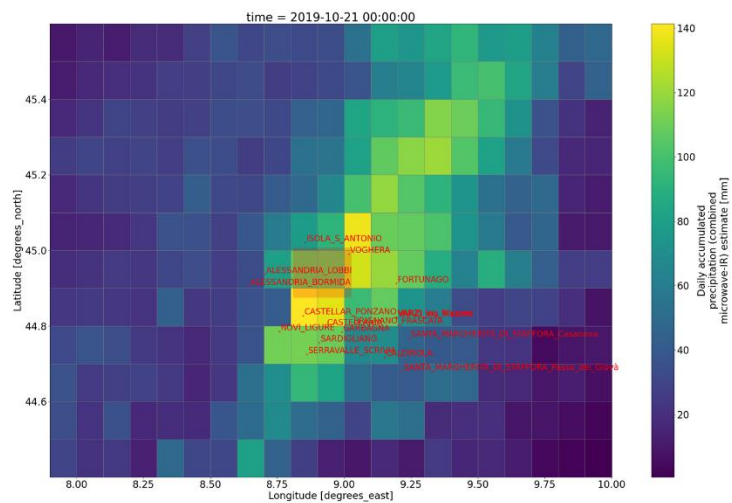


Figure 55 - GPM_3IMERGHH over the AOI.

GPM IMERG Late Precipitation L3 Half Hourly 0.1 degree x 0.1 degree V06 (GPM_3IMERGHHL)

In case of unavailability of GPM_3IMERGHH products, “GPM IMERG Late Precipitation L3 Half Hourly 0.1 degree x 0.1 degree V06 (GPM_3IMERGHHL)” (hereafter GPM_3IMERGHHL) products was considered. As described in the previous section, they lack rain gauge and climatological adjustments. Also in this case, precipitationCal variable was considered, which provides multi-satellite precipitation estimate.

Figure 56 shows the surface precipitation from GPM_3IMERGHHL.

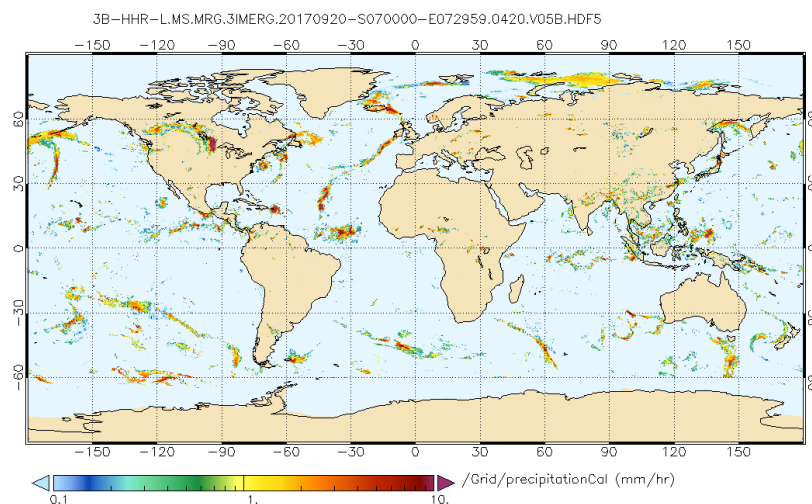


Figure 56. GPM IMERG Late precipitation L3 Half Hourly 0.1° x 0.1° (GPM_3IMERGHHL).

Data collection and processing:

GEE was used for data downloading and preprocessing. The GPM IMERG data collection includes

data from 01/06/2000, T 00:00:00 to 02/06/2024, T 18:30:00¹. In this collection provisional products are regularly replaced with updated versions when the data become available.

Table 7 summarizes the main characteristics of the considered precipitation products.

Data	GPM IMERG Final run
Version	06
Data availability	2000-06-01 – present
Frequency	Half-hour
Spatial resolution	10km (0.1°)
Variable	precipitationCal
Units	mm/hr

Table 7. Main characteristics of precipitation data.

For each day, 48 data are available.

Data processing follows the steps described in Figure 53.

Furthermore, satellite precipitation data were compared with rain gauge station data.

GLDAS Soil Moisture Data

This data was used for the estimation of the soil moisture parameter. Indeed, soil moisture plays a significant role in many hydrological processes, determines the partitioning of precipitation between infiltration and runoff and is also an important initial state of climate model. Not only surface soil moisture, that is the soil moisture in the top few centimetres (0–5 cm), is significant. In fact, root zone soil moisture is also very important for many applications. It carries memory from weekly to monthly time scales, and accurate root zone soil moisture information may help improve the prediction of precipitation. Soil moisture information can be obtained by measuring soil moisture in field, however, in situ measurements are only representative over a small spatial scale and they are often expensive and infeasible. Microwave remote sensing data can provide a means to estimate soil moisture at large scales however, only surface soil moisture can be obtained due to the limitation of microwave penetration depth. But soil moisture profile information can be derived also by modelling approaches, using either climate models or land surface models.

Several modelling systems can produce operational and spatiotemporally continuous soil moisture datasets and among them Global Land Data Assimilation System (GLDAS) is the most widely used (Bi, et al. 2016).

The following paragraphs describe the data and their characteristics.

At a first stage, data from the satellite mission Soil Moisture Active Passive (SMAP) by NASA was considered. This mission indeed was specifically developed for Earth's soil moisture monitoring and can provide data with a higher spatial resolution than GLDAS. However, first data availability was in 2015.

Data description:

GLDAS aims at combining satellite- and ground-based observational data products by means of advanced land surface modelling and data assimilation techniques, in order to generate optimal fields of land surface states. Hydrological products are also generated, including soil moisture

¹ On 16 July 2024

(NASA, GLDAS: Project Goals. 2024). Two versions of GLDAS products exist, including the GLDAS Version 1 (GLDAS-1) and the more recent GLDAS Version 2 (GLDAS-2). The main difference is that GLDAS-2 is climatologically more consistent. GLDAS can provide products with spatial resolution of both 0.25° and 1°. The 1.0° data range from 1979 to present, while the 0.25° data cover 2000 to present. Spatial resolution and data availability depend on the specific product. The temporal resolution of the GLDAS products is 3-hourly (Bi, et al. 2016).

GLDAS-2.1

The land surface model considered in GLDAS for soil moisture defines four soil layers: 0–10 cm, 10–40 cm, 40–100 cm, and 100–200 cm. For each of them, soil moisture is expressed as kg m^{-2} over the entire thickness of the indicated layer (NASA, GLDAS: Project Goals. 2024).

Figure 57 shows an example of the GLDAS-2.1 soil moisture.

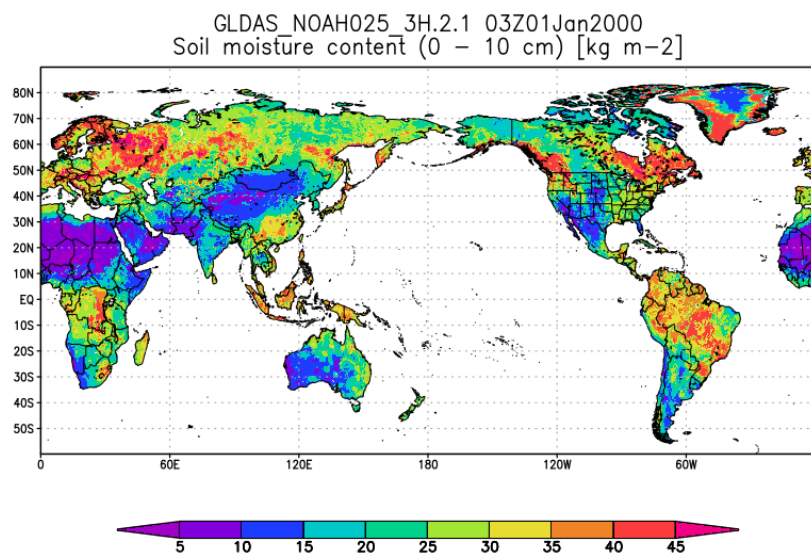


Figure 57. GLDAS-2.1 Noah 3-hourly 0.25 degree 0-10 cm soil moisture [kg m^{-2}] for 03Z Jan 01, 2000.

Data collection and processing: GEE was used for data downloading and preprocessing. The “GLDAS-2.1: Global Land Data Assimilation System” data collection includes data from 01/01/2000, T 03:00:00 to 19/06/2024, T 21:00:00². The **Table 8** summarizes the main characteristics of the considered soil moisture products.

² On 18 July 2024

Data	GLDAS
Version	2.1
Data availability	2000-01-01 – present
Frequency	3 hour
Spatial resolution	0.25° (approximately 28 km)
Variable	<ol style="list-style-type: none"> 1. SoilMoi0_10cm_inst 2. SoilMoi10_40cm_inst 3. SoilMoi40_100cm_inst 4. SoilMoi100_200cm_inst
Units	kg m-2

Table 8. Main characteristics of “GLDAS-2.1: Global Land Data Assimilation System”.

Figure 58 shows as an example GLDAS soil moisture data for the 1 January 2023 acquired over the AOI. Also rain gauge stations within the AOI are reported.

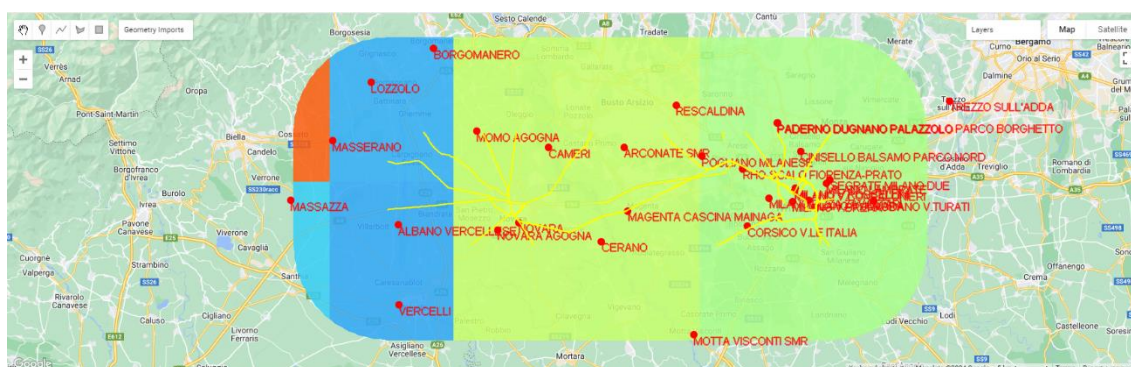


Figure 58. GLDAS soil moisture over the AOI (acquisition ID: NASA/GLDAS/V021/NOAH/G025/T3H/A20230101_0000).

MODIS Terra Data

This data was used to obtain the LST parameter. LST is the temperature of the most external part of the Earth surface and is a key parameter for land surface processing, including the hydrology field. MODIS LST data are the most commonly used, given their balance between spatial and temporal resolution, and their correspondence with in-situ measurements. MODIS LST data are freely available from NASA Land Data Products and Services (Phan and Kappas 2018). Compared to other LST products, MODIS LST was the most suitable given its characteristics in terms of beginning of the data availability and spatial resolution. The following paragraphs describe the data and their characteristics.

Data description:

MODIS stands for Moderate Resolution Imaging Spectroradiometer, a sensor aboard the Terra and Aqua satellites by NASA launched in 1999 and 2002, respectively. Terra's orbit is timed so that it passes from north to south across the equator in the morning, while Aqua passes south to north

over the equator in the afternoon. Terra and Aqua products are very similar with a few key differences, which include the launch date, since Terra was launched two years before Aqua and starts recording during 2000, and slight differences in snow products due to a detector failure on Aqua. The sensor has a temporal resolution of four times per day and a spatial resolution of 1 km and acquires data in 36 spectral bands.

The current MODIS data collection for the LST is the Collection-6 (C6) MODIS LST products. Figure 59 summarizes the available MODIS C6 LST products (NASA, MODIS 2024).

Earth Science Data Type (ESDT)	Product Level	Nominal Data Array Dimensions	Spatial Resolution	Temporal Resolution	Map Projection
MOD11_L2	L2	2030 or 2040 lines by 1354 pixels per line	1km at nadir	swath (scene)	None. (lat,lon referenced)
MOD11A1	L3	1200 rows by 1200 columns	1km (actual 0.928km)	daily	Sinusoidal
MOD11B1	L3	200 rows by 200 columns	6km (actual 5.568km)	daily	Sinusoidal
MOD11B2				eight days	
MOD11B3				monthly	
MOD11A2	L3	1200 rows by 1200 columns	1km (actual 0.928km)	eight days	Sinusoidal
MOD11C1	L3	360° by 180° (global)	0.05° by 0.05°	daily	equal-angle geographic
MOD11C2	L3	360° by 180° (global)	0.05° by 0.05°	eight days	equal-angle geographic
MOD11C3	L3	360° by 180° (global)	0.05° by 0.05°	monthly	equal-angle geographic

Figure 59. Summary of the C6 MODIS LST products (source: (NASA, MODIS 2024)).

Among the MODIS data products, the “*MODIS Land Surface Temperature and Emissivity (MOD11)*” is considered given its characteristics in terms of beginning of the data availability, product level, spatial resolution, and temporal resolution.

MODIS Land Surface Temperature and Emissivity (MOD11)

The daily level 3 LST product at 1km spatial resolution is a tile of daily LST product gridded in the Sinusoidal projection. A tile contains 1200 x 1200 grids in 1200 rows and 1200 columns. The exact grid size at 1km spatial resolution is 0.928km by 0.928km.

The C6 daily MOD11A1 LST product is constructed with the daily LST pixel values in each granule retrieved by the generalized split-window algorithm under clear-sky conditions.

In particular, the considered product is “*Land Surface Temperature/Emissivity Daily L3 Global 1km*” and the corresponding Terra product ID is MOD11A1.

LST_Day_1km variable is considered, that is the daytime LST expressed in Kelvin (K) (NASA, MODIS 2024).

Figure 60 shows as an example MOD11A1 data for the 1 January 2011 acquired over the AOI. Missing pixels are cloud-covered pixels.

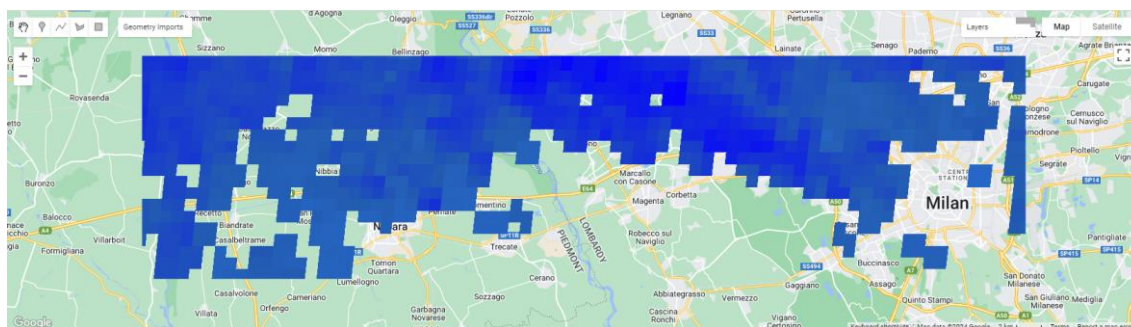


Figure 60. MOD11A1 over the AOI (acquisition ID: MODIS/061/MOD11A1/2011_01_01).

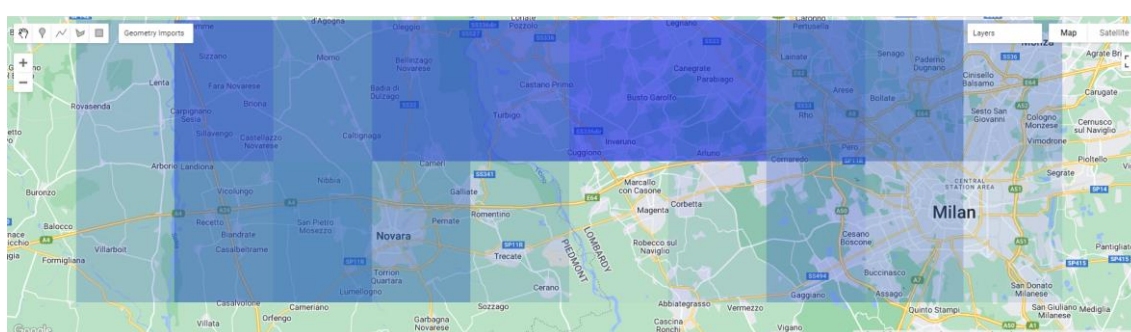
Data collection and processing GEE was used for data downloading and preprocessing. The “MOD11A1.061 Terra Land Surface Temperature and Emissivity Daily Global 1km” data collection includes data from 24/02/2000 to 15/07/2024³.

The following table summarizes the main characteristics of the considered precipitation products (Wan 2021).

Data	MOD11A1
Version	6.1
Data availability	2000-02-24 – present
Frequency	1 day
Spatial resolution	1 km
Variable	LST_Day_1km
Units	K

Table 9. Main characteristics of LST data.

Data processing follows the steps described in Figure 53. Additionally, a resampling step is performed in order to convert the spatial resolution to the one of precipitation and soil moisture data. The output of the resampling is shown in Figure 61.



7.1.3.3.2. Figure 61. MOD11A1 over the AOI (acquisition ID: MODIS/061/MOD11A1/2011_01_01) resampled to 10 km.
Data Processing and Correlation

³ On 18 July 2024

Considered data for precipitation, soil moisture, and LST parameters, respectively summarized in Table 8 were processed at different levels for their analysis. Section 7.1.3.3.1 and Figure 53 summarize data collection and processing operations.

This section provides further details on processing and data correlation.

As shown in Figure 53, the processing steps executed in GEE are in the blue area and can be summarized as follows:

1. **Input dataset collection:** dataset collection is imported in GEE considering the data available in the GEE Data Catalog;
2. **Dataset processing:** this step includes dataset filtering, i.e., the dataset is filtered based on area, time range and variable of interest;
3. **Output:** a CSV file for each considered year is produced.

It includes a number of rows that correspond to the number of available data within the considered year and a set of columns that include the acquisition date, acquisition time and the variable value for each pixel within the AOI.

The CSV files are used as input for further elaborations, implemented with Python programming language. They are outlined in the green part of Figure 53 and includes:

1. **Input (from GEE):** data collected in GEE are imported in Python;
2. **Dataset processing:** data are processed to produce the output. Processing steps include missing dates check;
3. Different outputs are obtained in the form of CSV files or graphs. If no different specified, the CSV includes a number of rows that correspond to the number of available data within the considered year, and a set of columns that include the acquisition date, acquisition time and the variable value for each pixel within the AOI. The different outputs are:

- 3.1. **Output – Hourly based:** a CSV file for each considered year is produced.

This output is produced for precipitation and soil moisture, since LST data are daily data. It includes hourly (or half-hourly, 3-hourly, depending on the input dataset) values of the parameter of interest reported in a CSV organized to facilitate subsequent elaborations. Only for precipitation, cumulative values at 1, 3, 6, 12, 24 hours are additionally calculated. These data are used as input to produce the *Output – Daily based* products;

- 3.2. **Output – Daily based:** a CSV file and a graph for each considered year is produced.

CSV file includes daily average values of the parameter of interest. The graphs report the time series trend of the parameter for the considered year. These data are used as input to produce the *Output – Monthly based* and *Output – Extreme values* products.

- 3.3. **Output – Monthly based:** the produced CSV files report: (1) monthly average value of the parameters for each considered year, (2) climatological mean of the parameter for the whole time period, and (3) anomaly values calculated based on the monthly average value and the climatological mean for each considered year. In this case the CSVs include a number of rows that correspond to the number of months, and a set of columns that include the variable value for each pixel within the AOI. More details about

climatological mean and anomalies are provided in the following Section “Climatological analysis”.

The produced graphs include (1) the time series trend of the anomalies of the parameter, (2) box plots calculated starting from the daily average parameter for each considered year, and (3) box plots for the whole time period calculated starting from the monthly average parameter. Further details related to box plots are provided in the following Section “**Box plot**”. These data are used as input to produce the *Output – Cross plot* products.

- 3.4. **Output – Extreme values:** the produced CSV files report parameter values corresponding to (1) the extreme meteorological event dates, (2) the 3 days before the beginning of the extreme meteorological event, (3) the 3 days after the end of the extreme meteorological event, (4) a value above a specific threshold set by the user, for each considered year. In this case the CSVs include a number of rows that correspond to the number of events, and a set of columns that include the variable value for each pixel within the AOI. Additionally, (5) daily maximum values for the considered parameter and the corresponding pixel are saved.

The produced graphs instead include the time series trend of the parameter values corresponding to the extreme meteorological event dates, the 3 days before and the 3 days after the extreme meteorological event dates.

These data are used as input to produce the *Output – Cross plot* products.

- 3.5. **Output – Cross plot:** the produced graphs plot precipitation values against soil moisture or LST for each considered year. Values reported in the graphs are obtained from *Output – Monthly based* and *Output – Extreme values* and include: daily values of the parameter during (1) the extreme meteorological event dates, (2) the 3 days before the beginning of the extreme meteorological event, (3) the 3 days after the end of the extreme meteorological event and the corresponding trendline. Additionally, the graphs also report (4) daily values of the parameter above a specific threshold and the corresponding trendline, (5) daily maximum values for the considered parameter, (6) annual mean values, (7) climatological mean values.

A CSV file reporting the value of the slope, r-value coefficient (Pearson coefficient), non-linear coefficient (Spearman coefficient) for the trendlines in the cross plots is also produced. Further details related to cross plots are provided in the following Sections.

The next table reports a summary of the produced outputs described above.

ID	Description
1	1, 3, 6, 12, 24 h cumulative values (precipitation only, for each pixel within AOI, for each year)
2	Daily values (for each pixel within AOI, for each year)
3	Monthly mean values (for each pixel within AOI, for each year)
4	Monthly anomaly values (for each pixel within AOI, for each year)
5	Monthly climatological mean values (for each pixel within AOI)
6	Box plots daily-values based (average value over the AOI, for each year)
7	Box plots monthly-values based (average value over the AOI)
8	Daily values during (1) the extreme meteorological event dates, (2) 3 days before the extreme meteorological event dates, and (3) 3 days after the extreme meteorological event dates (for each pixel within AOI, for each year)
9	Daily maximum values and corresponding pixel (for each year)
10	Daily values higher than a specific threshold (for each pixel within AOI, for each year)
11	Cross plot (1) precipitation - soil moisture, (2) precipitation – LST (for each year)
12	Slope, r-value coefficient, non-linear coefficient for the trendlines from the cross plot

Table 10. Summary of the produced output.

Figure 62 shows as an example an extract of the CSV with hourly and daily values for the precipitation parameter.

	A	B	C	D	E	F	G
1	acquisition_date	acquisition_hour	precipitationCal_1h_pixel_0	precipitationCal_1h_pixel_1			
2	0	01/06/2000	0	0			
3	1	01/06/2000	10000	0	0		
4	2	01/06/2000	20000	0	0		
5	3	01/06/2000	30000	0	0		
6	4	01/06/2000	40000	0	0		
7	5	01/06/2000	50000	0	0		
8	6	01/06/2000	60000	0	0		
9	7	01/06/2000	70000	0	0		
10	8	01/06/2000	80000	0	0		
11	9	01/06/2000	90000	0	0		
12	10	01/06/2000	100000	0	0		
13	11	01/06/2000	110000	0	0		
14	12	01/06/2000	120000	0	0		
15	13	01/06/2000	130000	0	0		
16	14	01/06/2000	140000	0	0		
17	15	01/06/2000	150000	0	0		
18	16	01/06/2000	160000	0	0		
19	17	01/06/2000	170000	0	0		
20	18	01/06/2000	180000	0	0		
21	19	01/06/2000	190000	0	0		
22	20	01/06/2000	200000	0	0		
23	21	01/06/2000	210000	0	0		
24	22	01/06/2000	220000	0	0		
25	23	01/06/2000	230000	0	0		

(a)

	A	B	C	D	E	F	G
1	acquisition_date	acquisition_hour	precipitationCal_24h_pixel_0	precipitationCal_24h_pixel_1			
2	0	01/06/2000	0	0			
3	1	02/06/2000	0	0			
4	2	03/06/2000	0	0			
5	3	04/06/2000	0	0			
6	4	05/06/2000	0	0			
7	5	06/06/2000	0	0			
8	6	07/06/2000	0	0			
9	7	08/06/2000	0	0			
10	8	09/06/2000	0	3.1032088	3.581991		
11	9	10/06/2000	0	5.755281	5.255914		
12	10	11/06/2000	0	31.334057	29.197955		
13	11	12/06/2000	0	4.0943985	7.764504		
14	12	13/06/2000	0	16.46017	15.356853		
15	13	14/06/2000	0	0	0		
16	14	15/06/2000	0	0	0		
17	15	16/06/2000	0	0	0		
18	16	17/06/2000	0	0	0		
19	17	18/06/2000	0	0	0		
20	18	19/06/2000	0	0	0		
21	19	20/06/2000	0	0	0		
22	20	21/06/2000	0	0	0		
23	21	22/06/2000	0	0	0		
24	22	23/06/2000	0	0	0.007237077		
25	23	24/06/2000	0	0	0		

(b)

	A	B	C	D
1	month	precipitationCal_monthly_mean_pixel_0	precipitationCal_monthly_mean_pixel_1	
2	1	6.925822141	7.167767237	
3	2	3.937745945	4.617807336	
4	3	2.493771133	2.600280284	
5	4	3.006220929	3.169928187	
6	5	1.969718336	1.954686197	
7	6	2.88596	3.010029008	
8	7	4.214000685	4.22836956	
9	8	2.790839572	2.857051159	
10	9	1.275267548	1.326645574	
11	10	2.272638655	2.509566965	
12	11	13.68483004	13.80932152	
13	12	3.424486172	3.435351431	

(c)

	A	B	C	D
1		precipitationCal_clima_mean_pixel_0	precipitationCal_clima_mean_pixel_1	
2	0	1.991388609	2.058466747	
3	1	1.880994897	1.924151012	
4	2	1.766120586	1.745171107	
5	3	2.495285305	2.565308856	
6	4	3.265437747	3.317668159	
7	5	2.116253147	2.142004173	
8	6	1.798209395	1.775616345	
9	7	2.309001173	2.310071626	
10	8	2.291707143	2.402083166	
11	9	3.514302158	3.569750851	
12	10	5.379659872	5.445738815	
13	11	2.388579943	2.461449446	

(d)

Figure 62. Example of CSV output. (a) cumulated 1 h, (b) daily, (c) monthly, (d) climatological average for precipitation parameter.

The following sections report more details about the most significant output obtained.

Climatological analysis

The anomaly of a variable is the variation relative to the climatological normal. The climatological normal is the monthly averages computed for a prolonged period of at least 30 consecutive years. Given the data availability for this specific case, the climatological average is considered instead, that is the mean of monthly values of a climate variable over a specified period of time. The period is typically 2-20 years.

The calculation of the monthly anomaly values for a specific variable is defined as:

$$Anomaly = x - x_{norm} \quad (15)$$

Where:

- x is the average value of variable in a specific month;
- x_{norm} is the average value of long-term variable over several years for the same month.

Figure 63 shows an example of the graphs obtained from the analysis of the anomalies for soil moisture parameter, year 2000, variable vsm_0_10 (vsm stands for volumetric soil moisture), that is the soil moisture between 0 and 10 cm soil depth. x-axis reports the month and y-axis the value of vsm_0_10 expressed as kg m⁻². The different lines represent the different pixels within the AOI. The red vertical lines represent the month in which a flood event occurred. The anomaly is calculated as in Equation (1), where x is the monthly average value of vsm_0_10 for each pixel and x_{norm} is the monthly average value of vsm_0_10 for each pixel averaged over the whole time period (from 2000 to 2023).

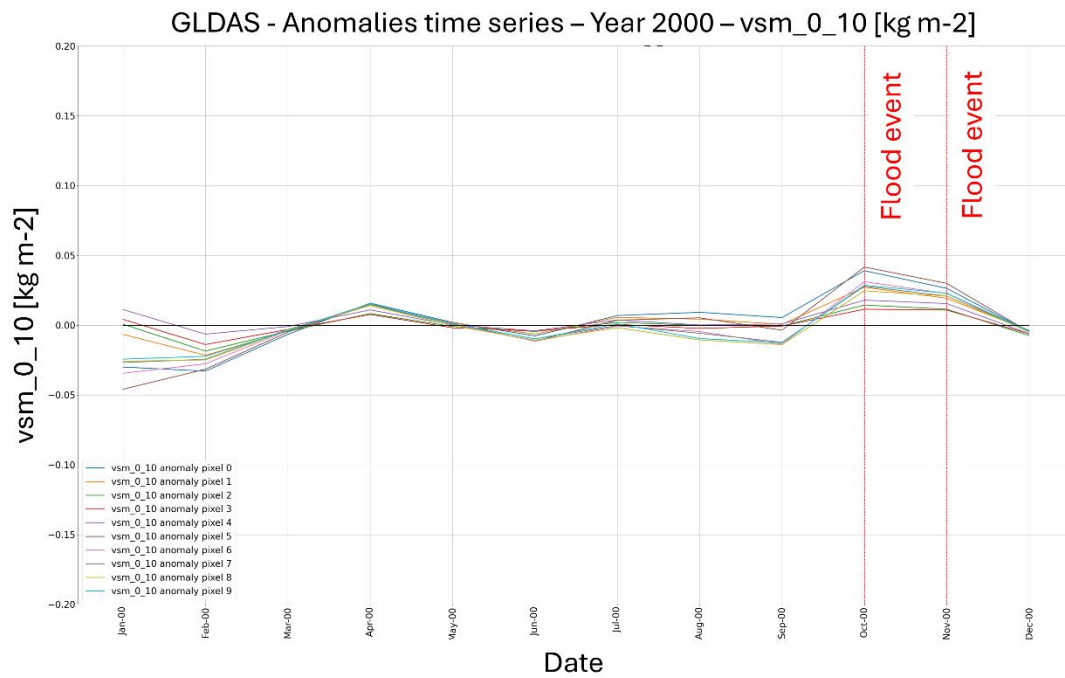


Figure 63. GLDAS anomalies series for year 2000 and variable vsm_0_10 (AOI Milano-Novara).

Similar graphs are shown in Figure 64 and Figure 65 for precipitation parameter, year 2002, precipitationCal variable and LST parameter, converted in Celsius degree, year 2023, respectively.

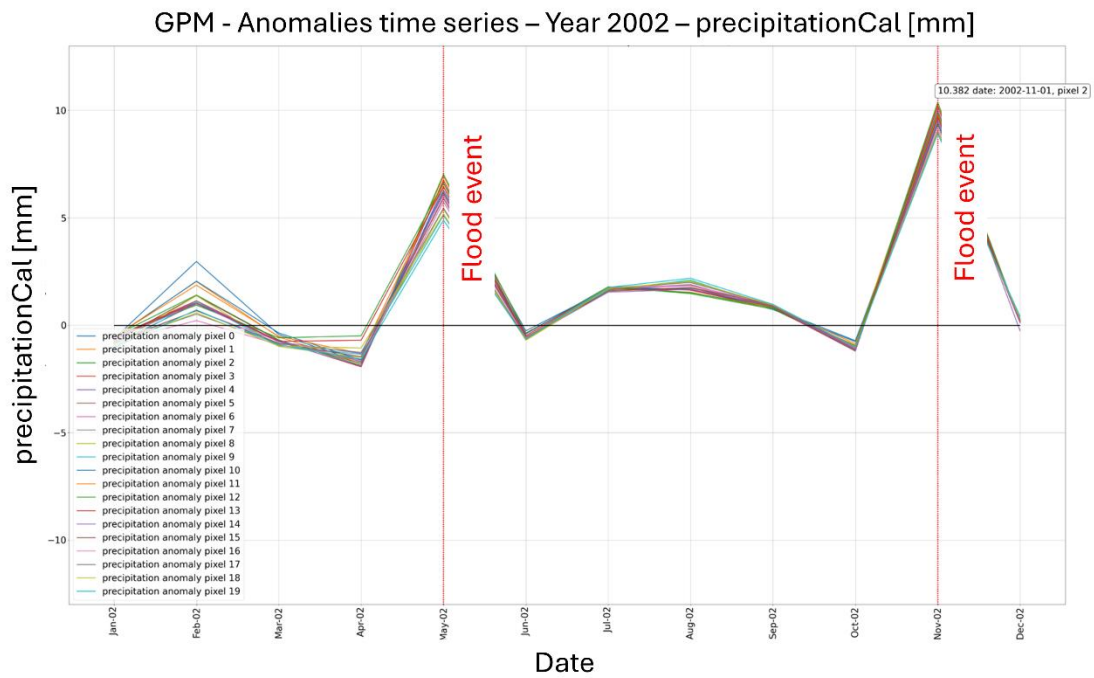


Figure 64. GPM anomalies time series for year 2002 and variable precipitationCal (AOI Milano-Novara).

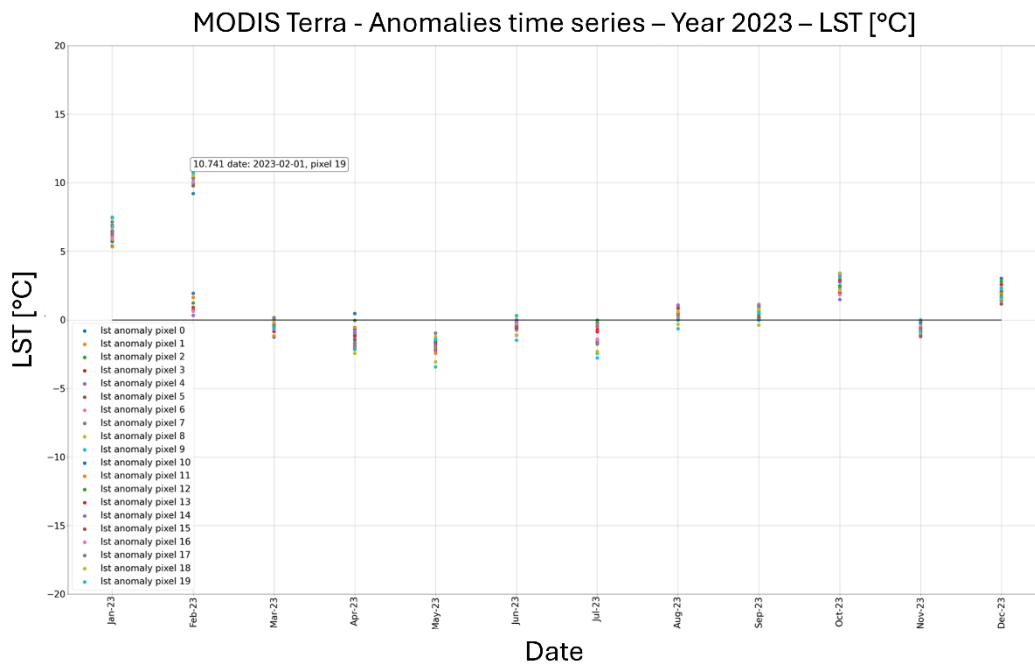


Figure 65. MODIS Terra anomalies time series for year 2023 and variable LST (AOI Milano-Novara).

Box plot

The box plot (or box and whisker plot) is calculated starting from the average value of the parameter computed over the AOI.

Figure 66 shows the box plot for GLDAS vsm_0_10 soil moisture. x-axis reports the month and y-axis the value of vsm_0_10 expressed as kg m⁻² calculated as the average value over the whole AOI. The box extends from the first to the third quartile of the data, with an orange line at the median and a green line at the average value. The whiskers extend from the box to the farthest data point lying within 1.5x the inter-quartile range from the box. Flier points are those past the end of the whiskers. For the flood event years, the red circles indicate the parameter values corresponding to the flood event dates, and the red squares the average value of the parameter for the flood event dates. The green squares instead, show the average value of the parameter for the 3 days before the event.

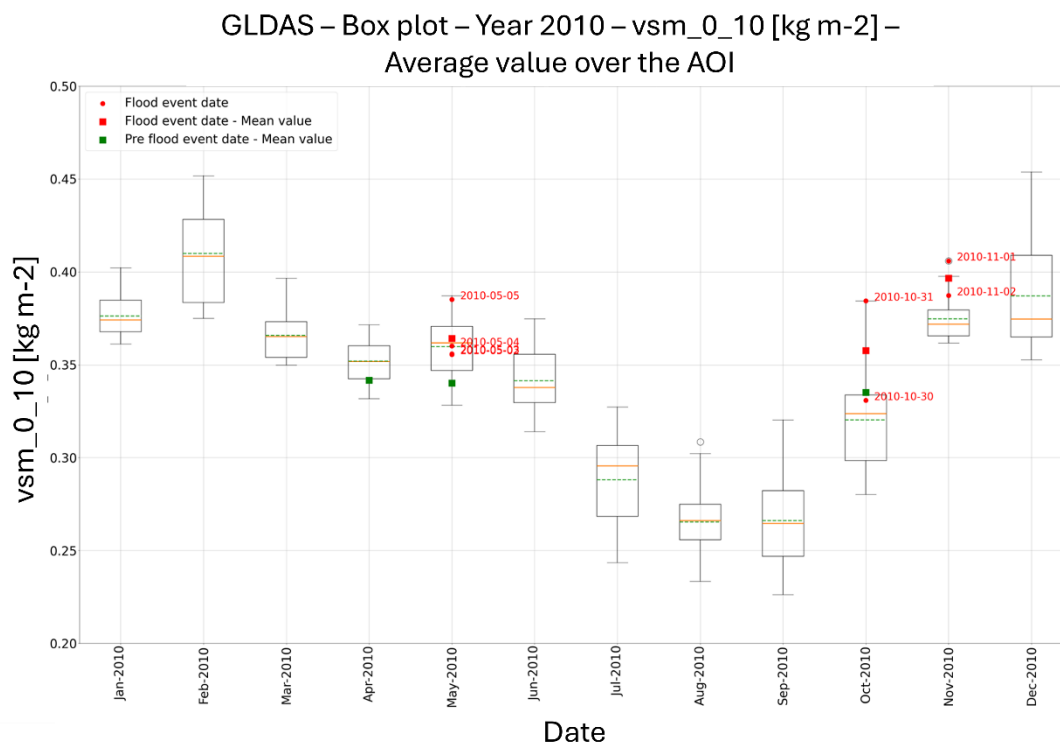


Figure 66. GLDAS box plot for year 2010 and parameter vsm_0_10 (AOI Tortona-Voghera).

Similar box plots are represented in Figure 67, Figure 68 for GPM and LST parameters, respectively.

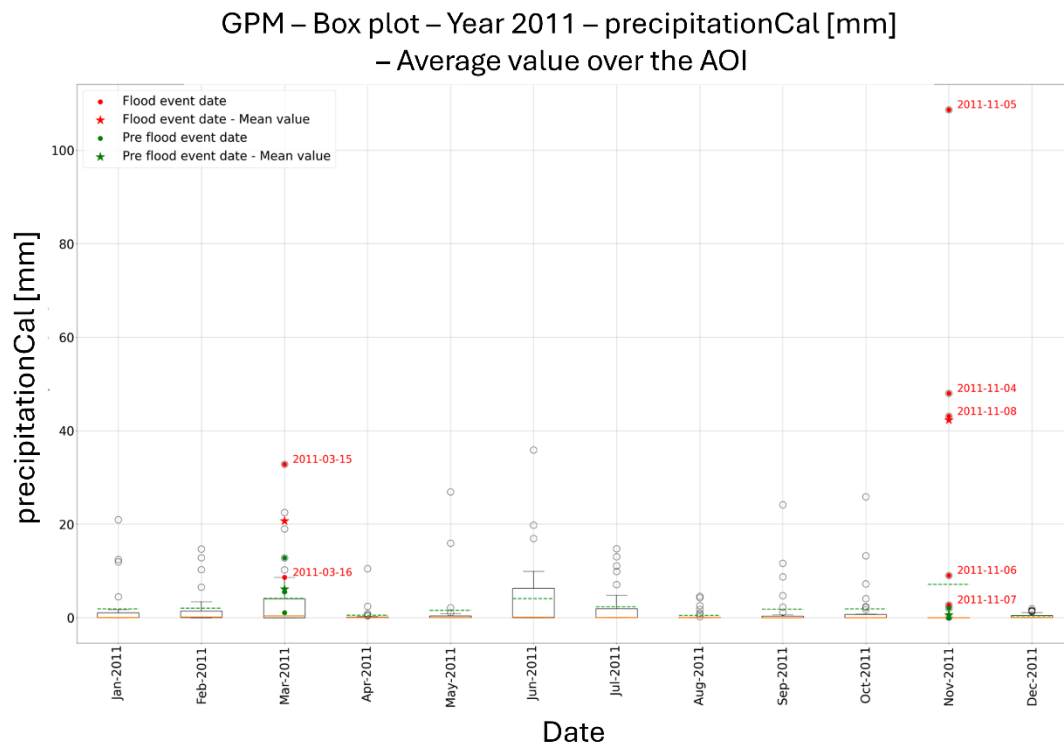


Figure 67. GPM box plot for year 2011 and parameter precipitationCal (AOI Tortona-Voghera).

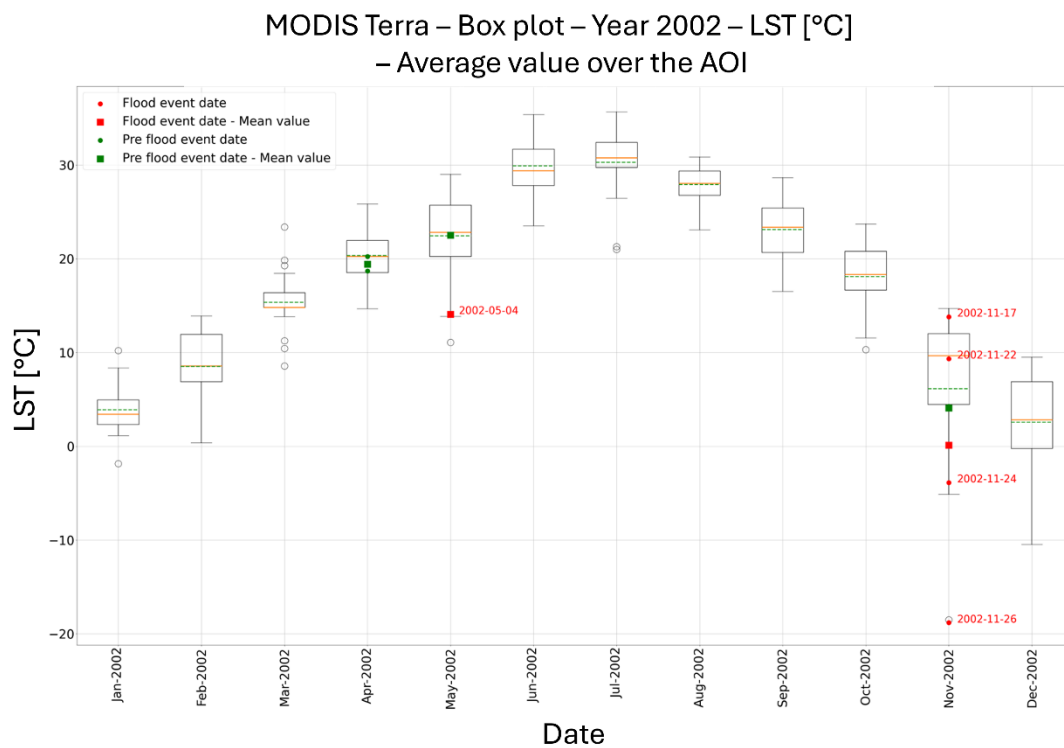


Figure 68. MODIS Terra box plot for year 2002 and parameter LST (AOI Tortona-Voghera).

Cross plot

These graphs aim at comparing the different parameters two by two. They report on the x-axis the precipitation parameter and on the y-axis the soil moisture or LST parameter. The first case is shown in Figure 69, where the x-axis refers to precipitationCal variable and y-axis to vsm_0_10 variable. The values are the average value over the AOI.

The values reported are listed below:

- Red stars are the precipitation-soil moisture couples related to the flood event dates. Regression line is also reported in red;
- Green stars are the average value of the precipitation-soil moisture couples related to the 3 days before the flood event dates. Green points are related to the single days before the event (i.e., 3 days before, 2 days before, and the day before). Regression line is also reported in green;
- Orange stars are the average value of the precipitation-soil moisture couples related to the 3 days before the flood event dates. Orange points are related to the single days after the event (i.e., the day after, 2 days after, and 3 days after). Regression line is also reported in orange;
- Blue squares are the precipitation-soil moisture couples related to the days of the year in which precipitation was higher than a predefined threshold (50 mm in this case). Regression line is also reported in blue;
- Blue point is the maximum precipitation and soil moisture values occurred during the year;
- Green square is the average precipitation and soil moisture values occurred during the whole period (from 2000 to 2023);
- Green point is the average precipitation and soil moisture values for the considered year.

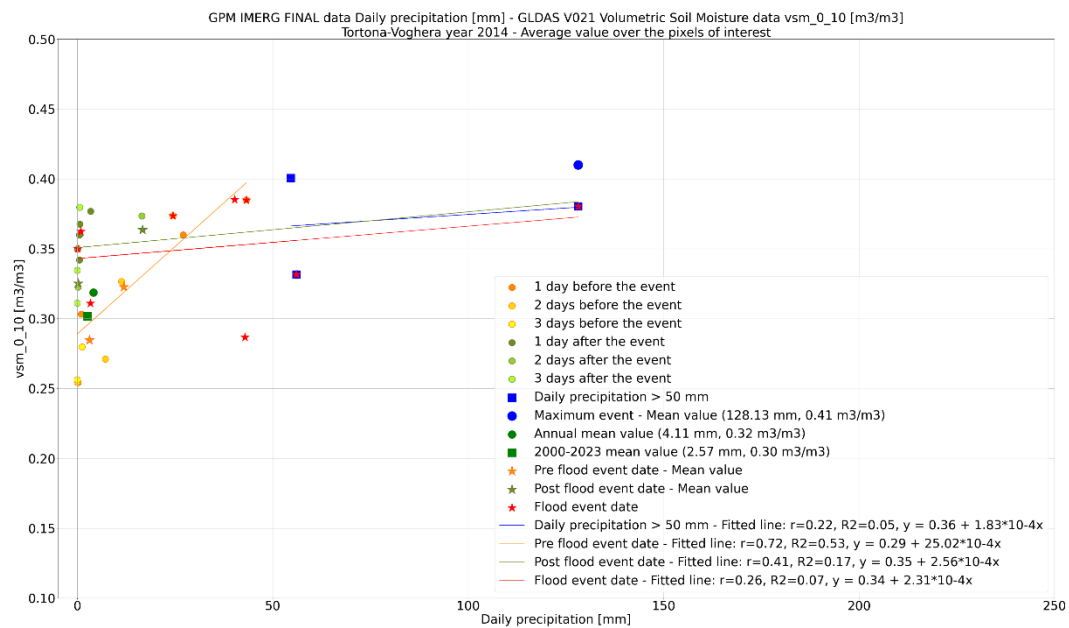


Figure 69. GPM cross plot precipitationCal-vsm_0_10 for year 2014 (AOI Tortona-Voghera).

Figure 70 shows the zoomed in version of the graph in Figure 69.

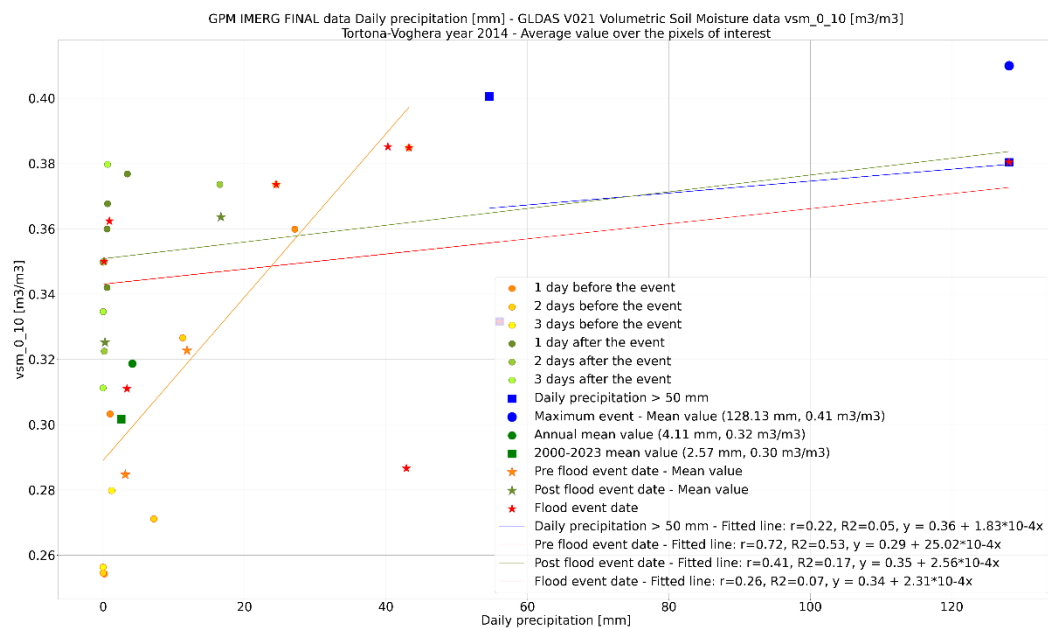


Figure 70. GPM cross plot precipitationCal-vsm_0_10 for year 2014 (AOI Tortona-Voghera).
Zoomed version.

Figure 71 similarly shows the same variables but for year 2015, for which any flood events occurred. In this and in similar cases, the values for the flood event dates and the 3 days before and after are the values of the variable for the analysed year (2015 in this case) on the days that correspond to a flood event date for the year in which a flood event occurs.

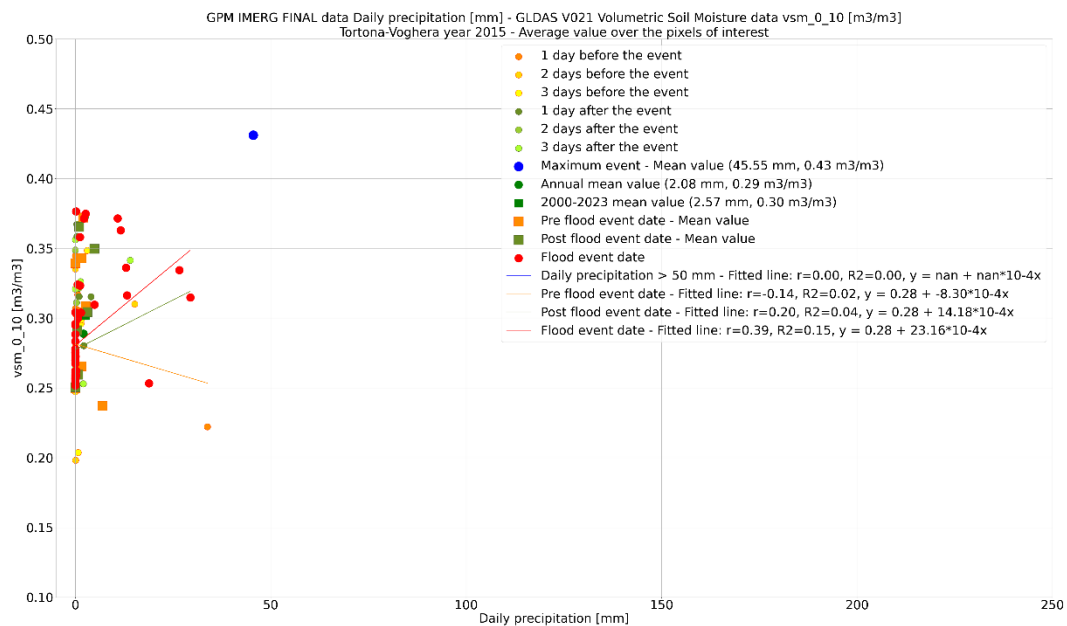


Figure 71. Cross plot precipitationCal-vsm_0_10 for year 2015 (AOI Tortona-Voghera).

Figure 72 is the zoomed in version of Figure 71.

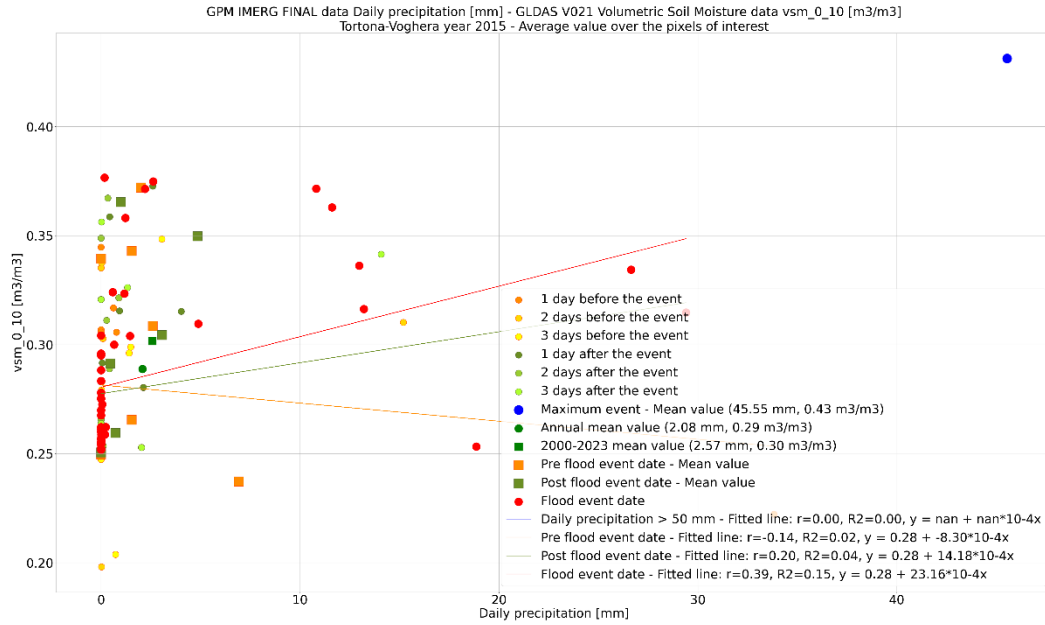


Figure 72. Cross plot precipitationCal-vsm_0_10 for year 2015 (AOI Tortona-Voghera). Zoom version.

Figure 73 is a similar graph that reports on the x-axis the precipitation parameter and on the y-axis the LST parameter.

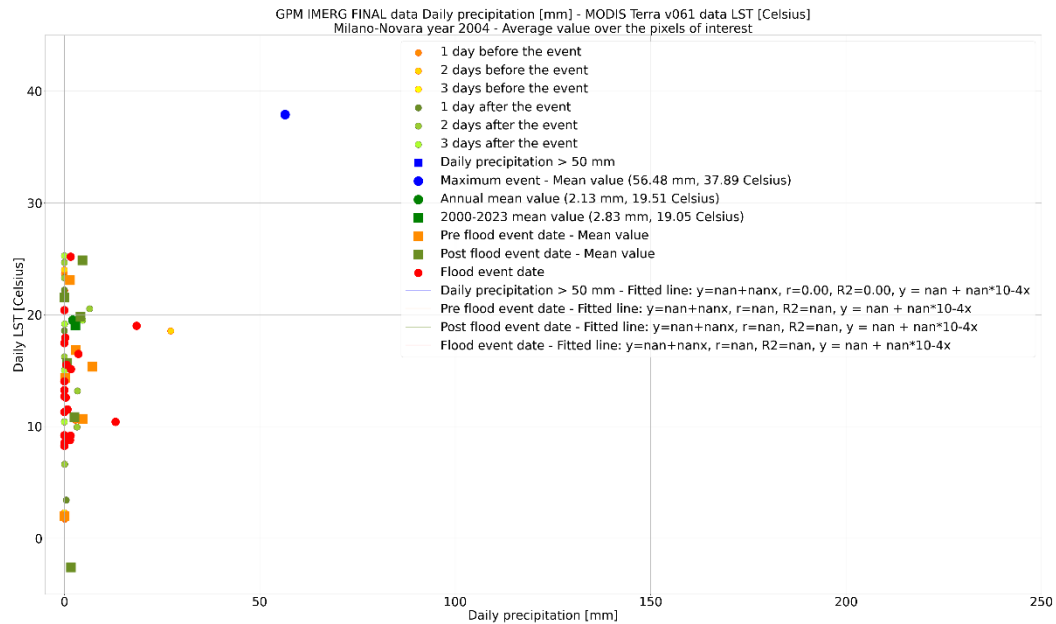


Figure 73. Cross plot precipitation Cal-LST for year 2004 (AOI Milano-Novara).

Figure 74 is the zoomed in version of the graph in Figure 73.

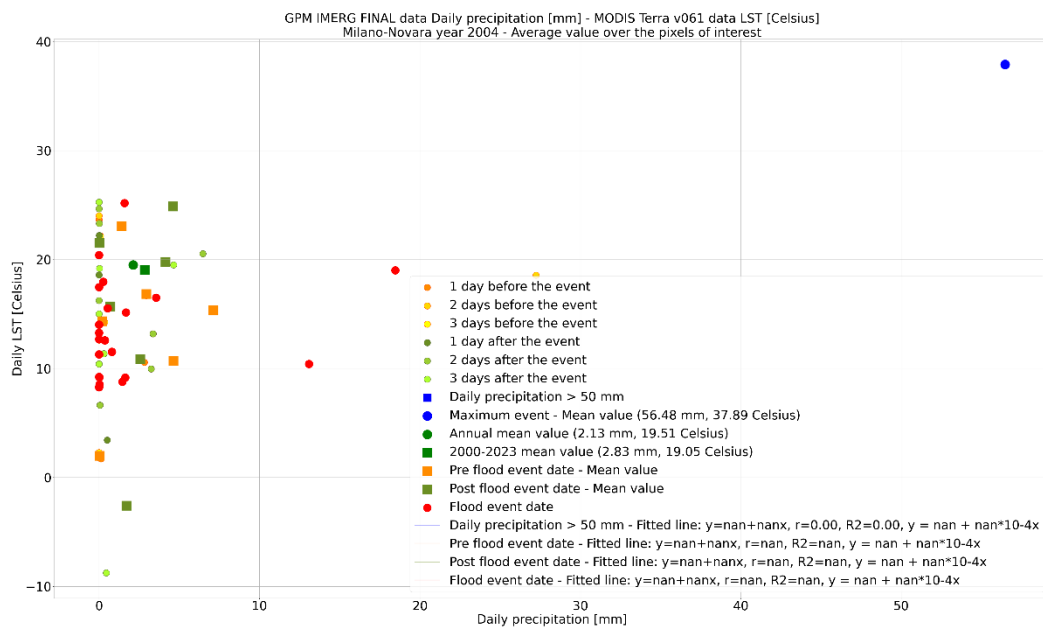


Figure 74. Cross plot precipitation Cal-LST for year 2004 (AOI Milano-Novara). Zoom version.

7.1.3.3.3. Workflow

The most significant output from elaborations described in Section 7.1.3.3.2 was selected in order to train a Neural Network (NN) model. A fully connected NN was developed to correlate the considered parameters, i.e., precipitation, soil moisture, and LST, with the extreme meteorological events. As shown in Figure 75, starting from the processed data described in Section 7.1.3.3.2 and **Table 10**, the most significant was selected and used in the NN design and development. Firstly, the dataset was created and then the model was trained and test.

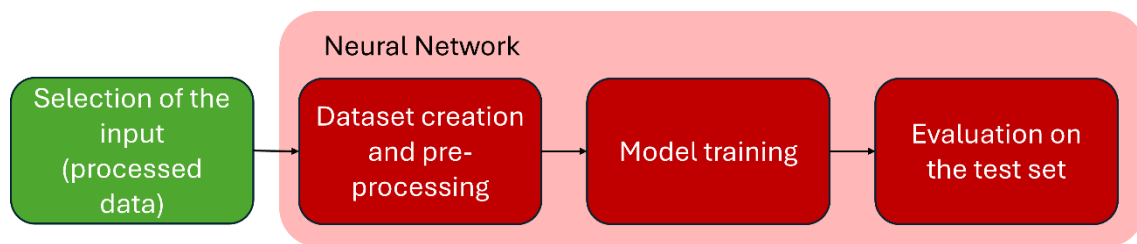


Figure 75. Workflow.

The following points (Dataset and NN model) describes the preliminary results obtained.

Dataset

In order to build the dataset, the whole number of flood events registered during the considered time period (2000-2023) was considered, for a total of 22 events. 22 non-event dates were randomly selected among the available to obtain a balanced dataset. For each event, the considered variable used as input for the NN are:

- vsm_0_10;
- vsm_10_40;
- vsm_40_100;
- vsm_100_200;
- precipitationCal.

The average value over the AOI in the 3 days before the event was considered.

The whole dataset is composed of 200 samples that were normalized between 0 and 1 and split into training, validation, and test sets with a proportion of 70%, 20%, and 10%.

LST variable was discarded at a first stage, since it exhibited a lower correlation with the events.

The addition of other parameters is under consideration for the next development, such as land cover and terrain slope.

NN model

Figure 76 shows a general scheme of a fully connected NN for a binary classification task.

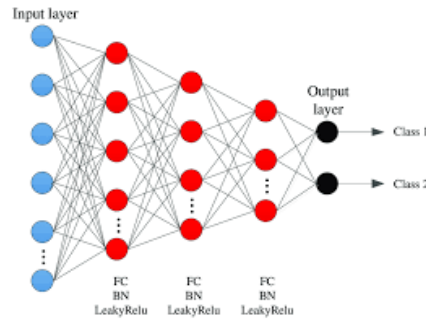


Figure 76. Fully connected NN architecture.

In this case, the input of the NN is a vector with 15 entries, that are the average value over the AOI in the 3 days before the event for each considered variable as in the following Equation (2):

$$\begin{aligned} \text{NN input} = & \text{vsm_0_10}_3, \text{vsm_0_10}_2, \text{vsm_0_10}_1, \text{vsm_10_40}_3, \text{vsm_10_40}_2, \text{vsm_10_40}_1, \\ & \text{vsm_40_100}_3, \text{vsm_40_100}_2, \text{vsm_40_100}_1, \text{vsm_100_200}_3, \text{vsm_100_200}_2, \\ & \text{vsm_100_200}_1, \text{precipitationCal}_3, \text{precipitationCal}_2, \text{precipitationCal}_1 \end{aligned} \quad (2)$$

The output instead is composed of one unit with *sigmoid* activation function to represent the class “event” and “non-event”.

The model was trained in Python with TensorFlow and Keras libraries (TensorFlow 2024, Keras 2024). One hidden layer with 2 units was considered with *relu* activation function. *sigmoid* activation function was used for the output layer. Binary crossentropy loss function and Adam optimizer were used.

7.1.3.3.4. Preliminary Results

The results presented here are preliminary results.

Different attempts were made to define the best NN architecture, which finally consists of 3 hidden layers with 15, 5, and 1 unit, respectively. Different learning rates (1e-2, 5e-3, 1e-3, 5e-4, 1e-4) and batch sizes (8, 16, 32, 64) were tested, and the early stopping algorithm was used to avoid overfitting.

The best configurations founded for the two different AOI are described in **Table 11** with the corresponding accuracy values evaluated on the test set.

	AOI	
	Milano-Novara	Tortona-Voghera
Learning rate	0.01	0.01
Batch size	64	16
Test accuracy	0.81	0.65

Table 11. Training configuration and test results.

Figure 77 and Figure 78 show the loss function and accuracy during training for Milano-Novara and Tortona-Voghera AOI, respectively, for the best configuration described in **Table 11**. Loss values and accuracy evaluated on both the training and validation sets are reported in the graphs.

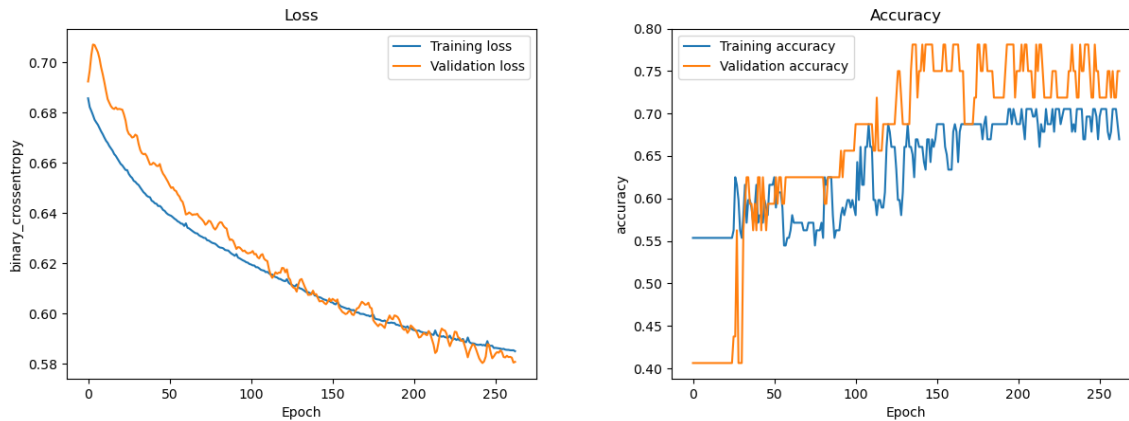


Figure 77. Loss function and accuracy for AOI Milano-Novara for training (in blue) and validation set (in orange).

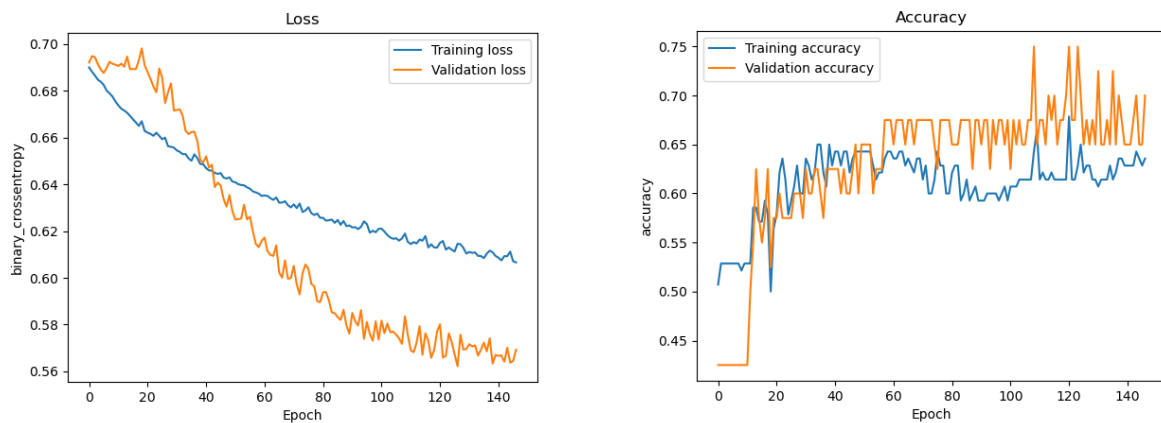


Figure 78. Loss function and accuracy for AOI Tortona-Voghera for training (in blue) and validation set (in orange).

7.1.3.4. Demonstration plan

The demonstration plan will include the integration of the collected data described above and pre-processed through neural networks in order to develop a predictive tool for flood events, based on "threshold" values of the analysed variables (i.e. precipitation, soil moisture, temperature), defined through the analysis of the same in the presence and absence of the event. The same procedure will also be developed for landslides / surface displacements, with the aim of obtaining the same result, i.e. a predictive tool for such phenomena.

7.1.4. Interferometric Analysis for subsidence

Synthetic Aperture Radar (SAR) will be used to monitor areas affected by hydrogeological risk and earthworks in general. DInSAR interferometry processing allows terrain displacement retrieval between dates, by mean of two successive SAR satellites acquisitions. This section is aimed to demonstrate these capabilities on selected areas pertaining two use cases, namely: Multiscale Monitoring of Civil Assets (Italy) and Bridges and Earthworks Asset Management aided by Geotechnics (Spain).

7.1.4.1. Selected equipment, technical specifications and justification

ESA Sentinel-1A and Sentinel-1B have been selected as data provider to support SAR analyses, particularly IWS SAR (Interferometric Wide Swath) has been selected as analysis' mode. Data are acquired in interferometric configuration (i.e. with the same geometry) by Sentinel-1A and Sentinel-1B with 12 days periodicity for single satellite (6 days considering both the satellites). The main orbital satellites parameters have been reported here below.

7.1.5. Orbital Parameters	Sentinel-1A	Sentinel-1B
Apogee Altitude	693 Km	693 Km
Inclination	98.18°	98.18°
Eccentricity	0,0016871	0,0016871
Anomaly	0°	180°
LTAN	18:00	18:00

Table 12. Sentinel-1A and Sentinel-1B orbital parameters.

Data used for analyses are IWS (Interferometric Wide Swath) as SAR Mode and SLC (Single Look Complex) as processing level.

Single look Complex provides data information in terms of module and phase for each pixel.

Sentinel-1 data can be both Single Pol (HH or VV) and Dual Pol (HH+HV or VV+VH), analyses have been concentrated on VV polarization that has a better penetration through vegetation allowing to detect better earth surface displacement.

IWS Sensor Mode is based on TOPS SAR Mode, described in following figure.

IWS mode captures three sub-swaths (from IW1 near range to IW3 far range) with progressive scan of the area to be acquired (TOPSAR), further each subswath is divided in up to 9 bursts in azimuth direction.

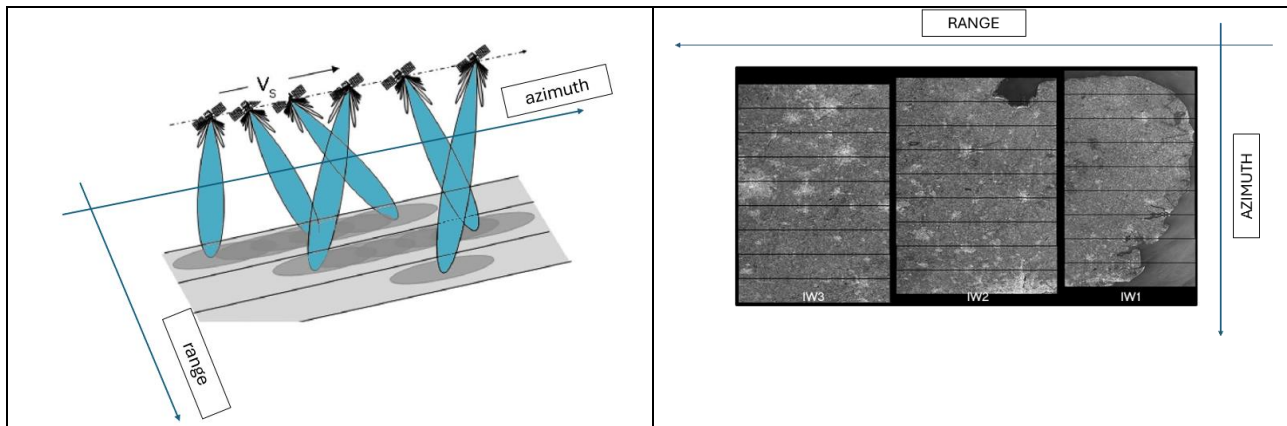


Figure 79. IWS TOPS SAR Mode Acquisition Scheme.

With the TOPSAR technique, in fact, in addition to beam steering the in range, it is also electronically steered from backward to forward in the azimuth direction for each burst, resulting in homogeneous image quality throughout the swath.

Table below reports off nadir and incidence angle for Intergerometric Wide-Swath Beams.

7.1.6.		IW1	IW2	IW3
Min Orbital altitude	Off-nadir	27.53-32.48	32.38-36.96	36.87-40.40
	Incidence	30.86-36.59	36.47-41.85	41.75-46.00
Max Orbital Altitude	Off-nadir	26.00-30.96	30.86-35.43	35.35-38.88
	Incidence	29.16-34.89	34.77-40.15	40.04-44.28

Table 13 IWS TOPS incidence and Offnadir per subswath.

Resolution and swath relevant to IWS SAR mode are reported below.

7.1		Range	Azimuth
Swath Size	[km]	~250	~250
Resolution	[m]	~5	~20

Table 14 Sentinel-1 IWS TOPS Swath and resolution geometric parameters.

7.1.9.2. Installation layout

The processing of retrieving earth surface displacement has been performed through two software, namely:

- SNAP (Sentinel's Application Platform)
- SNAPHU: Statistical-Cost, Network-Flow Algorithm for Phase Unwrapping

SNAP is open available under GNU GPL v3 licence, SNAPHU is a plugin for SNAP.

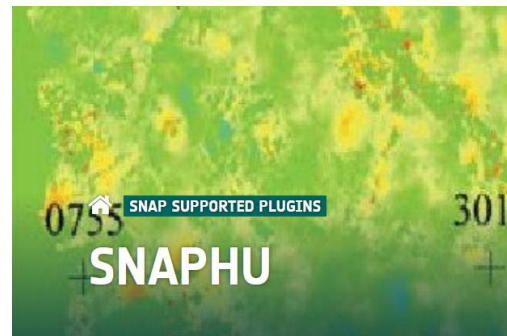


Figure 80 SW installed.

7.1.9.3. Initial data collection and results

Analyses have been performed on two areas:

- Cerignola Campagna in Italy [LAT = 41.31555556 LON= 15.89638889]
- Talud Briones in Spain [LAT = 42.55472222 LON=-2.828055556]

Both areas are interested by subsidence phenomena. These phenomena are tracked by the European Ground Motion Service available at EGMS (copernicus.eu). EGMS will be used as comparison for results obtained through SNAP processing; proving the successful incorporation of the SAR processing capability.

The EGM service covers the European area through several measures' points in which historical data from Sentinel-1A and Sentinel-1B are collected.

For each point displacement data measures are reported in a time interval between 2018 and 2022 in terms of:

- East-West displacement
- Vertical displacement

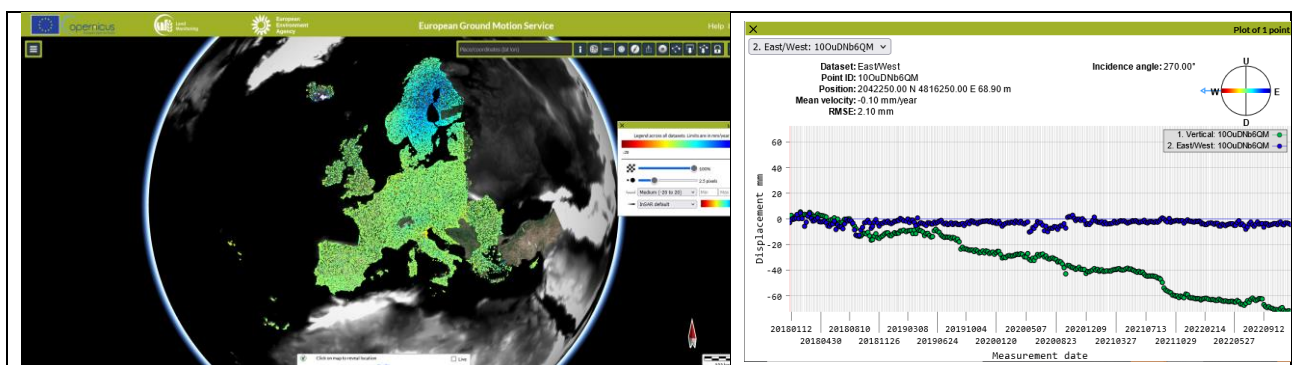


Figure 81. EGM Service and example of Reports per point (Vertical and East-West Displacement).

Here below are reported the displacements identified by EGM service on the areas of Figure 82 and Figure 83 report reported the displacements identified by EGM service on the areas of Cerignola Campagna (Italy) and Talud Briones (Spain).

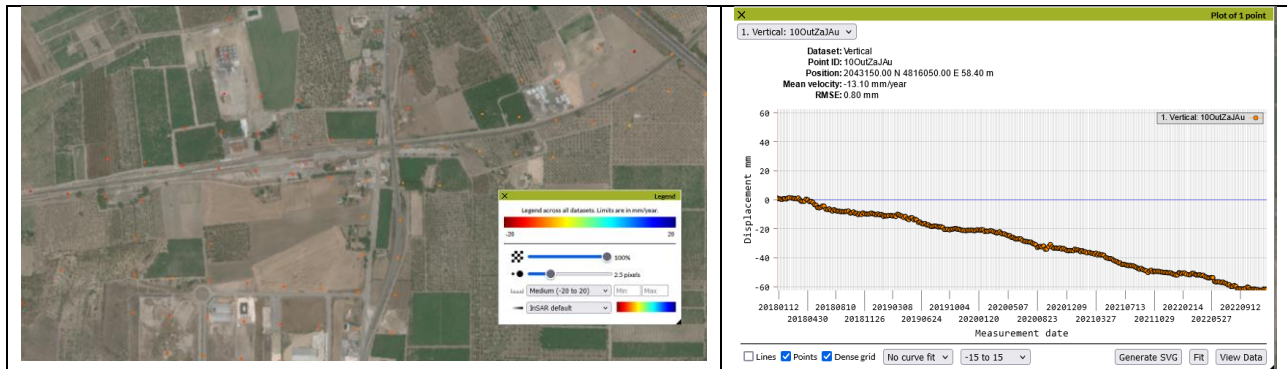


Figure 82 EGM Service Vertical Displacement on Cerignola Area.

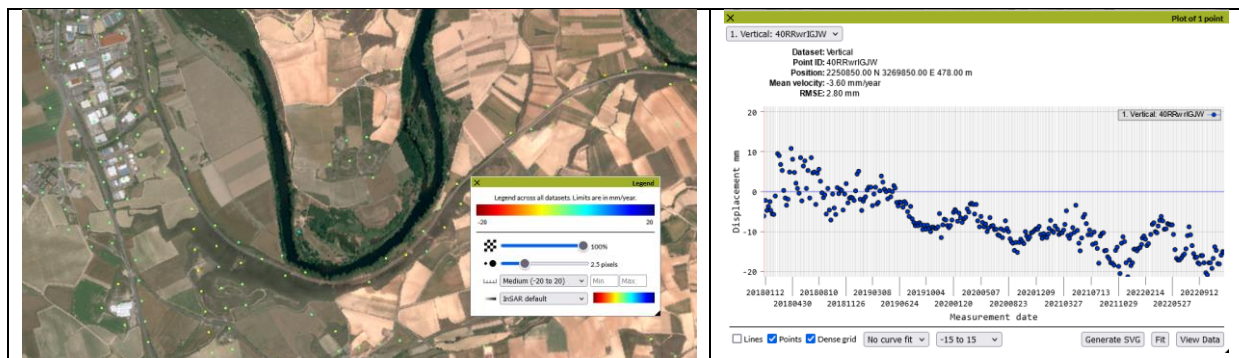


Figure 83 EGM Service Vertical Displacement on Talud Briones Area.

For Talud Briones, it is expected a worst-case displacement of around 2 cm in 4.5 years.

7.1.9.4. Data collection and process

Sentinel-1 SLC data, needed to perform interferometric analyses, have been retrieved from Copernicus Browser. The browsing of the data and respective downloads are available after user registration.

Data retrieval is supported by a set of filters based on: Geographical Area, Time Span, Processing Level, plus Satellite/Orbit Direction/Orbit Number/Acquisition Mode/Beam ID/Polarization

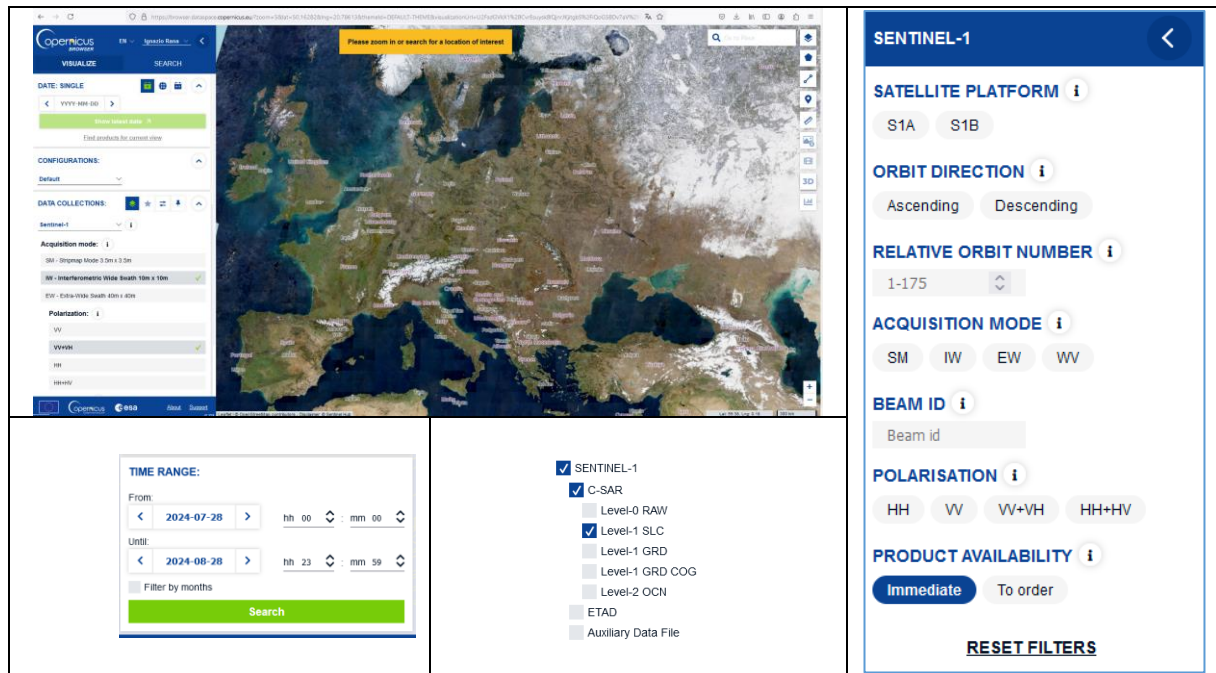


Figure 84 Copernicus Browsee and Data Download.

For Cerignola, we selected the following interferometric couple (reported has Start Time):

- START_TIME_1 = 20180108_165715
- START_TIME_2 = 20220908_165748

Likewise, for Talud Briones we selected:

- START_TIME_1 = 20181231_061647
- START_TIME_2 = 20220923_061800

7.1.9.5. Algorithms and implementation

The interferometry concept relates with Synthetic Aperture Radar observations from satellite.

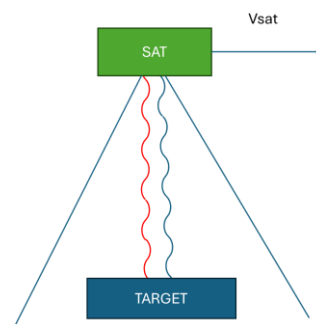


Figure 85 SAR Acquisition Concept.

From the satellite, an electromagnetic signal is sent downward to earth. From each point of the earth surface, the satellite receives signal and phase of the reflected signal (integrated for visibility time). This information is collected in L1 product level: Single-Look Complex Slant Products (SLC).

Gathering two or more acquisitions over the same area (having the same acquisition geometry), allows to assess earth surface movements (with cm precision).

For a given target, the same acquisition geometry is guaranteed by the repeating orbits track of satellites (picture below on the left). These orbits recur on the same track after a whole number of days (repeat cycle), for example Sentinel-1 has a repeat cycle of 12 days with a daily number of orbits equal to $14+7/12$. In the picture below, on the right, two fundamental concepts and terms relevant to interferometry are illustrated. These are driving the processing performance:

- Parallel Baseline (B_p in figure)
- Perpendicular Baseline (B_n in figure)

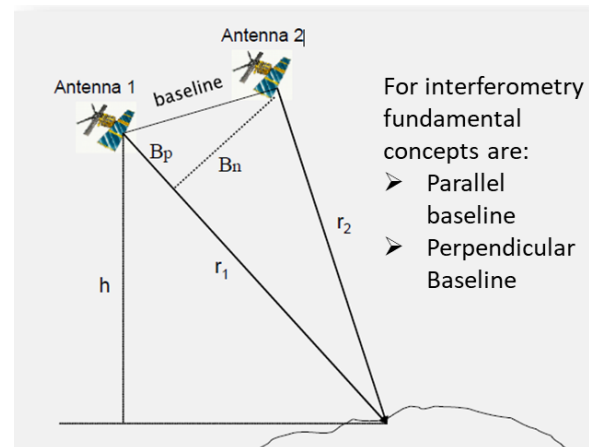
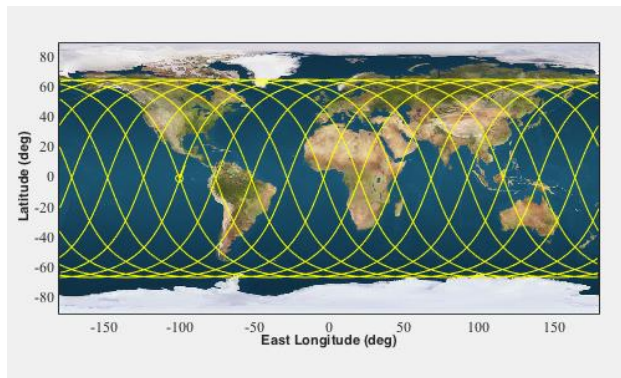


Figure 86. Left: repeating Ground Track. Right: Interferometric Concept.

Programming two acquisitions and requesting relevant Single-look Complex Slant (SCS) products on the same area displaced in time of a repeat cycle, enables the interferometric concept itself and associated processing.

For each pixel, SLC products report information pertaining to signal modulus and phase. Considering two corresponding pixels on two interferometric SLC products, the following signals are obtained:

$$S1 = A1e^{-j\varphi1} = A1e^{-j\frac{4\pi}{\lambda}r1} \quad (16)$$

$$S2 = A2e^{-j\varphi2} = A2e^{-j\frac{4\pi}{\lambda}r2} \quad (17)$$

Where $A1$ and $A2$ are the amplitude of respective signals and $r1$ and $r2$ are the distances between the satellites in the two positions and the pixel under analysis.

The interferogram is the pixel-to-pixel map of the phase differences between S1 and S2 obtained multiplying the first image by the complex conjugate of the second image.

$$S1S2^* = A1A2e^{-j\frac{4\pi}{\lambda}(r1-r2)} \quad (18)$$

$$\varphi_{TOT} = -\frac{4\pi}{\lambda}(r1 - r2) \quad (19)$$

The resulting phase difference is in general the sum of different contribution:

$$\varphi_{TOT} = \varphi_{FLAT} + \varphi_{TOPO} + \varphi_{DISPL} + \varphi_{ATM} + \varphi_{ERR} \quad (20)$$

Where:

- φ_{TOT} is the total interferometric phase
- φ_{FLAT} is the phase associated with earth curvature
- φ_{TOPO} is the phase associated with earth topography
- φ_{DISPL} is the phase associated with earth deformation during the two different acquisitions
- φ_{ATM} is the atmospheric phase
- φ_{ERR} is the noise (error) phase

Purpose of the InSAR processing is to calculate φ_{TOPO} (obtained neglecting or compensating the terms φ_{FLAT} φ_{DISPL} φ_{ATM} φ_{ERR}). Retrieving φ_{TOPO} provides the Digital Elevation Model (DEM).

Purpose of the DInSAR processing is to evaluate the earth surface displacement φ_{DISPL} between two time shifted observations (this is obtained by neglecting or compensating φ_{FLAT} φ_{TOPO} φ_{ATM} φ_{ERR}).

The main component φ_{TOPO} can be removed by having a high accuracy DEM.

The schematic of the sequence activities for DEM retrieval (InSAR) and displacement retrieval (DInSAR) are illustrated the picture below.

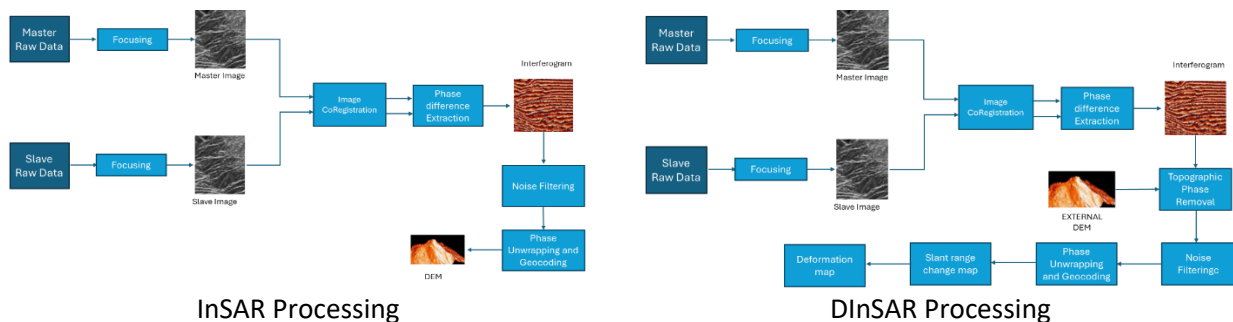


Figure 87 Operation sequence for DEM and displacement retrieval.

Details of the theoretical background are given in a dedicated Annex, provided with this document.

7.1.9.6. Workflow

Workflow Steps are thoroughly described in TRAINING KIT – HAZA03: LAND SUBSIDENCE WITH SENTINEL-1 using SNAP.

https://eo4society.esa.int/wp-content/uploads/2022/01/HAZA03_Land-Subsidence_Mexico-city.pdf

7.1.9.7. Preliminary results

The processing has been executed on Cerignola AOI taking two SAR products data between dates:

- START_TIME_1 = 20180108_165715
- START_TIME_2 = 20220908_165748

As can be seen the displacement retrieved between 01/2018 and 09/2022 is in the order of 3 cm, in line with expected results from EGM.

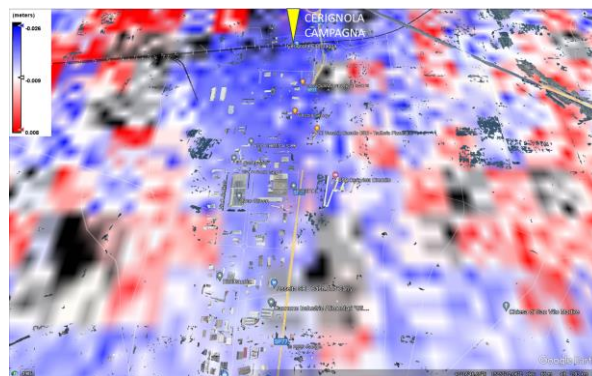


Figure 88. Subsidence on Cerignola AOI.

Same processing has been executed on Talud Briones AOI taking two SAR products data between dates:

- START_TIME_1 = 20181231_061647
- START_TIME_2 = 20220923_061800

The displacement retrieved between 12/2018 and 09/2022 is in the order of 2 cm; in line with expected results from EGM.

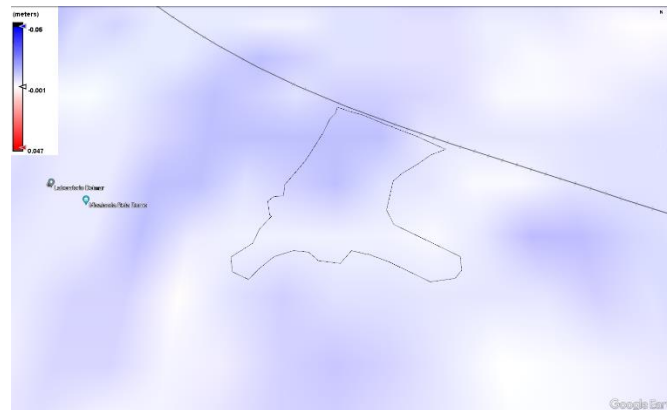


Figure 89. Subsidence on Talud Briones AOI.

Marginal discrepancies with the data of EGM results are expected. This is deemed to be related with the limited number of images processed (just 2 time-stamps, in years long time spans) for the mere sake of this demonstration.

7.1.9.8. Demonstration Plan

The areas proposed in these paragraphs (Cerignola and Talud Briones) are good examples of pathological areas, where terrain's instability occurs. SAR analysis will be provided on demand, or as available (e.g. satellite tasking or archive) to stakeholders dealing with Hydrogeological risks and Earthworks in different areas (Italy and Spain). Other areas could be inspected and tracked. Margin of improvement in the processing of the data will be explored. This could be attempted by selecting more accurate sources (other data providers) and by improving the processing chain.

7.2. Bridges and Earthworks Asset Management aided by Geotechnics (Spain)

7.2.1. Selected equipment, technical specifications, and justification

In this section the selected equipment, technical specification and justification will be described for the different UC pilots:

- Bridges.
- Earthworks.
 - Briones.
 - Vilar de Silva.

7.2.1.1. Bridge Assets Management

The monitoring system for both the support apparatus and the dynamic analysis of the structure shall consist of the following elements:

- **Sensors**, which are responsible for measuring displacements, inclinations, accelerations, temperatures and wind speed and direction.
- **Data acquisition equipment**, which is responsible for capturing the signals delivered by the sensors.
- **Processing and control equipment**, which is where the data captured by the acquisition equipment is processed and from where the entire system is controlled. This group also includes the equipment necessary for conditioning the power supply and for communications with the outside world.

Specifically, three companies (INECO, CEDEX and COMSA) will install their equipment and sensors in order to obtain the data required. The installation will be performed following the schemes of installation layout section.

The three companies that will be working on the viaduct will coordinate their activities with ADIF's R&D&I Project Department. This will ensure that they are able to work independently during the installation process.

CEDEX has awarded a contract for technological linking to the company Álava Ingenieros, which is responsible for supplying all the data acquisition and sensor equipment and for providing expertise in this field. The safety pilot will be provided by CEDEX, and all instrumentation will be confined to the interior of the board, with no sensors or equipment on the railway platform.

Furthermore, INECO will install a total of 30 triaxial accelerometers, capable of capturing the dynamic behaviour of the viaduct in the first five spans, also inside the deck, in the lower slab. INECO has safety pilots, which are necessary for access to the inside of the fence.

Finally, COMSA will install three chambers on the railway platform, each with an accelerometer and an inclinometer. This will enable us to correlate the data acquired on the surface with the data from the concrete structure itself. These devices are the only ones to be installed on the railway platform and will be assisted by COMSA safety pilots and track personnel from the Gabaldón Maintenance Base, to ensure that the proposed location and the execution itself does not affect maintenance tasks.

The three different installations performed for the bridge assets management are detailed below:

1. The monitoring system for POT bearings.

The objective of this installation is to analyse the POT support equipment in detail to analyse pathologies and service life and to optimise their maintenance. Most of the sensors and equipment will be concentrated in 5 zones or nodes distributed along the length of the viaduct. The corresponding layout is presented on the schemes of installation layout section. CEDEX will install, on 4 piles (P1, P5, P9 and P15) and on Abutment 1 a total of:

- **h14 LVDT units** (linear displacement sensors). An LVDT is an electromechanical device that converts vibrations or mechanical motion, specifically rectilinear motion, into electrical current, voltage, or variable electrical signals, and vice versa. These drive mechanisms are used primarily in automatic control systems or as mechanical motion sensors in the field of measurement technologies. The classification of electromechanical transducers includes conversion principles or types of output signals.

- 8 Inclinometers.
- 8 Resistance thermometers.

To ensure compatibility and interoperability with other monitoring systems to be installed on the viaduct, communications between the data acquisition equipment and the processing and control equipment will be carried out using the **EtherCAT** field bus standard. When the distances between nodes so require, physical media converters will be used for this bus, and **fibre optic** cables will be used. The monitoring system must be equipped with **GPS** precision absolute time, allowing cross-checking of the information obtained with events or observations made with other systems.

2. The monitoring system for dynamic analysis of the structure.

The objective is to identify any alteration in the dynamic behaviour of the structure resulting from a malfunction of the support devices (change in the boundary conditions) in the area of greatest stroke across the entire viaduct. This area coincides with the area of highest density of sensors for capturing support movement, which is the responsibility of CEDEX.

INECO will install a total of **30 triaxial accelerometers** in the first five spans of the viaduct. These will be bolted to the bottom slab and will be capable of capturing the dynamic behaviour of the viaduct. The accelerometers will be **powered by cable** from the power supply panel.

The specifications of the Triaxial accelerometers (Figure 90) are shown in Table 15.

Triaxial accelerometer $\pm 2g$		
General		
	Measuring range	$\pm 2g$
	Number of axes	3 (x, y, z)
	Signal conditioner	Integrated
	Operating temperature	-20 to +70 °C
Interface		
	Output type	EtherCat
	Connectors	RJ45
Feeding		
	Supply voltage	12 to 48 Vdc (via EtherCat)
	Consumption	<1.5W
Output (per axle)		
	Bandwidth	1kHz (-3dB)
	Sampling frequency	4 kHz
	Dynamic range	96 dB
	Noise	25 $\mu g/\sqrt{Hz}$
	Offset	$\pm 4 \text{ mg}$
	Offset derivative	< $\pm 0,15 \text{ mg/k}$
	Linearity error	< 0.1% of full scale
	Cross-sensitivity	< $\pm 1 \%$
Regulatory compliance		

Triaxial accelerometer $\pm 2g$		
	Environmental	Degree of protection IP66 (IEC 60529) IEC 60068
	EMC	EN 61326

Table 15. Triaxial accelerometer specifications.



Figure 90. Triaxial accelerometer image.

For further information, Annex 1 lists and gives a concrete and precise description of sensors, data acquisition equipment, processing and control equipment, electrical installation materials and auxiliary materials and equipment to be supplied by the contractor.

3. The monitoring system for correlation

The objective is to collate data in order to enable correlation with data measured by CEDEX and INECO and processed by CEMOSA through information received from the project database. This will facilitate the detection of any existing damage and observation of variations in the behaviour of the structure over time.

Furthermore, COMSA will install a gateway at abutment 1 or stack 1, which will be connected to the power supply and have a LoraWAN connection to the aforementioned sensors. The data acquisition system will be connected to the gateways. The specifications of the devices to be installed are:

- **LS-ACC-CELL-1C long-life batteries:** Saft LSH 14 C-size spiral cell battery (5.8Ah) for the LS-G6 family.

- The Gateway LSG6KIOGW8680 Load sensing LS-G6 outdoor gateway is a 868 MHz model with a 4G module and an internal 2.6 dBi radio antenna.
- Vibration meter (LSG7ACL-BILH-VIB)
- Three-axis inclinometer (LS-G6-TIL90-I, version with indoor antenna).

COMSA will install [three manholes](#), each equipped with sensors such as [accelerometers](#) and [inclinometers](#). The chambers will be prefabricated without a bottom, as detailed in Figure 91.

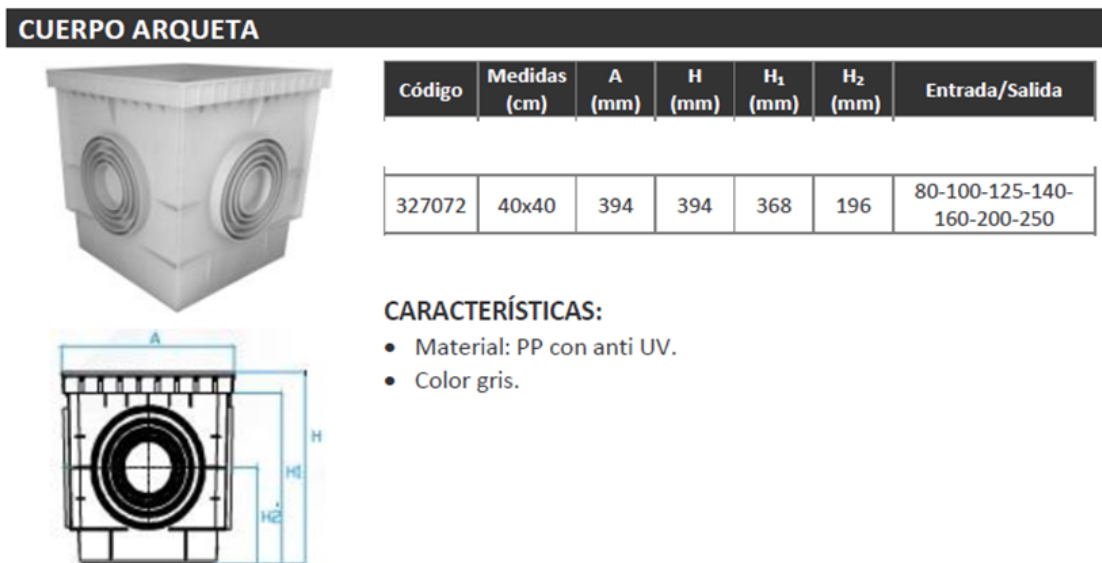


Figure 91. Concrete wall box 40x40 inside without bottom.

The manholes will be fixed at their base and the infrastructure will be sealed with mortar or other material to prevent displacement. If necessary, a silicone or sealant will be applied to make them more watertight. The three manholes will be installed in the trench where the catenary posts are anchored, between the communications duct and the wall containing the ballast bed, in the direction of Madrid (west), on the inside side of the curve (north). No action will be taken between the tracks in the ballast area, thus minimising risks. In addition, a more detailed analysis will be carried out of the behaviour of the POT and structural supports of the viaduct and their correlation with the data to be recorded with the CEDEX and INECO sensors. This location allows for better connectivity and simplicity in case any additional intervention is required.

7.2.1.2. Earthworks Assets Management

[Wireless tiltmeters](#) are sophisticated instruments designed to measure the angle of slope inclination and detect minute changes in slope movements.

These devices are strategically placed on slopes adjacent to railway tracks to continuously monitor their stability. The use of wireless technology in these tiltmeters offers several key advantages:

- Real-time Data Transmissions

- Remote Monitoring
- Cost-Effective Deployment
- Scalability and Flexibility
- Data Integration and Analysis

In summary, the use of wireless tiltmeters in the railway sector represents a significant advancement in monitoring unstable slopes. By providing real-time, remote, and cost-effective monitoring solutions, these devices enhance the safety and efficiency of railway operations. As technology continues to evolve, the integration of wireless tiltmeters with other monitoring systems will further improve the ability to predict and mitigate the risks associated with unstable slopes.

The specification will be described following the two pilots regarding earthworks: (1) Briones and (2) Vilar de Silva.

7.2.1.2.1. Briones

The general scope of the action is represented by the development of the following activities:

1. [Installation of the equipment](#), configuration of the nodes, and data transmission.
2. [The provision of access and license](#) for one year to a web platform for the visualization of data generated in the field, including the capacity to manage alarms and trigger actions, with no impact on the change.
3. [The dismantling of the various pieces of equipment](#).

The objective is to implement a network of low-cost sensors to collect data in real time, in situ, and correlated with data from existing instrumentation on the slope.

The proposed instrumentation is of the [WSN \(wireless sensor network\) type](#), i.e., a network of contact sensors that measure terrain or environmental variables but communicate without wiring. In other words, it is a data acquisition network based on [IoT technology](#), capable of autonomously and reliably capturing data at remote measurement points by means of dataloggers with telematic capacity without the need for external connectivity and low power consumption.



Figure 92. Example of Gateway + solar panel installed on catenary pole.



Figure 93. Detail of the Gateway and the solar panel to be installed on the catenary pole that is located in front of the unstable slope.

The system comprises **14 wireless clinometers**, which are connected either individually or in small groups to reading nodes. These act as local dataloggers, **measuring, recording and sending** data to a network or directly to a gateway, which acts as a central datalogger or hub. Communications are by radio using the Flat Mesh protocol. The clinometers will be distributed across the entire surface of the slope and installed on 25-30mm diameter corrugated bars embedded in the ground.

Figure 94 and Figure 95 depict the installation of the 2-meter corrugated bars, which serve as support for the sensors. These bars are installed with a sledgehammer in a 1-meter embedment depth and 1-meter elevation above the soil and vegetation.



Figure 94. Type clinometers to be installed on the slope on rebar. Specifically, 14 clinometers of the same type as the one shown on the right of the image will be installed.



Figure 95. Mode of installation of rebar.

The system is completed by a [weather station](#) capable of simultaneously reading [rainfall](#), [ambient temperature](#), and [relative humidity](#). This station will be installed on an existing hut next to the track in a safety area on a mast. A [video camera](#) will be placed on a catenary pole to determine whether the system alarm is false or true.

The two devices will be integrated into the dashboard, web viewer, or digital platform. The communications gateway will be located next to the track on a catenary pole and powered by a solar panel. It will transmit all the data via Internet telephony through [cellular connectivity \(4G\)](#) and integrate the data from the sensors to a digital platform for alarm management.



Figure 96. Example of a weather station installed on a shed.



Figure 97. Type video camera installed on catenary pole.



Figure 98. Detail of the Inclinator installed.



Figure 99. Inclinator installed on the Corrugated Bar

The digital platform or web viewer serves to complete the scheme and has no impact on the proposed change. It is included here for a complete understanding of the system to be installed. Figure 100 outlines the proposed architecture.

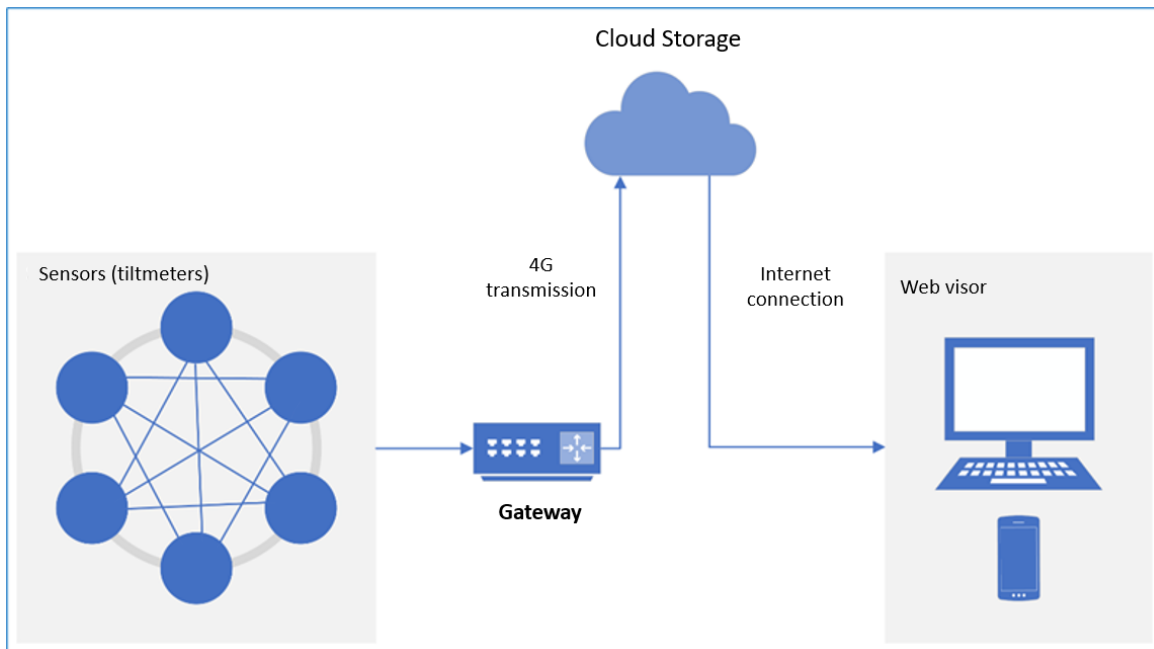


Figure 100. Schematic of the proposed architecture.

The slope monitoring system under study will be composed of:

- **Sensor network**, formed by **wireless clinometers**, in charge of measuring displacements, inclinations, temperatures, rainfall and relative humidity. These sensors will be installed on the surface, inside the unstable slope.
- **Gateway**, in charge of capturing the signals delivered by the sensors in the local network and from where the whole system is controlled at the level of communications with the exterior. This device will be in charge of the bidirectional communication between the sensor network, as well as with the database hosted in the cloud. The Gateway must ensure a continuous data flow for the instrumentation and its radius of action must cover the entire slope, whose surface area is approximately 6,000 m². It must allow the generation of customized CSV files for any combination of nodes / channels, as well as individual files for each node. In addition, it must be robust enough to minimize maintenance operations. The Gateway will be powered by solar panel and battery, which will be installed next to the device on the catenary pole in front of the unstable slope to be monitored.
- **Web visor**, for the consultation of the evolution of the slope movements.
- **A video camera**, which will be placed on a catenary pole to determine whether the system alarm is true or false.

7.2.1.2.2. Vilar de Silva

This case study deals with a slope in north western Spain located at the entrance of a tunnel. This area which suffers from high frequency rainfall and the presence of a reservoir with continuous rising and falling of the water level, which exacerbates the instability of the slope that consequently can cause problems in the infrastructure.

ADIF deployed a data acquisition network based on IoT Worldsensing technology, capable of autonomously and reliably capturing data at remote measurement points using telematics-enabled dataloggers with no need for external connectivity and low power consumption.

The sensor network responsible for measuring displacements, slopes, temperatures, rainfall and relative humidity. It is composed of the following elements:

- **Wireless tiltmeters - LS-G6-TIL90-X / LS-G6-TIL90-I.** Tiltmeters, alone or in close clusters, act as a local datalogger, measuring, recording and sending data to a gateway that acts as a central datalogger or hub.
The tiltmeters are distributed over the entire surface of the slope and can be installed on the ground as well as on rock or concrete. On this occasion, 4 tiltmeters have been installed on the sleeper, 3 tiltmeters on rock, 2 tiltmeters on the concrete wall or tunnel gable and 7 tiltmeters on the ground.
The tiltmeters and their installation can be seen in Figure 101, Figure 102, Figure 103, Figure 104 and Figure 105.
- **The Gateway - 4G Rugged Gateway – Edge.** The gateway is in charge of capturing the signals delivered by the sensors in the local network. It is the device from which the entire system is controlled at the level of communications with the outside, being these communications by radio using the LoRa (Long Range) protocol, a low power consumption wireless network. The gateway has been powered by a solar panel.
- **Weather station - Rain-O-Matic Professional Rain Gauge:** The system is completed by a meteorological station capable of simultaneously reading rainfall, ambient temperature and relative humidity. Its purpose is to monitor rainfall in the study area, as it critically affects the hydrology and geotechnics and, therefore, the slope stability conditions and the properties of the soil itself.

The technical specifications of the three elements are detailed in their datasheets of Annex 4.



Figure 101. Installation of tiltmeter on a mast embedded in the ground.



Figure 102. Tiltmeter orientation.



Figure 103. Clinometer power batteries.



Figure 104. Tiltmeter installed on a rock.

These systems allow a higher sampling frequency, and increase the adaptability, reliability and cost-effectiveness of predictive monitoring of slope instabilities and potential landslides that could affect infrastructures.

In its maintenance programs, ADIF relies on digital solutions because they are more environmentally friendly and safer for the railway sector. Remote monitoring solutions extend the useful life of infrastructures while meeting safety requirements and improving the reliability, availability and capacity of the railway system. It also minimizes costs and improves the management of the entire asset lifecycle.



Figure 105. Tiltmeter installed on sleeper.

The complete information regarding the equipment, layout and installation is gathered in Annex 3.

7.2.2. Installation layout

In this section, the layout of the installations with the equipment and specification presented in section 7.2.1 is presented for every pilot and scenario englobed in the UC.

7.2.2.1. Bridge Assets Management

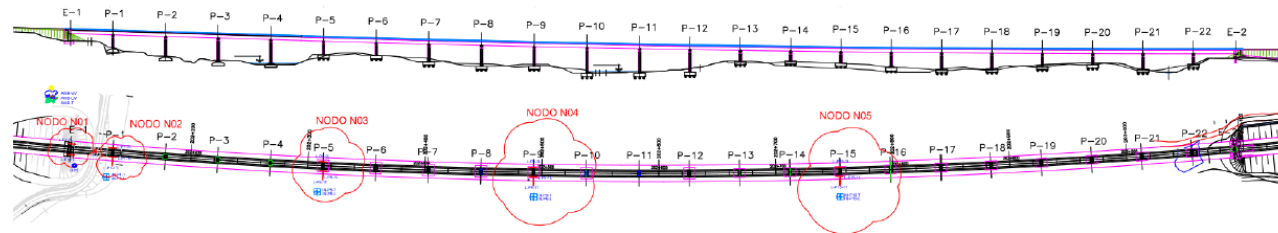
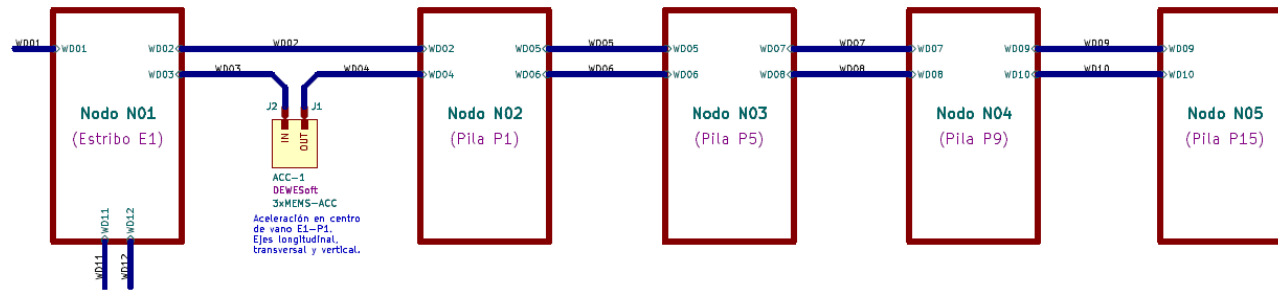
The layouts from the different installations planned for Bridge Assets Management defined are described below:

1. The monitoring system for POT bearings.

The layout planned for the Bridge Assets Management is displayed on Figure 106. The main node, Node 1, will contain the processing and control equipment and the sensors and acquisition equipment necessary to monitor the relative movements between the E1 abutment and the deck. A temperature measurement point and two relative longitudinal displacement measurement points will be set up. A weather station for measuring wind speed and direction will be installed near this node.

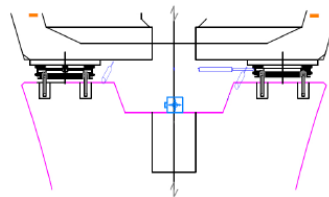
Once the electrical connection has been made from cabinet 9 of the safety installations with their respective circuit breakers, which will be carried out by the maintenance contract, a low voltage power supply cable (230V) will be laid to the inside of the panel, near Abutment 1. At this point, CEDEX will connect the cable to a power supply panel to be installed on the inside side wall of the panel, from which all the equipment and sensors will be supplied with electricity.

The remaining four nodes, stack nodes Node 2 to Node 5, will contain the sensors and acquisition equipment necessary to carry out the measurements on the P-1, P-5, P-9 and P-15 pile supports. At each of these, temperature will be measured at two points, relative longitudinal stack-board displacement at two points, relative transverse stack-board displacement at one point and stack tilt at two perpendicular axes. Furthermore, acceleration measurements in three perpendicular axes shall be performed at two points on stack node P-1.



WD01 Entrada de alimentación 230V
WD02 Alimentación 48V a Nodo N02
WD03 Bus EtherCat Cobre
WD04 Bus EtherCat Cobre
WD05 Alimentación 48V a Nodo N03
WD06 Bus EtherCat Fibra
WD07 Alimentación 48V a Nodo N04
WD08 Bus EtherCat Fibra
WD09 Alimentación 48V a Nodo N05
WD10 Bus EtherCat Fibra
WD11 Alimentación 230 para el Sist. Análisis Dinámico
WD12 Red LAN para el Sist. Análisis Dinámico

Ver composición de cables en página 9



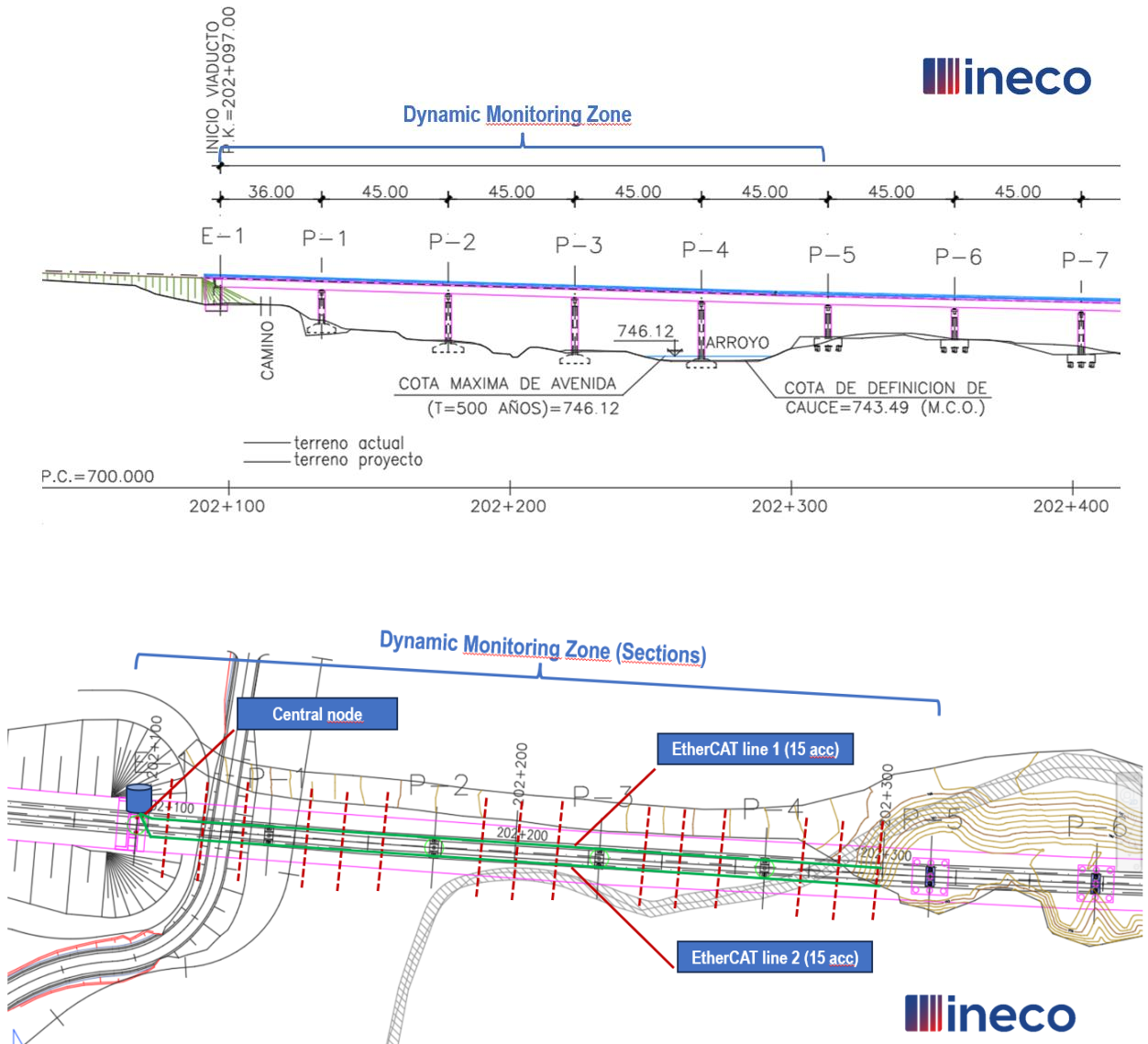
CEDEX
CENTRO DE ESTUDIOS
Y EXPERIMENTACIÓN
DE OBRAS PÚBLICAS

Project:
ADIF Viaducto Arroyo de las Huertas de Mateo
Sistema de monitorización de aparatos de apoyo
Title:
Bloques
Date: 2024-02-22 Rev: 1.0

Figure 106. Installation scheme.

2. The monitoring system for dynamic analysis of the structure.

The 30 accelerometers described in the previous section are installed in the first five spans of the viaduct of study following the schematic of Figure 107.



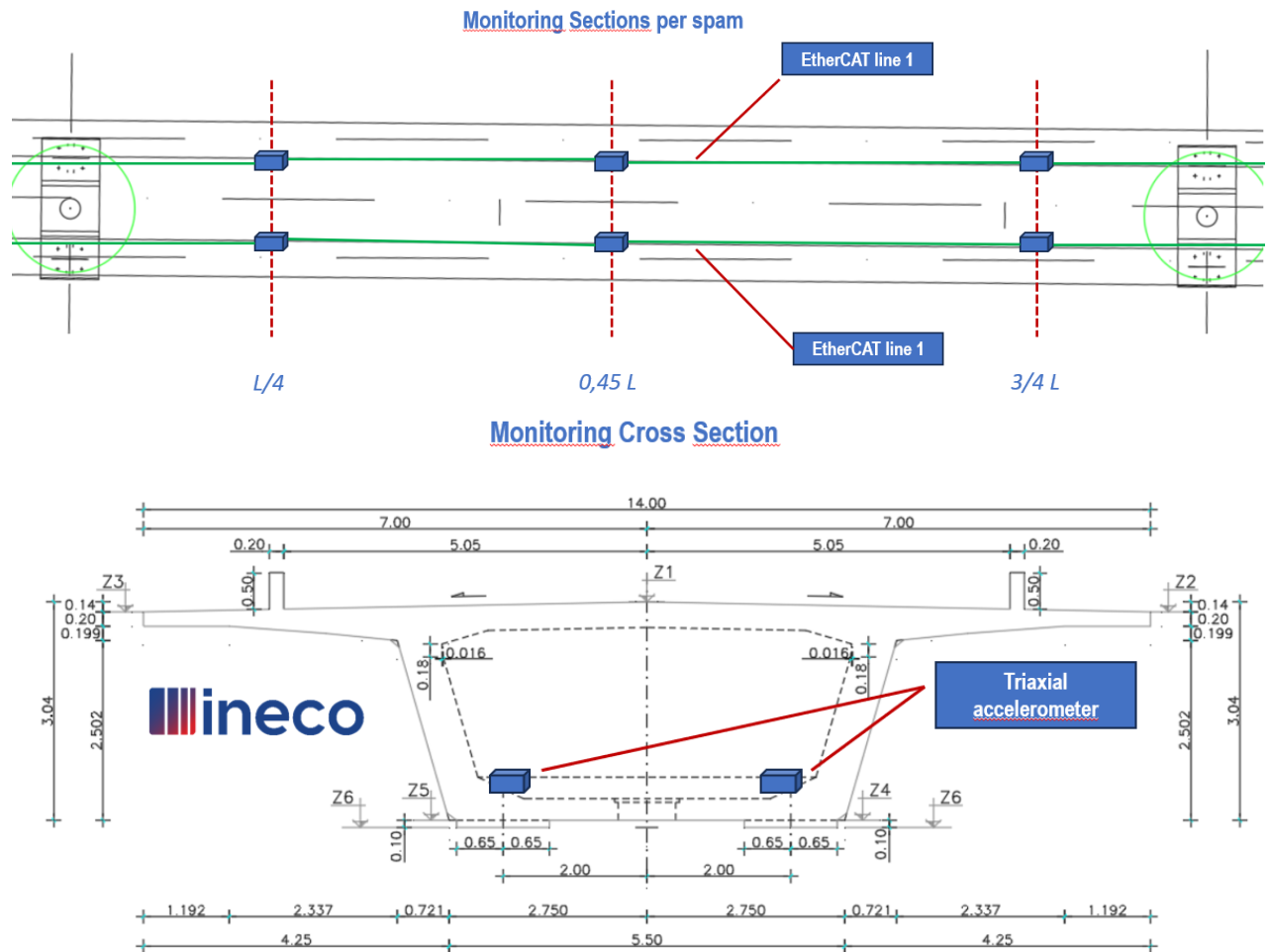


Figure 107. Plans of the installation of the monitoring system for dynamic analysis of the structure.

3. The monitoring system for correlation

The location of the sensors defined in the previous section is indicated in the cross section of Figure 108 on the left side and the photos of Figure 109.

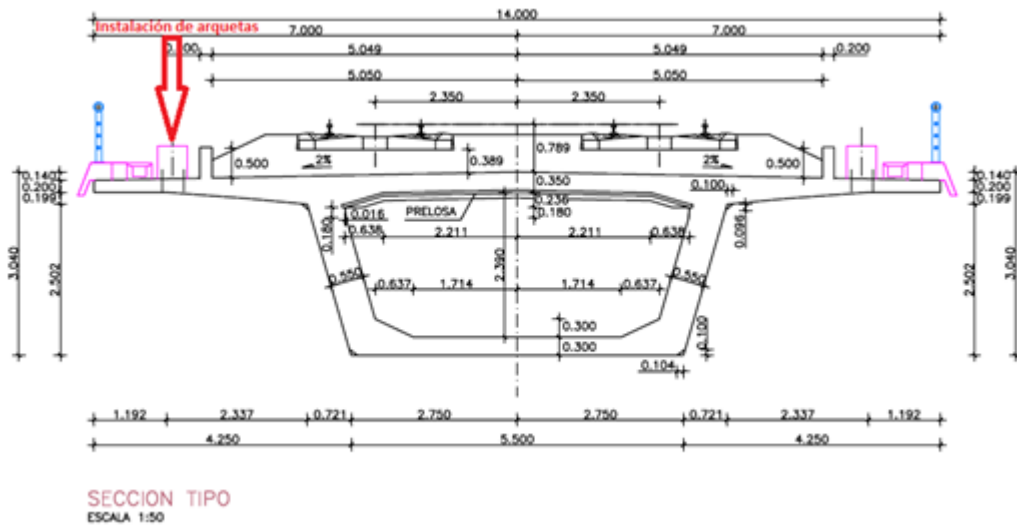


Figure 108. Viaduct cross-section.

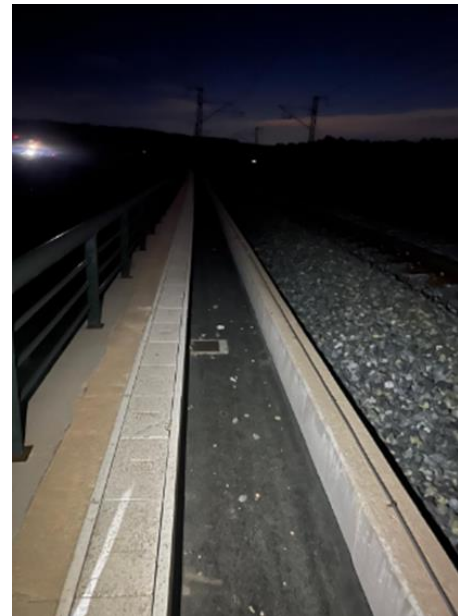


Figure 109. Trench between communications channel and wall.

The three manholes installed are the following:

- **Pit A:** To be installed on abutment 1, with inclinometer and Gateway to correlate data with the LVDT of CEDEX.
- **Pit B** will be installed on pile 1, with an inclinometer to correlate data with the LVDT and CEDEX inclinometer on the POT support. In the event that there is no adequate LoraWAN coverage, the Gateway initially planned for installation in pit A will be proposed for installation in pit B. This is to be considered, given that pit B is located in the middle of the three pits, although a little further away from the electrical cabinet.

- **Pit C** will be installed in the middle of the span between piles 1 and 2. It will include an inclinometer and accelerometer to correlate accelerations with the INECO sensors. Please refer to the image below for the location.

The three locations are shown in the elevation and plan sections of Figure 110.

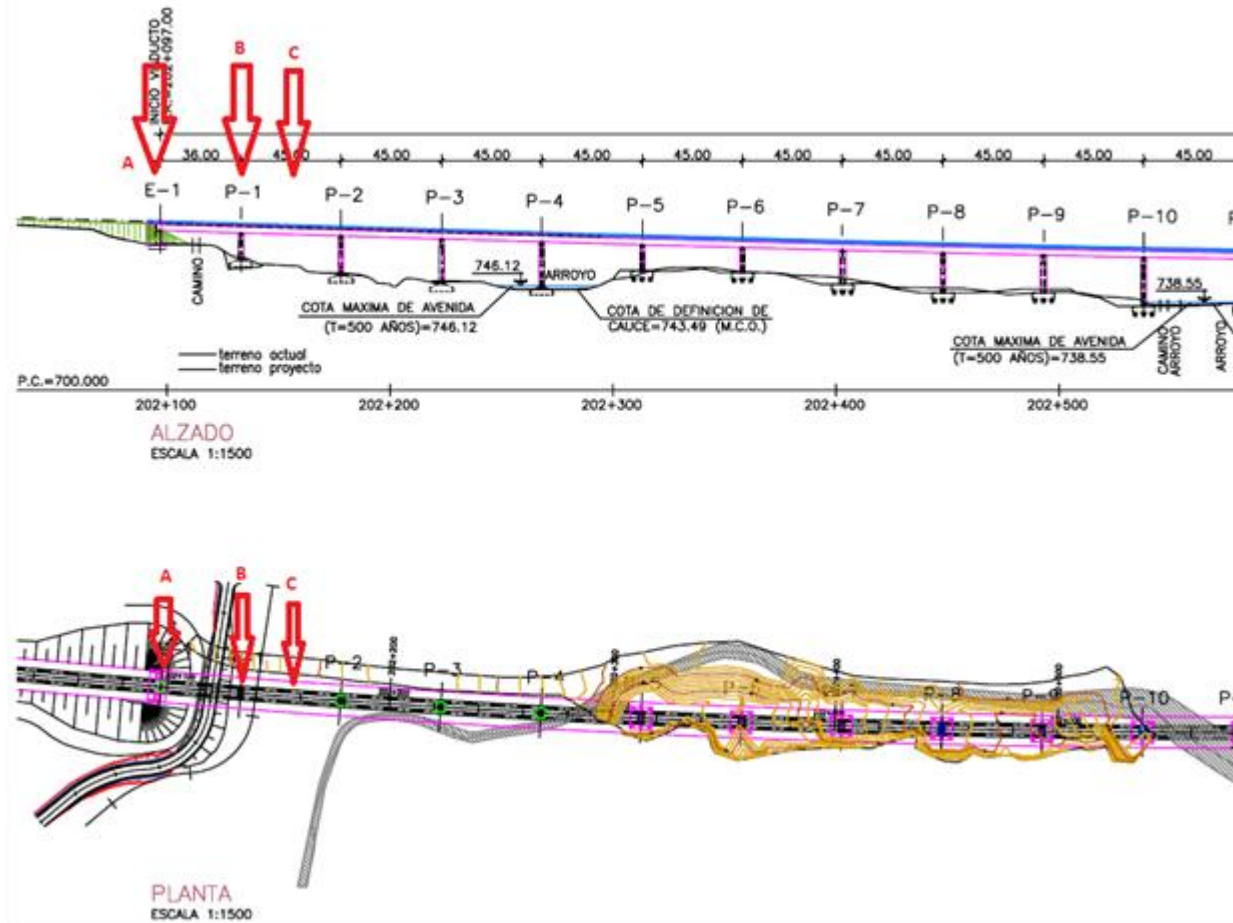


Figure 110. Elevation section and plan of the viaduct.

7.2.2.2. Earthworks Assets Management

The specification will be described following the two pilots regarding earthworks: (1) Briones and (2) Vilar de Silva.

7.2.2.2.1. Briones

The slope is located on the 700 line of the Conventional Network Castejón-Bilbao, specifically in the Briones – Haro section, between PP.KK. 124+050 and 124+100. This section has experienced numerous incidents affecting traffic safety, primarily material dislodgements onto the railway infrastructure.

The location of the monitoring system installed in Briones is shown in Figure 111 and Figure 112.

The general layout of its architecture is shown in Figure 113.

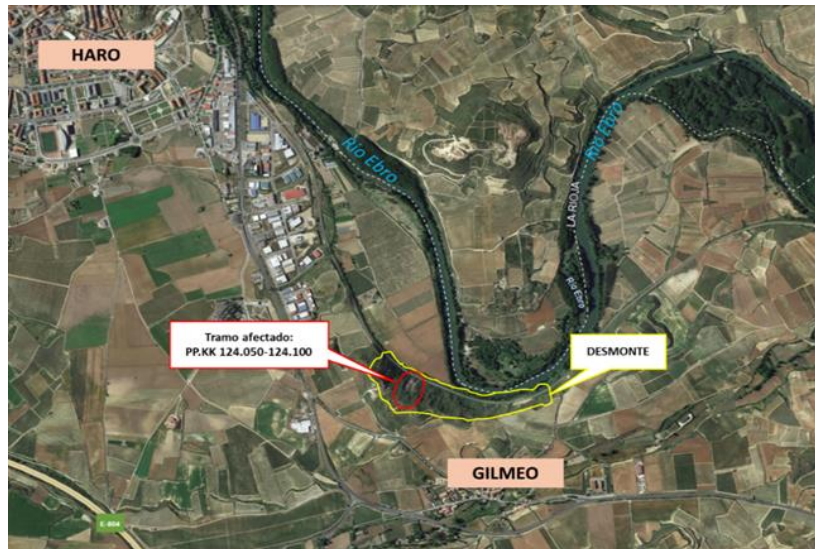


Figure 111. Affected section of Adif's RC Line 700.



Figure 112. Detail of the slope slip.



Figure 113. General architecture for the study slope.

Sensor Type	Label	X-axis Beam Displacement	Y-axis Beam Displacement	Installation Location
CLINOMETER	1	-0,8796	0,932	SLOPE
	2	-0,6946	0,5253	
	3	-4,3913	-2,1572	
	4	-0,2112	-0,5986	
	5	-3,8363	0,0087	
	6	0,6039	0,0035	
	7	0,6772	-1,1502	
	8	-8,4808	-1,6493	
	9	-0,2025	-0,1676	
	10	-0,658	-2,8257	
	11	1,0001	-3,9829	
	12	-0,2251	-0,0122	
	13	0,0332	1,6127	
	Clino Ref.	-1,3683	-1,967	

Table 14. Information on the location of installed clinometers.

7.2.2.2.2. Vilar de Silva

Figure 114 indicates the location of the slope in question within the Iberian Peninsula. In particular, it is situated at the entrance to tunnel 40 on the conventional line 800 between Palencia and La Coruña (ppkk 277+100 – 277+457), approximately one kilometre to the east of the town of Vilar de Silva, situated in the province of Ourense. To the east, the embankment is adjacent to the Peñarrubia dam, which is situated on the Sil river and marks the border between the autonomous communities of Galicia and Castilla y León.

Table 3 presents the data for the 16 clinometers installed on the embankment, including the label, serial number, latitude, longitude and installation location for each device. The sensors layout is displayed in Figure 115.



Figure 114. Location of the unstable slope under study.

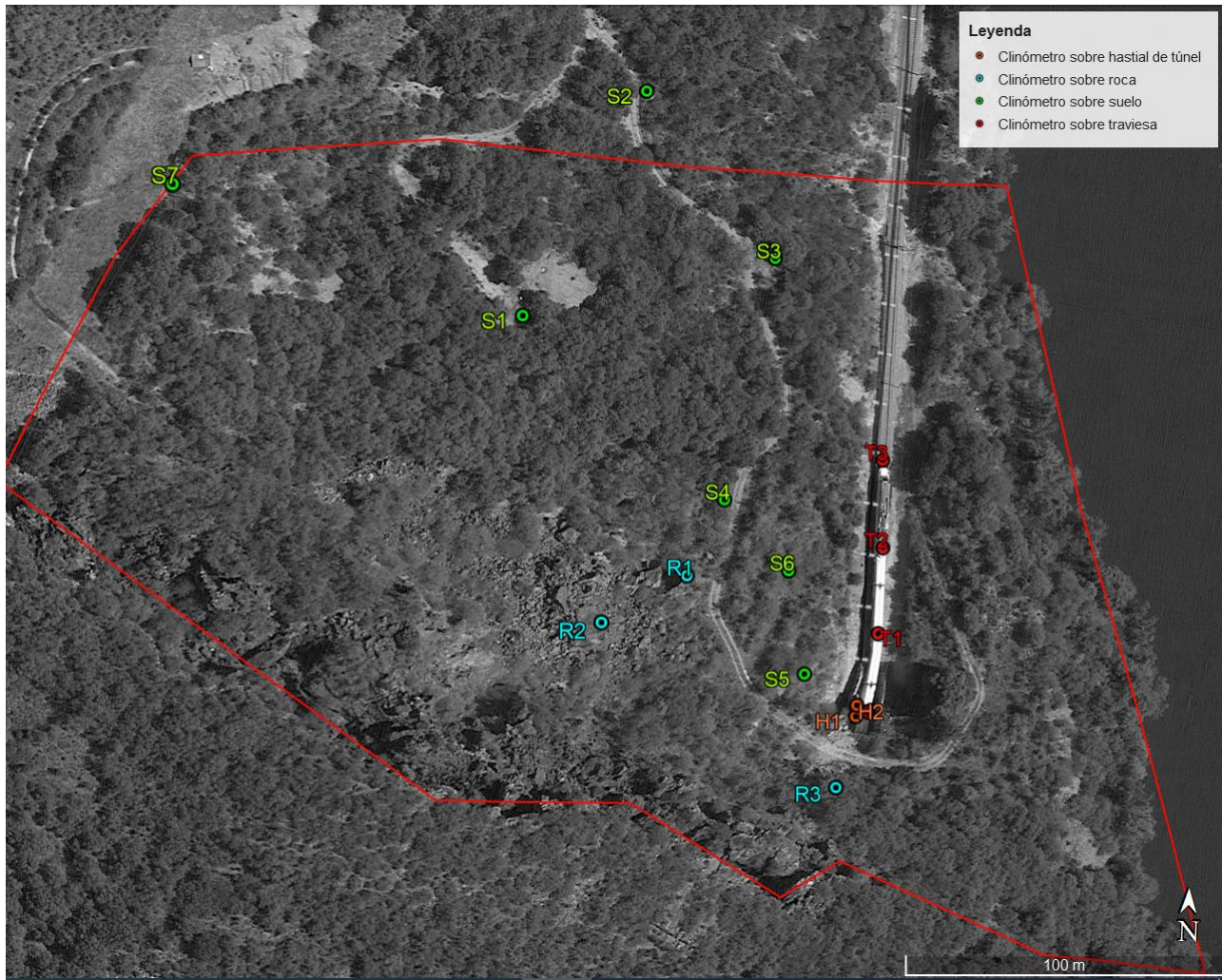


Figure 115. Location plan of installed clinometers.



		INSTALACIÓN DE EQUIPOS Y ADQUISICIÓN DE DATOS PARA LA AUSCULTACIÓN DE LA LADERA DE ENTRADA AL TÚNEL 40 EN LA LÍNEA 800 DE RED CONVENCIONAL PALENCIA-LA CORUÑA (PP.KK. 277+100 - 277+457)			Numero Rev.0
					Data: 14-12-2023
					
TIPO SENSOR	ETIQUETA	Nº SERIE SENSOR	LATITUD	LONGITUD	UBICACIÓN INSTALACIÓN
CLINOMETRO	S1	91776	42°27'47.74"N	6°48'58.66"O	SUELO
	S2	91785	42°27'49.75"N	6°48'57.29"O	
	S3	91848	42°27'48.43"N	6°48'55.61"O	
	S4	91858	42°27'46.29"N	6°48'56.21"O	
	S5	91909	42°27'44.82"N	6°48'55.21"O	
	S6	91973	42°27'45.70"N	6°48'55.40"O	
	S7	91979	42°27'48.56"N	6°49'2.45"O	
	R1	91987	42°27'45.64"N	6°48'56.68"O	ROCA
	R2	91988	42°27'45.24"N	6°48'57.68"O	
	R3	91993	42°27'43.88"N	6°48'54.83"O	
	H1	92002	42°27'44.46"N	6°48'54.55"O	HASTIAL
	H2	92029	42°27'44.56"N	6°48'54.54"O	
	T1	102876	42°27'45.17"N	6°48'54.23"O	TRAVIESA (SIN ANTENA)
	T2	103220	42°27'45.92"N	6°48'54.15"O	
	T3	103799	42°27'46.71"N	6°48'54.14"O	
	T4	103364	42°27'44.50"N	6°48'54.40"O	

Table 16. Information on the location of installed clinometers.

Further details on the clinometer's installation, location and orientation are gathered in Annex 2.

7.2.3. Initial data collection and results

7.2.3.1. Bridge Assets Management

This chapter presents the methodology and general approach for detecting and locating bridge damage. The damage identification problem is typically organized into a hierarchical structure of increasing complexity:

- Level I: Detection.
- Level II: Localization.
- Level III: Classification.
- Level IV: Extension.
- Level V: Prognosis.

Damage assessment can generally be conducted using unsupervised learning (UL) and supervised learning (SL) tools. Unsupervised techniques, particularly statistical pattern recognition and anomaly detection, have become popular due to their independence from structural models and related uncertainties, as well as their straightforward implementation in continuous SHM schemes. However, a major drawback of UL is its limitation to damage detection (Level I), with location and quantification of defects possible only in specific cases. While this may suffice for the maintenance of singular constructions, SL techniques, which allow for higher levels of damage identification, may be crucial for managing architectural ensembles and coordinating field inspections with emergency services after natural disasters such as earthquakes. These techniques, often referred to as Structural Identification (St-Id), involve constructing and

calibrating a physics-based model of a structure based on experimental performance data. The calibration of such models is typically conducted through model updating approaches, which aim to bridge the gap between numerical models and real systems by tuning model parameters to minimize the mismatch between experimental and theoretical observations. The rapid advancements in machine learning (ML) and artificial intelligence (AI), along with the decreasing cost of sensor technologies in recent years, have enabled the integration of SL approaches into the emerging concept of Structural Digital Twins (S-DT).

The workflow of the implemented S-DT based continuous Structural Identification (St-Id) approach is sketched in Figure 116. The process iteratively acquires experimental data from the physical asset, conducts St-Id by inverse calibration of the S-DT, and identifies the potential presence of damage. To attain quasi-real-time damage identification, it is of pivotal importance to guarantee that the total computational time involved in the signal processing, inverse calibration of the S-DT, and the damage assessment is lower than the acquisition time. If so, at any step $j+1$, the damage identification can be conducted in parallel with the previous acquisition j without accumulating time delays. In this light, the procedure comprises four consecutive steps:

- (A) **Automated OMA.** Ambient vibrations are periodically recorded by a data acquisition system (DAQ) and stored in separate data files containing a certain time duration. Then, a set of modal signatures (resonant frequencies f_j , mode shape Φ_j , and damping ratios ξ_j) is extracted through automated OMA.
- (B) **Removal of environmental and operational conditions (EOC).** The presence of benign fluctuations driven by EOC in the previously identified modal signatures is minimized through statistical pattern recognition.
- (C) **S-DT-based St-Id.** This step relates the St-Id of the asset through the model updating of the S-DT. This is accomplished by solving an optimization problem with an objective function $J(\mathbf{x})$ accounting for the mismatch between the theoretical predictions of the model and the previously identified experimental modal signatures. As a result, certain damage-sensitive model parameters \mathbf{x} are calibrated $\hat{\mathbf{x}}$ and collected in an observation matrix $\hat{\mathbf{X}}$.
- (D) **Damage identification.** Finally, the appearance of structural damage can be appraised by novelty analysis of the time series of modal signatures and model parameters contained in $\hat{\mathbf{X}}$. Since the latter are defined according to certain structural elements or damage mechanisms, the identification of permanent variations in their time series provides direct assessment of the location and severity of the damage.

To perform the S-DT-based St-Id, an objective function $J(\mathbf{x})$ including the relative differences between the l target modes of vibration determined experimentally, and their theoretical counterparts is introduced as follows:

$$J(\mathbf{x}) = \sum_{i=1}^l [\alpha \varepsilon_i(\mathbf{x}) + \beta \delta_i(\mathbf{x})] + \frac{\eta}{l} \sum_{i=1}^l \frac{(k_i - 1)^2}{1.2 - 0.7} \quad (21)$$

With

$$\varepsilon_i(\mathbf{x}) = \frac{|f_{exp}^i - f_{surr}^i|}{f_{exp}^i}, \quad \delta_i(\mathbf{x}) = 1 - MAC_i(\mathbf{x}) \quad (22)$$

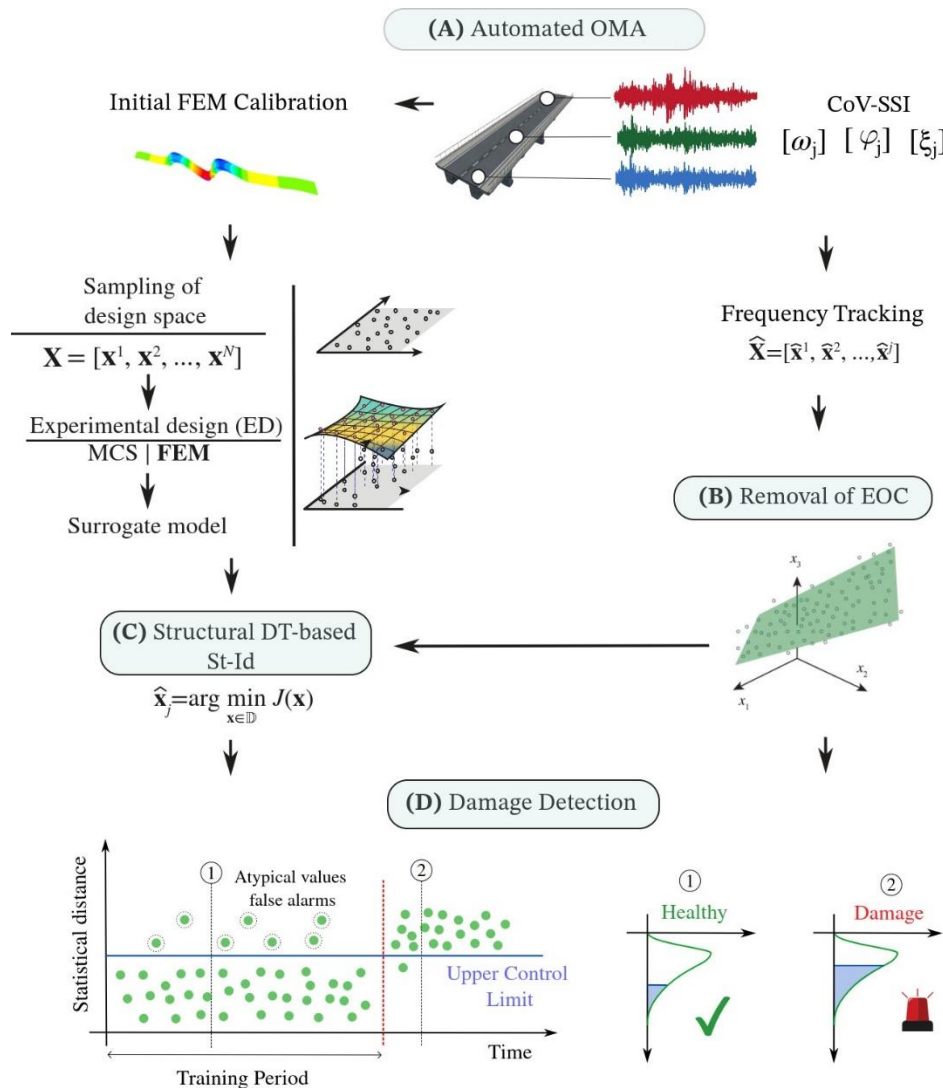


Figure 116. Flowchart of the implemented S-DT-based continuous St-Id of bridges.

Damage detection in Pot Bearings based on vibration measurements involves analyzing the dynamic response of the bearings when high-speed trains pass over the bridge. The vibrations caused by the passing trains are recorded using sensors placed strategically on the structure. By comparing these vibration signals with baseline data from an undamaged bearing, anomalies can be identified. Advanced signal processing techniques, such as frequency analysis and mode shape extraction, are used to detect changes in the bearing's behaviour. A significant deviation from the baseline indicates potential damage, allowing for early maintenance and repair to prevent further deterioration.

7.2.3.2. Earthworks Assets Management

The specification will be described following the two pilots regarding earthworks: (1) Briones and (2) Vilar de Silva.

7.2.3.2.1. Briones

The process iteratively acquires real-time data from the inclinometers, which is then analysed to facilitate real-time anomaly detection. The system will be completed by a weather station capable of simultaneously reading precipitation, ambient temperature, and relative humidity.

GENERAL SYSTEM OVERVIEW

The remote monitoring system with wireless sensors is composed of three main elements: Sensors, communication system (Gateway), and web viewer.

The sensors are installed at each location of interest to be monitored and take measurements at the frequency defined in each case. The obtained data is transmitted via WiFi/Radio to the Gateway, and from there to the server through 4G/Ethernet, where the Database storing the observations is hosted. We can access and visualize the data using the WebMonitor web viewer from anywhere and with any device (smartphone, tablet, or laptop).

The system consists of 14 wireless inclinometers, they will be distributed across the entire slope and installed on masts or tetracers embedded in the ground. These are connected either individually or in very close groupings to reading nodes, which act as local data loggers, measuring, recording, and sending data either through the network or directly to a Gateway that serves as the central data logger or hub. These communications are done via radio using Flat Mesh protocol:

- The FlatMesh NanoMacro is an extremely high precision and exceptionally stable three axis tilt sensor which reports its measurements through Senceive's FlatMesh wireless communications network to a FlatMesh Gateway.
- The FlatMesh NanoMacro is highly robust, has a long battery life, and comes with Near Field Communication (NFC)[™] capability, enabling on the spot interactions with the node.
- The FlatMesh 4G Gateway is a fully integrated unit which provides all the functionality required to operate a FlatMesh wireless sensor network in a remote location.
- No fixed IP address is required for the cellular service; the Gateway simply initiates the connection with the FlatMesh WebMonitor software over the Internet.

The system includes a range of standard anchoring accessories to install the sensor according to the circumstances, prioritizing a secure, easy, and quick installation.

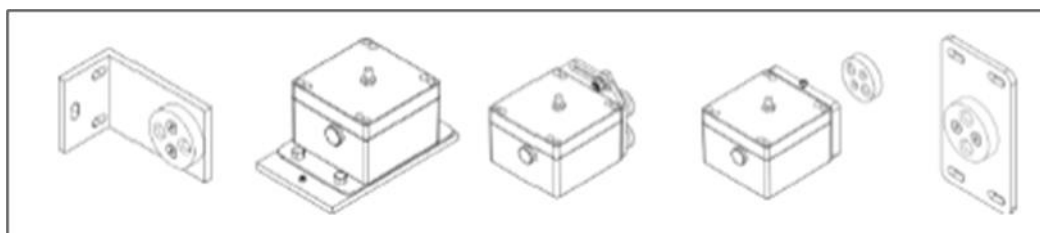


Figure 117. Example of standard anchoring accessories.

As the final component of the chain, we have a web viewer that can be accessed at any time using any device with internet access. It allows you to view measurements both graphically and in alphanumeric format, such as CSV.

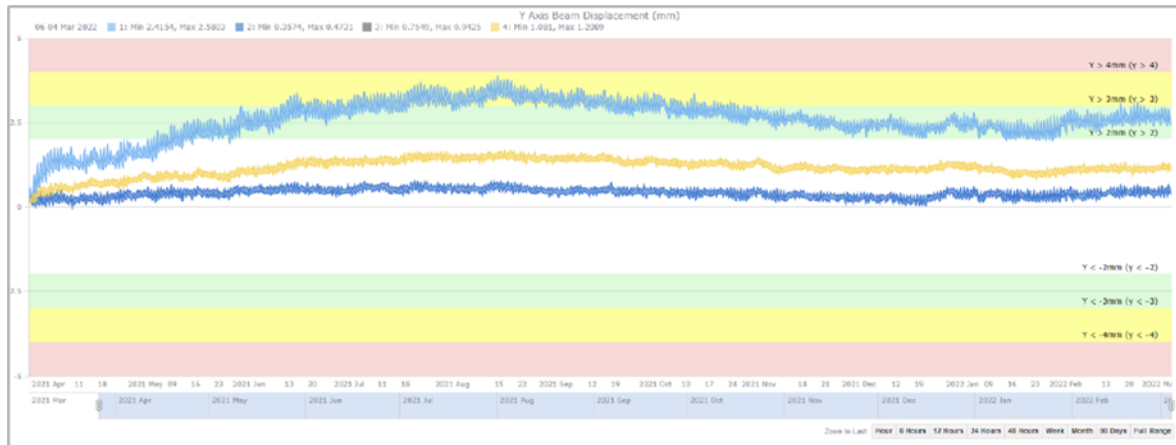


Figure 118. Example of Differential Settlement Evolution – 9 Months of Observation.

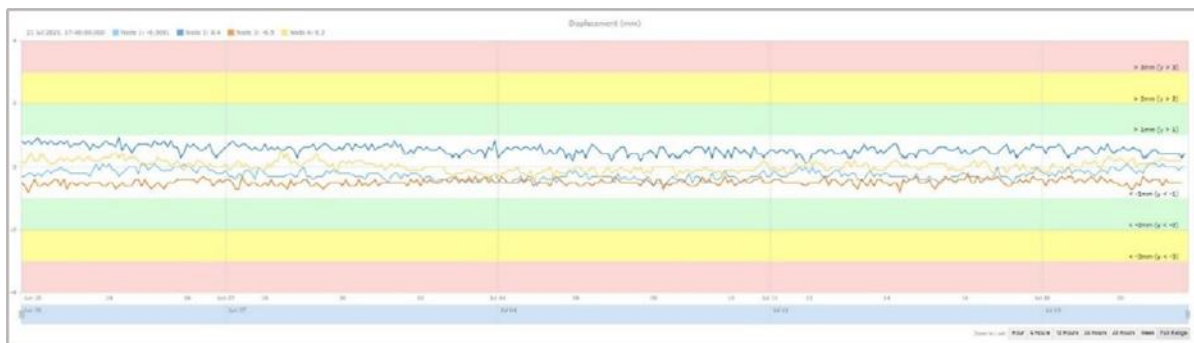


Figure 119. Example of Convergence Monitoring – 4 Months of Observation.

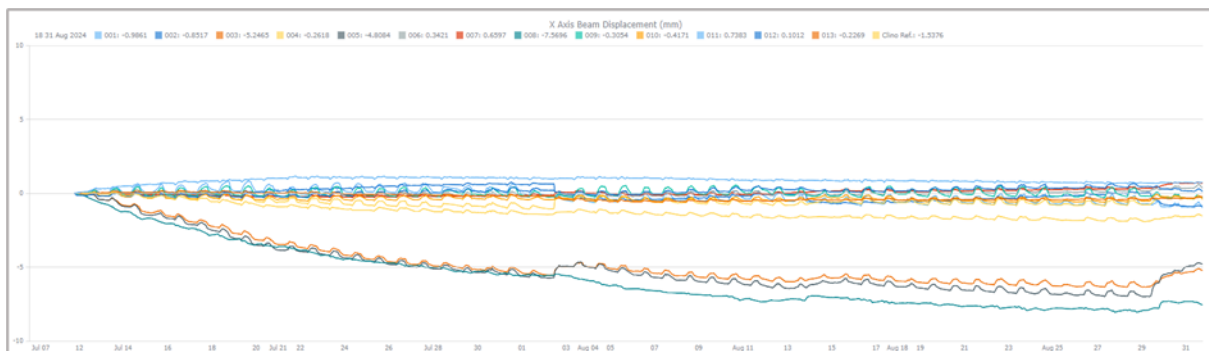


Figure 120. X Axis beam displacement - Briones.



Figure 121. X Axis beam displacement- Briones.

The viewer also has the tools necessary to define alarm thresholds and automatically send an email and SMS when measurements reach the defined values.

Date	Location	Trigger Description	Status
16/03/2022 15:38:30	10	> -0.127° ángulo Y	Active
16/03/2022 15:38:30	10	> -33mm Y	Active
05/03/2022 23:38:31	10	0.064 a 0.127° ángulo Y	Active
04/03/2022 12:38:32	10	4.5 a 9 mm Y	Active
03/03/2022 13:38:30	10	> 0.127° ángulo X	Active
03/03/2022 13:38:30	10	> 0.127° ángulo Y	Active
03/03/2022 13:38:30	10	> 9 mm Y	Active
14/01/2022 04:34:46	07	-0.032 a -0.054° ángulo Y	Active
06/01/2022 05:27:00	06	> -0.054° ángulo Y	Active
06/01/2022 05:27:00	06	< 0.032° ángulo X	Active
01/01/2022 16:26:15	04	< 0.032° ángulo Y	Active

Figure 122. Record of Sent Alarms.

In the specific case of the Briones slope, the sensors have been recording and accumulating data installation date through. Overall, no significant changes have been observed, but it is important to highlight that on August 2, a minor event was noted:

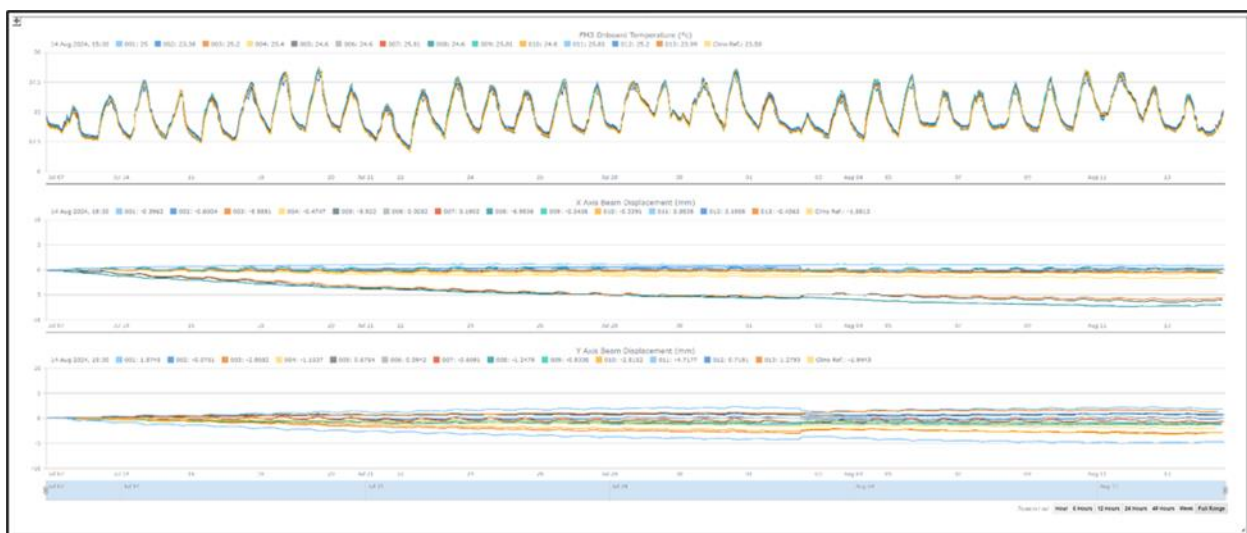


Figure 123. Analysed graph.

The nearby station was queried to verify that precipitation had indeed occurred on that day, it's observed that the slope reacts to the precipitation:

Últimos treinta días reportados por la estación HARO.

FECHA	PRECIPITACIÓN	T. MEDIA	T. MÍNIMA	T. MÁXIMA
10/08/2024	0,0	28,8	18,3	39,4
09/08/2024	0,0	26,2	18,5	33,9
08/08/2024	0,0	25,7	19,1	32,3
07/08/2024	0,0	24,4	19,3	29,6
06/08/2024	0,0	24,8	19,6	29,9
05/08/2024	0,0	25,2	15,8	34,5
04/08/2024	0,0	24,1	13,9	34,3
03/08/2024	0,0	22,6	15,5	29,7
02/08/2024	8,4	19,8	17,5	22,2
01/08/2024	0,0	24,3	18,9	29,7
31/07/2024	0,0	28,1	18,7	37,5
30/07/2024	0,2	28,0	19,9	36,1
29/07/2024	0,4	29,3	22,5	36,1

Figure 124. Precipitation Table, Haro Station.

7.2.3.2.2. Vilar de Silva

The workflow for the analysis and detection of anomalies on the case study is shown in Figure 117. The process iteratively acquires real-time data from the inclinometers, which is then analysed to facilitate real-time anomaly detection. In this light, the procedure consists of five main tasks:

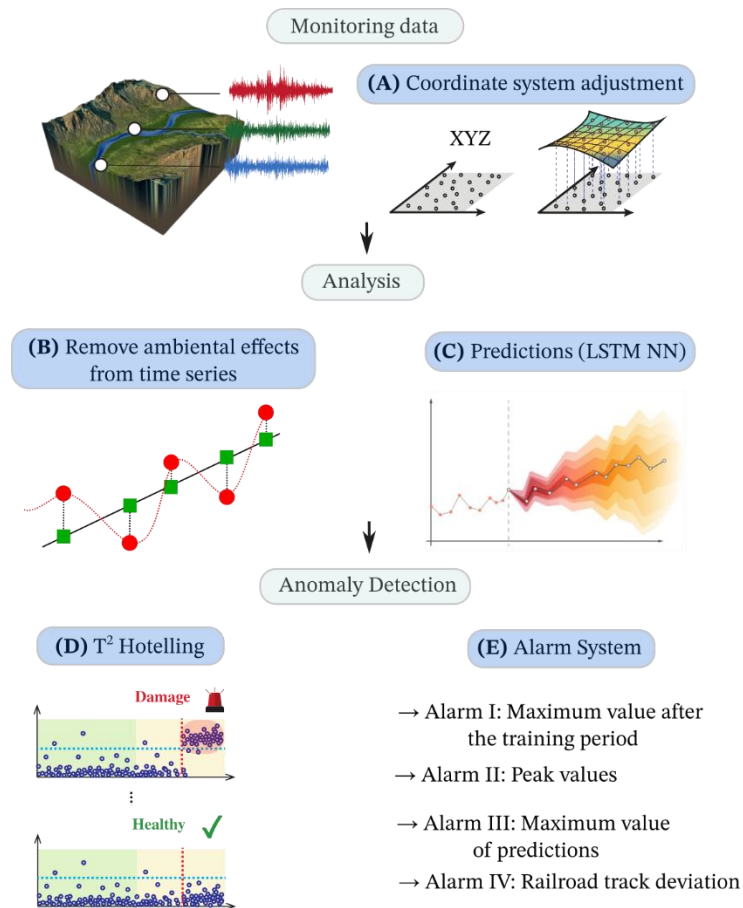


Figure 117. Flowchart for the analysis and detection of anomalies in tiltmeter time series.

- **Coordinate system adjustment.** The Figure 118 shows the layout of the different tiltmeters across the study area and their corresponding local coordinate systems. As observed, the sensors do not share the same coordinate system. Therefore, a global coordinate system (the yellow axis) needs to be established by transforming the local coordinate axes. To achieve this, each sensor is treated individually, with its local coordinate system rotated using its respective rotation matrix to align with the global system. The rotation angles were calculated based on the orientation information provided by the installers, measured with a compass.

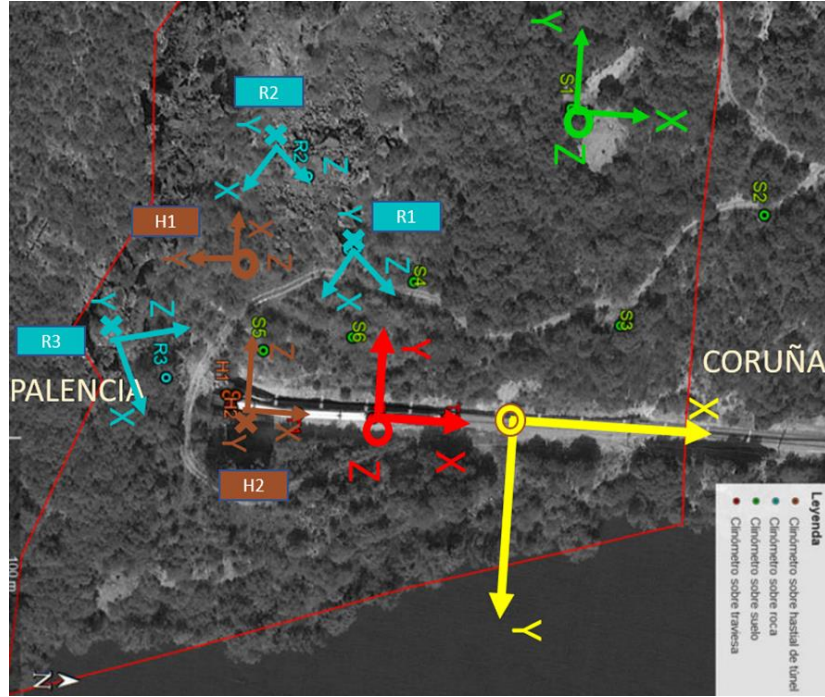


Figure 118. Tiltmeters installation with local coordinates systems.

- Removal of environmental effects from the time series.** Benign fluctuations caused by varying environmental conditions are minimized using statistical pattern recognition. In this case, the method employed is Linear Regression. Let us denote the time series from the tiltmeters in the observation matrix $Y = [y_1, \dots, y_f] \in \mathbb{R}^{N \times 2}$ containing the N observations. In this context, data normalization involves subtracting the reversible variability in the selected features of Y induced by benign environmental and operational conditions (EOC). This can be achieved by training a certain statistical model over a set of training period samples from Y defining a baseline in-control population. This baseline dataset must represent the healthy condition of the structure under all possible EOC being a one-year period often adopted. Among the wide variety of data normalization techniques available in the literature, Multiple Linear Regression (MLR) models represent a simple but powerful approach. MLR models exploit linear correlations between the selected features in Y (estimators) and a set of p independent exploratory variables (predictors or independent variables), which are typically taken from monitoring data of EOC (e.g. temperature, humidity). The predictions by MLR (\hat{Y}) of the observation matrix Y are obtained as:

$$\hat{Y} = \bar{P}\bar{\beta} = [1_{N \times 1}, P] \begin{bmatrix} \beta_0^T \\ \beta \end{bmatrix} \quad (23)$$

where $1_{N \times 1}$ is a column vector of ones and $P = [p_1, \dots, p_p] \in \mathbb{R}^{N \times p}$ is an observation matrix with columns containing the time series of the p selected predictors. Term $\beta_0 \in \mathbb{R}$ is a vector of intercept terms and $\beta \in \mathbb{R}$ is a matrix of linear regression coefficients. Assuming normally distributed errors between the estimators and the predictions by the MLR model over the training

period, the least squares estimate of the coefficient's matrix reads:

$$\bar{\beta} = (\bar{P}_{tp}^T \bar{P}_{tp})^{-1} \bar{P}_{tp}^T Y_{tp} \quad (24)$$

where subscript “ tp ” has been included to explicitly state that the MLR model is trained considering the set of predictors and estimators within the training period. Once constructed, the predictions of the MLR model \hat{Y} from Eq. (24) can be used to remove the variance due to EOC from Y through the so-called residual error matrix $E \in \mathbb{R}^{N \times 2}$, that is:

$$E = Y - \hat{Y} \quad (25)$$

When the system remains healthy, matrix \hat{Y} reproduces the part of the variance driven by EOC, while E only contains the residual variance stemming from modelling errors. Conversely, if a certain damage develops, matrix \hat{Y} remains unaltered while matrix E concentrates the damage-induced variance, being thus apt for damage identification.

- **Predictions (LSTM Neural Network).** Long Short-Term Memory (LSTM) neural networks are a specialized type of recurrent neural network (RNN) designed to effectively capture long-term dependencies and temporal patterns in time series data. Unlike standard RNNs, LSTMs address the issue of vanishing and exploding gradients, which can occur during training when dealing with long sequences. In this case, the designed network maintains a cell state that acts as a memory, allowing them to retain information over long periods. This memory helps the network remember important information and forget irrelevant data. Besides the network use three types of gates—input, forget, and output gates—to regulate the flow of information into, out of, and within the cell state: the “Input Gate” that controls how much new information is added to the cell state. The “Forget Gate” that decides which information from the cell state should be discarded and the “Output Gate” Determines the output based on the cell state. The compact forms of the equations for the forward pass of an LSTM cell with a forget gate are:

$$f_t = \sigma(W_f x_t + U_f h_{t-1} + b_f) \quad (26)$$

$$i_t = \sigma(W_i x_t + U_i h_{t-1} + b_i) \quad (27)$$

$$o_t = \sigma(W_o x_t + U_o h_{t-1} + b_o) \quad (28)$$

$$\tilde{c}_t = \sigma(W_c x_t + U_c h_{t-1} + b_o) \quad (30)$$

$$c_t = f_t \odot c_{t-1} + i_t \odot \tilde{c}_t \quad (29)$$

$$h_t = o_t \odot \sigma_h(c_t) \quad (30)$$

where the initial values are $c_0 = 0$ and $h_0 = 0$ and the operator \odot denotes the Hadamard product (element-wise product), σ and \tanh correspond to the sigmoid and hyperbolic tangent activation functions, respectively. The subscript t indexes the time step. Letting the superscripts h and d refer to the number of input features and number of hidden units, respectively. $x_t \in \mathbb{R}^d$ corresponds to input vector to the LSTM unit, $f_t \in (0,1)^h$ is the activation vector of the forget gate, $i_t \in (0,1)^h$ is the activation vector of the input (update) gate, $o_t \in (0,1)^h$ is the activation vector of the output gate, $h_t \in (-1,1)^h$ is the hidden state vector also known as output vector of the LSTM unit, $\tilde{c}_t \in (-1,1)^h$ is the cell input activation vector, $c_t \in \mathbb{R}^h$ is the cell state vector, finally $W \in \mathbb{R}^{h \times d}$, $U \in \mathbb{R}^{h \times h}$ and $b \in \mathbb{R}^h$ are the weight matrices and bias vector that need to be learned during training.

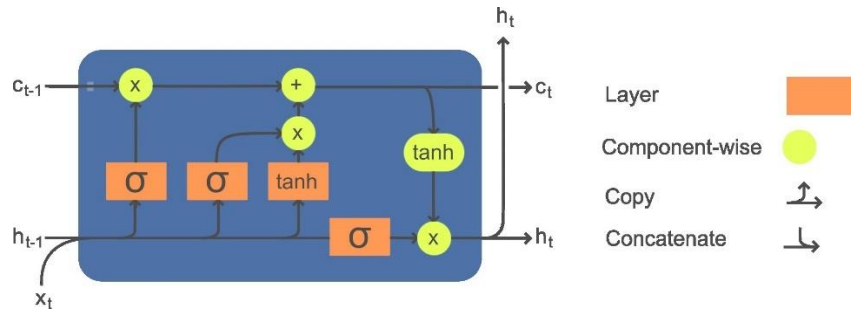


Figure 119. LSTM network architecture.

- **T² Hotelling:** is a multivariate statistical test used to assess whether the mean vector of a multivariate sample differs significantly from a hypothesized mean vector. It extends the concept of the Student's t-test to multiple dimensions, making it useful for analysing multivariate data. The statistic is calculated using the formula:

$$T^2 = n(\bar{x} - \mu)^T S^{-1} (\bar{x} - \mu) \quad (31)$$

where \bar{x} is the sample mean vector, μ is the hypothesized mean vector, S is the sample covariance matrix, and n is the sample size. For this case study, this statistical method is used to determine if significant differences exist between two sets of data by delimiting the time series for each sensor using a training period defined as “healthy”. Thus, the differences are assessed relative to the healthy case study.

- **Alarm System:** Based on the behaviour of the time series data collected from each tiltmeter, several types of alarms have been defined, corresponding to various potential damage mechanisms that the object under study might experience. The process begins with the

acquisition of real-time data, which is expected to have an average value of approximately zero. Fixed averages are determined for the training period to establish baseline conditions. Each sensor records two components of rotation: the first corresponds to the rotation around the x-axis, and the second corresponds to the rotation around the y-axis (refer to Figure 118). It is important to note that the direction of the steepest slope aligns with the direction of rotation around the x-axis. Once the initial conditions are established, the types of alarms are defined as follows:

Alarm I: Maximum value after the training period. Figure 120 shows the main characteristics that trigger the alarm mechanism in question. The process begins by establishing a training period, with the primary assumption that the structure is considered healthy throughout this period. Defining this period allows for the establishment of upper and lower limits for each sensor. Once these values are set, the behaviour of the data post-training period is analyzed. If the predefined thresholds are exceeded, it is considered that there is damage to that sensor, as shown in Figure 120 (a). This failure mechanism has the limitation that under environmental conditions not previously experienced at the study location, these thresholds can be exceeded with relative ease. Therefore, the activation of the alarm depends on detecting anomalous values in three sensors in close proximity, as shown in Figure 120 (b).

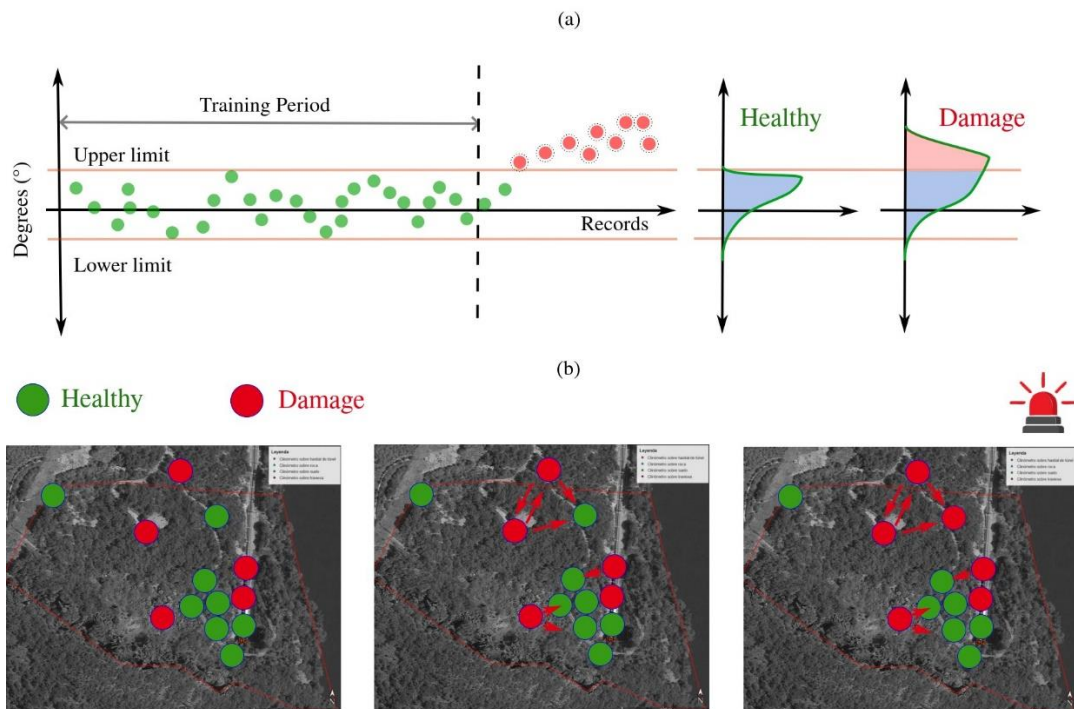


Figure 120. (a) Definition of limits based on the training period. (b) Alarm activation mechanism.

Alarm II: Peak values. This alarm is triggered by storing the differences between records during the training period so that peak values can be determined in the post-training period. If the data shows peaks that surpass this amplified threshold during analysis, it indicates potential damage or anomalies in the sensor readings. This mechanism is designed to detect significant deviations that

may signal critical issues, as illustrated in Figure 121.

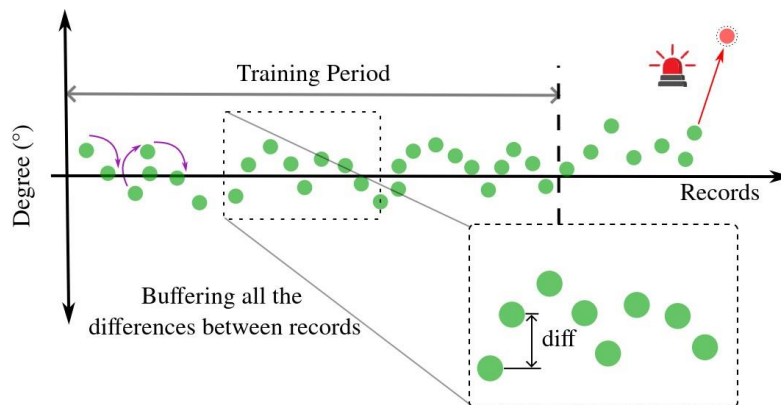


Figure 121. Recording Differences to Identify Peak Values.

Alarm III: Maximum value of predictions. Once the differences corresponding to the degree records for each sensor are stored, the next step is to determine if the predictions (48-hour period – LSTM Neural Network) indicate any anomalous values. This neural network has been constructed based on the behavior of each time series (degrees), with extreme precipitation defined as a variable. The damage mechanism scheme is shown in the following figure:

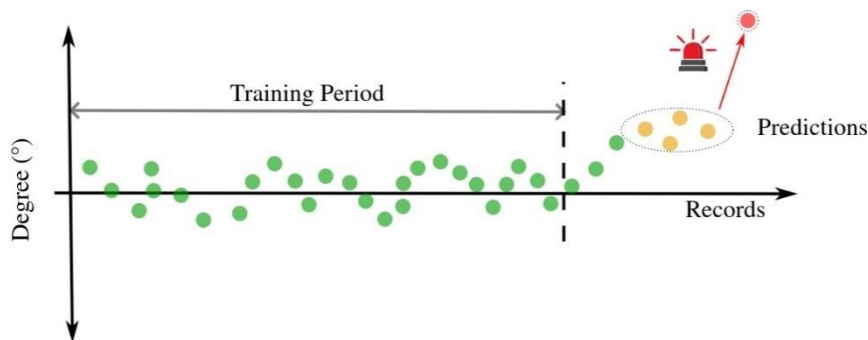


Figure 122. Alarm mechanism based on value predictions.

Alarm IV: Railroad track deviation. This alarm is only applied to sensors located on the railroad ties of the train line. By knowing the dimensions of the support element for the sensors, it is possible to determine the rotation (in the longitudinal direction) of four railroad ties on the train line. Figure 123 (a) illustrates the procedure for calculating the deviation of the tie based on its rotation. In our opinion, this rotation is attributed to changes in the water levels of the nearby lake. According to NAV 3-0-5.2 'Track Geometry Parameters' regulations, the deviation must not exceed 25 mm. Therefore, using this value as a reference, Figure 123 (b) outlines the conditions for activating this failure mechanism.

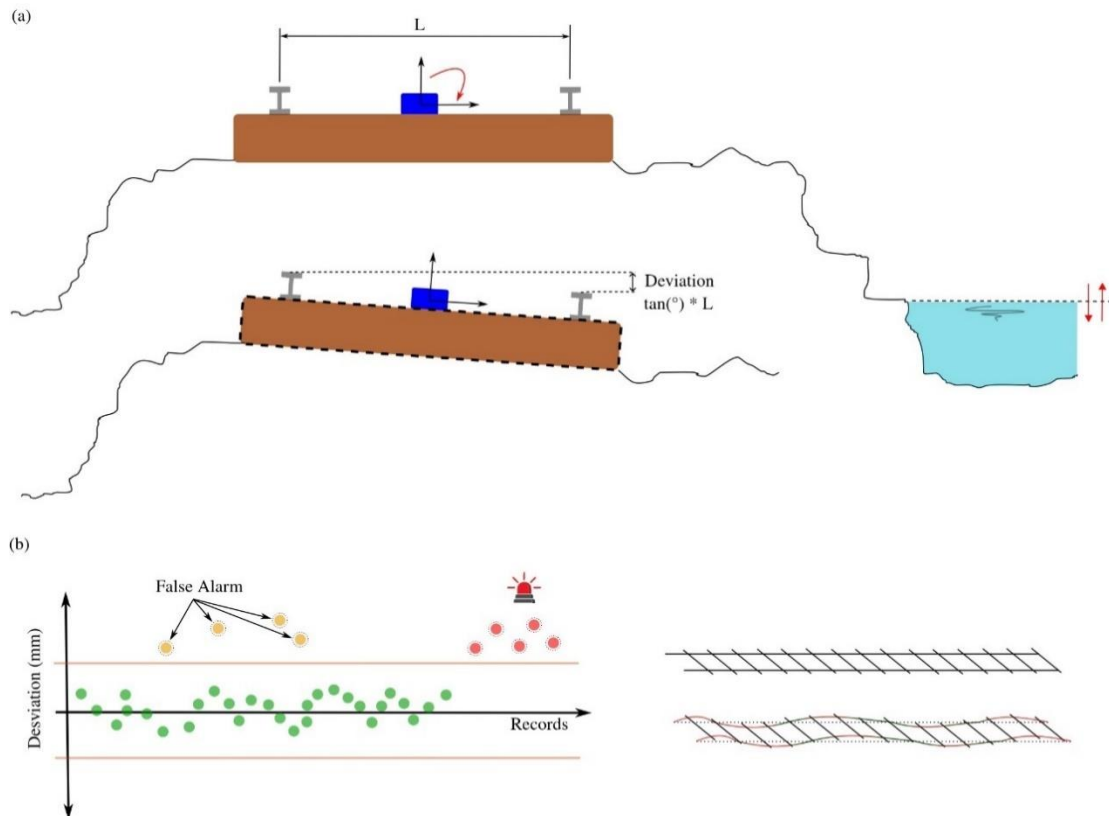


Figure 123. (a) Deviation in railway sleepers and (b) damage mechanism based on deviation limit values.

7.2.4. Demonstration Plans

Bridges and Earthworks Asset Management aided by Geotechnics Use Case analyses real-time data coming from the installed monitoring system in various scenarios, therefore its demonstration is closely linked with the developments and results throughout the project. In all pilots presented, a final platform which integrates the previously defined developments in an efficient and user-friendly manner which can be defined as the UC demonstration. In this section the plans and actual state of these platforms is presented.

7.2.4.1. Bridge Assets Management

At the moment of this deliverable preparation, the bridge assets management use case is at the installation phase. Since the monitoring system is not in place the connection and reception of information cannot be performed, and therefore the platform integration development could not be started.

Nevertheless, different interfaces are planned for the final integration:

- **Management interface.** This interface displays information regarding the different assets and elements of study, providing all the useful information of the assets, the

monitoring elements such as sensors and any other information needed for the management.

- **Inspection.** This interface displays available information regarding inspection campaigns outside the scope of the monitoring. This will depend on the information provided by the pilot.
- **Monitoring.** The monitoring interface displays two types of information:
 - Sensors data. Data coming from the installed sensors to be visualized in real time.
 - Analysis. Different analysis performed on the sensors data to analyze the asset condition and detect damage.

All these interfaces will be shown next to a BIM-GIS environment visor which will allow the interaction between the displayed information and the different elements from the visualization. In mid-July, assessments were conducted at the Álava Ingenieros facilities. These assessments are tests in a controlled environment to ensure the proper functioning of the entire monitoring system before its installation on the viaduct (Figure 124, Figure 125, Figure 126 and Figure 127).

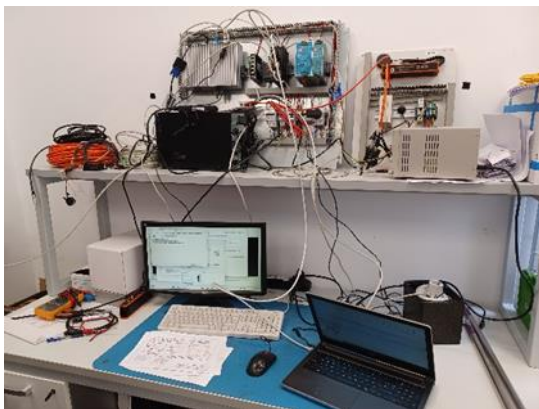


Figure 124. Tests set-up. Example 1.

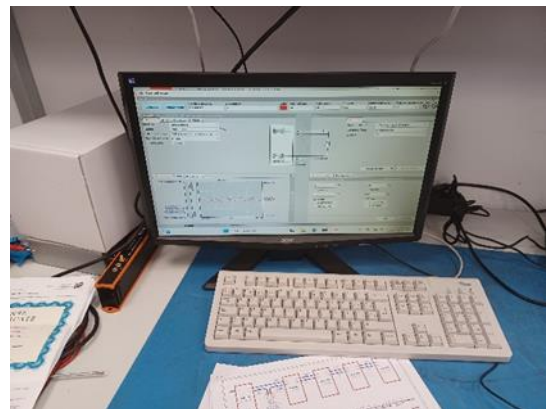


Figure 125. Tests set-up. Example 2.

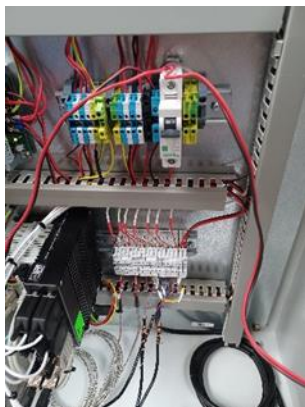


Figure 126. Tests set-up. Example 3.



Figure 127. Tests set-up. Example 4.

7.2.4.2. Earthworks Assets Management

The specification will be described following the two pilots regarding earthworks: (1) Briones and (2) Vilar de Silva.

7.2.4.2.1. Briones

This section describes the platform for the Briones pilot. The first thing visible is the slope viewer, which displays the different sensors, allowing the selection of the installed elements: the 14 inclinometers and the Gateway.

This platform has the following features and functionalities:

- **Graphical Interface:** It includes a situational screen compatible with maps or diagrams, graphical alerts, alert lists, and controls for modifying installation parameters. Layer management should be possible within the interface.
- **Alarm List:** Displaying alarms with date, time, classification, and location.
- **Profile Management:** Allowing different users to load various profiles created by themselves while operating under a single user login. This can be used for different analysis states or simply for personal preferences.
- **Data Recording Control:** To manage the recording of observed data.
- **Report Generator:** Enabling the extraction of data based on geographic references, dates, etc. Reports should be exportable to Excel or compatible formats and images to PNG/JPG formats.

This system, which will operate TWENTY-FOUR (24) hours a day, SEVEN (7) days a week, will provide remote web access to ADIF for various users with viewing capabilities.

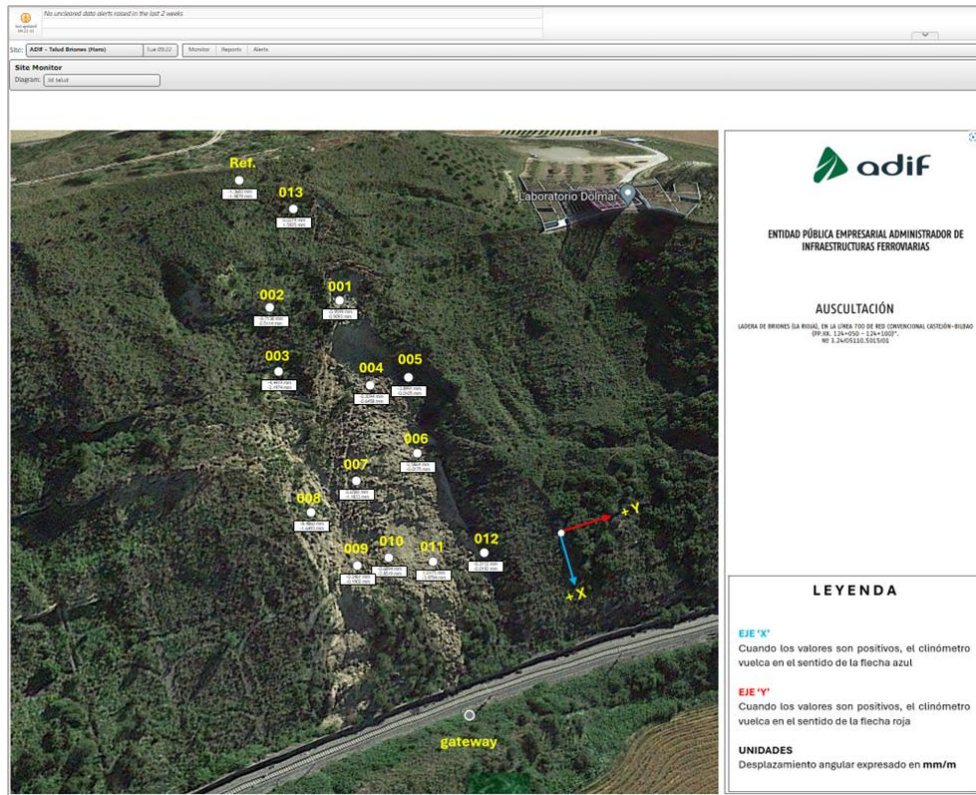


Figure 128. Platform interface.

Date	Location	Trigger Description	Status
16/03/2022 15:38:30	10	> - 0.127 ángulo Y	Active
16/03/2022 15:38:30	10	> - 33mm Y	Active
05/03/2022 23:38:31	10	0.064 a 0.127° ángulo Y	Active
04/03/2022 12:38:32	10	4.5 a 9 mm Y	Active
03/03/2022 13:38:30	10	> 0.127 ángulo X	Active
03/03/2022 13:38:30	10	> 0.127° ángulo Y	Active
03/03/2022 13:38:30	10	> 0 mm Y	Active
14/01/2022 04:34:40	07	- 0.032 a - 0.054° ángulo Y	Active
06/01/2022 05:27:00	06	> -0.064° ángulo Y	Active
06/01/2022 05:27:00	06	< 0.032° ángulo X	Active
01/01/2022 16:26:15	04	< 0.032° ángulo Y	Active

Figure 129. Example of log of alarms.

7.2.4.2.2. Vilar de Silva

In this section the Platform for Vilar de Silva pilot is described. The general platform layout is the same for all the interfaces: on the left the BIM-GIS visor of the slope displaying the different sensors included in the platform, which allows the navigation and the selection of elements and on the right the information which corresponds to the different interfaces like it is showcased in the examples of Figure 130 and Figure 131.

Different elements are included in the platform both with dynamic and static data. Dynamic elements are connected to IoT sensors which provide real-time monitoring, these include tiltmeters and a weather station. The static data is information coming from a database which is updated punctually with information coming from inspections. This data corresponding with inclinometers, piezometers, levelling and others is included in the platform for its consultation, and the structure is prepared to update the information whenever new inspections are performed.

Besides the visualization on the monitoring and inspection data, the platform will integrate a series of interfaces relative with to the previously defined UC developments: trends, alarms, predictions, etc. displayed in a user-friendly way for the end-users.

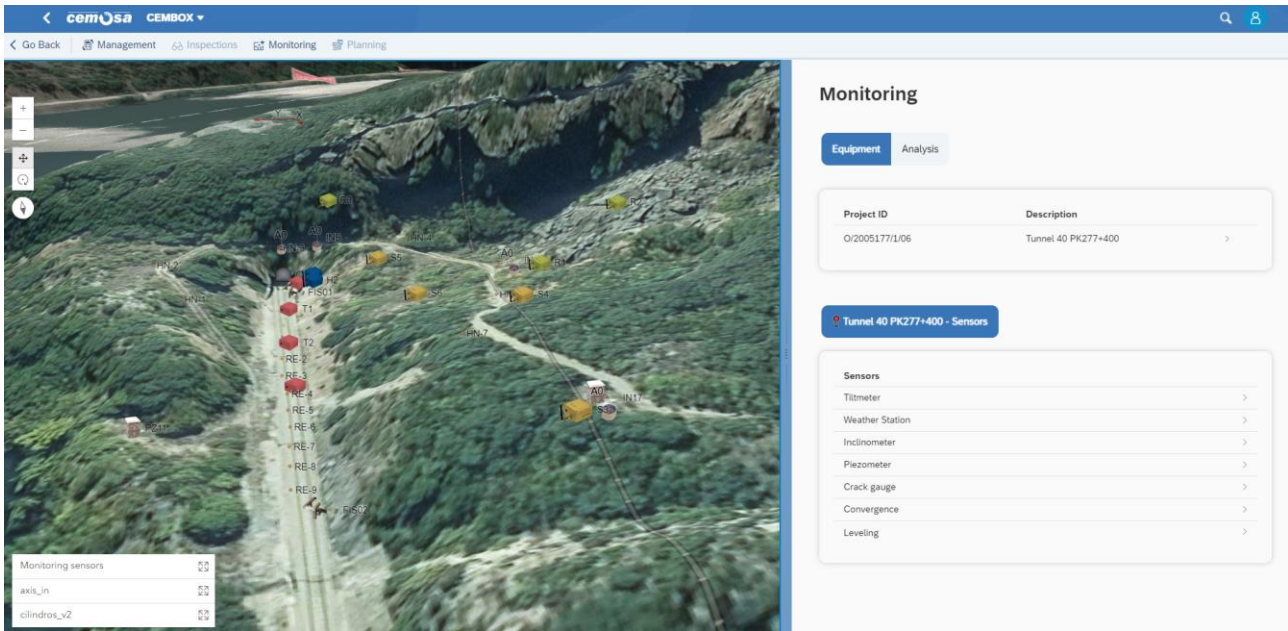


Figure 130. Platform interface. Example 1.

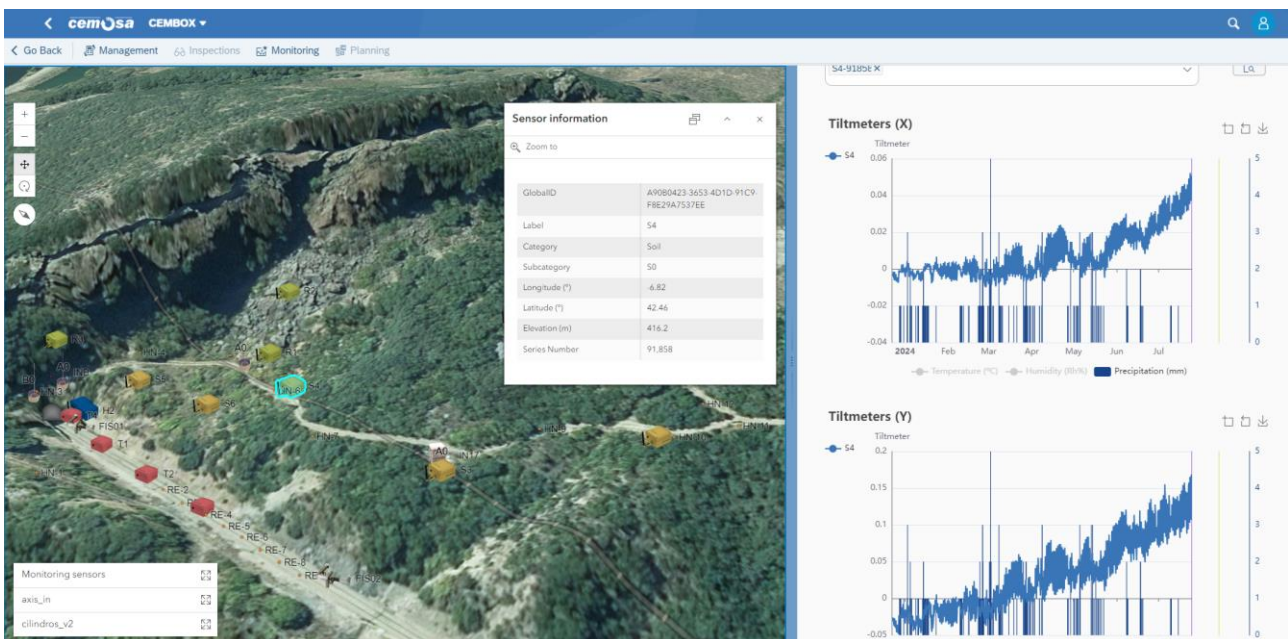


Figure 131. Platform interface. Example 2.

7.3. Monitoring of Tunnel, Sub-ballast layers, Subsoil (France)

7.3.1. Monitoring of sub-ballast layers and subsoil

7.3.1.1. Selected equipment, technical specifications and justification

Seismic wave propagation is studied to image and analyse the subsoil, much like echography and scanning in the medical field. Two methods are used based on wave generation.

The first is the **active** method (called Multichannel Analysis of Surface-Waves or MASW), where a hammer (see Figure 132) or weight-drop generates waves for targeted, time-specific subsoil characterization.

The second is the **passive** method (called passive-MASW), which continuously monitors the subsoil using waves naturally generated by passing trains.

For the active method, vertical component geophones from the company Geometrics are used: 24 bit, ultra-high resolution 20 kHz bandwidth (8 to 0.02 ms sampling), low distortion (0.0005%), low noise (0.2uV), stacking accuracy (1/32 of sample interval).

For the passive method, MEMS accelerometers from the company Sercel are used. MEMS sensors offer linear and flat amplitude and phase responses from DC to 800 Hz in the acceleration domain. Their specifications are not affected by temperature, ageing or manufacturing tolerances, making the signal recorded accurate in both phase and amplitude on the entire seismic bandwidth of interest. The preservation of amplitudes has been recognized for amplitude versus offset applications.

Fundamentally, the choice between the two methods relies in the desired investigation depth and the need for a continuous or punctual characterization.



Figure 132 : Photograph of the hammer-type active seismic source on a metal plate between two geophones (black and blue).

7.3.1.2. Installation layout

For both methods, the acquisitions are carried out on the cess to have better coupling between geophones and the soil (from 2020 to 2023).

Preliminary studies conducted by SNCF Réseau and Sorbonne University (France) during an internal research program have shown that a device with a small spacing (less than 0.5 m) provides sufficient resolution of the first few meters of soil. For example, concerning the active acquisition, a system of 72 geophones spaced 0.25 m apart with an active hammer-type source provides sufficient resolution to characterize the first 5 meters along the cess.

Passive acquisitions with 2D arrays, with 5 lines of 42 accelerometers have shown great results (see Figure 133). The sensors are spaced by 3 m and each parallel line is spaced 4.75 m. The setup was installed in late 2020 and has been recording daily train passages ever since. In late 2022, two piezometers were added to the setup to correlate groundwater variations with the changes observed in the seismic data.

The type of seismic device (type of sensors, number, length, etc.) plays a role in the resolution and depth of investigation and must be adapted to answer the desired imaging requirements and must be adapted to answer the desired imaging requirements.

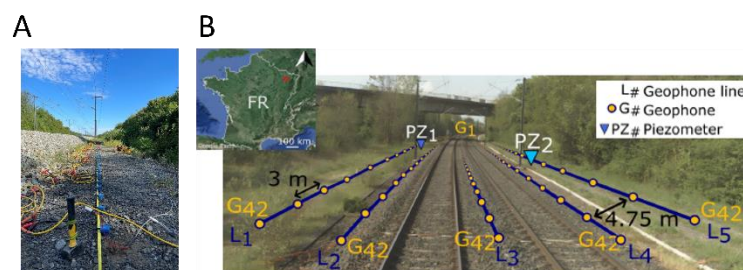


Figure 133 : (A) Photograph of a seismic setup placed on the cess and of the hammer-type source used during seismic active acquisitions (2022). (B) Seismic setup recording seismic waves generated by the train passage (2022).

7.3.1.3. Initial data collection and preliminary results

The main objective of this project is to develop non-invasive tools for the characterization of the railway track bed (i.e., sub-ballast layers) and earthwork (i.e., subsoil). Characterizing these structures is essential for understanding natural hazard (e.g. sinkholes, poor mechanical properties of geological layers) that could be the cause of disorders affecting the track.

The geophysical method used for this project is the seismic method particularly MASW (Multichannel Analysis of Surface Waves). This is the only method that can be used to estimate the mechanical properties of soils in the railway context. These properties are defined according to the shear-wave velocity and the associated mechanical shear modulus.

The methodology of data acquisition and processing is as follows (see Figure 134 and Figure 135):

- Seismic setup installation;

- Record of seismic waves (particularly surfaces waves) generated by a hammer or induced by train passages;
- Processing surface waves;
- Inverse process of the data to recover the shear-waves velocity profile of the tracked and/or earthwork.

The **processing** of collected data relies on the study of the dispersion of surface waves presents in the entire wave field collected. The behavior of these surface waves reflects the properties of the ground. For example, by studying their velocity and propagation type, it was possible to detect a layer of lower velocity. This would be the cause of recurring disorders, as the supporting soil would be in poor condition and would not allow the superstructure to be properly maintained.

An additional step, called seismic interferometry, is needed in the passive method before extracting dispersion.

Inverse process calculation tools are being developed to recover the velocity profile in a simple way. The uncertainties associated with these inversion calculations are also considered.

Artificial intelligence (AI) has been applied to this inversion procedure and has shown great results and processing precision, speed, and automation. Passive methods combined with AI were used to retrieve groundwater table height maps and precise geological descriptions helping the interpretation of the results and decision-making.

The following objectives will be to optimize (and automate) even further all these steps to obtain a complete and relevant characterization tool for railway track bed and earthwork diagnosis.

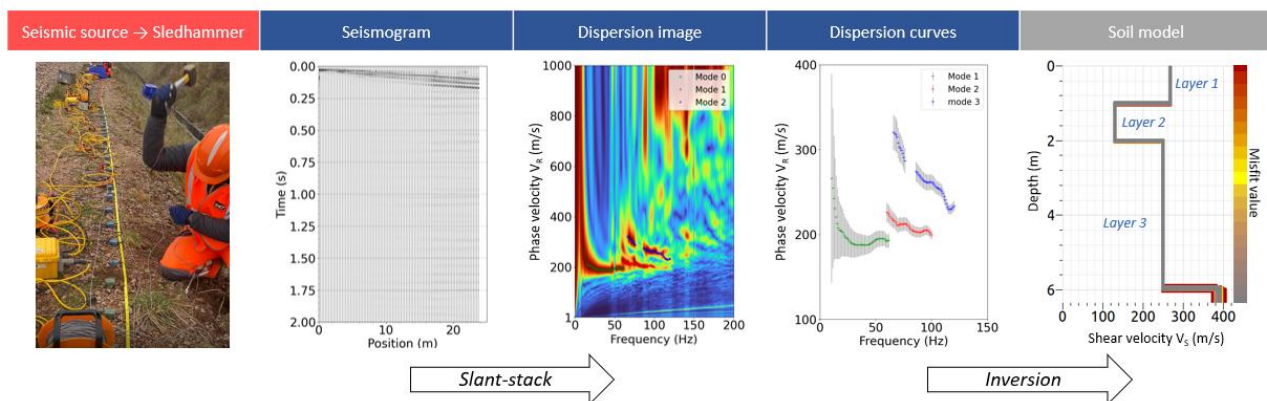


Figure 134. Workflow of the active seismic method.

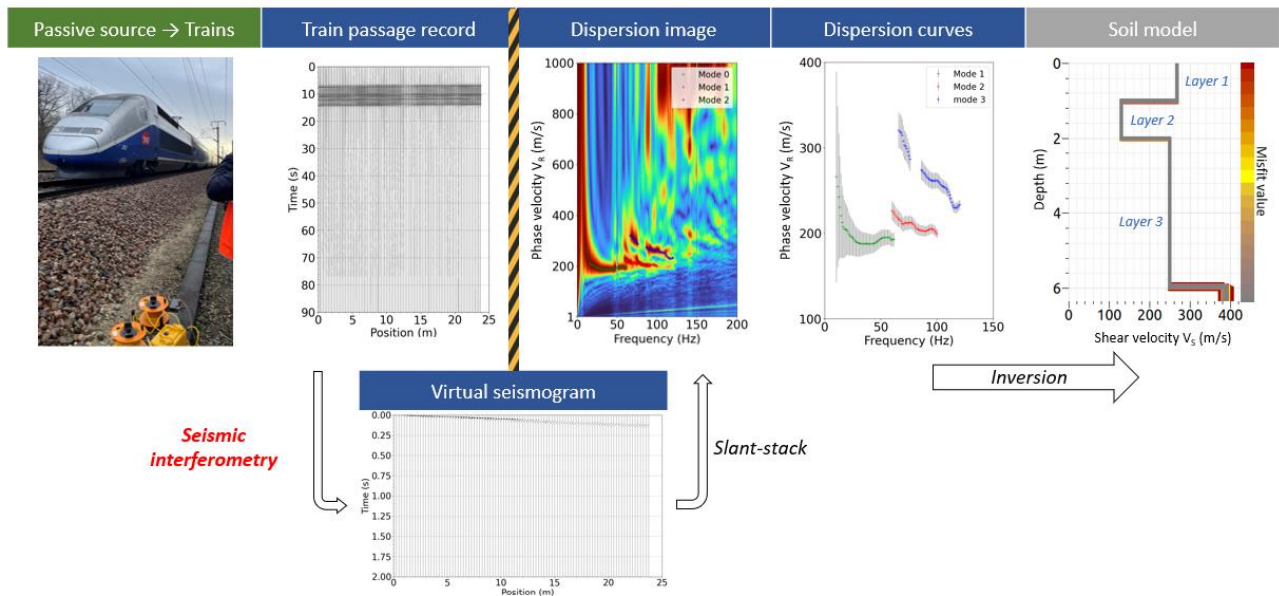


Figure 135. Workflow of the passive seismic method.

Pseudo-section of shear-waves velocity shows the evolution of a lower velocity soil layer with an increase in thickness along the study area (Figure 136). This layer is thought to be the cause of the disruption to the railway trackbed. By superimposing the radargram on the 2D shear-waves velocity profile, the complementarity between dielectric permittivity variations (radargram) and mechanical property variations with V_s (seismic profile) can be highlighted.

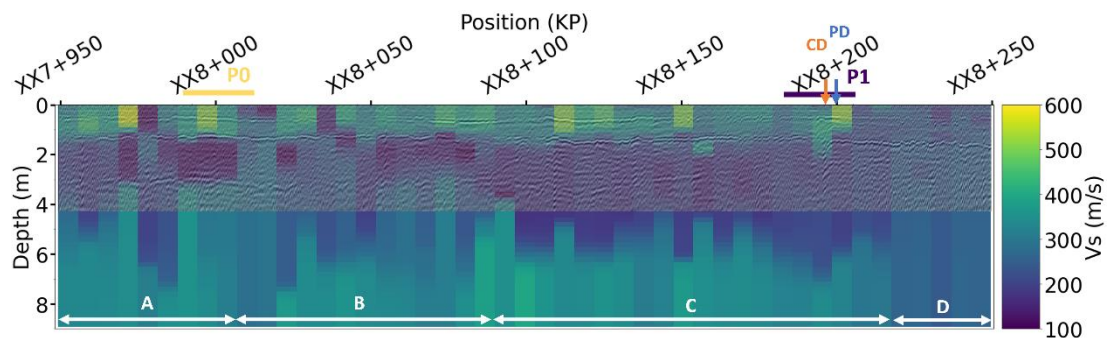


Figure 136. Example of shear-waves velocity pseudo-section and complementarity with GPR data along a railway trackbed disorder zone.

The resulting dispersion curves can either be inverted into ground models or into petrophysical and hydrogeological models.

We developed inversion procedures based on Monte-Carlo algorithms and Artificial Intelligence to retrieve the mechanical and hydrogeological properties of the soil over time (Figure 137).

The results from the AI models were validated with drilling and piezometric data, and enable a deep understanding of the site subsoil.

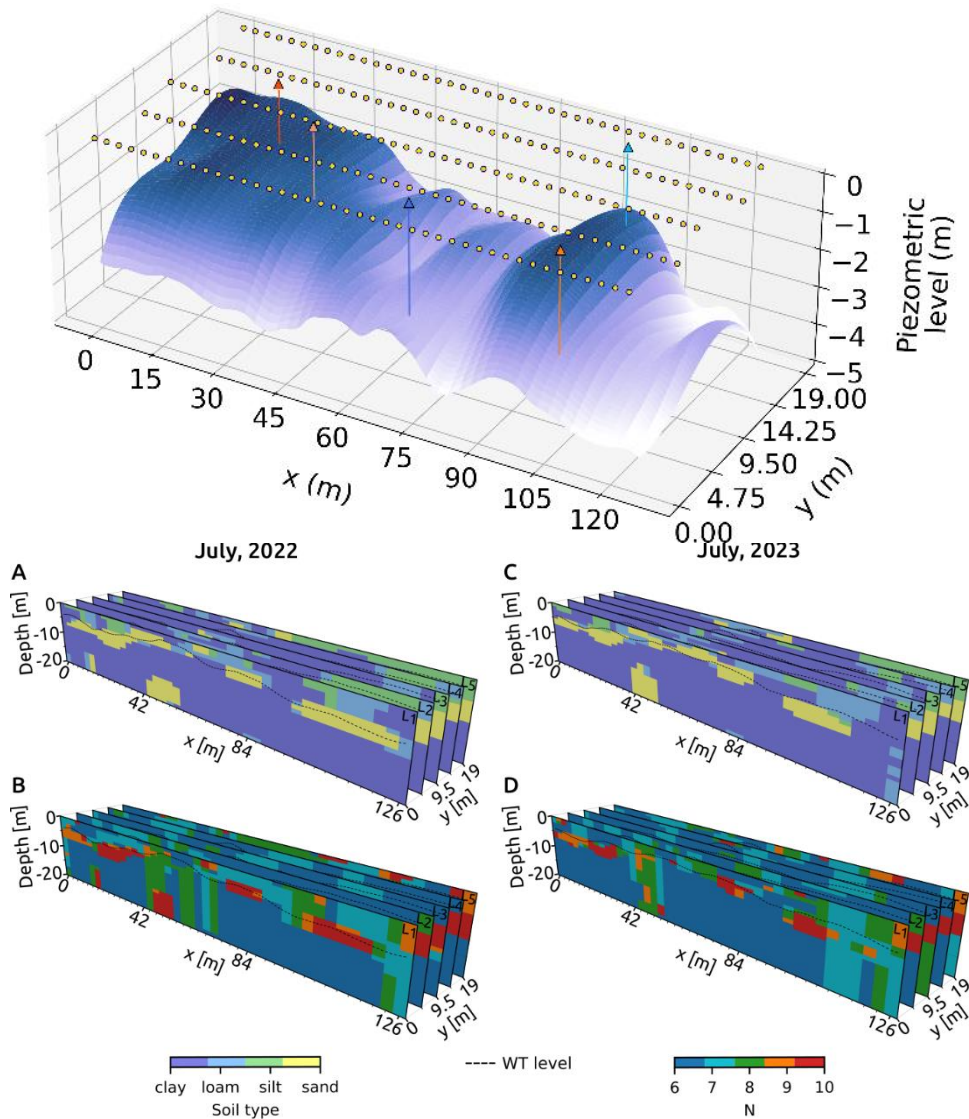


Figure 137. (top) Example of groundwater table map generated using passive MASW and Artificial Intelligence. (bottom) Example of geologic profiles and groundwater table profiles inferred using passive MASW and Artificial Intelligence.

7.3.1.4. Demonstration plans

The passive data could also be used to infer soil permeability values, however this is still under development. We are also developing the use of land streamers (towed geophones) to enhance the acquisition efficiency of the active seismic method (see Figure 138)

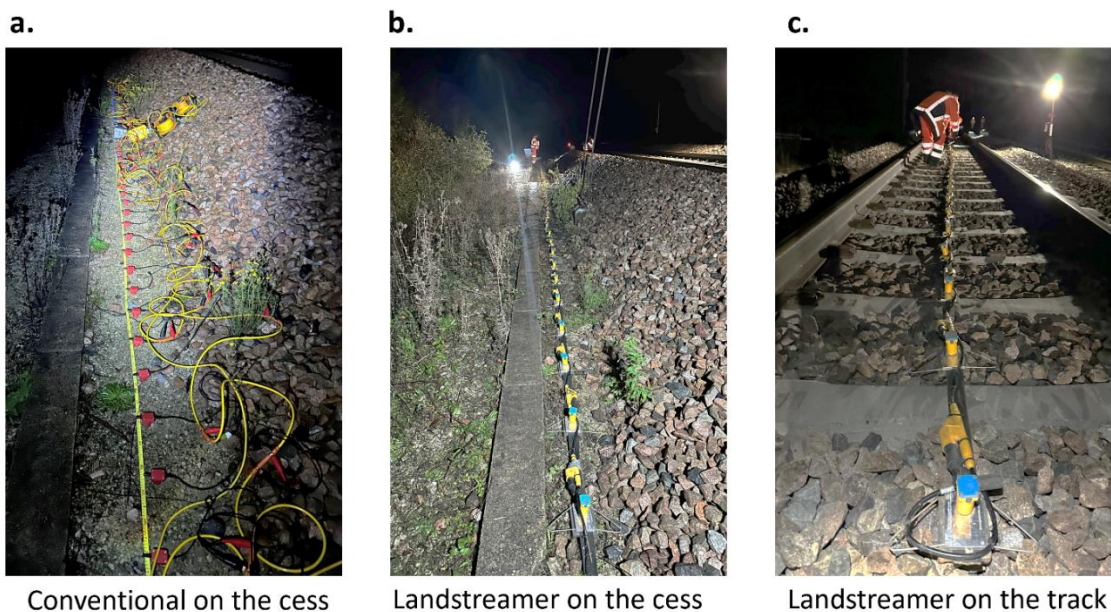


Figure 138. Active seismic device : a. Conventional on the cess, b. Landstreamer on the cess, c. Landstreamer on the track.

7.3.2. Predictive maintenance for tunnels

7.3.2.1. Selected equipment, technical specifications and justification

SNCF Réseau's digital strategy in support of maintenance

For several years, SNCF Réseau's digital strategy has led to the creation of various tools designed to capitalize on, pool, and enhance both historical and new digital data related to underground structures. Today, these tools serve as a source of digital data and notably provide improved traceability for surveillance and maintenance actions. They also enable all stakeholders involved in monitoring to access reliable and high-quality information for direct operational use. The PREDICT research project is fully integrated into this digital strategy by drawing directly from these tools to perform in-depth analyses of the heritage of underground structures.

RADIS tool - Acquisition of digital data for underground structures

Since 1995, SNCF Réseau has equipped itself with a tool for creating detailed inspection reports of underground structures. The RADIS application (Detailed Computerized Record of Underground Defects) operating under AutoCAD has helped standardize practices and limit the risks of heterogeneity, particularly in the representation of defects. It has defined the various elements (linings, equipment, defects) found in the structures, as well as their characteristics. From its inception, the tool included data archiving functions, allowing for data preservation and processing.

In 2002, SNCF Réseau's engineering department leveraged these entries to automatically retrieve and centralize a set of information such as surface areas of linings by type, linear meters of cracks, etc. The first use of these data in a structured database enabled the implementation of an automatic rating tool for underground structures (see Figure 139).

This rating system follows these principles:

- The obtained rating is a numerical representation of the density of defects recorded throughout the entire length of the structure.
- The rating is calculated over the entire length of the structure, in 10 m sections.
- The rating comprises 15 different sub-ratings, each considering one or more types of defects that can be weighted by their specific characteristics (for example, cracks are characterized by their width).
- The sum of the 15 weighted sub-ratings gives the overall rating for a zone.

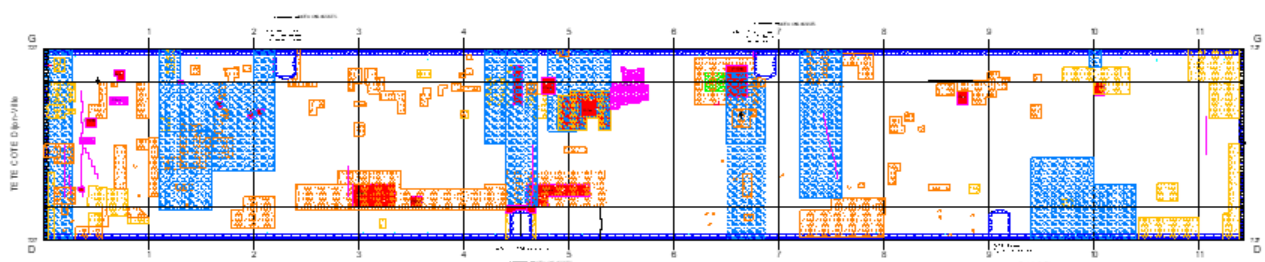


Figure 139. Example of a defect survey conducted using the RADIS module (AutoCAD software).

The rating of the underground structure ranges from 0 to a maximum of 100 points, with defined condition classes (Good condition, Fair, Mediocre, Poor, Very poor). A structure in good condition has a low rating, while a degraded area has a high rating.

Above is an example of a rating, showing the variability in the rating of an underground structure. In this example, only 8 out of the 15 sub-ratings have been detected.

RADIS heritage tool - Data processing

The exploitation of historical data for the entire SNCF Réseau infrastructure has been developed around the “RADIS Patrimoine” tool, a data analysis tool specifically designed for experts in underground structures. This tool offers analyses in the form of tables and graphs, enabling the monitoring of a given infrastructure (globally, by region, by UIC group, etc.).

It has helped experts establish a maintenance policy for these structures. Over the years, the database has been continuously enriched. To date, more than 5,800 archiving operations have been carried out since the implementation of the RADIS tool (see Figure 140).

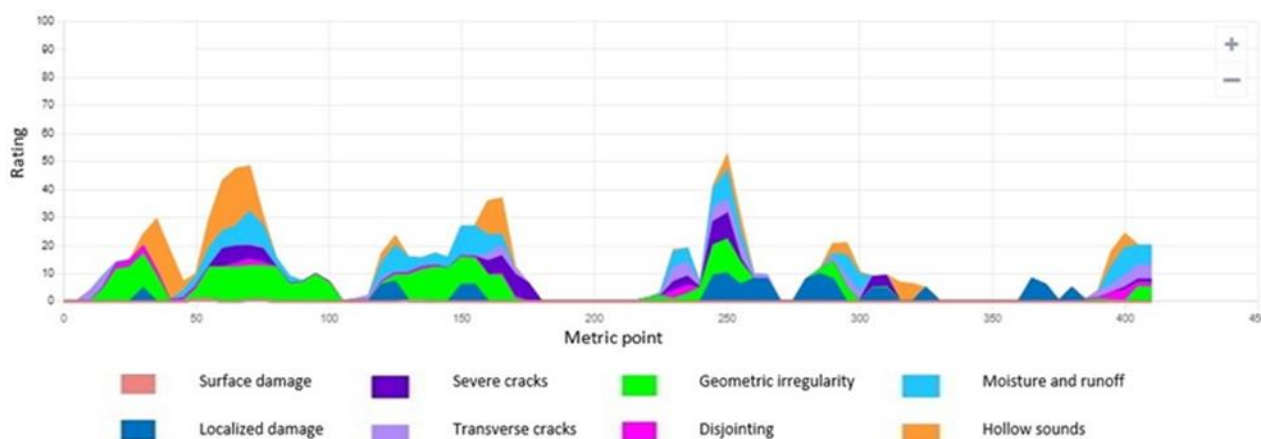


Figure 140. Example of rating for an underground structure (source database 2023).

7.3.2.2. Installation layout

Analysis of available SNCF data sources by a specialized predictive maintenance company

In 2022, a company specialized in data science and predictive maintenance analysed the SNCF data sources to assess data quality and determine the feasibility of a predictive maintenance project.

The determining factors

Several factors (length of the structure, age of the structure, type of predominant coating, etc.) are available in the data. The correlation analysis did not reveal any obvious relationships between the factors, and therefore did not help in reducing the number of dimensions. However, by studying the aging rate of a structure relative to each factor individually, we compiled a list of factors that influence the aging of the structures (see Table 17. Influence of factors on speed (examples)). For example, we observed that the entries and exits of the structures age faster than the center of the structures. Factors with missing data for several underground structures were excluded from the analysis because the models are unreliable with missing data (see Figure 141). This is particularly the case for geology, which is not currently precisely characterized along the length of each structure.

Factor	Influence on speed
Rating	A higher minimum rating leads to higher speeds
The year of inspection	The most recent inspections record lower speeds
The position or metric point	Speeds are higher at the ends of the structures
The size of the structure	Smaller structures age more quickly than medium-sized ones

Table 17. Influence of factors on speed (examples).

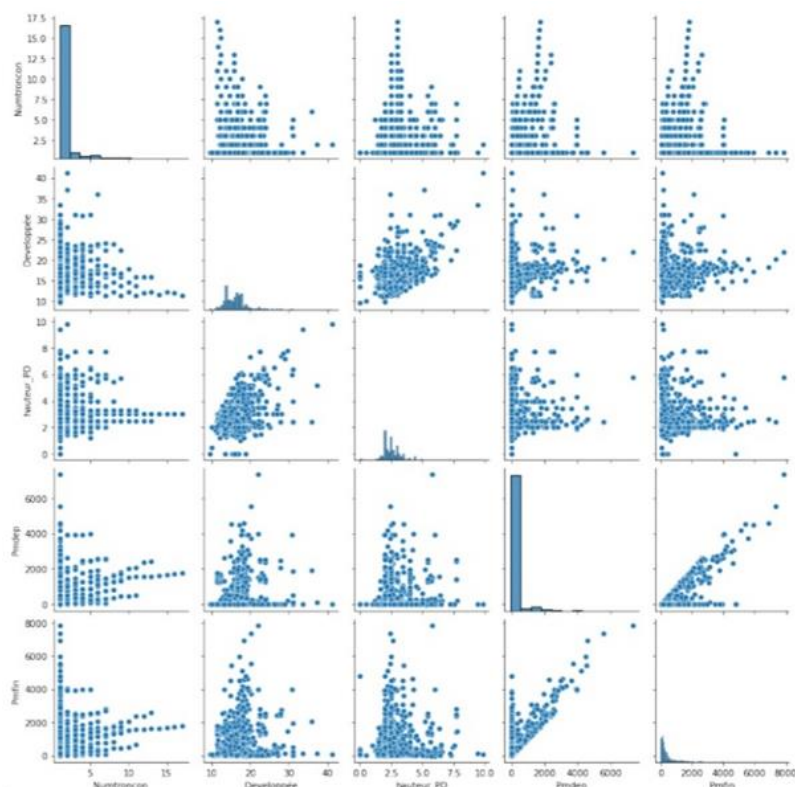


Figure 141. Analysis of the relationships between the identified factors of change.

The variability of the rating

Measurement error serves as a reference to evaluate the quality of models, which must have an error lower than that of the measurement to be considered relevant. The calculation of measurement error is based on the variability of the rating obtained after smoothing by the mean. The result depends on the size of the smoothing window used. For a defect with an influence extending over 30 meters, the measurement error is 5 ratings. For a defect with a local influence (<10 meters), the measurement error is 3 ratings.

Cleaning of inspection data

Some inspections show anomalies. For example, we observe very close inspection dates, leading to high aging rates, or rating repetitions in the case of partial inspections, resulting in zero aging rates and introducing bias into the data.

The quality of predictions directly depends on the quality of the data, which is why the inspections have been processed. On one hand, SNCF Réseau has conducted a series of additional analyses using AutoCAD RADIS drawings to validate certain numerical data from field surveys. On the other hand, retained inspections must have less than 50% zero speeds, which helps to exclude from the analysis partial inspections covering only a small part of a structure.

Modeling, assumptions, and constraints

According to the model, we predict a speed or a rating. The variable to be predicted depends on the influencing factors represented by the variable θ , the inspection t , and the position x .

$$y(t,x) = f(\theta(t,x))$$

The remainder of this study is dedicated to finding the optimal function f .

We also state the assumptions defining the learning framework related to the prediction objectives:

Learning is based solely on degradations.

Weighting of degradations: more recent inspections have greater weight in the learning process.

The models are also constrained to predict only degradations.

The study of sub-ratings

The rating present in the data is the result of a business calculation based on sub-ratings, which are derived from the defects recorded on-site. Assuming that the developments may vary depending on the type of defect, it seems relevant to analyze and model the types of sub-ratings individually. Statistical work has been carried out to provide an overview of the sub-ratings and any potential correlations with the identified factors.

The modeling was conducted according to the following principles:

- Calculation of the evolution rate of the sub-ratings.
- Modeling these rates.
- Application of business rules to calculate the rating.

It is worth noting that, due to a lack of evolution in certain types of sub-ratings, the modeling was simplified by using the values from previous sub-ratings. This method has several advantages for future work:

- Use of different models depending on the types of sub-ratings.
- Comparison of rating models based on sub-ratings and existing business rules.
- Consideration of new external factors affecting certain types of sub-ratings.

However, this method also presents some difficulties:

- Increased complexity: additional data processing, longer computation times, more intricate parameter settings, and more tedious arbitration and evaluation.
- Lack of data for certain types.

Decision tree model

A decision tree (see Figure 142) is a decision-support tool that represents a set of choices in the graphical form of a tree. The different possible decisions are located at the ends of the branches (the 'leaves' of the tree) and are reached based on decisions made at each step. A variant is known as a 'Random Forest.' This algorithm combines the concepts of random subspaces and 'bagging'

by learning multiple decision trees and then applying a rule to make a single decision (typically majority voting).

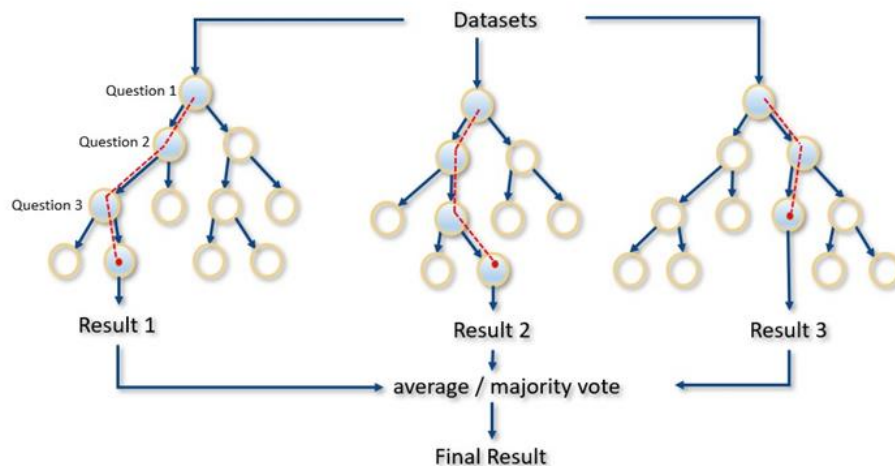


Figure 142. Synthetic example of how a decision tree model works.

Neural network model

The proposed architecture is a neural network (see Figure 143) designed to handle spatial correlations of ratings and archival data; it is divided into two sub-models. Initially, the time series of neighbouring ratings and the rating to be predicted are encoded using convolutional layers. This first sub-model addresses the spatial aspect of the data. The encoded time series is then fed into a second model, along with the influencing factors. This second sub-model is a neural network that handles temporal dependencies.

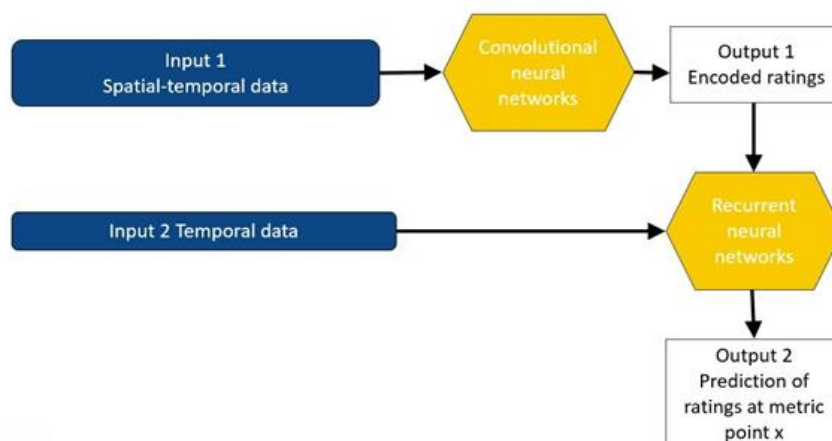


Figure 143. Synthetic example of how a neural network model works.

7.3.2.3. Initial data collection and results

Results and Performance of Each Model

Model evaluation is carried out by comparing predictions with observations. Two metrics are used to assess the performance of models and to choose the one with the best performance on SNCF Réseau data:

1. **Mathematical Indicator:** The Mean Absolute Error (MAE), which measures the average of the absolute errors between a prediction and its observation across a total of n observations. The difference between the prediction and the observation is called a residual. The closer the residuals are to 0, the better the prediction. This indicator is preferred over the Mean Squared Error because it is more robust to outliers present in the data.
2. **–Percentage within the Interval [rating-5; rating+5]:** This score is obtained by counting the number of points within the tolerance interval, divided by the total number of points. The tolerance thresholds are defined relative to the human error margin of ± 5 ratings between two inspections.
3. **Business Indicator:** The total length by speed class. This indicator calculates the distance covered by each aging speed interval for the infrastructure. Results are calculated both from observed speeds and predicted speeds.

Performance of the neural network model

The neural network predicts a rating per PM. The distribution of the prediction error (or residual) is centered around 0 and is concentrated within the $[-5; 5]$ rating interval. However, it is slightly skewed towards negative values, indicating a tendency to underestimate observations. It should be noted, however, that the model performs well regardless of the observation value, with high ratings being predicted accurately (see Figure 144).

Due to the difficulty in explaining the prediction process despite highly satisfactory results, SNCF decided not to continue with this model, as it is too opaque (black box).

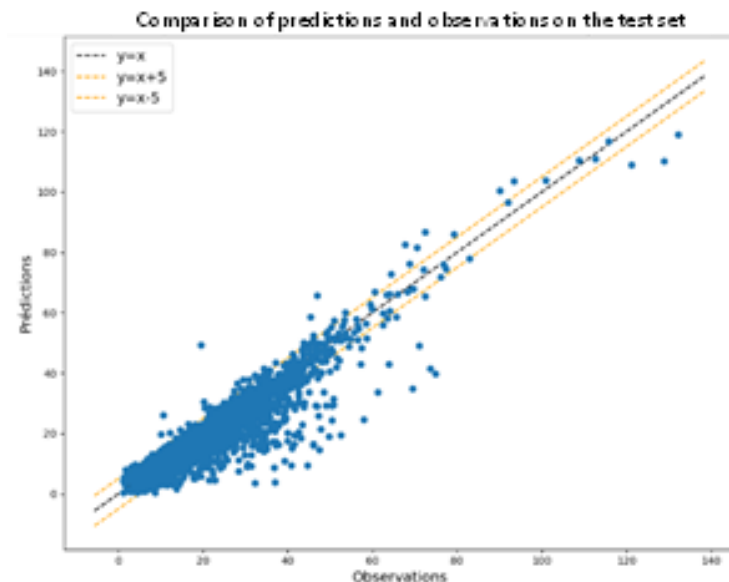


Figure 144. Performance results for the neural network model. 75% of the predictions fall within the [rating-5; rating+5] interval.

Performance of the decision tree model: Gradient Boosting

The gradient boosting model predicts a speed per metric point. The rating per metric point is reconstructed from this predicted speed. The performance shown by this model (76.6% within [-5; 5]) is better than the results provided by the neural network (75% within [-5; 5]). At the end of 2023, SNCF decided to retain this model in order to integrate it into the digital decision-making tool, with the aim of improving transparency and the understanding of its outcomes (see Figure 145).

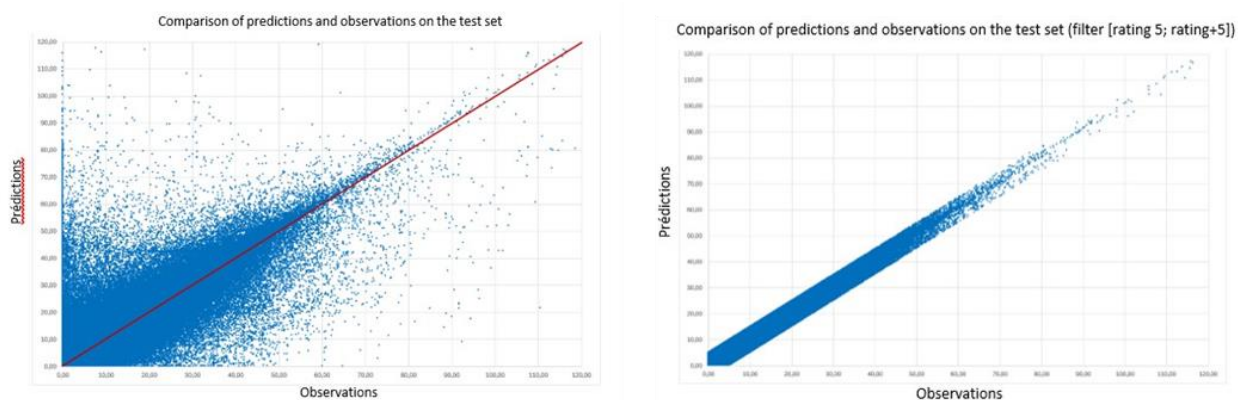


Figure 145. Performance results for the Gradient Boosting model. 76,6% of the predictions fall within the [rating-5; rating+5] interval.

Model limitations

The limitations of forecasting models are primarily evident through several critical aspects, including:

The inability to predict significant price increases without prior indicators or linked to an unforeseen event.

Forecasting models generally rely on past trends, historical correlations, and rational assumptions. However, they show their limitations when it comes to anticipating sudden or unpredictable events, such as natural disasters, extreme climate events, unexpected structural disruptions, or repair operations. These events, which can cause sharp price increases or decreases, often do not fit into any of the modelled trends, making them difficult to account for. Traditional models fail to predict these movements as they lack clear early warning indicators and are often incapable of reacting to unmodeled external factors.

The quality of input data

The reliability and accuracy of models directly depend on the quality of the data provided to them. If the input data is incomplete, inaccurate, or biased, the model will produce forecasts that deviate from reality. Data management is therefore crucial: its collection, cleaning, and updating must be done with care. Models are thus exposed to misinterpretation or suboptimal decisions when the data is insufficient or skewed.

In conclusion, while forecasting models are powerful tools, they remain limited, particularly when faced with the unpredictability of sudden events and the variability of input data quality. These factors must be considered to avoid placing excessive trust in the results provided by these models.

7.3.2.4. Demonstration plan

Development of a Decision Support Tool for SNCF Tunnel Expertise

A decision support tool (ADN OST – Analysis of Digital Data for Underground Structures), assisted by AI, was developed in 2024. It builds on research conducted in 2022 and 2023 (Figure 146).

The tool incorporates a Machine Learning model (Gradient Boosting) and a prediction module that allows visualization of the projected aging of underground structures using two indicators:

The potential rate of tunnel degradation evolution and a forecast of the condition rating of the structures at future dates (see the dashed blue and green curves below representing the forecasts for 2035 and 2050).

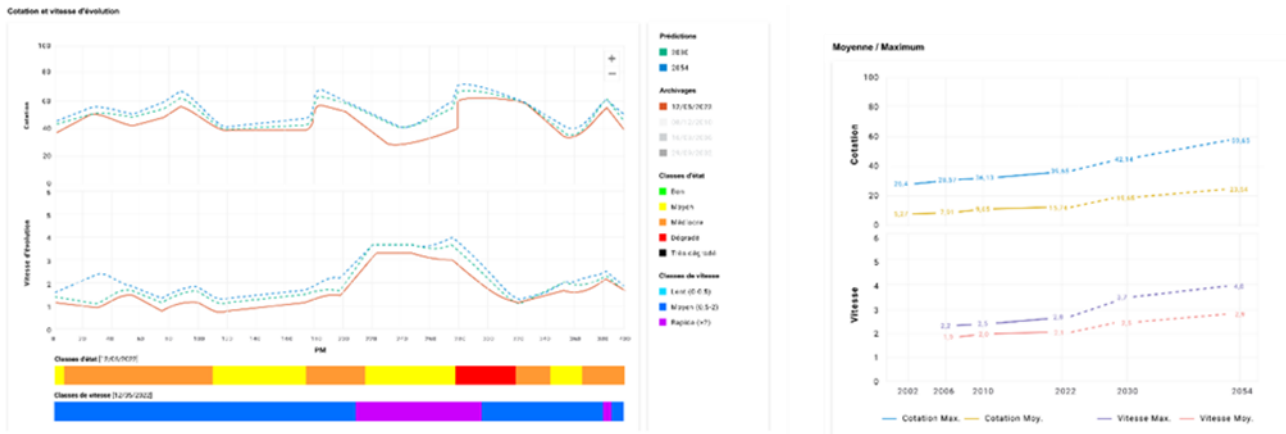


Figure 146. Screenshot of the Decision Support Tool Developed by SNCF.

The screenshot shows the decision support tool developed by SNCF, with the blue and green dashed curves representing the forecasts for 2035 and 2050 for a given structure.

The tool leverages and enhances the intrinsic characteristics of tunnels, their pathologies, and their environment. The integration of future RADIS survey data into the heritage database will refine the compliance rate. The prediction model will be retrained at defined intervals (3 to 6 years) to ensure its reliability. This model approximates the aging laws of these infrastructures based on their typology and environment.

The tool will assist experts in their daily work and enrich risk analyses for decision-making. It also marks the beginning of a new phase in the maintenance policy for underground structures, with three main objectives:

- Near-Automatic Prioritization of Tunnel Regeneration Operations
- Identification of Regeneration Needs
- Projection of Financial Trajectories for Tunnels in the Medium and Long Term

7.3.3. High efficiency tunnel inspection systems

7.3.3.1. Selected equipment, technical specifications and justification

The tunnel inspection systems use three types of sensors:

- **Photographic sensors.** The aim is to obtain a high-resolution colour image of the tunnel intrados. The minimum resolution expected is 1 mm/pxl. Two types of sensors are used:
 - **Linear cameras (or line-scan cameras):** These cameras can reach acquisition speeds of several tens of kilometres per hour (60 km/hr or even more). However, these cameras require a continuous supply of light to illuminate the capture line. This is provided by a LED ring that requires a large power source. For this reason, this type of camera needs to be installed on a large piece of equipment such as a train or road/rail truck (see Figure 147).



Figure 147. TS4 system from German company SPACETEC with line-scan cameras.

- **Matrix cameras:** These sensors are similar to conventional cameras. Flashes are used to bring in light. With these cameras, the system is lightweight, and battery powered. It can therefore be installed on a light lorry, making it easy to operate. The disadvantage is the low acquisition speed (a few kilometres per hour).

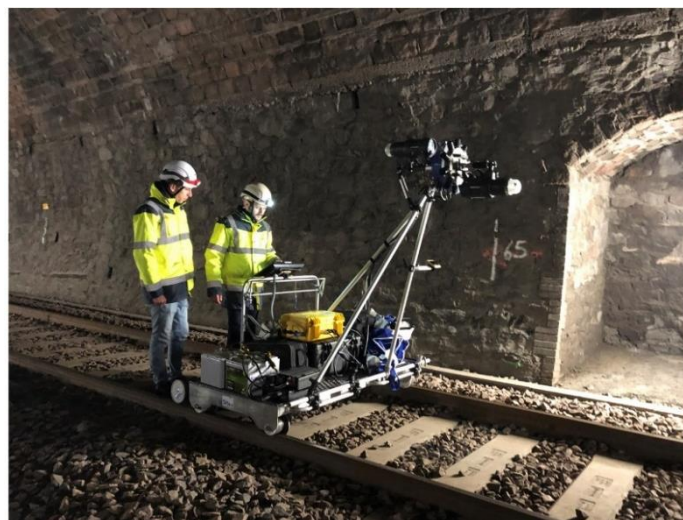


Figure 148. Scantubes system from the French company SITES with matrix cameras.

In both cases, a calibration step, of varying speed, is necessary before the start of the measurement to adapt to the geometry of the tunnel (Figure 148).

- **Lidar/lasergrammetry sensors.** Lasergrammetry uses motorised digital sensors, or scanners, to measure points in X, Y and Z coordinates with a relative accuracy of around 0.5 mm.

The resolution of the point cloud depends on the characteristics of the scanner (speed of rotation and number of points measured per revolution), the forward speed of the vector and the distance of the measured object from the scanner. The optimum speed should be between 2 and 5 km/hr to obtain sufficient transverse resolution to identify masonry joints. For concrete structures, the speed can be higher (Figure 149).



Figure 149. ELISE system from the Swiss company AMBERG for SNCF Réseau.

- **Infrared thermography sensors.**

For all the sensors, an oedometer sensor is also required to adjust the position of the data in relation to the tunnel. Data collection is monitored live from a computer.

Three independent systems produced by private companies are used:

- TS4 from the German company SPACETEC, which uses photographic sensors, lidar and infrared thermography. The system must be installed on a train or rail/road vehicle;
- Scantubes from the French company SITES, which has photographic and infrared thermography sensors. The system is installed on a light lorry;
- Elise, a lidar sensor from Swiss company AMBERG. Spacetec also has an equivalent system. The system is installed on a light lorry.

7.3.3.2. Installation layout

From 2019 to 2022, tests were conducted in a railway tunnel to identify the contribution of these technologies to tunnel inspection.

The installation must be on a mobile vector and is different depending on the type of sensors.

Linear cameras require significant lighting with high energy consumption. This is why it requires a vector (train or road-rail truck) that can power the system or accommodate a generator.

The other systems can be powered by batteries and can therefore be installed on lightweight lorries.

In a railway context, lorries are simpler to deploy between traffic. However, the efficiency is lower if several tunnels must be measured in the same period.

7.3.3.3. Initial data collection and results

Several results are obtained and useful for the inspection of tunnels.

- **Photogrammetry: orthophotography of the intrados at high resolution and in color:**

The resolution achieved of around 1 mm/pxl makes it possible to visualize cracks with an opening of approximately 0.3 mm.

This orthophotography can be directly used to carry out damage surveys to facilitate the reporting of disorders and the detection of developments. It also constitutes an excellent support for preparing visits and self-checking at the end of the mission. However, it does not offer any notion of depth (see Figure 150).

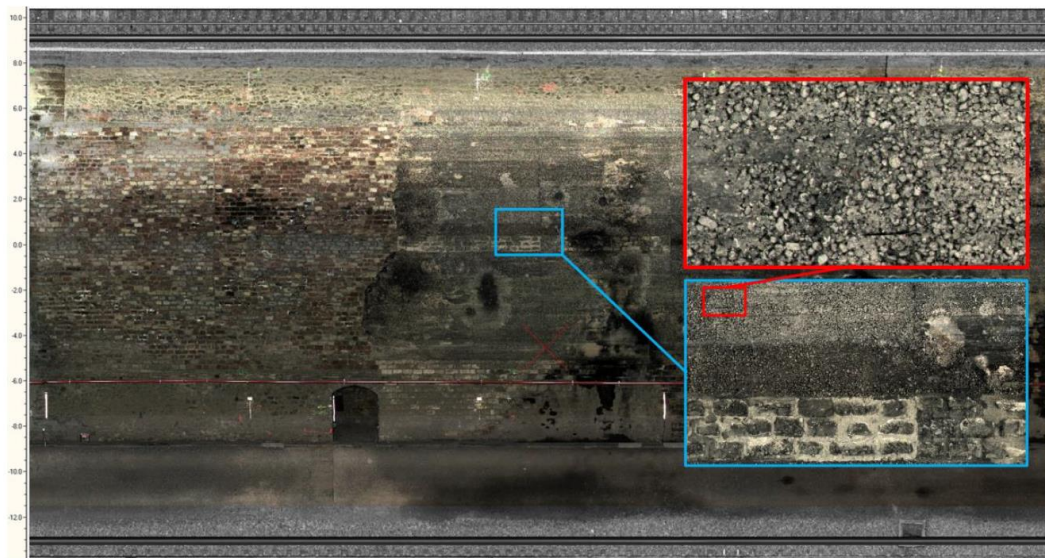


Figure 150. ELISE system from the Swiss company AMBERG for SNCF Réseau.

- **Photogrammetry: photorealistic 3D model (mesh and textured point cloud)**

Although the precision of the point cloud of several millimeters/centimeters at the scale of the section does not allow fine geometric analyzes to be carried out, it is possible to visualize geometric irregularities of large amplitude (several tens of centimeters) (see Figure 151).

This type of data is especially interesting for preparing the visit in order to have another vision of the work in addition to the orthophotography.



Figure 151. Example of a photorealistic 3D model.

- **Lasergrammetry: pseudo-orthophotography of the lower surface in black and white:**

It is obtained thanks to the representation of shades of grey associated with the reflectivity values of the measured points and by a “flat” projection according to the development of the tunnel.

The resolution is much lower than orthophotographs obtained with photographs (2.5 to 5 mm/pixel) but still facilitates the identification and positioning of damage observed on site (see Figure 152).

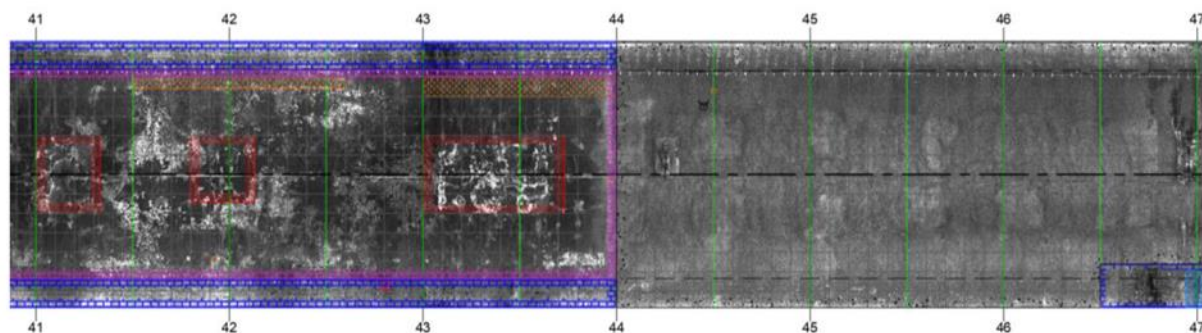


Figure 152. Superposition of a damage survey with a pseudo-orthophotograph obtained from a scanner.

- **Lasergrammetry: 3D point cloud**

The superior precision of point clouds from photogrammetry makes it possible to carry out geometric analyzes making it possible to characterize geometric irregularities or loss of materials (disjointedness and surface damage). Identification can be made automatically by comparing the measured profiles with one or more theoretical profiles (see Figure 153).

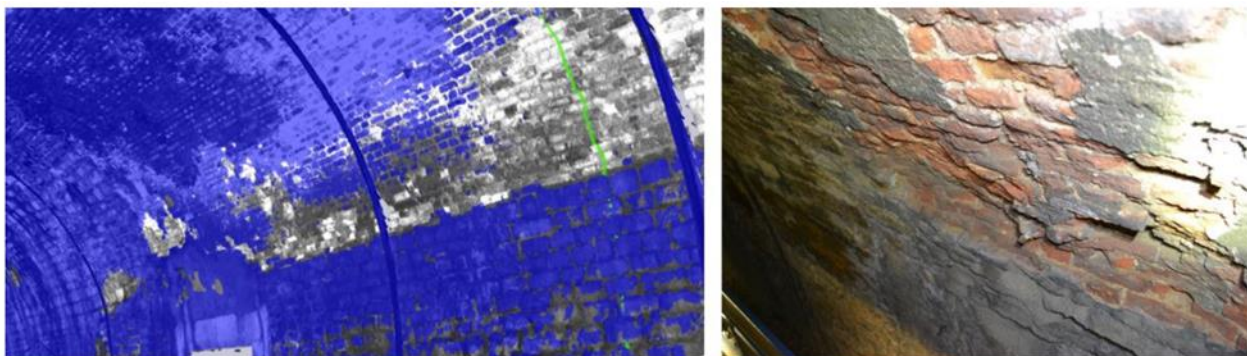


Figure 153. Automatic detection of a brick exfoliation zone by comparison between the profiles measured by a scanner and a theoretical profile and photograph of the zone taken in-situ during an inspection.

- **Infrared Thermography Card**

The restitution of a temperature map on the scale of the intrados allows use in a damage survey. It is also possible to overlay this map with an orthography to correlate the presence of damage to areas of humidity (see Figure 154).



Figure 154. Superposition of an orthophotograph with the temperature reading.

New tunnel inspection assistance technologies can provide valuable assistance in identifying and characterizing damage. They offer a gain in the precision of the surveys and therefore in the evaluation of the degradation of the structures. They also provide assistance in preparing for inspections and self-checking at the end of the mission.

It is however necessary that the acquisition and processing protocols be uniform for the three technologies. This is all the more important to allow a comparison of the results of acquisitions carried out in two different periods.

In 2022 and 2023, the measures continued and concerned the capacity of photogrammetry to automatically detect changes in the state of the tunnel between two measurements. It is important to mention that knowing the position of the damage is important but knowing its evolution is even more important.

The measurements were carried out with the SCANTUBE system from the company SITES in 2022 and 2023.

The measurement carried out in 2022 concerned an operated railway tunnel which show progressive damages due to sensitive terrain and structure. The aim of this measurement was to carry out an initial inventory and then, in 2024/2025, carry out a second measurement to automatically detect changes using photogrammetry analyses (see Figure 155).



Figure 155. Superposition of an orthophotograph with the temperature reading.

In 2023, automatic damage detection tests were carried out in an abandoned tunnel with SITES company.

Damages were deliberately generated and measurements were taken at different stages of degradation (see Figure 156, Figure 157 and

Figure 158).



Figure 156. Creation of damages.



Figure 157. Measurement.

In post-processing, the photographs were processed by photogrammetry to generate a 3D model and orthophotographs. These treatments were carried out for each measurement corresponding to different stages of degradation (by SITES company). The different orthophotographs have been superimposed to the nearest pixel. A similar approach was carried out with 3D models.



Figure 158. Examples of orthophotographs corresponding to different degradation moments.

With the perfect superposition of images and 3D models, it is possible to automatically identify the location of areas of degradation as well as their centimetre depth (see Figure 159 and Figure 160).

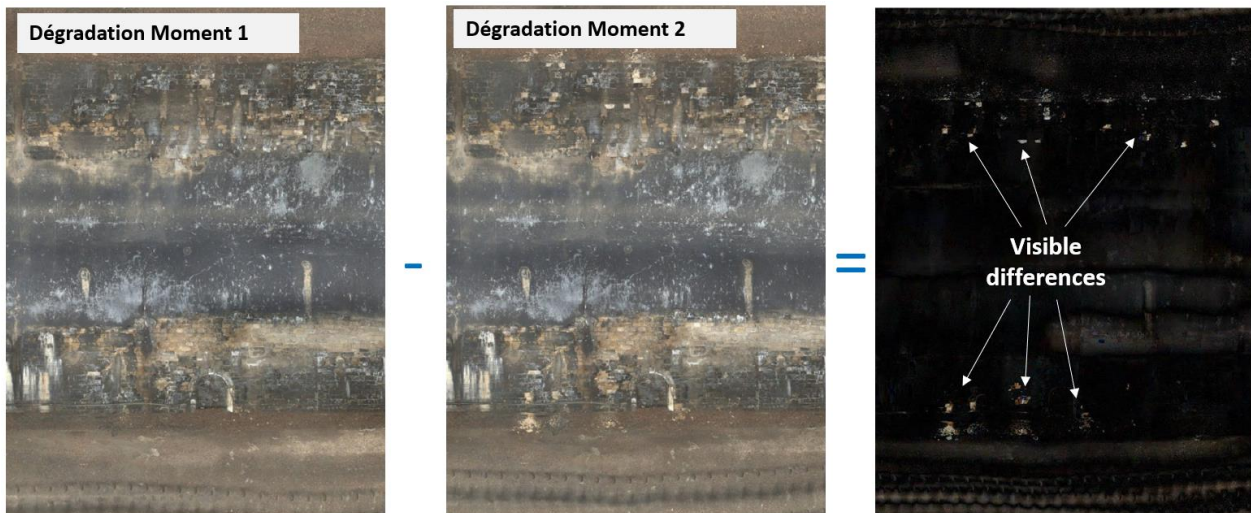


Figure 159. Pixel-to-pixel subtraction and identification of visible differences between two moments (ScanTubes® – SITES) – SNCF Network Tunnel.

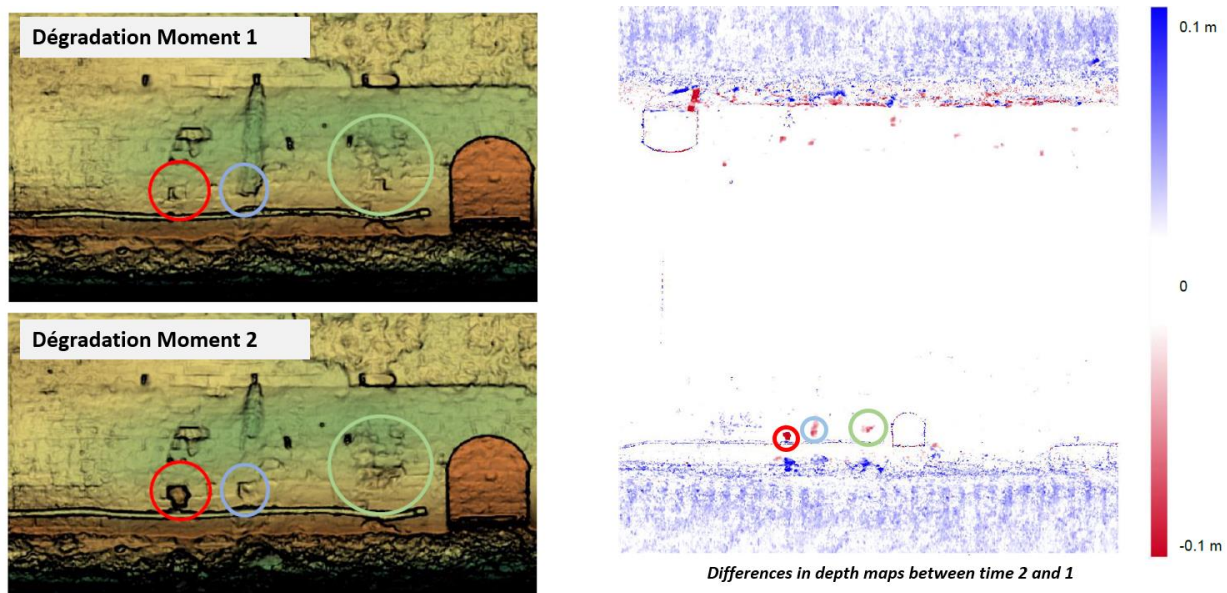


Figure 160. Geometric processing and detection of damage depths between two moments (ScanTubes® – SITES) – SNCF Network Tunnel.

7.3.3.4. Demonstration plan

The validation tests of the algorithms are continued over the year 2024 with additional measurements in the tunnel measured in 2022 for which the disorders are known.

7.3.4. Passive contactless magnetic microwire sensor arrays for high-definition tunnel convergence monitoring systems in tunnels.

Currently, the measurement to check if a tunnel in question has experienced relative displacements in its contours are performed using topographic methods, which involve the need to invade the track to place the measurement equipment, in addition to the qualified personnel needed to perform the in-situ measurements with this instrumentation.

Since these measurements are invasive, they are not compatible with railway traffic, which significantly limits the capacity to obtain more data. For these reasons, these measurements have high costs and also pose a greater risk to the safety of workers.

As a search for a replacement for these methods, the possibility arises of using a new non-invasive sensor element to perform the inspection of railway tunnel convergence. The material used for this sensor is called magnetic microwire.

The microwire, in turn, would not require interruptions in traffic and could obtain data continuously, meaning that it would be continuous monitoring of the infrastructure that also would not require personnel in situ to take the measurements, offering a great advantage in terms of both safety and economics.

Once this brief introduction has been made, the microwire, the tests it has undergone, and the results obtained in them with their relevant conclusions will be defined.

7.3.4.1. Selected equipment, technical specifications, and justification

The magnetic microwire is a **filament** with a **microstructure** composed of different materials: the **core**, made of a **metal alloy**, most commonly iron and cobalt, and an **outer layer** of **Pyrex** that provides insulation. Throughout this research, the microwire used has a core with the following composition: Co72.75 Fe2.25 Si10 B15. The **manufacturing** process involves an **ultra-rapid cooling** technique that allows for the production of these microwires in coils with a maximum diameter of **100 microns**. In the Figure 161 the microwire appears from the microscope.

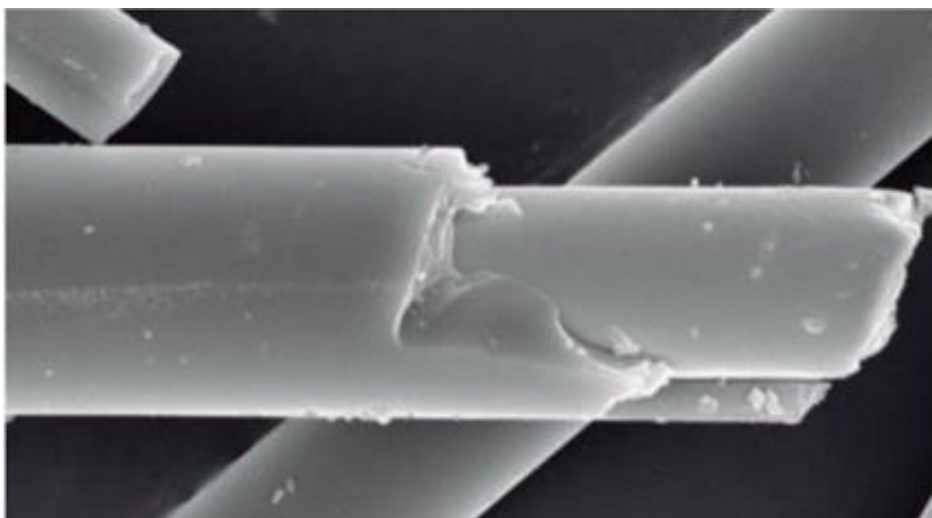


Figure 161. View of the microwire under the microscope. Source: IMA

The reason for using these microwires in the inspection of railway tunnel convergence lies in their properties, as they are **magnetostrictive** materials, a specific property of ferromagnetic materials. Ferromagnetic materials are those in which their spins (the magnetic moments of the material) are always aligned in the same direction without the need for an external magnetic field.

Magnetostriction is the **ability** of a **material** to **change its shape** in the **presence of magnetic fields**.

The structure of these ferromagnetic materials includes **two domains**, each being a magnetically polarized region. When a magnetic field is applied to the material, the **boundaries** between these domains **shift** until they rotate; that is, the **spins** begin to **change direction** until they align in the opposite direction. As a result, this change is **reflected** in the **material's dimensional shape**.

This property of the material to change shape in the presence of magnetic fields is called magnetostriction.

When the spins are in one position and begin to shift to their **opposite position**, reaching the point where they are all aligned in the opposite direction, it is said that the **saturation level** has been reached. If this process is repeated over and over, what we know as a **hysteresis cycle** is formed. Previous research has shown the potential of the microwire, which possesses these characteristics (ferromagnetic material with magnetostrictive properties), and that in the **presence of electromagnetic waves** at a specific frequency, this material could be used as a **sensor element**.

To use the microwire as a sensor element, it must be placed between **two helical antennas**, with one functioning as the **transmitting** antenna and the other as the **receiving** antenna. Using a **vector network analyzer (VNA)**, the transmission, reception, and analysis of the signal are captured.

Simultaneously, the microwire is subjected to an **alternating magnetic field** of a specific **frequency** and **amplitude**. The microwire acts as a **modulator** when the wave emitted by the transmitting antenna passes through it, and the data from this are recorded in the time domain as periodic functions.

While the **microwire** undergoes a **change** in the **stress** it is subjected to, these **graphs will change**, **allowing** the **identification** of the **changes** the microwire undergoes, thereby **serving as a sensor element to detect small variations in the geometry of railway tunnels**.

7.3.4.2. Initial data collection and results

The aim of the laboratory tests is to determine the optimal installation conditions for the microwire so that the detection of possible deformations is as sensitive as possible and can be detected by the systems even when the deformations are on a millimeter scale.

This research project on microwires has been carried out mainly at the **Instituto de Magnetismo Aplicado (IMA) UCM-ADIF, Salvador Velayos Laboratory**.

The research has consisted of an **initial stage of study and technical understanding** of the microwire, followed by **practical tests with it**. The methodology followed in this project consists of a series of tests which can be seen in Figure 162.

These practical tests can be divided into several stages, culminating in the final part, which is the objective of this project: **finding the relationship between a magnetic parameter, in this case, S_{21} , and the stress applied to the microwire, so that it can be used as a sensor element in the measurement of railway tunnel convergence**.

The stages of the research project were:

1. Selection of microwire length
2. Selection of the number of wires
3. Selection of the working frequency
4. Placement of the wires in the prototype
5. Application of load on the prototype
6. Voltage-to- S_{21} parameter variation relationship

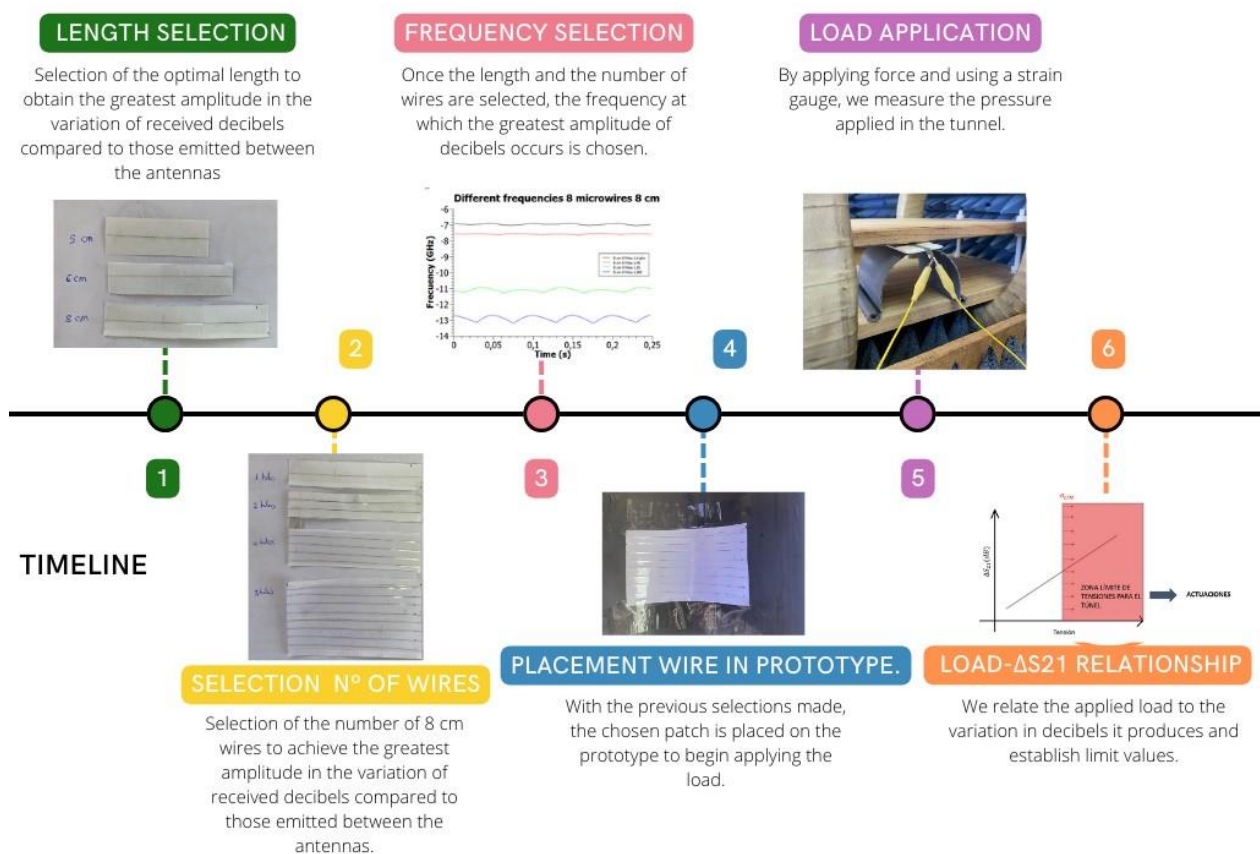


Figure 162. Project Timeline. Source: Own Elaboration

Stage 1: Selection of microwire length

In this first stage, the goal is to determine the most suitable length to achieve the greatest variation of the S_{21} parameter, which can be identified and measured using the VNA and, therefore, allows us to monitor the system. The greater the variation in S_{21} provided by the microwire, the easier it will be to detect small changes that may occur in the infrastructure.

In Figure 163, an example of 3 patches of different lengths can be observed:

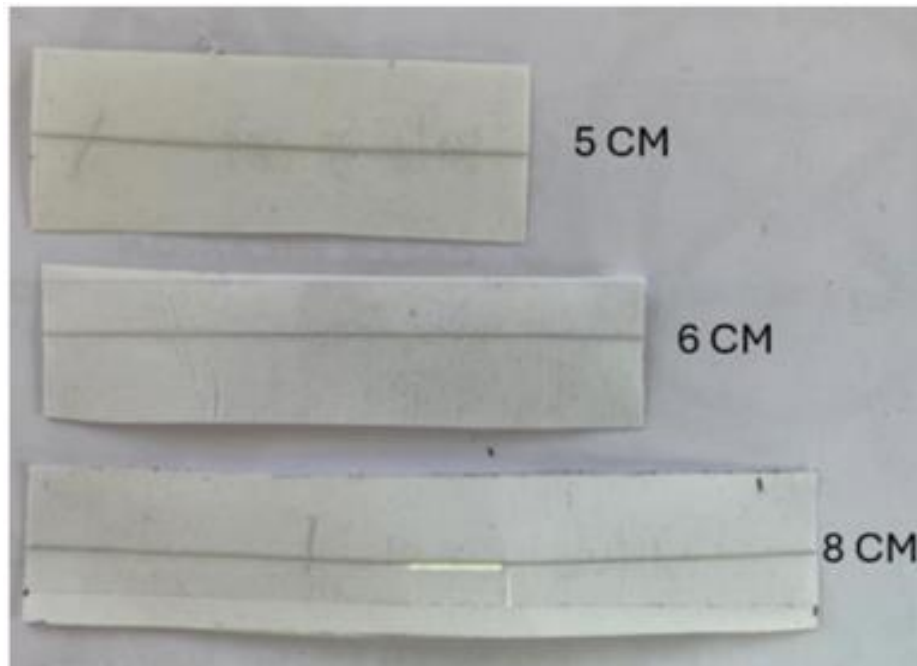


Figure 163. Microwire patches of different lengths. Source: Own Elaboration

Stage 2: Selection of the number of microwires

The number of microwires was determined in the same way as the microwire length. Figure 164 illustrates the optimal patch identified in the course of this research.



Figure 164. Optimal microthread patch. Source: Own elaboration

Stage 3: Selection of the working frequency

Once the aforementioned patch is ready, the working frequency must be selected for the tests when applying the load. To conduct these measurements, a frequency domain measurement is first performed on the patch with 8 microwires, each 8 centimetres long, to determine the frequency at which the greatest variation in S_{21} occurs. This frequency will then be used as the basis for subsequent measurements.

Stage 4: Placement of the patch on the prototype

In this stage, as mentioned, the patch with 8 microwires, each 8 centimetres long, is placed at the crown of the tunnel to later conduct the required tests.

In Figure 165, you can see how the patch is installed on the tunnel prototype.

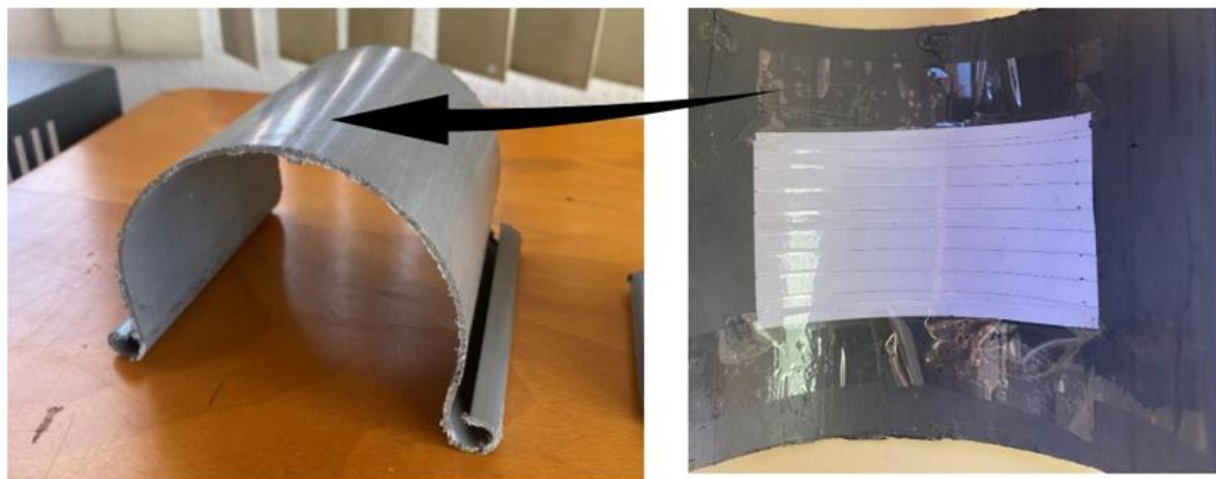


Figure 165. PCV prototype with microwire patch. Source: Own elaboration

After that, the prototype is introduced into the setup, and everything is ready for load application.

Stage 5: Load application on the prototype

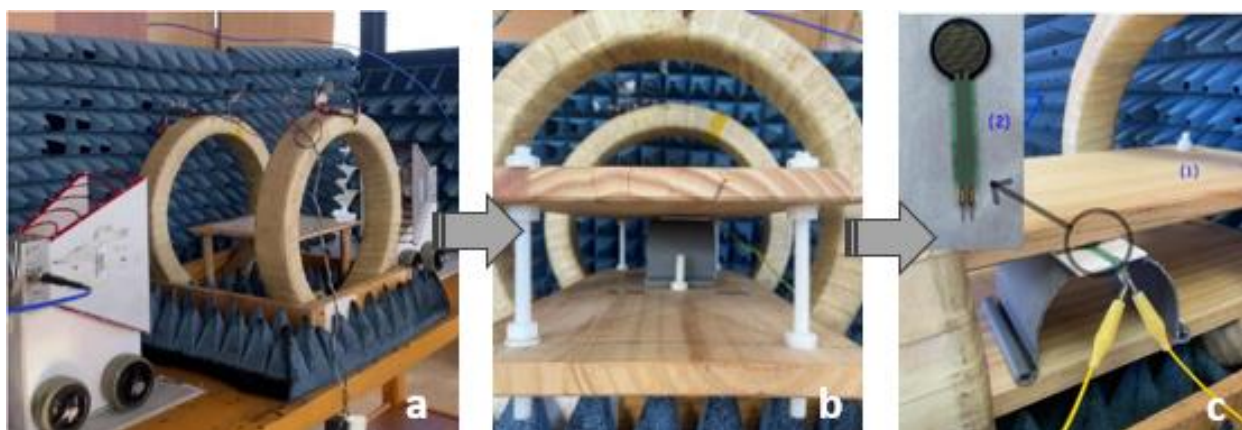


Figure 166. Parts of the experimental setup. Source: Own elaboration

In the setup, the **system designed for load application must be placed**. This system consists of **two wooden** boards connected by **PVC screws**, with nuts on each side of the board responsible for applying pressure to lower the upper board, exerting force on the prototype.

This force is recorded with a strain gauge, as shown in the Figure 166, which is connected to a voltmeter and, with the help of a datasheet, indicates the pressure being applied to the microwire. Additionally, we can measure how much the prototype has descended as a result of the applied load and how much its width has increased, thus covering all the parameters that provide information about the effects of the load application on the prototype.

While the load is being applied, the variation in the previously mentioned parameter, S_{21} , is simultaneously measured using the VNA.

Stage 6: Voltage-to- S_{21} parameter variation relationship

The principal objective of this research is to construct a graph that correlates the load and S_{21} . This graph will serve as a crucial reference point for the implementation of corrective measures in the event of a voltage shift, which may be indicative of a disruption in the S_{21} parameter.

The findings of this research demonstrate that the microwire is a technically viable sensing element for measuring minute deformations in the surrounding material. Consequently, it has the potential to serve as an effective and precise sensing element for the continuous monitoring of railway tunnel convergence when necessary.

The results indicate that, with further development and testing, the material could transform and revolutionise the way railway infrastructure is monitored, markedly enhancing safety and reducing maintenance-related operational costs.

7.4. Data Analysis for Condition Monitoring (The Netherlands, Norway)

7.4.1. Selected equipment, technical specifications, and justification

7.4.1.1. The Netherlands-Track condition monitoring

The final goal of the task is to monitor embankment stability with ABA-based technology. Railway bridge transition zones are considered case studies as they exhibit significant changes in track support conditions. According to the architecture, two data sources (the developed ABA measurement system and the track inspection vehicle) are included, and their specifications are given as follows.

The ABA measurement system, TU Delft patented technology (Li and Molodova 2011), consists of four major components, as shown in the next table. The operational speed in the conventional Dutch railway network is typically no higher than 140 km/h. Therefore, the lowest positioning resolution of the ABA dataset is approximately 1.5 mm based on the sampling rate of 25.6 kHz.

Components	Description
Axle box accelerometers	A one-directional accelerometer with linear characteristics up to 10 kHz is mounted on each axle box of a wagon and aligned with the center of each axle box to measure the vertical acceleration. In total, 8 channels of acceleration signals are recorded with a sampling rate of 25.6 kHz.
Tachometer	The tachometer that can detect pulses at approximately 1 MHz is used to calculate the rolling distance of the wheel. One channel is recorded in the database with a sampling rate of 25.6 kHz. Later, the running speed of the instrumented wagon can be obtained based on the measured distance.
GPS receiver module	The high-precision GPS module with a real-time kinetic function that can receive the GPS coordinates with a sampling rate of 1 Hz is utilized to determine the instrumented wagon position. In total, three channels (Latitude, Longitude, and time) are recorded in the database with a sampling rate of 1 Hz. Later, GPS coordinates are interpolated to 25.6 kHz and synchronized with all remaining signals.
Data acquisition system	NI compact RIO module with the in-house control software records signals with synchronized sampling between all channels. The measured dataset is recorded at the sampling rate of 25.6 kHz.

Table 18. Description of the measured signals from the ABA measurement system.

The track inspection vehicle of model UFM 120 is from EUROSCOUT, which ProRail contracts to conduct track geometry measurements following EN 13848. The measurement campaign is conducted at least once, up to four times yearly. After post-processing, the measured dataset is transferred to the BBMS system, in which track geometry parameters are reported every 0.25 m and all positioned in the Dutch railway reference system. The description and specification of track geometry parameters used in this research are shown next.

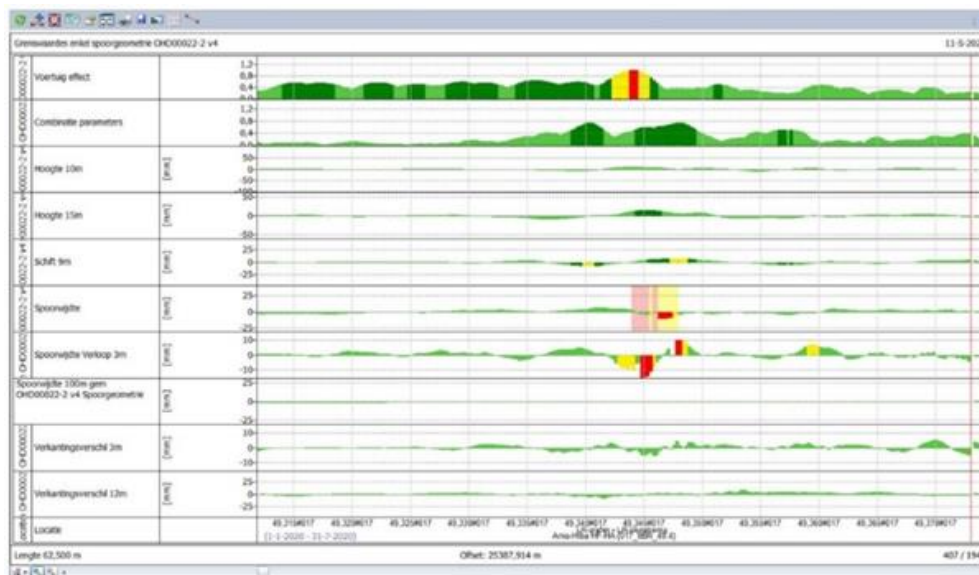


Figure 167. BBMS system interface (ProRail, Factsheet ProRail - Dataset Spoorgeometrie 2022).

Name	Description
Hoogte_D1_O and Hooqe_D1_I	Longitudinal level: deviation of the top of the railhead at a particular rail in the vertical direction from the reference line. This work considers signals in D1 wavelength (3~25 m).
Schift_D1_O and Schift_D1_I	Alignment: deviation of the side of the railhead at a particular rail in the lateral direction from the reference line. This work considers signals in D1 wavelength (3~25 m).
Spoorwijdte	Track gauge: perpendicular distance between the inner side of 2 railheads at a particular location. The difference from the standard value is reported.
Verkanting	Cross-level (so-called cant or superelevation): different heights between the top of 2 railheads at a particular location.

Table 19. Description of the considered track geometry parameters.

Parameter	Measuring range	Resolution	Uncertainty
Hoogte_D1 (Longitudinal level)	± 50 mm	≤ 0.1 mm	≤ 1 mm
Schift_D1 (Alignment)	± 50 mm	≤ 0.1 mm	≤ 1.5 mm
Spoorwijdte (Track gauge)	- 25 to + 60 mm	≤ 0.1 mm	≤ 1 mm
Verkanting (Cross-level)	± 225 mm	≤ 0.1 mm	≤ 5 mm

Table 20. Specification of the considered track geometry parameters (ProRail, Factsheet ProRail - Dataset Spoorgeometrie 2022).

7.4.1.2. Norway–Condition assessment of existing concrete bridge and transition zones

The purpose of this use-case is to develop methodology and techniques for improved monitoring of concrete bridges including the transition zones. Particularly, two main failure modes have been identified as the focus:

1. Loss of prestress in tendons – how is it affecting the resonance frequency of the bridge?
2. Loss of stiffness in transition zones – how is it affecting the dynamic loading of the bridge?

In addition, the measurement system data will be utilized to evaluate bridge response for train passing of trains with higher axel loads (up to 32.5 tons) than today's maximum (31 tons), over time, to evaluate possibility of increasing the axel load permanently for the bridge. The measurement data will be correlated with response from finite element (FE) model response of the same bridge, to analyse the bridge's structural integrity of the most common damage and deteriorating processes for this type of concrete structure, including the transition zones.

The scope of the measurement system includes:

- **Structural integrity:** Measure deformation, stress and vibrations in the concrete structure and deformations and vibrations in the transition zones during train passings. A nearby weighing station already in operation will supply weight of passing trains.
- **Environmental factors:** Measure air temperature and air humidity.

- **Data collection:** Collect measurement data from each train passing and store data in cloud solution where data will be available for further processing and analysis.

The measurement system shall register the following data categories:

- Structural deformation at selected locations including deformation, deformation and bending of the bridge during train passing.
- Vibrations and dynamic response of bridge and transition zones during train passing.
- Displacement and vibrational phenomenon in the track during train passing.
- Weather data.
- Track temperature.

Specifications	Description
Sensors	The measurement system includes accelerometers, inclinometers, LVDTs, and temperature and humidity sensors for continuous measurements. The system shall also include sensors for measuring bending response in transition zones and bridge span for train passing with known weight for calibration. This will be through vertical laser measuring vertical distance between bridge deck and ground, and high-speed cameras but will not be permanently installed.
Data logging	Storing of measurement data shall be triggered by train passing.
Displacement measurements	Displacement measured by LVDT and inclinometers shall measure across approximately 1 meter length. Inclinometer shall measure close to each abutment and LVDT at bridge center and shear-deformation close to each abutment. Measurement frequency shall be in the range of 10-20 samples per second. Inclinometers shall have measurement accuracy higher than 0.0005 degrees. LVDT shall have measurement accuracy higher than 2 microns.
Bridge vibration measurements	Vibrations shall be measured by 3-axis accelerometers with at least 500 samples per second. Expected measurement range is below 0.5g.
Transition zone vibration measurement	Vibrations shall be measured by 1-axis accelerometers mounted on sleepers in vertical direction at 1000 samples per second. Expected measurement range is below 2g. Today's sleepers are made of wood but will be changed to concrete so the sensors must be de- and re-mountable.
Communication	The measured data shall be stored in a cloud solution through internet. Area has good 4G and 5G coverage, and fibre-based Internet is available.
Robustness	The measurement system needs to withstand harsh weather conditions including at least $\pm 30^{\circ}\text{C}$ ambient temperature conditions, severe rain, snow and wind conditions and dust. Thus, environmental rating should at least be IP65.

Table 21. List of major specifications for bridge measurement system.

The summary of the planned measurement system is shown in Table 22.

Bridge 1	
Type of sensor	Number of units
Accelerometers (transition zone)	8 (4 on each transition zone)
Accelerometers (bridge span)	1
Inclinometers	2 (at bridge centre)
Bridge 2	
Type of sensor	Number of units
Accelerometers (transition zones)	12 (6 on each transition zones).
Accelerometers (bridge span)	2 (1 on each span)
Inclinometers	2 (at bridge centre)
LVDTs	5 (1 at bridge centre, 4 next to abutments)

Table 22. Summary of the planned measurement system.

7.4.2. Installation layout

7.4.2.1. The Netherlands-Track condition monitoring

The next figure shows an example of the instrumentation of a passenger wagon with the developed ABA-based measurement system. Eight axle boxes of the four wheelsets of the wagon are mounted with axle box accelerometers. GPS antenna is mounted on the roof of the wagon, and a tachometer is mounted on the second wheelset of the wagon.

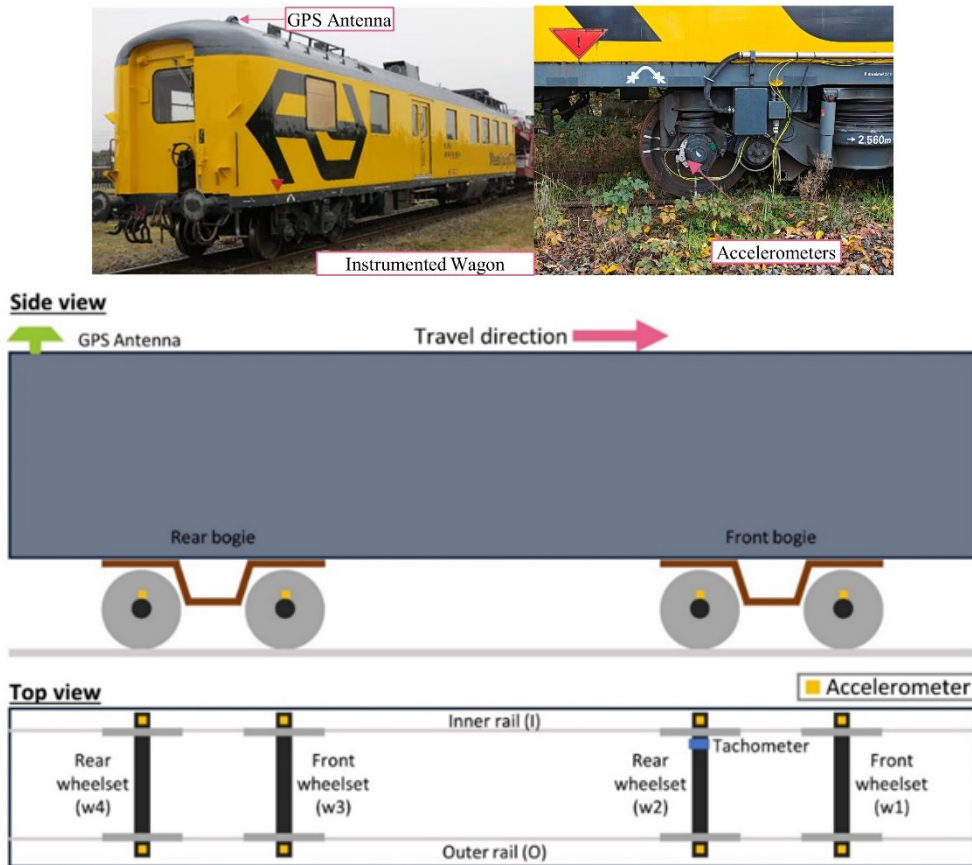


Figure 168. ABA measurement system sensor layout.

The next figure shows the UFM120 track inspection vehicle consisting of comprehensive measurement modules. The track geometry measurement module is highlighted with the box.

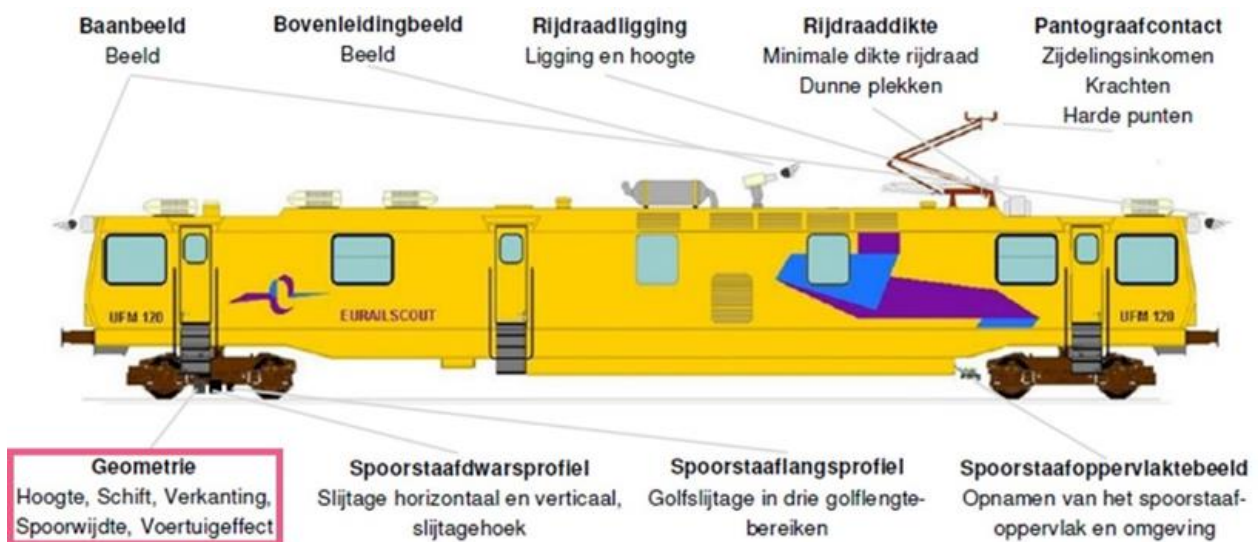


Figure 169. UFM120 sensors layout (ProRail, Factsheet ProRail - Meetsystemen UFM120 2022).

7.4.2.2. Norway–Condition assessment of existing concrete bridge and transition zones

The Sømsterbekk bridges are located on the Ofoton railway. The bridges are located approximately 100 and 300 meters from the Sømsterbekk railway station (Figure 170).



Figure 170. Situational map of Sømsterbekk area on Ofotbanen railway line.

The installation plans for both bridges are depicted in Figure 171 and Figure 172. The acquisition equipment will be placed inside a shed next to the station where Internet by optical fibre and 230 VAC will be available.

Suggestion for instrumentation - Søsterbekk bridge-1

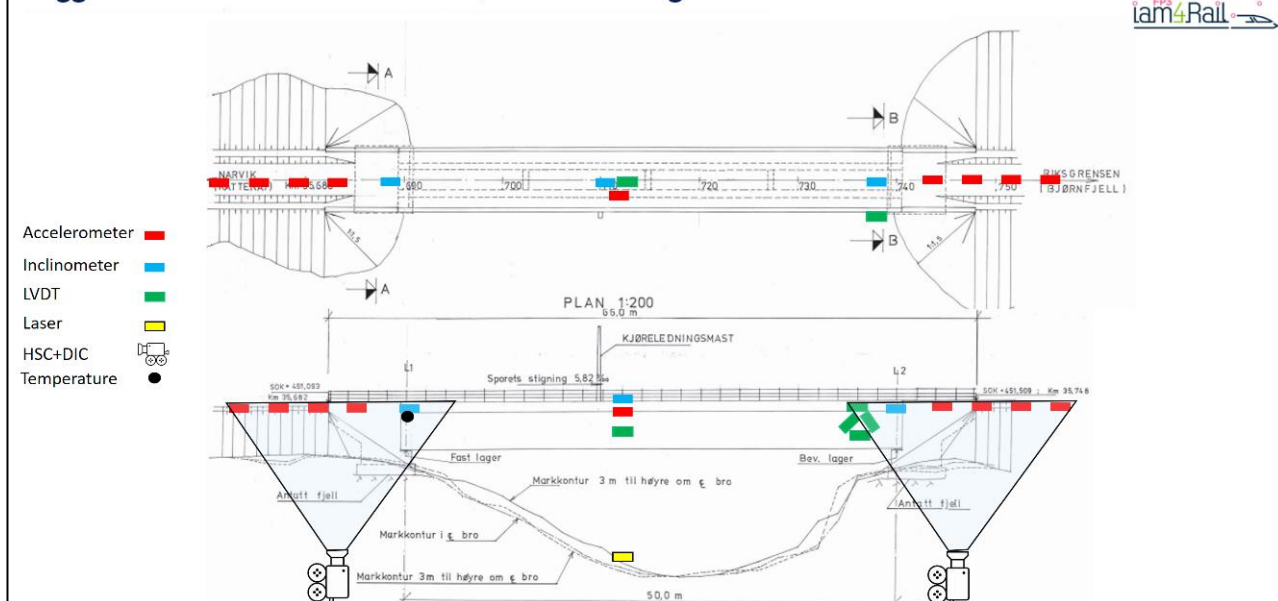


Figure 171. Installation plan for Søsterbekk bridge 1.

Suggestion for instrumentation - Søsterbekk bridge-2

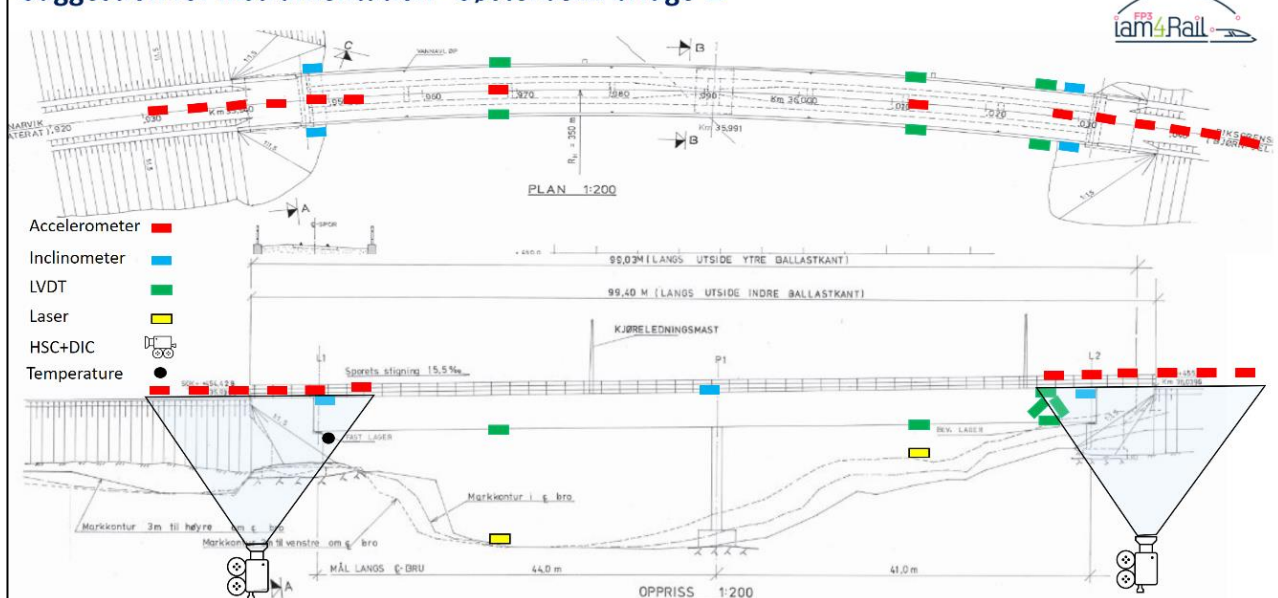


Figure 172. Installation plan for Søsterbekk bridge 2.

7.4.3. Initial data collection and results

7.4.3.1. The Netherlands-Track condition monitoring

Considering the availability of measurement data, we selected the track section between Dordrecht and Lage Zwaluwe as the initial case study for this period. There are nine bridges in this

track section, and multiple measurements have been taken. The track section and the transition zones are shown next.



Figure 173. Transition zones between Dordrecht station and Lage Zwaluwe station (Unsiwilai, et al. 2023).

In 2019, two measurements were conducted at a particular transition zone with different speeds upon train operational conditions. We then analyze the ABA signals from different wheelsets and different speeds.

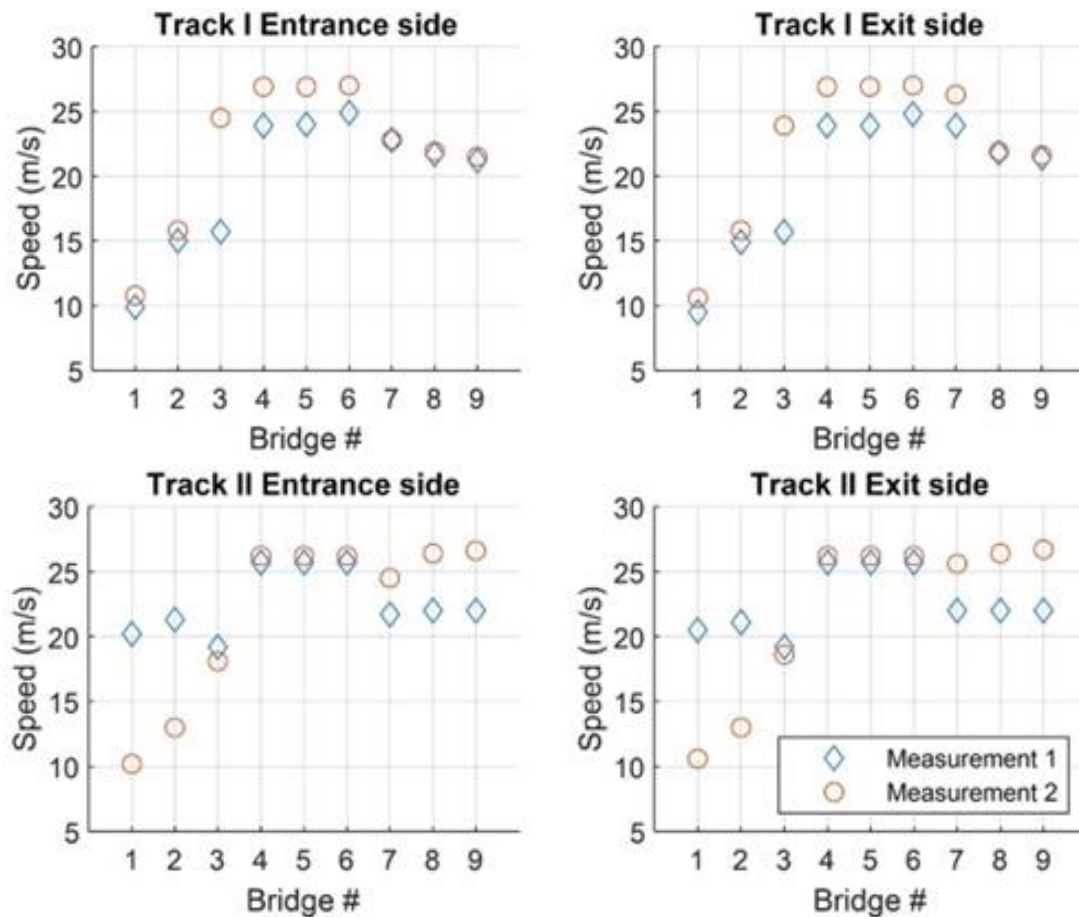


Figure 174. The average speed of the ABA measurement system at each transition zone. Multi-ABA responses at different wheelsets (Unsiwilai, et al. 2023).

To showcase the results of different wheelsets, the transition zones of Bridge 6 are selected since it is relatively isolated from insulated joints (the closest is 42.8 m away) and other bridges. Signals from all the wheelsets provide strong responses at positions close to both abutments. For Bridge 6, the responses near the South Abutment are stronger than the responses near the North Abutment. Similar dominant peaks at the entrance and exit sides close to abutments are found from the four signals (see dashed rectangles 1 and 2). The wavelet power spectrum (WPS) of the ABA signals from the four wheelsets follows similar patterns.

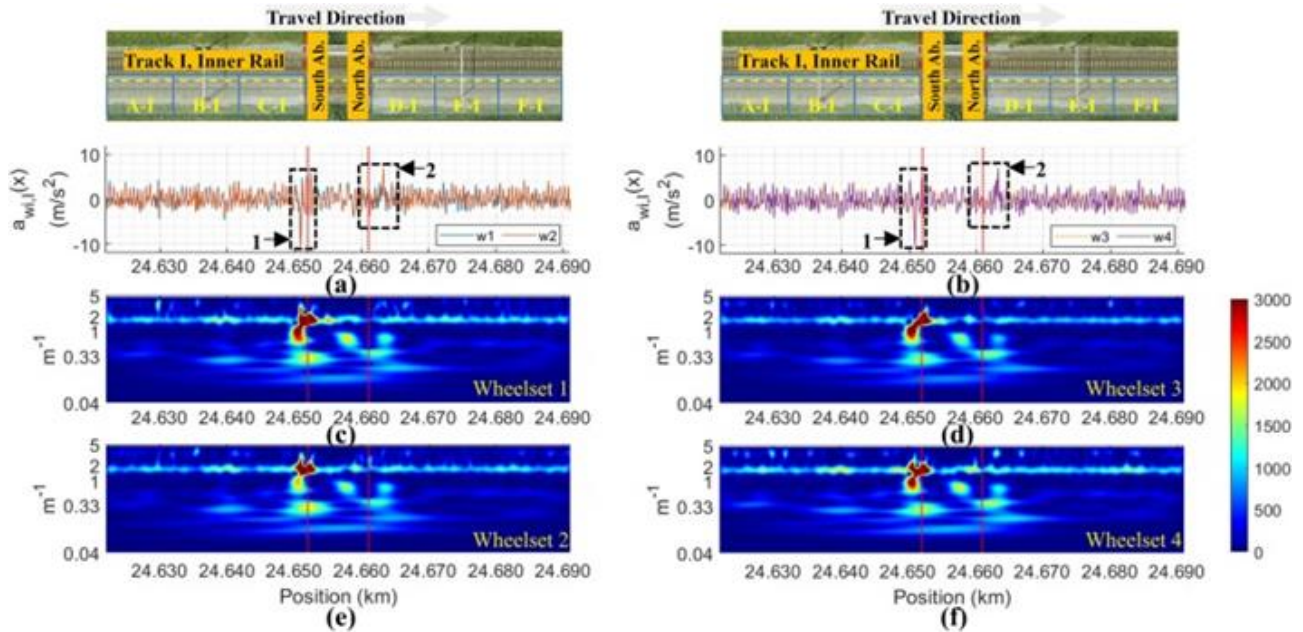


Figure 175. Responses of the ABA signals from 4 wheelsets measured at the inner rail of Track I at Bridge 6, ABA signals with 100 Hz cutoff frequency (source of aerial photographs: BBMS, ProRail) (Unsiwilai, et al. 2023).

The next figure shows that the GWPS responses from different wheelsets in each study area contain the same number of dominant peaks with slight amplitude differences. For Track I of Bridge 6, in the considered spatial frequency range from 0.04 m^{-1} to 0.33 m^{-1} , the closer the area is to the bridge, the higher the total energy. Furthermore, the dominant peak at each area varies in frequency and amplitude, as indicated by the blue rectangles in the next figure. Note the common peak outside the region of interest at 1.68 m^{-1} , which corresponds to a 0.60 m wavelength that is sleeper-related.

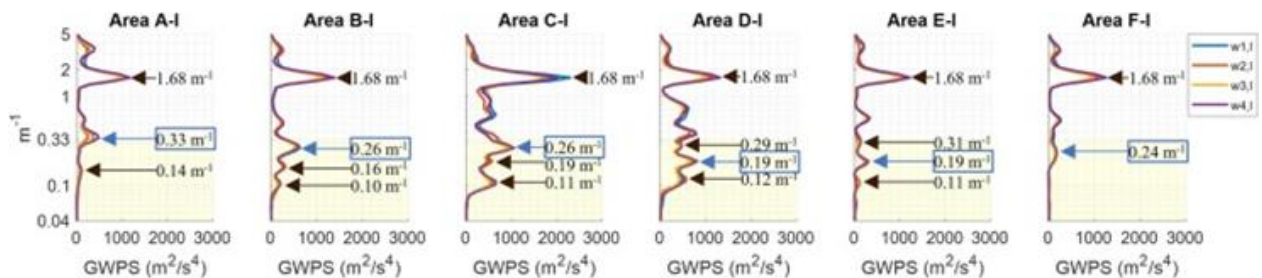


Figure 176. GWPS of the ABA signals of the transition zones at the inner rail of Track I at Bridge 6. A-I to C-I are areas on the entrance side, and D-I to F-I are areas on the exit side (Unsiwilai, et al. 2023).

The next figure presents the SAWP in the spatial frequency range from 0.04 m^{-1} to 0.33 m^{-1} from the four wheelsets. Although similar SAWP patterns are observed, differences are found in the peak locations and amplitudes. For example, the peaks in Area C-I have amplitudes between $0.48 \text{ m}^2/\text{s}^4$ and $0.67 \text{ m}^2/\text{s}^4$, and the positions of the peaks vary within a range of approximately 1 m . In

the case of Area D-I, the peaks have amplitudes between $0.31 \text{ m}^2/\text{s}^4$ and $0.47 \text{ m}^2/\text{s}^4$ with less than 1 m variation in the position of the peaks.

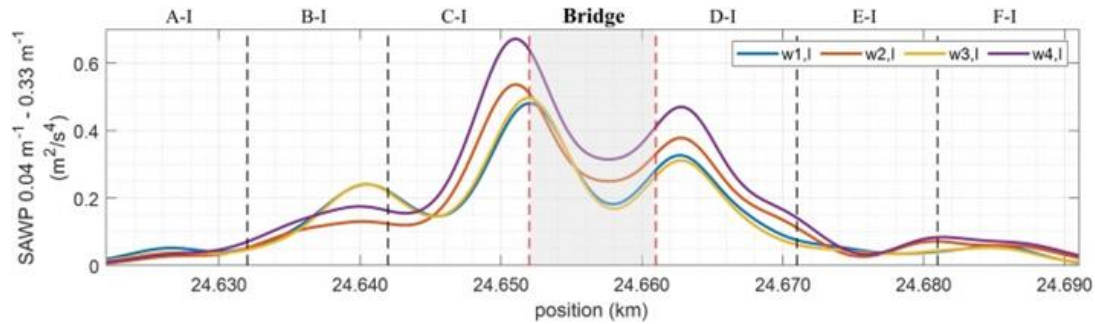


Figure 177. SAWP of the ABA signals from 4 wheelsets at the inner rail of Track I at Bridge 6 (Unsiwilai, et al. 2023).

Finally, different wheelsets provide similar responses when analyzing other transition zones. Thus, the average GWPS and SAWP can be considered to account for the minor variabilities between wheelset responses. Furthermore, we observed local changes in the spatial frequency range between 0.04 m^{-1} and 0.33 m^{-1} for different transition zones. Thus, the total energy of the SAWP is a good candidate for determining a general KPI for transition zones.

To showcase the results of different speeds, the transition zones of Bridge 3 were selected since they have the largest speed variations from the measurement campaign (15.7 m/s and 24.2 m/s). For Bridge 3, the ABA signal responses of wheelset 1 are shown in the next figure. The peak locations of the ABA signals are similar, but the amplitude of each peak is larger and has a faster measurement speed. Measurements at different speeds show different WPS and GWPS responses in terms of the energy level, but the locations of the corresponding dominant spatial frequencies are similar. We observe similar numbers of dominant peaks and notable alignment of peaks in all the different study areas. This shows good repeatability of the measurements.

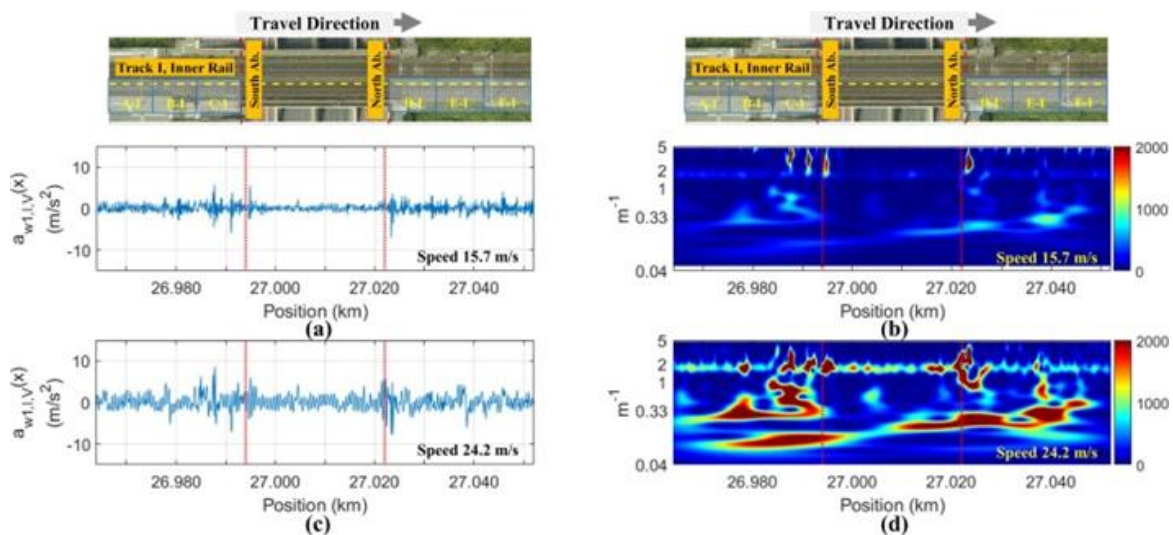


Figure 178. ABA responses (with 100 Hz cutoff frequency) at Bridge 3 in wheelset 1 on the inner rail of Track I: (a) and (b) ABA and its WPS, measured at 15.7 m/s ; and (c) and (d) ABA and its WPS, measured at 24.2 m/s (source of aerial photographs: BBMS, ProRail) (Unsiwilai, et al. 2023).

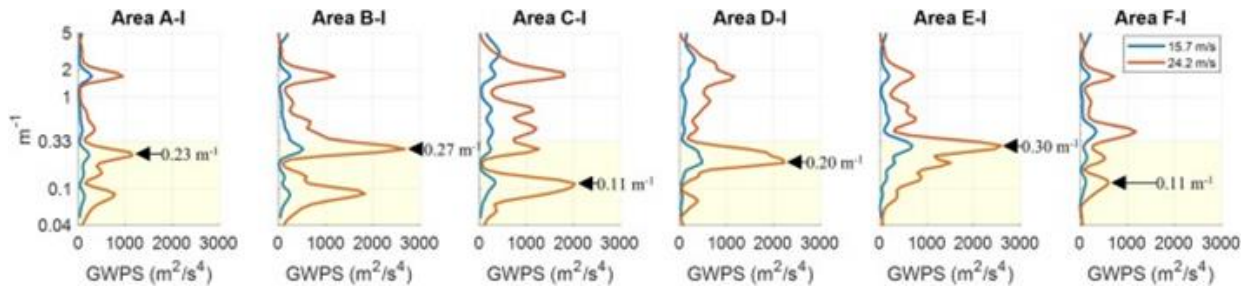


Figure 179. GWPS of ABA signals from two different measurement speeds at Bridge 3 in wheelset 1 on the inner rail of Track I (Unsiwilai, et al. 2023).

Furthermore, a comparison of the SAWP values of the ABA signals from the two measurement speeds is presented next. The result shows that a signal from a particular wheelset provides similar peak positions despite the different measurement speeds. Moreover, the amplitude is larger with a faster measurement, and the differences are more prominent than with a slower measurement. Varying peak positions of approximately 1 m for different wheelsets are observed between measurements.

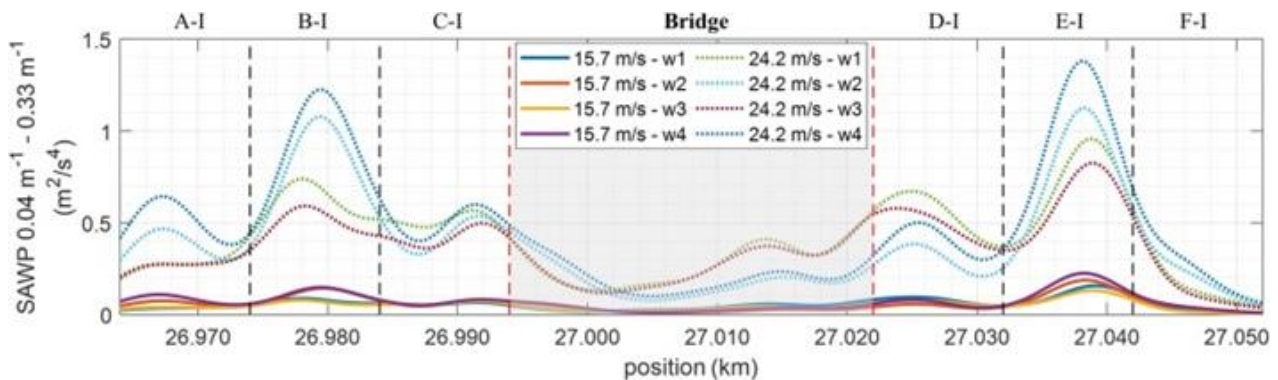


Figure 180. SAWP of the ABA signals from two different measurement speeds at Bridge 3 for the inner rail of Track I (Unsiwilai, et al. 2023).

Finally, similar findings are obtained when analyzing other transition zones. That is, speed variations in the multi-ABA measurement have a minor influence on the location of the dominant peaks. However, the measurement speeds strongly influence the multi-ABA responses in terms of energy. As expected, faster speeds lead to larger dynamic responses of the train-track interactions (Esveld 2003). The multi-ABA data characterize the responses of the whole track system under a very strong input excitation given by the moving load (train). For substructure condition assessment, a faster measurement speed is preferable in the design of KPIs for transition zones since it provides more noticeable responses due to the higher excitation level than a slower speed, particularly in the low-frequency range. Still, other track components are also more excited, necessitating further studies to separate the responses from each track component, for instance, from the subgrade, sub-ballast, ballast, and sleepers.

Bridge 6, Track I are selected as an example to showcase the variation in track geometry parameters, measured in 2019, at railway transition zones, as shown next. We found a

considerable variation in track geometry parameters, especially in Area C and Area D on both tracks. This finding might relate to the reported relationship between the longitudinal level and the track substructure conditions (Audley and Andrews 2013, Auersch 2015, Paixão, Fortunato and Calçada 2016, Lazarević, et al. 2019, Nielsen, et al. 2020).

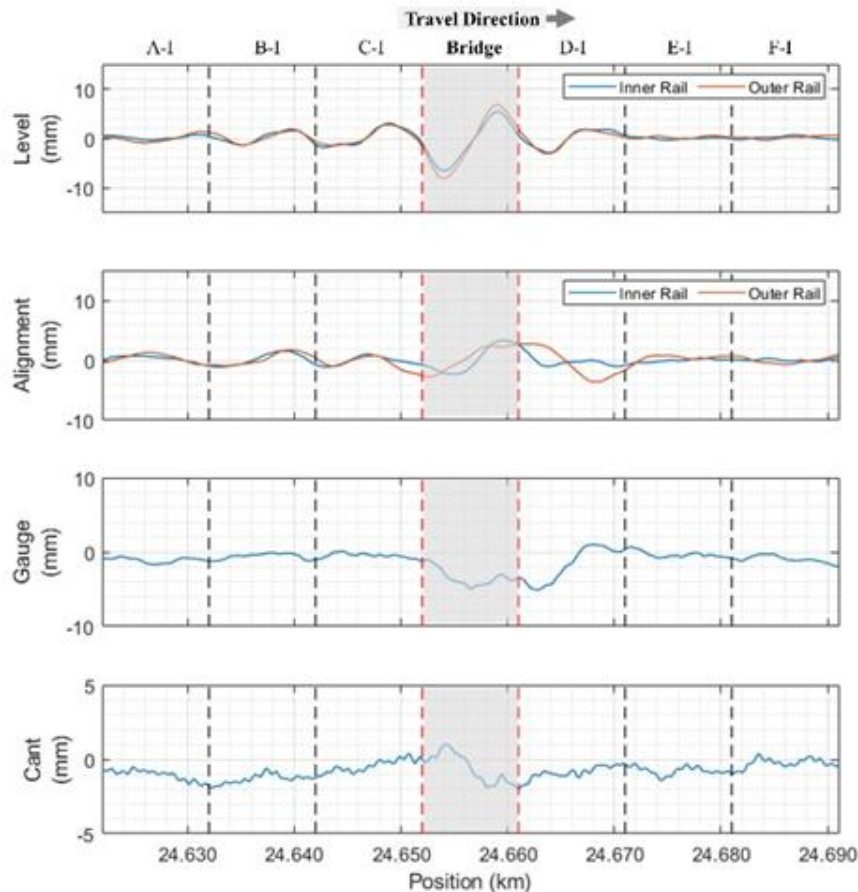


Figure 181. SAWP of the ABA signals and track geometries at Bridge 6, Track I (Unsiwilai, et al. 2023).

7.4.3.2. Norway–Condition assessment of existing concrete bridge and transition zones

The installation of the measurement system is planned to be installed in the yearly maintenance period for Ofotbanen, divided into the two separate time spans 02.06.2025 - 29.06.2025 and 21.07.2025-07.09.2025.

7.4.4. Demonstration Plans

7.4.4.1. The Netherlands-Track condition monitoring

The developed track condition monitoring technology is currently being tested and assessed based on the measurements on the track section between Dordrecht and Lage Zwaluwe. A future use case is to demonstrate this technology on the track section between Delft and Schiedam. This

railway line is one of the oldest in the Netherlands, and it was constructed in the moist soil of the polder area. The overview of this railway line is shown next. In addition, the first round of ABA measurement on this line was conducted in May 2023.



Figure 182. The overview of Delft – Schiedam Line (source of the map and aerial photographs: BBMS, ProRail).



Figure 183. The ABA measurement train passed the Delft Campus station (between Delft and Schiedam).

7.4.4.2. Norway–Condition assessment of existing concrete bridge and transition zones

7.4.4.2.1. Bridge monitoring

Numerical modelling of the concrete bridge structures will allow studying methods and models for structural assessment management. The numerical model will allow introducing and analysing faults from train-based track measurements and artificial anomalies. Further, anomaly detection algorithms will be developed using the model and will be applied based on measured data in the field. Modelling work will be performed by using multibody software to assess the acceleration and behaviour of bridges with full and degraded structural integrity.

Structural assessment management of concrete bridges - More advanced calculations (e.g., nonlinear FE analysis) together with detailed inspections (Non-Destructive Inspections - NDI), and bridge monitoring measurements of the use case will be demonstrated to investigate the current load-bearing capacities and residual service life of railway bridges made of concrete. Structural assessment and modelling will identify failure modes in an earlier stage to increase the safety of infrastructure assets. A digital twin will be established to investigate the effects of known failure modes on concrete bridge structures and predict future structural degradation for maintenance and repair mitigation planning. The model will also be used to investigate possible higher load-bearing capacities and constitute a basis for upgrading/strengthening remedies if needed.

Methods developed from this use case could be used as a methodology for structural assessment on other railway concrete bridges and to improve bridge performance, reduce costs, and make it possible to improve designs for better and longer-lasting bridge designs. The general principle is to extend the service life of large concrete structures instead of demolishing and building new ones. This has the potential to save Norwegian society and industry for at least NOK 100 billion. In addition, it can help to reduce the national greenhouse gas emissions by at least 10,000 tonnes over the next ten years.

7.4.4.2.2. Embankment stability – Transition zones

For the Norwegian railway, we will establish a numerical model of embankment stability in a chosen transition zone on the Ofoten line inspired by the ongoing project in In2Track3 in Sweden. We will characterize the degradation mode and response of the system to the passage of different trains over time. Finite Elements model, discretization of parts, and connection in a transition zone will be evaluated to see the effect of modifications, to set boundary conditions for design, and to monitor them. A numerical model will be established and used for track structure design in order to optimize the track structure dynamic stiffness in railway superstructure and substructure. In transition zones such as tunnels, bridges, culverts, etc.) for both existing railways and the design of new railway tracks. There is a need for a smooth transition in track elasticity between open track and stiffer constructions e.g., bridges, tunnels, and culverts.

8. Conclusion

This deliverable presents all the technologies and demonstration scenarios associated with the four defined project UCs, addressing the challenges these technologies aim to solve, their current state within research and industry and other details referring to their impact and influence. The architecture of the WP and the applied standards used to ensure interoperability are defined. Also, the progress made at the time of this deliverable has been detailed, with a particular focus on the initial stages of monitoring system installation, as well as the first data reception and analysis.

The first four sections of the deliverable address in detail the problem which the different technologies will solve, analyzing the current state of the industry to analyze where these technologies fit and how they are needed within an economic, social and industrial point of view. The challenges and needs covered by the development are described in detail and different Key Performance Indicators (KPIs) are presented in order to measure in a quantitative manner the impact of the technologies once they are applied.

The architecture of the project database is presented, which aligned with FAIR principles describe its different elements and interconnections, as well as the visual interface for its management. The different standards applied during the project are gathered in relation to interoperability and retrievability and the different UCs.

The last section describes the installation and preliminary analysis and results from the different UCs and their technologies:

- Multiscale Monitoring of civil assets:
 - Vegetation encroachment and asset recognition. This section details how raw data and the ground truth data are obtained and processed. The algorithms and workflows applied are described. The preliminary results in relation to the classification in terrain, vegetation, buildings is showcased and the technology demonstration plans is presented.
 - Bridge inspection. The information provided and used for the training of the models is described. Conclusions from the first analysis of the provided data is reported and the two AI processing strategies for addressing the problem are described. Conclusions and demonstration plan are also included.
 - Hydrogeological risk. In this section it is described how Satellite data will be collected and processed using Google Earth Engine (GEE) platform and how the integration of collected and pre-elaborated data will carry out through neural networks algorithms, on the basis of which the monitoring and forecasting tool will be developed. The best NN configurations are discussed, and the demonstration plan presented. Interferometric Analysis for subsidence describes how Synthetic Aperture Radar (SAR) will be used to monitor areas affected by hydrogeological risk and earthworks in general.
- Bridges and earthworks aided by geotechnics:

- Bridge assets management. The monitoring and installation plans for the bridge monitoring are detailed as well as the methodology for detecting and locating bridge damage. The planning of the visualization platform is presented as demonstration plan.
- Earthworks asset management. The installation details about the earthworks monitoring are described for both Briones and Vilar de Silva. The workflows and analysis developed for the earthworks instability analysis based among others on the removal of environmental defects, a LSTM NN and an alarm system is presented. As well as the visualization of the platform as demonstration plan.
- Monitoring of tunnel, sub-ballast layers and subsoil.
 - Monitoring of sub-ballast layers and subsoil. The acquisition system based on geophones is described and the analysis based on the data process as well as how passive methods combined with AI were used to retrieve groundwater table height maps and geological descriptions are presented.
 - Monitoring of tunnel. RADIS tool for the acquisition of data is described, as well as the high efficiency sensor installation are described for the tunnel monitoring capabilities.
 - Passive contactless magnetic microwire sensor arrays for high-definition tunnel convergence monitoring systems in tunnels. The new non-invasive sensor element (magnetic microwire) to perform the inspection of railway tunnel convergence installation and description is presented.
- Data Analysis for Condition Monitoring.
 - The Netherlands - Track condition monitoring using a combination of ABA and track geometry measurements is proposed. First, the limitations of track geometry measurement, which is the current practice in the track condition assessment, have been discussed. ABA measurement system has been introduced to improve the efficiency of the assessment. The analysis and preliminary results at railway transition zones, where the composition of the embankment is changed, have been discussed. The findings suggested significant changes in ABA signal characteristics at transition zones. This suggests the potential to detect different conditions of the embankment. In the next phase, the relationship between dynamic train loading with respect to ABA signals and the rate of change of track geometry will be investigated. Then, a track quality indicator combining ABA signals and track geometry will be proposed. The first analysis will be conducted in the Dordrecht-Lage Zwaluwe line. Then, we will evaluate this framework on the track section between Delft and Schiedam.
 - Norway–Condition assessment of existing concrete bridge and transition zones. In this section the specifications of the sensing systems, the data logging and other elements from the monitoring system to be installed are described.

This deliverable not only meets the project's objectives but also provides a detailed roadmap for



the continued development and integration of innovative technologies within the framework of WP12 and WP13.

9. References

- Andrade, A., and P. Teixeira. "Assessing temporary speed restrictions and associated unavailability costs in railway infrastructure." *International Journal of Civil Engineering* 16 (2018): 219–228.
- Audley, M., and J. D. Andrews. "The effects of tamping on railway track geometry degradation." *Proceedings of the Institution of Mechanical Engineers, Part F: Journal of Rail and Rapid Transit*. 227, no. 4 (2013): 376–391.
- Auersch, L. "Excitation of ground vibration due to the passage of trains over a track with trackbed irregularities and a varying support stiffness." *Vehicle System Dynamics* 53, no. 1 (2015): 1–29.
- Azim, M. R., and M. Gul. "Data-driven damage identification technique for steel truss railroad bridges utilizing principal component analysis of strain response." *Structure and Infrastructure Engineering: Maintenance, Management, Life-Cycle Design and Performance* 17, no. 8 (2021): 1019–1035.
- Beskhryoun, S., T. Oshima, and S. Mikami. "Wavelet-based technique for structural damage detection." *Structural Control and Health Monitoring* 17, no. 5 (2010): 473–494.
- Bi, H., J. Ma, W. Zheng, and J. Zeng. "Comparison of soil moisture in GLDAS model simulations and in situ observations over the Tibetan Plateau." *Journal of Geophysical Research: Atmospheres* 121, no. 16 (2016): 2658–2678.
- Brownjohn, J. M. W., P. Q. Xia, H. Hao, and Y. Xia. . "Civil structure condition assessment by FE model updating: methodology and case studies." *Finite Elements in Analysis and Design* 37, no. 10 (2001): 761–775.
- Catbas , F. N., H. B. Gokce, and M. Gul. "Nonparametric analysis of structural health monitoring data for identification and localization of changes: Concept, lab, and real-life studies." *Structural Health Monitoring* 11, no. 5 (2012): 613–626.
- CEN. "NEN-EN 13848-1:2019 (E) - Railway applications - track - track geometry quality - part 1: characterization of track geometry." 2019.
- CEN. "NEN-EN 13848-5:2017 (E) - Railway applications - track - track geometry quality - part 5: geometric quality levels - plain line, switches and crossing." 2017.
- CEN. "NEN-EN 13848-6:2014 (E) - Railway applications - track - track geometry quality - part 6: characterization of track geometry quality." 2014.
- Dang, H. V., M. Tatipamula, and H. X. Nguyen. "Cloud-based digital twinning for structural health monitoring using deep learning." *IEEE Transactions on Industrial Informatics* 18, no. 6 (2022): 3820–3830.
- Esveld, C. *Modern railway track*. 2nd. Zaltbommel: MRT-productions, 2003.
- Friswell, M. I., J. E. Mottershead, and H. Ahmadian. "Finite-element model updating using experimental test data: parametrization and regularization." *Philosophical Transactions: Mathematical, Physical and Engineering Sciences* 359, no. 1778 (2001): 169–186.
- Ghiasi, A., C. T. Ng, and A. H. Sheikh. "Damage detection of in-service steel railway bridges using a

fine k-nearest neighbor machine learning classifier.” *Structures*. 45, 1920–1935. 45 (2022): 1920–1935.

Google. *Google Earth Engine*. 2024. <https://earthengine.google.com/> (accessed July 16, 2024).

Guo, W. C., A. D. Orcesi, C. F. Cremona, J. P. Santos, S. Z. Yang, and L. Dieleman. “A vibration-based framework for structural health monitoring of railway bridges.” *Proceedings of the 3rd International Symposium on Life Cycle Civil engineering (IALCCE)*. Vienna, Austria, 2012.

Huffman, G., E. Stocker, D. Bolvin, E. Nelkin, and J. Tan. *GPM IMERG Final Precipitation L3 Half Hourly 0.1 degree x 0.1 degree V06*. Greenbelt, MD: Goddard Earth Sciences Data and Information Services Center (GES DISC), 2019.

Imam, B. M., and M. K. Chryssanthopoulos. “Causes and consequences of metallic bridge failures.” *Structural Health Monitoring* 22, no. 1 (2012): 93–98.

Keras. 2024. <https://keras.io/>.

Laory, I., N. B. H. Ali, T. Trinh, and I. Smith. “Measurement system configuration for damage identification of continuously monitored structures.” *Journal of Bridge Engineering* 17, no. 6 (2012): 857–866.

Laory, I., T. N. Trinh, D. Posenato, and I. F. C. Smith. “Combined model-free data-interpretation methodologies for damage detection during continuous monitoring of structures.” *Journal of Computing in Civil Engineering* 27, no. 6 (2013): 657–66.

Lazarević, L., D. Vučković, M. Vilotijević, and Z. Popović. “Application of seismic tomography for assessment of the railway substructure condition.” *Structural Health Monitoring* 18, no. 3 (2019): 792–805.

Li, D., A. Meddah, K. Hass, and S. Kalay. “Relating track geometry to vehicle performance using neural network approach.” *Proceedings of the Institution of Mechanical Engineers, Part F: Journal of Rail and Rapid Transit* 220, no. 3 (2006): 273–281.

Li, Z., and M. Molodova. *Method and instrumentation for detection of rail defects, in particular rail top defects*. WO 2011019273 (A1), 2011.

Loidolt, M., and S. Marschnig. “The impact of short-wave effects on deterioration of track geometry.” *Proceedings of the Institution of Mechanical Engineers, Part F: Journal of Rail and Rapid Transit* 238, no. 2 (2024): 175–184.

Maes, K., L. V. Meerbeeck, E. P. B. Reynders, and G. Lombaert. “Validation of vibration-based structural health monitoring on retrofitted railway bridge KW51.” *Mechanical Systems and Signal Processing* 165 (2022): 108380.

NASA. *GLDAS: Project Goals*. 2024. <https://ldas.gsfc.nasa.gov/gldas>.

—. *MODIS*. July 18, 2024. <https://modis.gsfc.nasa.gov/data/dataproduct/mod11.php>.

—. *Precipitation Data Directory*. 2024. <https://gpm.nasa.gov/data/directory>.

Neves, A. C., I. Gonzalez, and R. Karoumi. “Development and validation of a data-based SHM method for railway bridges.” In *Structural Integrity: Structural Health Monitoring Based on Data Science Techniques*, by A. Cury, D. Ribeiro, F. Ubertini and M. D. Todd, 95–116. New York: Springer, 2022.

- Ngoc, H. T., S. Khatir, G. D. Roeck, and T. B. Tien. "An efficient artificial neural network for damage detection in bridges and beam-like structures by improving training parameters using cuckoo search algorithm." *Engineering Structures* 199 (2019): 109637.
- Nielsen, J. C. O., E. G. Berggren, A. Hammar, F. Jansson, and R. Bolmsvik. "Degradation of railway track geometry – correlation between track stiffness gradient and differential settlement." *Proceedings of the Institution of Mechanical Engineers, Part F: Journal of Rail and Rapid Transit* 234, no. 1 (2020): 108–119.
- Oshima, T., Y. Miyamori, S. Mikami, T. Yamazaki, S. Beskhyroun, and M. F. Kopacz. "Small damage detection of real steel bridge by using local excitation method." *Journal of Civil Structural Health Monitoring* 3 (2013): 307–315.
- Paixão, A., E. Fortunato, and R. Calçada. "A contribution for integrated analysis of railway track performance at transition zones and other discontinuities." *Construction and Building Materials* 111 (2016): 699–709.
- Parisi, F., A. M. Mangini, M. P. Fanti, and J. Adam. "Automated location of steel truss bridge damage using machine learning and raw strain sensor data." *Automation in Construction* 138 (2022): 104249.
- Phan, T. N., and M. Kappas. "Application of MODIS land surface temperature data: a systematic literature review and analysis." *Journal of Applied Remote Sensing* 12, no. 4 (2018): 041501.
- Pradhan, R. K., et al. "Review of GPM IMERG performance: A global perspective." *Remote Sensing of Environment* 268 (2022): 112754.
- ProRail. "Factsheet ProRail - Dataset Spoorgeometrie." 2022.
- ProRail. "Factsheet ProRail - Meetsystemen UFM120." 2022.
- ProRail. "Instandhoudingsspecificatie - Spoor - Deel 1: Onderhoudswaarden, Interventiewaarden, Onmiddellijke actiewaarden." 2021.
- Rageh, A., D. G. Linzell, and S.E. Azam. "Automated, strain-based, output-only bridge damage detection." *Journal of Civil Structural Health Monitoring* 8 (2018): 833–846.
- Sarmadi, H., A. Entezami, B. Behkamal, and C. D. Michele. "Partially online damage detection using long-term modal data under severe environmental effects by unsupervised feature selection and local metric learning." *Journal of Civil Structural Health Monitoring* 12 (2022): 1043–1066.
- Sonbul, O. S., Rashid, M. "Algorithms and techniques for the structural health monitoring of bridges: Systematic literature review." *Sensors* 23, no. 9 (2023): 4230.
- Sunca, F., M. Ergun, A. C. Altunisik, M. Gunaydin, and F. Y. Okur. "Modal identification and fatigue behavior of Eynel steel arch highway bridge with calibrated models." *Journal of Civil Structural Health Monitoring* 11 (2021): 1337–1354.
- Svendsen, B. T., G. T. Froseth, O. Oiseth, and A. Ronnquist. "A data-based structural health monitoring approach for damage detection in steel bridges using experimental data." *Journal of Civil Structural Health Monitoring* 12 (2022): 101–115.
- Svendsen, B. T., O. Oiseth, G. T. Froseth, and A. Ronnquist. "A hybrid structural health monitoring approach for damage detection in steel bridges under simulated environmental conditions

using numerical and experimental data.” *Structural Health Monitoring* 22, no. 1 (2023): 540-561.

TensorFlow. 2024. <https://www.tensorflow.org/>.

Torres, B., P. Poveda, S. Ivorra, and L. Estevan. “Long-term static and dynamic monitoring to failure scenarios assessment in steel truss railway bridges: A case study.” *Engineering Failure Analysis* 152 (2023): 107435.

Unsiwilai, S., L. Wang, A. Núñez, and Z. Li. “Multiple-axle box acceleration measurements at railway transition zones.” *Measurement* 213 (2023): 112688.

Vagnoli, M., R. R. Prescott, and J. Andrews. “Railway bridge structural health monitoring and fault detection: State-of-the-art methods and future challenges.” *Structural Health Monitoring* 17, no. 4 (2018): 971–1007.

Wan, Z., Hook, S., Hulley, G. *MODIS/Terra Land Surface Temperature/Emissivity Daily L3 Global 1km SIN Grid V061*. NASA EOSDIS Land Processes Distributed Active Archive Center, 2021.

Wang, Y., P. Wang, X. Wang, and X. Liu. “Position synchronization for track geometry inspection data via big-data fusion and incremental learning.” *Transportation Research Part C: Emerging Technologies* 93 (2018): 544–565.

Xu, L., Zhai, W. “A novel model for determining the amplitude-wavelength limits of track irregularities accompanied by a reliability assessment in railway vehicle-track dynamics.” *Mechanical Systems and Signal Processing* 86 (2017): 260–277.

Yano, M. O., E. Figueiredo, S. D. Silva, A. Cury, and I. Moldovan. “Transfer learning for structural health monitoring in bridges that underwent retrofitting.” *Buildings* 13, no. 9 (2023): 2323.

Zhou, X., C. W. Kim, F. L. Zhang, and K. C. Chang. “Vibration-based Bayesian model updating of an actual steel truss bridge subjected to incremental damage.” *Engineering Structures* 260 (2022): 114226.

10. Annexes.

1. Annex 1. Technical Specification Huerta Mateo (Bridge Spain).
2. Annex 2. Layouts Huertas Mateo (Bridge Spain).
3. Annex 3. Study and Installation Vilar de Silva (Earthwork Spain).
4. Annex 4. Sensors Technical Specifications – Earthworks – Vilar de Silva.
5. Annex 5. Selected theoretical Framework for InSAR and DInSar.
6. Annex 6. Technical and functional requirements Sørsterbekk bridges (Norway).
7. Annex 7. Asset digitization.